Investigating metabolic, vascular and structural neuroplasticity in healthy and diseased brain using advanced neuroimaging techniques

Eleonora Patitucci

A thesis submitted to Cardiff University for the degree of Doctor of Philosophy

February 2021

Supervisors – Professor Richard Wise and Dr Valentina Tomassini

ACKNOWLEDGMENTS

Firstly, thank you to *Wellcome* for funding my PhD and making this research possible.
I would like to thank my supervisors for their support and guidance through these years. Richard, your incredible patience and experience was invaluable throughout my PhD and Valentina, your critical thinking skills made all your feedback and our discussions amazing. I was supervised by two great researchers with complementary skills and I look forward to new incredible projects together.

Thanks to all the people in CUBRIC that made the working environment one of the best places in which to learn and to stimulate discussions. In particular thanks to Ilona, Rachael and Hannah for getting me started with MRI and for all the work we did together.
Thanks to all the people who I shared my life outside academia, for our countless meals together, for our limitless board-game sessions and for the several walks around Wales during the rare sunny days. Especially thanks to our 'bubble', to keep sharing our lives despite this particular year.
Thank you to all my lifelong friends, for being in each other's lives despite the thousands of miles between us.

Thank you to my immediate and extended family, who have always given me support and who tried hard to understand what I am doing. Especially, my little sister who is growing up so fast and she has now learnt to be encouraging as an older sister too.

Finally, thanks to Jacopo, just for deciding every day to be in my life. Your love and humour make every day a better day. And a special thanks to our son, baby Ludo, who made me feel in great company during the writing-up, and now he entertains our working-from-home days with countless smiles.

THESIS SUMMARY

The brain's lifelong capacity for reorganization is termed 'plasticity'. It relies on molecular signalling translated into long lasting modifications. MRI has been widely used to assess neuroplasticity *in vivo*, showing brain's ability to undergo functional and structural reorganization. However, there is a lack of understanding of the physiological events supporting neuroplasticity and advanced MRI techniques could help in the investigation of the biological meaning of these events and their alterations during neuroinflammation.

This thesis has two main aims. Neuroscientifically, it aims to better understand mechanisms supporting neuroplasticity in the healthy and diseased brain. Methodologically, it aims to explore new MRI approaches to the study of neuroplasticity. The early experiments investigate the mechanisms underlying long-term neuroplasticity in MS. The studies then aim to elucidate the changes in brain energetics underlying adaptation in healthy and MS brain using calibrated fMRI. I explored new approaches to analyse the relative oxygen consumption during task adaptation in the same population. A new task to study short-term neuroplasticity was validated and used to demonstrate changes in resting blood flow *after* task execution. The same task was used to investigate the relationship between GM myelination and functional activity during task execution.

Overall, we show the feasibility of using quantitative methods to study neuroplasticity, encouraging their application to improve biological interpretation in imaging studies. Our results highlight the importance of studying the brain as a network and the advantages of integrating different MRI modalities. We also show that our methods are applicable to MS populations, despite the observed metabolic impairment with neuroinflammation. Our methods

may, in future, contribute to the study of disease progression and to the development of targeted interventions to limit the damage of inflammation.

CONTRIBUTORS

The study design and data collection presented in Chapters 2 and 3 were carried out by Ilona Lipp. I originated new research questions applied to these data, as well as analysing all the data to answer these new questions (except for lesion drawing by Ilona Lipp) and writing up.

The data presented in Chapters 4 and 5, I collected together with the research team in CUBRIC including Hannah Chandler, Rachael Stickland, Neeraj Saxena and Sharmila Khot. Catherine Foster was also involved in the early study design. Hypothesis generation and data analysis were performed by me, except for lesion drawing by Shona Bhome-Dhaliwal. Mike Germuska developed the MRI sequence and part of the analysis pipeline to calculate physiological parameters related to absolute oxygen consumption. Appropriate acknowledgements are given in the relevant chapters.

I designed the experiments, collected the data, and analysed and wrote up all the data presented in Chapters 6 and 7.

PUBLICATIONS RESULTING FROM THIS THESIS

PRE-PRINT

Chandler, H. L., Stickland, R. C., Germuska, M., **Patitucci, E**., Foster, C., Bhome-Dhaliwal, S., Lancaster, T.M., Saxena, N., Khot, S., Tomassini, V. & Wise, R. G. (2021) Using dual-calibrated functional MRI to map brain oxygen supply and consumption in multiple sclerosis. *bioRxiv*, 2021-01.

ABSTRACTS

Patitucci, E., Stickland, R.C., Chandler, H.L., Germuska, M., Foster, C., Khot, S., Saxeena, N., Tomassini, V. and Wise, R.G. (2020) Voxel-wise CMRO2 mapping reveals focally-reduced task-related oxygen consumption in multiple sclerosis. Oral Presentation In *ISMRM 28th Annual Meeting.*

Patitucci, E., Stickland, R.C., Chandler, H.L., Germuska, M., Foster, C., Khot, S., Saxeena, N., Tomassini, V. and Wise, R.G. (2020) A novel pipeline to investigate brain oxygen metabolism at a voxel-wise level. Oral Presentation In *PG-BCISMRM.*

Patitucci, E., Foster, C., Stickland, R.C., Chandler, H.L., Germuska, M., Khot, S., Saxena, N., Tomassini, V. and Wise, R.G. (2019) Quantitative fMRI to investigate the energetics of brain plasticity in the healthy and MS brain. Oral Presentation In *European Society for Magnetic Resonance in Medicine and Biology (ESMRMB).*

Patitucci, E., Lipp, I., Foster, C., Stickland, R.C., Davidson, A.E., Wise, R.G. and Tomassini, V. (2019). Imaging mechanisms of brain plasticity underlying the early stages of functional recovery in MS. Poster Presentation In *25th Annual Meeting of the Organization for Human Brain Mapping (OHBM).*

Patitucci, E., Foster, C., Stickland, R., Chandler, H., Germuska, M., Khot S., Saxena N., Tomassini, V. and Wise, R.G. (2019). Energetics of brain plasticity in the healthy and MS brain: a quantitative fMRI study. Poster Presentation In *25th Annual Meeting of the Organization for Human Brain Mapping (OHBM).*

Patitucci, E., Stickland, R.C., Chandler, H.L., Germuska, M., Foster, C., Khot, S., Saxeena, N., Tomassini, V. and Wise, R.G. (2019) Energetics of brain plasticity in the healthy and MS brain: a quantitative fMRI study. Poster Presentation In *PG-BCISMRM.*

Chandler, H.L., Stickland, R., Germuska, M., **Patitucci, E**., Foster, C., Khot, S., Saxena, N**.**, Bhome-Dhaliwal, S., Tomassini, V., Wise, R.G. (2019). Quantification of cerebral grey matter vascular and metabolic function in multiple sclerosis using dual-calibrated fMRI. In *ISMRM 27th Annual Meeting.*

Patitucci, E., Lipp, I., Foster, C., Stickland, R., Davidson, A. E., Wise, R.G., & Tomassini, V. (2018). Investigating brain plasticity underlying the early stages of functional recovery in MS. Poster Presentation In *ECTRIMS-Multiple Sclerosis Congress 2018*.

Patitucci, E., Lipp, I., Foster, C., Stickland, R.C., Davidson, A.E., Wise, R.G. and Tomassini, V. (2017). Investigating microstructural damage in an MS sample. Poster Presentation In *School of Brain Cells & Circuits "Camillo Golgi": From cell physiology to integrated signals and emerging brain function.*

ABBREVIATIONS

Frequently used shown in bold

9-HPT	9-Hole Peg Test
ASL	**Arterial Spin Labelling**
ATP	**Adenosine Triphosphate**
B_0	Static Magnetic Field
BBB	Blood brain barrier
BOLD	**Blood Oxygenation Level Dependent**
CaO_2	Arterial Oxygen Content
CASL	Continuous Arterial Spin Labelling
CBF	**Cerebral Blood Flow**
CBV	Cerebral Blood Volume
$CMRO_2$	**Cerebral Metabolic Rate of Oxygen**
CNS	Central Nervous System
CO_2	Carbon Dioxide
CSF	Cerebrospinal Fluid
D_C	Effective Oxygen Diffusivity
DEXI	Dual-Excitation
DGMS	Deep Grey Matter Structures
dHb	**Deoxyhaemoglobin**
DMT	Disease modifying treatment
DTI	Diffusion Tensor Imaging
DWI	Diffusion Weighted Imaging
EDSS	Expanded Disability Status Scale
EPI	Echo Planar Imaging
FA	Fractional Anisotropy
FID	Free Induction Decay
FLAIR	Fluid Attenuated Inversion Recovery
fMRI	**Functional Magnetic Resonance**
FSMC	Fatigue Scale for Motor and Cognitive Functions
GE	Gradient Echo
GLM	General Linear Model

GM	**Grey Matter**
GRE	Gradient Recalled Echo
HC	**Healthy Controls**
Hct	Haematocrit
LTD	Long-Term Depression
LTP	Long-Term Potentiation
MP2RAGE	Magnetization Prepared 2 Rapid Acquisition Gradient Echoes
MPRAGE	Magnetization prepared rapid acquisition with gradient echo
MR	Magnetic Resonance
MS	**Multiple Sclerosis**
MSIS-29	Multiple-Sclerosis Impact Scale
NVC	Neurovascular Coupling
O_2	Oxygen
OD	Oxygen Diffusivity
OEF	Oxygen Extraction Fraction
PaO_2	Partial Pressure of Oxygen
PASAT	Paced Auditory Serial Addition Test
PASL	Pulsed Arterial Spin Labelling
PCASL	Pseudo-Continuous Arterial Spin Labelling
PD	Proton Density
$P_{ET}CO_2$	Partial Pressure of End-Tidal Carbon Dioxide
$P_{ET}O_2$	Partial Pressure of End-Tidal Carbon Oxygen
PLD	Post-Labelling Delay
PVE	Partial Volume Effects
RF	Radiofrequency
ROI	**Region of Interest**
RSN_S	Resting State Networks
RT	**Reaction Time**
SaO_2	Oxygen Saturation
SDMT	Symbol Digit Modalities Test
SE	Standard Error
SNR	**Signal to Noise Ratio**
SRT	**Serial Reaction Time**
T25-FW	Timed 25-foot-walk
TBSS	Tract-Based spatial statistic

TE	**Echo Time**
TFCE	Threshold-free cluster enhancement
TR	**Repetition Time**
VBM	Voxel-Based Morphometry
WM	**White Matter**

TABLE OF CONTENTS

INDEX OF FIGURES

INDEX OF TABLES

INDEX OF EQUATIONS

CHAPTER 1

General Introduction

1.1 INTRODUCTION TO BRAIN METABOLISM AND MRI METHODS

1.1.1 CEREBROVASCULAR ANATOMY

The brain is dependent on a continuous supply of blood through the cerebral vasculature to function. The cerebral circulation is composed of a supplying arterial circulation and a draining venous circulation. The arterial system can be subdivided according to anatomical position into anterior and posterior cerebral circulations. The arterial circulation can also be divided by size: where the macrocirculation is considered to comprise the gross branches of the cerebral vascular responsible for the regional perfusion of the brain. On the other hand, the microcirculation is defined as the microscopic site of oxygen and nutrient exchange within the vasculature and blood-brain barrier (BBB).

The main arteries supplying the oxygenated blood necessary to maintain the brain and all its many crucial functions are the internal carotid arteries (ICA), which give rise to anterior brain circulation and supply the cerebrum, and vertebral arteries (VA), which give rise to posterior circulation and join to form the basilar artery that supplies brainstem and cerebellum. They are interconnected through the circle of Willis located in subarachnoid cisterns at the base of the brain (**Figure 1.1**). The circle of Willis is an important anastomosis formed by the communicating arteries between the posterior and middle cerebral arteries, and between the middle and anterior cerebral arteries. This vascular ring gives rise to three pairs of arteries

(anterior, middle and posterior) that cover the external surface of the cerebral cortex. The arteries then divide into progressively smaller arteries penetrating the brain tissue and supplying blood to specific regions.

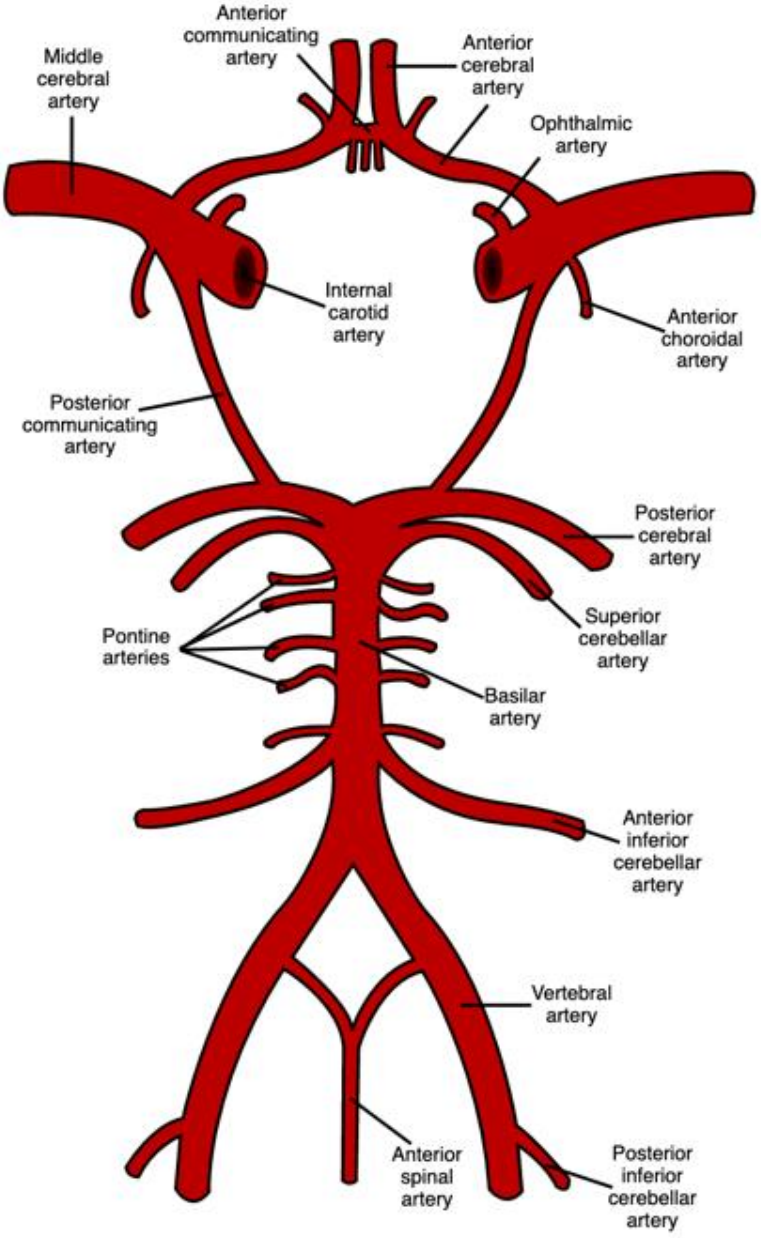

Figure 1.1. Schematic representation of the circle of Willis.

Cerebral arterial walls are composed by three layers: 1. The inner tunica intima that contains a single layer of endothelium cells. 2. The tunica media that contains smooth muscle cells, elastin and collage fibres. 3. The outer layer, the tunic adventitia, that contains collagen fibres and perivascular nerves.

Penetrating vessels are separated from the brain by the Virchow-Robin space containing the cerebrospinal fluid (CSF). Astrocytes are on the outer side of the Virchow-Robin space and they give rise to glial membranes. Deeper in the brain, the Virchow-Robin space disappears, and the vascular membrane is in direct contact with astrocyte end feet. Arterioles become progressively smaller and they lose the smooth muscle cell layer becoming capillaries. The density of brain capillaries is heterogeneous across the brain and it depends on regional blood flow and metabolic demand (Girouard & Iadecola, 2006; Ward & LaManna, 2004).

Constriction and/or dilation of cerebral arteries is dependent on the tone of the smooth muscle cells within the arterial walls. Many different mechanisms can influence smooth muscle cell tone affecting the level of free Ca^{2+} within the cells, such as factors present in the blood (neurotransmitters, carbon dioxide, nitric oxide), changes in blood pressure and local factors in the surrounding extracellular area (ion concentrations, electrical coupling, astrocytes and pericytes).

Overall, neurons and glia work together releasing different vasoactive factors that act together in order to target cerebral endothelial cells, pericytes, and smooth muscle cells that coordinate vascular adjustments to increase the cerebral blood flow (Attwell & Laughlin, 2001; Iadecola, 2017). The process involving local neural activity and changes in vessel tone (and so in local cerebral blood flow), is known as neurovascular coupling (NVC – **Figure 1.2**); this spatial and temporal coupling is the basis of fMRI. NVC is supported by the neurovascular unit that implicates interaction of neuronal, glia and vascular cells. Neurons can communicate directly

to blood vessels (Attwell & Iadecola, 2002) or to astrocytes in order to release vasoactive agents (Petzold & Murthy, 2011).

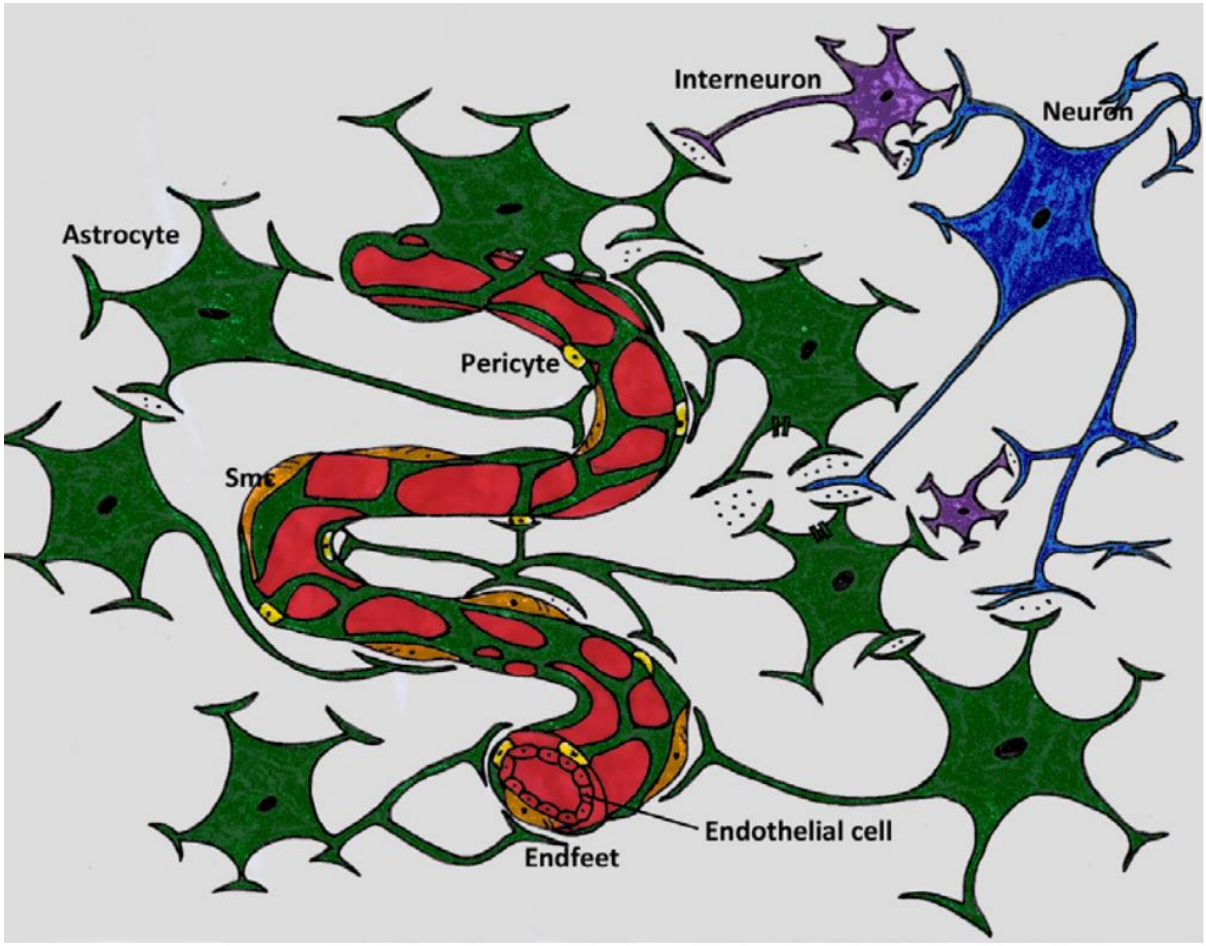

Figure 1.2. Neurovascular Unit*. Figure taken from Muoio et. al (Muoio, Persson, & Sendeski, 2014) showing the component of the neurovascular unit (NVU). Neurons (blue) establishes synapses with interneurons (purple) and with astrocytes (green). The point of contact between astrocytes and the vasculature is the end-feet, which can be in touch directly with endothelial cells (red), pericytes (yellow) or myocytes (orange).*

1.1.2 CEREBRAL ENERGY METABOLISM

Neural activity is a highly energy demanding process where most of the resources are allocated to restore ionic gradients to their baseline, after they change due to action potentials (Buxton, 2013). Brain energy metabolism and the flow of energy-yielding substrates via the cerebral blood flow are very closely related to brain activity and functions. Neurons need a source of free energy in the form of Adenosine Triphosphate (ATP), a molecule that can store and transport chemical energy. Cellular activity increases ATP demand, metabolic fluxes, ATP production and the rate of blood flow is augmented in order to activate the tissue.

The brain is not able to store energy, and given its high metabolic demand a constant adequate supply of energy, in the term of oxygen and glucose, is required (Clarke & Sokoloff, 1999).

Glucose is the main energy substrate for the brain and nearly all the glucose is oxidized during resting, but when the brain is activated glucose utilization usually increase more than oxygen consumption (Mckenna, Dienel, Sonnewald, Waagepetersen, & Schousboe, 2012). When glucose is available, it is converted to usable energy, first by glycolysis where it is converted to pyruvate (part of the pyruvate may be stored as lactate and transported back and forth between neurons and astrocytes in response to energetic request) and then from pyruvate to carbon dioxide (CO_2) (Krebs cycle); ATP is produced at both stages, but during the Krebs cycle is slower and oxygen consumption is required. The general energy use by human brain is approximately around 21 μmol ATP/g/min. Local metabolic rates in grey matter are considerably higher and more variable than in white matter.

The close coupling between local neuronal energy metabolism and functional brain activity means that neuroimaging techniques can detect signals that are directly related to energy delivery and use (Logothetis, Pauls, Augath, Trinath, & Oeltermann, 2001). It is worth noting that environmental changes can lead to an adaptive response in brain cells, such as

strengthening of existing synapses, the formation of new synapses and the production of new neurons from stem cells; at the molecular level, the consequence is a new regulation of brain energy metabolism (Camandola & Mattson, 2017).

In this thesis oxygen metabolism is used as a marker of energy consumption, but some energy could be also available for non-oxidative processes, meaning that we may not have the full pictures in term of energy (or specifically, in number of ATP molecules).

1.1.3 PRINCIPLES OF MAGNETIC RESONANCE IMAGING

Atomic nuclei act like tiny bar magnets (they possess a magnetic moment related to their property of quantum spin) and as such they interact with external magnetic fields, allowing us to measure and manipulate their magnetic state. The hydrogen nuclei within the water and fat molecules or the body are usually the main target of MRI. In the absence of an external magnetic field, they can be considered to point randomly in different directions. Application of a strong magnetic field can create some partial alignment, indicated schematically in **Figure 1.3**. The strong magnetic field is known as B_0 and the strength of the magnetic field is reported in units of tesla - T. The sum of the magnetic vectors of the atomic nuclei is known as the macroscopic net magnetization and it is this that we measure during MRI.

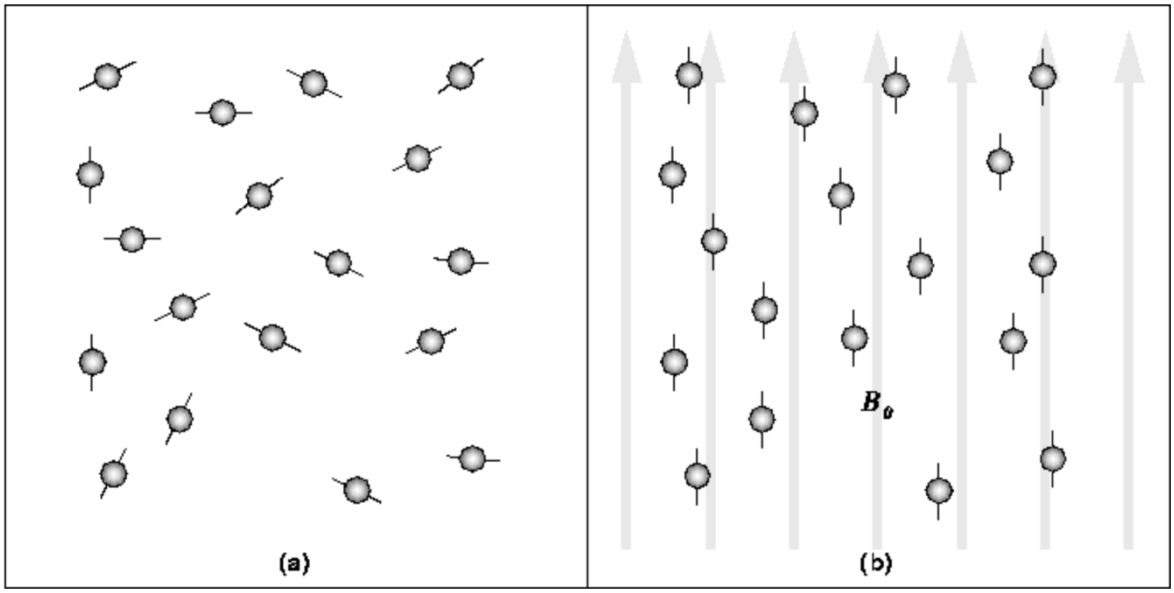

Figure 1.3. Hydrogen Nuclei. *(A) In the absence of a strong magnetic field, hydrogen nuclei are randomly pointing to different directions. (B) When a strong magnetic field (B_0) is applied, the hydrogen nuclei point to the same direction.*

At equilibrium, the net magnetization is aligned with B_0; but, in this strong magnetic field, if perturbed from equilibrium, it will precess or rotate around the axis of the B_0 field, at a frequency proportional to the strength of the magnetic field as ruled by the Larmor equation (**Equation 1.1**).

$$\omega = \gamma B_0$$

Equation 1.1. Larmor equation. *ω is the precessional frequency, γ is the gyromagnetic ratio and B_0 is the magnetic field.*

Specifically, the frequency of precession for a hydrogen nucleus is 42.58 MHz times the main B_0 field strength in tesla, also known as the resonant frequency: the frequency at which the ensemble of nuclear 'magnets' absorbs and emits radiofrequency energy. The Larmor relation, that embodies the property of resonance, is exploited by using an additional magnetic field (B_1 field) at that frequency in order to move the magnetization away from the longitudinal axes and to generate an MR image. In this process, the hydrogen nuclei experience the static B_0 field plus the B_1 field, consequently the magnetization will rotate away from the axis of B_0. After the application of the B_1 field we can then measure the precessing magnetization of the hydrogen nuclei from the voltage that they induce in a system of receiver coils. The net magnetization will be subsequently realigned with B_0 as it returns to an equilibrium state. This process is called relaxation. The component of the net magnetization detected by a receiver coil is perpendicular to B_0. The measured signal decays relatively rapidly as described by the T_2 time constant (typically milliseconds to hundreds of milliseconds in biological tissues). A tissue with a long T_2 time constant will continue to produce a signal for longer than one with a short T_2. The amount of T_2 relaxation obtained can be manipulated with the choice of the RF pulse timing parameters. The echo time (TE) is the time between the RF pulse and the peak of the signal in the receiver-coil and it can be manipulated in order to generate a contrast between different tissues with different characteristic T_2 time constants. Different tissues types vary in the amount of interaction between hydrogen nuclei. Therefore, they take a distinctive and different amount of time to lose their transverse magnetisation, after the RF pulse has been turned off. This offers a mechanism for creating image contrast between tissue types.

There are two forms of T_2 relaxation: the true T_2 and the time constant that we observe (T_2*) in many pulse sequences based on 'gradient-echo' (GE). T_2' constant is the difference between these two ($1/T_2^* = 1/T_2 + 1/T_2'$). Its relaxation effect is a static effect that can be compensated

for using a spin echo (SE) to eliminate dephasing effects and obtain a pure T_2 weighted image, by using a refocussing RF pulse with flip angle of 180˚.

The true T_2 relaxation time is a spin-spin relaxation due to magnetic field of nearby nuclei interacting. The rate of decay is an exponential process, and it causes irreversible dephasing of the transverse magnetisation. T_2* relaxation can also cause dephasing, but this is because of magnetic field inhomogeneities occurring due to magnetic susceptibility differences of different tissues present in the sample or image voxel.

T_1 relaxation is the recovery of the net magnetisation component aligned with the B_0 field, which is slower than T_2 decay. After an excitation, it is possible to excite again when the net magnetization is recovered at least partially along the axis parallel to the B_0 field (**Figure 1.4**).

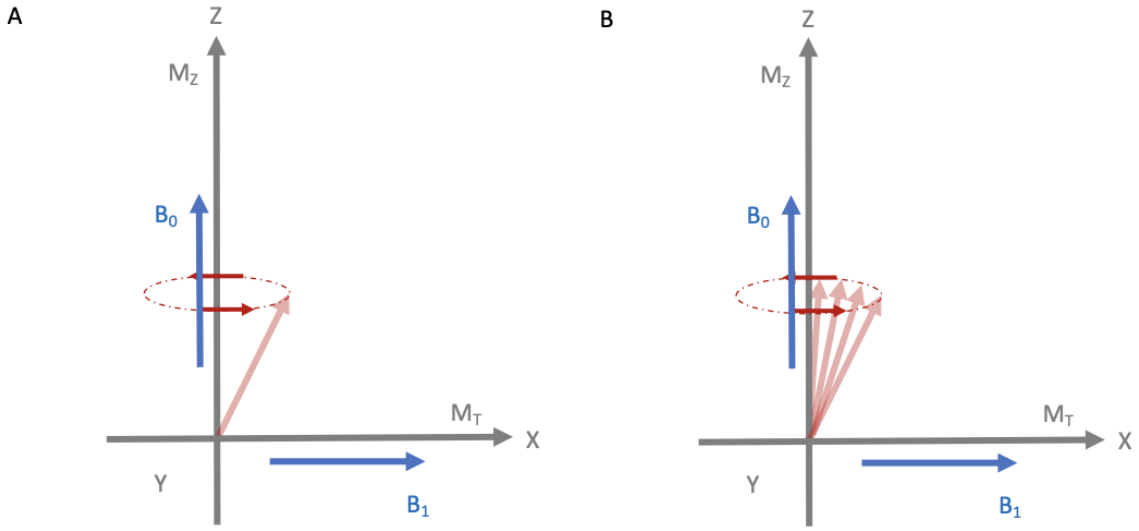

***Figure 1.4. Net magnetization**. (A) Hydrogen nuclei precess around the direction of the magnetic field (B_0) at a fixed angle when placed in a strong field. (B) The orientation of the net magnetization is changed by the excitation, moving it away from B_0 field axis. Mz=longitudinal magnetization. Mt=transverse magnetization.*

The time between successive excitations is called the repetition time (TR). The recovery of the longitudinal magnetization is due to nuclei giving up energy to their surrounding environment (known as the spin lattice): the total nuclear magnetic moment vector which is parallel to the constant magnetic field relaxes and goes from a non-equilibrium state to thermodynamic equilibrium with its lattice. The process occurs with the characteristic time dependent on tissue composition, the spin-lattice relaxation time. The magnetization recovers exponentially over time, and T_1 characterizes the rate at which the longitudinal magnetization recovers exponentially towards the thermodynamic equilibrium. T_1 relaxation time is the time required for the longitudinal magnetization to reach 63% of its maximum (equilibrium) value (**Figure 1.5**).

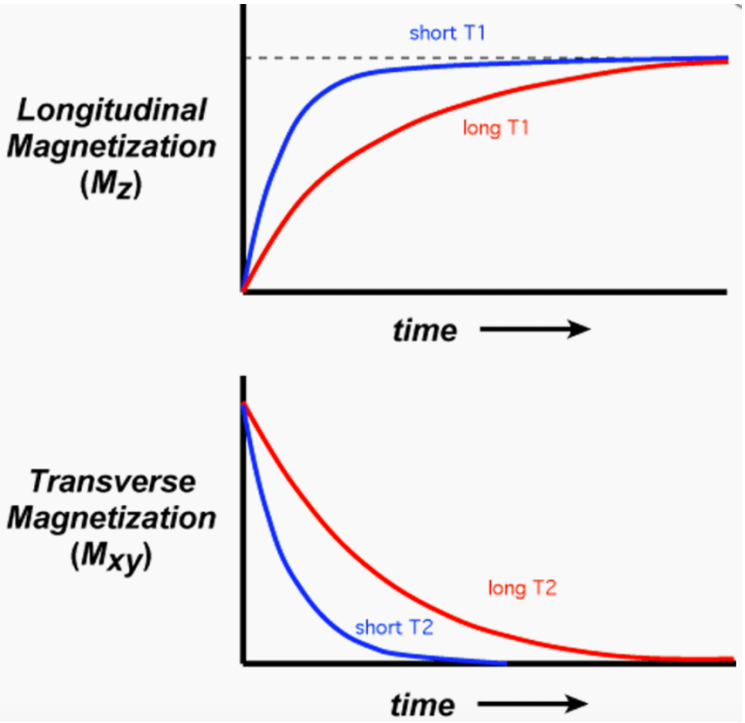

Figure 1.5. Longitudinal and Transverse Magnetization. *T1 reflects the length of time it takes for regrowth of M_z back toward its initial maximum value. T2 reflects the length of time it takes for the MR signal to decay in the transverse plane.*

Taken together, magnetization in the longitudinal plane increases (‘recovery’), while the magnetisation in the transverse plane decreases (‘decay’). The MR receiver coil detects these changes in the signal; this process is known as free induction decay (FID) and it can be observed immediately after RF excitation is complete.

A gradient recalled echo (GRE) or gradient echo (GE) for short is a manipulation of the FID signal that begins by applying an external dephasing gradient field across the tissue. This gradient causes a calibrated change in local magnetic fields and then alters the resonance frequencies across the tissue resulting in accelerated dephasing of the FID. These types of sequences are sensitive to both T_2 relaxation and dephasing effects, so they produce T_2* weighted images (where T_2* is always shorter than T_2).

RF pulses and gradients can encode the information about the spatial distribution of the transverse magnetization into the frequency and phase of the signal. The gradient coil manipulates the static magnetic field, which induce a spatial variation in Larmor frequency, and imaging is feasible because the local precession frequency is proportional to the local magnetic field. The manipulation of the magnetic field is done by slice selection, frequency encoding and phase encoding.

The slice selection is determined by its position and geometry of the field of view. Gradient coil generates a linear gradient in B_0 in order to select the slice. Therefore, each slice has a different Larmor equation based on its location in the field and the selection is successful if the B_1 magnetic field is oscillating with frequency equal to hydrogen spins in the slice of interest.

In order to encode the distribution of the transverse magnetization in the x and y plane, two additional coils are used. The first one is a spatial gradient along the x direction which encodes the frequency encoding in the x plane and the information on the position of the transverse magnetization is acquired. A second one is for encoding the spatial information in the phase of

the signal detected in the y plane, where different components of the transverse magnetization will have diverse phase depending on their position along the y axis, but not of their precession frequency. In order to get the final MR image, we need to transform the signal from the time domain, where numbers are stored in an array called k-space, to the frequency domain, through the Fourier transformation. There are several ways to sample k-space data, here we consider the Cartesian read-out, where data are acquired line-by-line. Moreover, in echo planar imaging readout (EPI) all the lines are acquired after one or a small number of excitations (single shot and multi-shot EPI respectively), therefore an entire 2D plane is collected following a single RF-excitation pulse. To do so, the gradients are rapidly switching in order to scan k-space.

1.1.4 MAIN MRI MODALITIES

A wide variety of images can be acquired on an MRI scanner and different type of images capture different information about the brain according to the image contrast delivered by the pulse sequence. The three modalities that are the most commonly used in this thesis are: structural, diffusion and functional imaging.

Structural Imaging

CSF and blood tend to have long T_1 and T_2 times due to the unobstructed movement of their water molecules. On the other hand, solid tissues like grey and white matter, tend to have shorter relaxation times than biological fluids, as the water molecules interact with macromolecules. Brain morphological characteristics are then obtainable because of the differences in relaxation rates that produces an adequate signal contrast.

Structural imaging can provide information about the anatomical structure in the brain, as well as focal differences in brain anatomy, such as inflammatory lesions in the context of multiple sclerosis (MS), by showing the boundaries between tissues types.

Diffusion Imaging

Diffusion weighted imaging (DWI) relies on the detection of the random microscopic motion of free water molecules known as Brownian movement to provide information about microstructure and anatomical connectivity within the brain.

The most common method used for diffusion weighted imaging is to incorporate two symmetric motion-probing gradient pulses into a single-shot spin echo T2-weighted sequence, one on either side of the 180˚ refocussing pulse. During the first part of the spin echo a gradient is applied in order to cause the hydrogen nuclei in different locations to have a higher or lower frequency. Then water molecules move around experiencing different fields, and their magnetization falls out of synchronization, as each one is moving differently. This effect is like an additional T_2 decay, and so the spin echo is able to recover less signal from hydrogen nuclei that have been moving around than from those staying near or in the same location. Therefore, DWI provides a measure of the averaged distance travelled by water.

The sensitivity of diffusion-weighted imaging to diffusion can be augmented by increasing the amplitude, duration, and temporal spacing of the two motion-probing gradients. These gradient properties determine the b value (expressed in seconds per square millimetre), an index of the degree of diffusion weighting. Therefore, the strength of the influence of the diffusion weighting can be varied by adjusting the timing of the spin echo or increasing the strength of the gradient field that is applied. The effect depends on the chosen direction and it is only sensitive to movement along that direction. It is possible to use a combination of different direction and different b-values to get more detailed information about the movement of water

within the voxels in the image and this is the basis of diffusion tensor imaging and diffusion tractography that yield information about the microstructural anisotropy of brain tissue.

Functional Imaging

Functional Magnetic Resonance Imaging (fMRI) normally uses fast imaging methods, such as gradient-echo echo planar imaging, to acquire functional information on blood oxygenation changes linked to local blood flow changes either in response to specific stimuli or in relation to spontaneous brain activity (Ogawa, Lee, Kay, & Tank, 1990). Blood oxygenation level dependent (BOLD) imaging has been widely employed to map brain function.

Brain changes in metabolic demand are reflected in changes in localised blood volume, blood flow and oxygen extraction, which affect the local B_0 field due to the magnetic properties of deoxygenated blood. BOLD signal relies on the de-oxyhaemoglobin having a different magnetic susceptibility compared to oxyhaemoglobin (**Figure 1.6**).

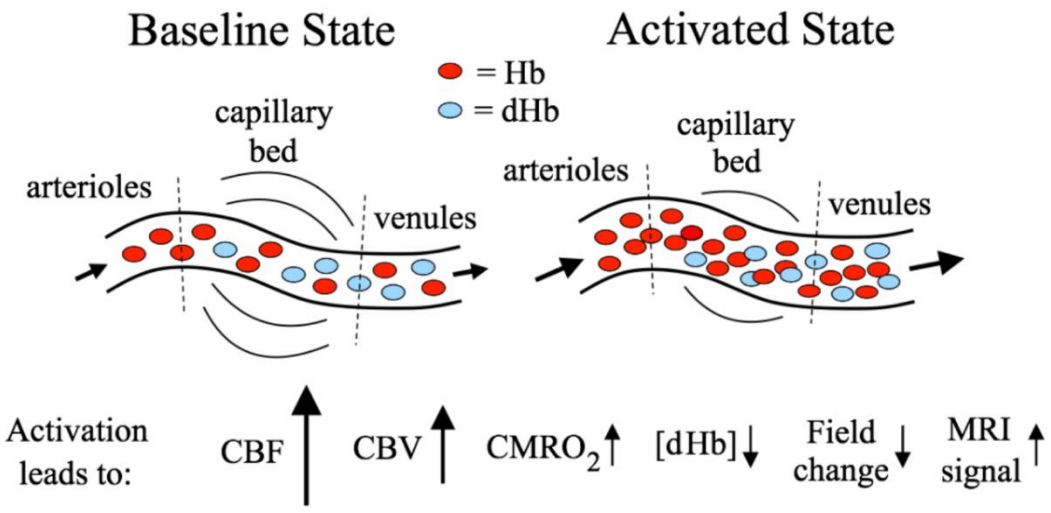

Figure 1.6. BOLD effect. *Figure adapted from (https://www.fmrib.ox.ac.uk/primers/appendices/mri_physics.pdf) showing the BOLD effect. An increase in local neuronal activation is accompanied by large increases in CBF, CBV, modest changes in $CMRO_2$. Therefore, an overall increase in the amount of Hb compared to dHb is observed.*

BOLD is a T_2* dependent contrast that relies on the different magnetic properties of oxygenated and deoxygenated haemoglobin within the blood. Oxyhaemoglobin is diamagnetic: it has analogous magnetic properties to the surrounding tissue. De-oxyhaemoglobin is paramagnetic: it distorts the surrounding magnetic field causing shorter T_2 and T_2* relaxation times, hence the MR signal decays faster. When neural activity increases, the amount of de-oxyhaemoglobin decreases in the imaged voxel leading to longer T_2 and T_2* relaxation times, and increased signal measured with a T_2- or T_2*- weighted sequence. Therefore, by acquiring images that have T_2* weighting, it is possible to detect changes associated with changes in blood oxygenation and thus map neuronal activity. Consequently, spin-echo sequences are generally not used as the spin-echo removes most of the T_2' component, leaving the image only sensitive to T_2 relaxation. Gradient-echo, that is sensitive to T2*, has become the common standard in fMRI.

Perfusion MRI

The BOLD response provides qualitative information about changes in neural activity, commonly revealing the difference between a stimulus and a rest condition. Quantification of the BOLD response is difficult because the BOLD imaging is not directly sensitive to the brain metabolic activity, but rather to the amount of deoxygenated haemoglobin in the capillaries

and venules of the brain tissue. BOLD response reflects changes in cerebral blood volume (CBV), cerebral blood flow (CBF) and cerebral metabolic rate of oxygen ($CMRO_2$); increases in CBV and $CMRO_2$ cause a decrease in the BOLD signal, whereas an increase in CBF causes an increase in the BOLD signal. It is worth noting that the BOLD response is also dependent on the physiological state of the tissue, determined by blood haematocrit, resting oxygen extraction fraction (OEF) and resting CBV. Given the qualitative nature of the BOLD response, comparing populations with different baseline states may not be a valid reflection of differences in neural activity. Advanced MRI techniques that aim to quantify individual physiological variables, with physical units, are desirable in order to better understand the physiological meaning of the changes underlying the BOLD signal.

Arterial spin labelling for CBF measurement

Arterial spin labelling (ASL) exploits the ability of MRI to magnetically label arterial blood below the imaging slab using the inversion of the hydrogen nuclei that are in water within blood, whilst the blood is in the arteries of the neck. Therefore, the tracer is a magnetic label applied to water molecules of flowing blood. Usually, the magnetic label is produced by inverting the longitudinal component of the MR signal. The main goal is to obtain a labelled image and a control (unlabelled blood) image, in which the static tissue signals are identical but the magnetisation of the inflowing blood is different, the difference between the two images then representing the local perfusion or blood flow.

The labelled blood travels into the brain where it replaces non-labelled blood and it alters the local tissue's longitudinal magnetization once blood water has transferred into the tissue. The tagged (or labelled) blood flows into the imaging slices and relaxing all the time towards equilibrium; after a delay (called TI – inversion time) an image is acquired, known as tag image. In order to remove the contribution of the static tissue to the tag image, a control image of the

same slice is acquired in which inflowing blood is not tagged. The process creates then two different images: with and without the labelling; shown by a reduced T_1-weighted signal in the tag image compared to the control image where blood is fully relaxed.

The two images can be subtracted ($\Delta M = M_{control} - M_{tag}$) to show the quantity of labelled blood-water that has reached the brain; considering that ΔM depends on the delivery of magnetization by venous outflow and longitudinal relaxation. The perfusion weighted image represents the amount of arterial blood delivered to voxels in the slices of interests within the TI, also called the post-labelling delay (PLD) time. The parameter derived is CBF. CBF is then a measure of the volume of blood passing through a point in the brain circulation per unit time and cerebral perfusion is the delivery of the blood to the capillary bed. The standard unit for CBF measurement is *millilitres of blood/100g of tissue/minute*; with a typical value in human grey matter (GM) of *60mL/100g/minute* (Buxton et al., 1998; Liu & Brown, 2007).

There are two main classes of ASL methods that vary according to the dependence of the magnetic labelling process on the location and velocity of the flowing blood (**Figure 1.7**).

Pulsed ASL (PASL). The tagging is based on the location. Short RF pulses (5-20ms) are used to saturate or invert a slab of spins, known as the tagging region, which is proximal to the imaging slice of interest, so that all spins are excited instantaneously. The advantages are high inversion efficiency and little RF power use. The technique has also some disadvantages like the dependency on the coverage and uniformity of the transmit RF field to determine the geometry of applied tag and less perfusion weighted signal compared to continuous ASL sequence.

Continuous ASL (CASL). The tagging is based on location and velocity and spins are continuously labelled as they flow through a narrow tagging band. More specifically, long RF pulses (1-3s) are used in conjunction with a constant gradient field to expose a narrow plane of

spins to RF energy. Although CASL provides higher perfusion contrast than other types of labelling, it has two main disadvantages: the considerable magnetization transfer effects and high level of the energy deposited in the tissue. To overcome this issue and to facilitate practical implementation, *pseudo-continuous ASL (PCASL)* has been implemented (Dai, Garcia, Bazelaire, & Alsop, 2008). It involves multiple short RF pulses in place of the single long pulse, making the label duration longer than in PASL.

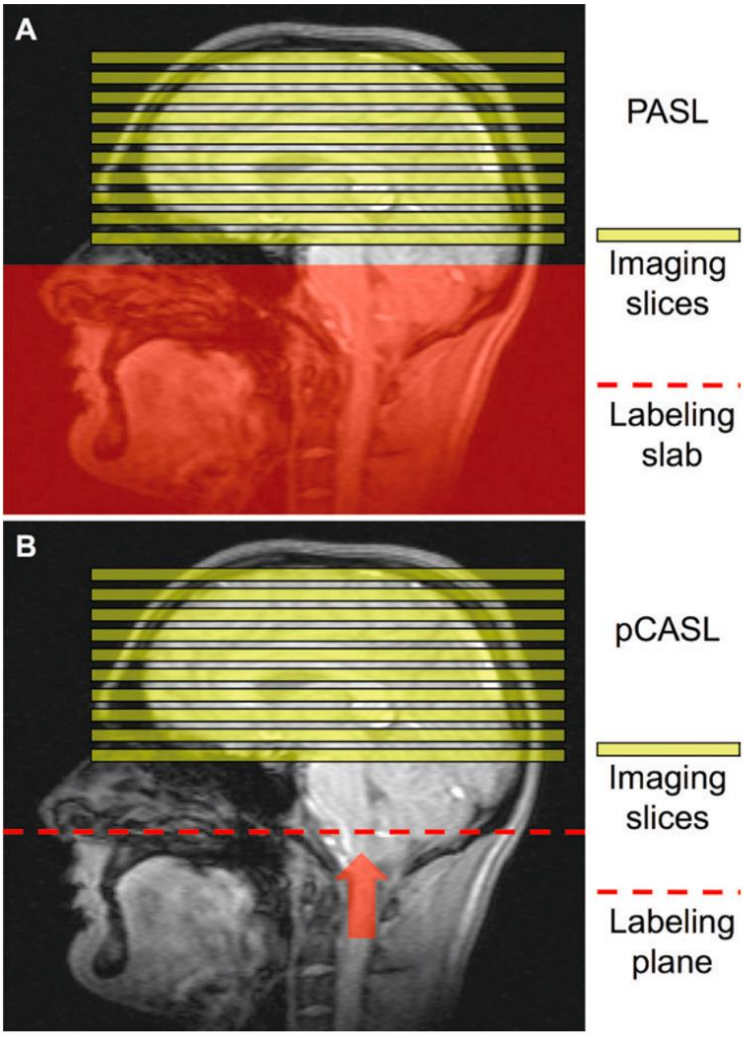

Figure 1.7. ASL labelling scheme*. Figure taken from Haller et. al (Haller et al., 2016) showing ASL labelling schemes.*

(A) PASL sequence. An inversion slab is place proximal to the imaging volume to label blood in the arterial feeding vessels supplying the brain. The pulse is short and all the blood is inverted simultaneously.

(B) PCASL sequence. The inflowing arterial blood is continuously inverted as it flows through the labelling plane. The pulse train is typically applied for a period of approximately 1-2 seconds.

Quantitative fMRI

As explained before, the relative changes in CBF and $CMRO_2$ alone do not determine the amplitude of the BOLD response, but it is also determined by the individual baseline physiological state. This baseline is determined by the total amount of de-oxyhaemoglobin present in the voxel, which is a function of haematocrit (Hct), baseline OEF and baseline CBV (**Figure 1.8**). To interpret the BOLD signal in a quantitative manner we need to calibrate the BOLD signal, aiming to measure the baseline condition through a calibration experiment.

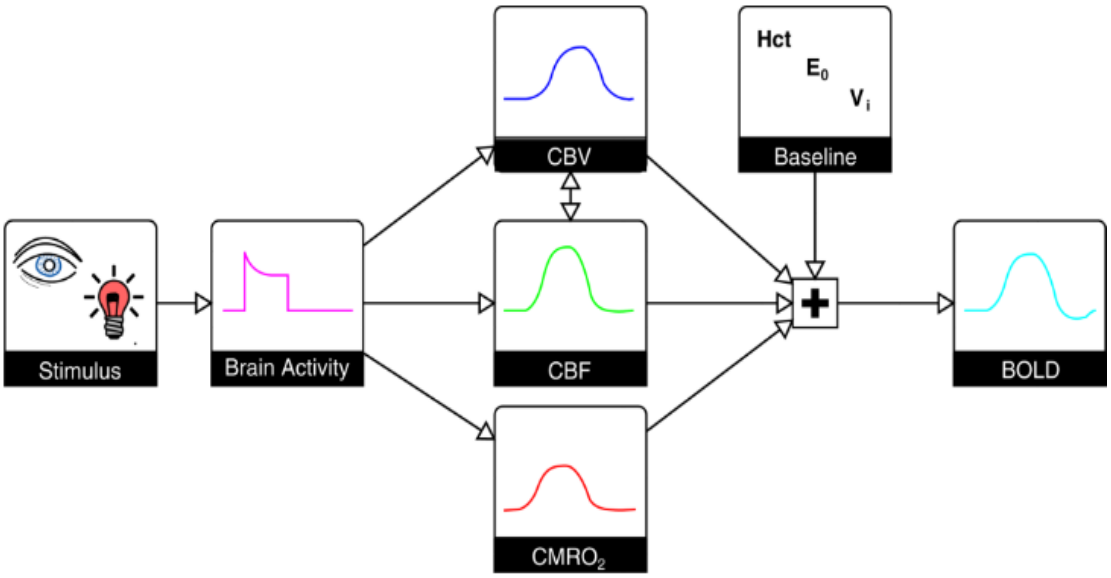

Figure 1.8. BOLD components. *Figure taken from Blockley et al. (Blockley, Griffeth, Simon, & Buxton, 2013) showing how the BOLD response is a complex signal.*

A fundamental component of the calibrated BOLD method is a model describing how the BOLD signal depends on the underlying physiological changes. Davis et al. (Davis, Kwong, Weisskoff, & Rosen, 1998) described a new method in which changes in BOLD signal and CBF during hypercapnia could be used to calibrate the BOLD signal, resulting in a quantitative

estimate of oxygen consumption relative change from subsequent BOLD and CBF measurements acquired during tasks execution.

The rationale behind the calibrated MRI is very similar to the one behind the ASL: if ASL aims to isolate the pure flow component to get the specific physiological parameter of blood flow, calibrated MRI tries to isolate the signal component dependent on [dHb] at rest.

This parameter was initially called M (Davis et al., 1998), and empirically it indicates the maximum possible increase in BOLD signal from a specific baseline (see chapter 4 – methods section for detailed explanations). M is usually expressed as hypothetical percent signal change relative to the resting T2*-weighted MRI signal, therefore the value is accurate only for specific echo-time, field strength, and macrovascular weighting applicable for that particular measurement. The same conditions need to be also applied during measurement of task response in order to compute valid $CMRO_2$ changes using that M.

Hypercapnic calibration is the technique most used to provide the calibration factor M. The method consists of a small increase of the inspired level of CO_2. This induces hypercapnia in the subject causing an increase CBF, which reduces [dHb] and increases CBV to maintain optimal gas concentrations, as blood flow is sensitive to changes in arterial CO_2. Mild hypercapnia is not thought to affect resting $CMRO_2$ and so this stimulus is considered isometabolic.

An alternative calibration method was also proposed that replaces carbon dioxide with air enriched with oxygen (Chiarelli, Bulte, Wise, Gallichan, & Jezzard, 2007). Rather than modulate [dHb] indirectly by increasing flow, hyperoxia affects the venous blood oxygenated directly. During hyperoxia, venous haemoglobin saturation increases as the additional oxygen carried in the plasma results in less desaturation due to resting metabolic oxygen consumption. It is worth noting that hyperoxia can also cause vasoconstriction and hence a reduction in flow, so that CBF measurements also are required to estimate M. The change in deoxyhaemoglobin

concentration need to take into accounts the arterial PO_2 (PaO_2), that is inferred from measurements of end-tidal PO_2 in mmHg, and it is affected on arterial saturation, SaO_2; which is needed to calculate the oxygen content of arterial blood during hyperoxia (CaO_2).

The interpretation of relative changes in $CMRO_2$ could be problematic when the $CMRO_2$ baseline may be altered by disease or drug action (Iannetti & Wise, 2007). Therefore, in recent years methods have been developed to measure absolute $CMRO_2$. Dual calibrated fMRI involves the use of both hypercapnia and hyperoxia challenges to induce CBF and BOLD signal changes in order to estimate venous deoxyhaemoglobin concentration and thus OEF and absolute $CMRO_2$ (Bulte et al., 2012; C. J. Gauthier & Hoge, 2012; Wise, Harris, Stone, & Murphy, 2013).

1.2 INTRODUCTION TO NEUROPLASTICITY IN HEALTHY AND DISEASED BRAIN

1.2.1 NEUROPLASTICITY

Numerous studies in primate and non-primate animals agree on the notion that experience, learning of a new skill and damage to the nervous system can all cause reorganization of the brain. The reorganization mechanisms are broadly termed 'plasticity' and the brain's lifelong capacity to alter its structure and function is seen as a mechanism for healthy development to ensure adjusted functioning of neural networks and to maintain homeostasis in changing surroundings (Butz, Wörgötter, & Ooyen, 2009; Nagy & Turecki, 2012).

Neuroplasticity can occur at different levels of neural function and time scales (Le Bihan, 2003, 2012). Mechanisms involved in neuroplasticity at the neuronal level include long-term potentiation (LTP) and long-term depression (LTD) (Rioult-Pedotti, Friedman, & Donoghue, 2000), synaptogenesis (Xu et al., 2009), neurogenesis (Gould, Beylin, Tanapat, Reeves, & Shors, 1999), changes in neuronal morphology (Lerch et al., 2011; Tronel, Fabre, Charrier, Oliet, & Gage, 2010) and long-lasting new neuronal connections, such as those carried by dendritic trees (Holtmaat & Svoboda, 2009). Non-neuronal tissue components have also a main role in neuroplasticity, like astrocytes, microglia (Kettenmann, Kirchhoff, & Verkhratsky, 2013), oligodendrocytes and myelin (Fields, 2010; Gibson et al., 2014; Haroutunian et al., 2014), angiogenesis (Black, Zelazny, & Greenough, 1991; Kerr, Steuer, Pochtarev, & Swain, 2010), changes in glial cell density and morphology (Dong & Greenough, 2004). Taken together, long-term plasticity of the central nervous system is triggered by changes in the environment which lead to activation of numerous intracellular signalling cascades. Then they are integrated to achieve the appropriate neuronal response. Therefore, neuroplasticity relies

on a molecular machinery that transduces molecular changes into long lasting structural and functional modifications at the cellular and brain systems level.

1.2.2 MRI TO INVESTIGATE NEUROPLASTICITY

In vivo MRI enables non-invasive investigation of the entire brain with the possibility of probing functional, structural (macro and micro anatomy levels), metabolic and vascular events in the living brain. Therefore, MRI techniques have been widely used to assess humans brain plasticity *in vivo*.

Structural MRI has been used to show the ability of the adult brain to undergo structural modifications following periods of training (Draganski & May, 2008; May, 2011; Tardif et al., 2016b). Early cross-sectional experiments have used voxel-based morphometry methods (VBM) to demonstrate differences in people with specific expertise such as larger hippocampal volume in expert taxi drivers (Maguire et al., 2000) or increased white matter and volume in Broca's area of the left inferior frontal gyrus in expert orchestra musicians (Sluming et al., 2002). The same method was also applied longitudinally to study learning related changes in grey matter (Draganski et al., 2004, 2006). White matter changes have been also investigated using diffusion weighted imaging (DWI) in both cross-sectional and longitudinal studies (Johansen-Berg, Della-Maggiore, Behrens, Smith, & Paus, 2007; Taubert et al., 2010) and changes in white matter associated with learning have been demonstrated (Bengtsson et al., 2005; Blumenfeld-katzir, Pasternak, Dagan, & Assaf, 2011; Scholz, Klein, Behrens, & Johansen-Berg, 2009; Thiebaut De Schotten et al., 2014). Furthermore, studies have found that brain rewiring can occur between anatomical distant areas and the rewiring could be used as a marker of brain damage and reorganization (Johansen-Berg, 2007). All together, these studies

show the dynamic properties of the grey and white matter tissue (Assaf, Johansen-Berg, & Thiebaut de Schotten, 2019).

Numerous studies have used BOLD signal to show anatomical location of activation changes during the task, their correlation with behavioural changes (Doyon & Benali, 2005) and network-level changes following specific training (Albouy et al., 2012; Mackey, Miller Singley, & Bunge, 2013; Steele & Penhune, 2010). Motor learning has been particularly studied in the context of neuroplasticity. Specifically, different stages of learning have been demonstrated (Karni et al., 1995; Kleim et al., 2004; Korman, Raz, Flash, & Karni, 2003), as well as the distinctive networks recruited during the phases of motor learning (Floyer-Lea & Matthews, 2005). Motor cortex reorganization after injuries has also been investigated; specifically, Ward et al. demonstrated a relationship between recovery and task-related activation (Ward, Brown, Thompson, & Frackowiak, 2003).

fMRI has also been employed to study changes in resting state networks. Particularly, the changes in resting state have been investigated after training (Albert, Robertson, Miall, & Hall, 2009) and they have been related to changes in task performance (Xiong et al., 2009). Furthermore, the relationship between learning and changes in functional connectivity has also been demonstrated (L. Ma, Narayana, Robin, Fox, & Xiong, 2011).

Despite BOLD signal having been used in numerous studies to investigate brain functional changes, it is worth noting that the interpretation of BOLD is not straightforward, given the co-existence of many physiological ambiguities (Buxton, 2010); moreover, BOLD signal represents a relative change from an unknown baseline. Although advanced neuroimaging techniques to investigate quantitatively functional activation in the brain exist, they have only been used in a few neuroplasticity studies so far.

Early studies have used blood flow to investigate changes in brain functional activity, their anatomical localization during motor learning task execution (Grafton, Hazeltine, & Ivry, 1995a; Seitz & Roland, 1992) and to demonstrate that different sets of cortical regions are dynamically employed in implicit and explicit motor sequence learning (Honda et al., 1998). Later studies have found a coupling between CBF and $CMRO_2$ increases during motor task execution in the contralateral primary motor cortex, as well as in other regions involved in motion activity (Vafaee & Gjedde, 2004).

Metabolic measures have also been used to investigate adaptation and changes in signals; Fernandez-Seara et al. (Fernández-Seara, Aznárez-Sanado, Mengual, Loayza, & Pastor, 2009) is one of the first studies showing the association between CBF changes and explicit learning task. Xiong et el. (Xiong et al., 2009) have found an association between an altered resting metabolic activity and changes observed during task performance. A recent PET-fMRI study has monitored the metabolic and connectivity changes during a visuomotor task and researchers found the occurrence of aerobic glycolysis, a particular metabolic pathway of glucose, in conditions of high synaptic plasticity and remodelling (Shannon et al., 2016).

1.2.3 NEUROPLASTICITY IN DISEASED BRAIN

Neurodegenerative disorders and brain injuries can affect the mechanisms that allow the nervous system to be shaped by the experience. Studies have reported changes in the expression of genes, proteins and generation of new neurons and blood vessels, and increase of synaptic connections after brain injuries (Albensi, 2001; Li & Chopp, 1999). Researchers have demonstrated the ability of brain to rewire and remodel after stroke and trauma (Brown, 2006). Neuroplasticity is seen as the expression of cellular responsiveness and may be considered as the capability of the brain to adapt its function to different demands. Furthermore, preserved

neuroplasticity mechanisms have been exploited in animal studies to enhance treatment and recovery through changes in neurogenesis (Chen et al., 2009), angiogenesis (L. Wang, Zhang, Wang, Zhang, & Chopp, 2004), synaptogenesis (Chen et al., 2003) and structural changes in the brain (Li et al., 2005). Humans studies of brain damage have shown reorganization of brain functions at different systematic levels reflecting molecular, synaptic and cellular events (Cramer, 2008; Nudo, 2006) that support functional recovery after the damage (Cramer, 2008).

Neuroplasticity in multiple sclerosis

Multiple sclerosis (MS) is a chronic inflammatory disease of the central nervous system leading to demyelination, neurodegeneration and axonal loss; but the clinical course is highly variable across individuals.

The acute inflammation can impair different domains, such as motor, visual and cognitive functions. Different mediators released during the inflammation can affect the neural functions, like LTP/LTD expression (Di Filippo et al., 2013; Mori et al., 2014), and therefore influence the course of the development of the functional impairments in the disease (Stampanoni et al., 2017). Altered connectivity has also been observed in the early phase of the disease and it has been linked with cognitive and clinical deficits (Bullmore & Sporns, 2009; Faivre et al., 2012; Hawellek, Hipp, Lewis, Corbetta, & Engel, 2011; Liu et al., 2017; Roosendaal et al., 2010; Shu et al., 2016). Furthermore, reduced structural and functional connectivity has been linked to white matter lesion load and cortical atrophy (Cruz-gómez, Ventura-campos, Belenguer, Ávila, & Forn, 2014; Rocca et al., 2018; Rocca, Valsasina, Martinelli, Misci, & Falini, 2012; Zhou et al., 2014), confirming the hypothesis that inflammation may alter brain activity and reorganization (Di Pasquale et al., 2016; Hannestad et al., 2012). Studies have shown that the ability to undergo neuroplasticity at the systems level are preserved in patients with MS, despite the inflammation (Tomassini, Johansen-Berg, et al., 2012). Among the first studies

investigating functional reorganization in MS, Morgen et al. (Morgen et al., 2004) showed that additional neural resources are needed for MS patients to perform a task and although the ability to perform a motor task is preserved, patients show a different neural adaptation compared to controls. The authors hypothesized that more prolonged training may show a similar trend to the one observed in controls. Later studies have demonstrated that short-term learning during a serial reaction time task (SRT) is preserved in patients with MS, however other learning circuits could be impaired, like implicit motor learning (Tacchino et al., 2014). In contrast, Deroost et al. (Deroost, Smetcoren, Vandenbossche, Hooghe, & Kerckhofs, 2014) found that explicit learning was more impaired than implicit learning in patients with MS. The sample used in the latter study reported more severe EDSS compared to the former; suggesting that the learning component might be affected by disease severity. Lastly, Tomassini et al. (Tomassini et al., 2016) showed that MS inflammation alters short-term plasticity given that greater adaptation effects were observed in patients compared to healthy controls.

In MS it has been shown that brain plasticity has a main role in the recovery of functions (Bosnell et al., 2011; Nudo, 2003); specifically, studies reported that changes in activation patterns occur in parallel to recovery of motor function (Mezzapesa, Rocca, Rodegher, Comi, & Filippi, 2008; Reddy et al., 2000), local remapping of cortical representation (M. Lee et al., 2000), increased activation in cortical areas (Rocca et al., 2009, 2004) and higher activation in the ipsilateral hemisphere (Rocca et al., 2004; Wegner et al., 2008).

Recent studies showed valuable outcomes of motor training on brain structure in patients with MS (Barghi et al., 2018; Bonzano et al., 2014; Ibrahim et al., 2011; Prosperini et al., 2014), suggesting that functional recovery is sustained by remyelination processes leading to repair of damage.

1.2.4 CONCLUSION

Neuroplasticity can be observed on multiple scales, such as adaptive behaviour, learning, brain reorganization and recovery, thanks to molecular interactions with underlying synaptic, cellular and neuronal circuits. In the context of brain disease, advanced neuroimaging techniques would allow a better understanding of the physiology supporting neuroplasticity events leading to the development of targeted interventions to limit the damage of inflammation on brain structure and function.

CHAPTER 2

Deep grey matter structures and their relevance for functional recovery in multiple sclerosis: MRI evidence

ABSTRACT

Damage within deep grey matter structures (DGMS) is a major contributor to disability in multiple sclerosis (MS) and the involvement of DGMS in higher motor control and motivation can explain the clinical impact of DGMS damage in MS. The connectivity of DGMS to cortical regions and their "hubness" in the human connectome make them targets of therapeutic interventions aimed at regaining or adapting lost functions through selective pharmacological modulation or electrophysiological stimulation. Here we aim to improve the understanding of the localised changes occurring in the DGMS as a consequence of MS damage and their impact on performance improvements with training.

29 MS patients and 19 matched volunteers underwent a structural and DWI scan, as well as functional scan in order to identify DGMS involved in SRT execution. For each participant, task-related DGMS were segmented and between-groups differences in shape and volume were assessed. The relationships between DGMS shape and volume and performance improvements during 4 weeks' SRT home training were also investigated, as well as brain-behaviour

relationship group differences. The behaviourally relevant regions were identified with respect to their structural connectivity to the cortex.

Thalamus, caudate and putamen bilaterally were involved in SRT execution. Among these, MS patients showed a reduction in the volume of left thalami and differences in the shape of both thalami suggesting their pathological involvement. The relationship between performance improvements and shape of DGM structures was different between groups. Furthermore, the connectivity-based parcellation of behaviourally-relevant DGMS showed a group difference in quantity and spatial distribution of subcortical-cortical connections. Taken together, they indicate a compensatory mechanism of reorganization of the behaviourally relevant DGMS areas and their cortical connections in order to improve their performance during the training. DGMS circuits can be identified through connectivity-based parcellation and, as such, they may constitute targets for selective pharmacological manipulation or cortical electrophysiological modulation in order to enhance functional recovery.

KEY WORDS

Multiple Sclerosis - Basal Ganglia - Grey Matter - Volume and Shape Analysis - Diffusion Imaging

2.1 INTRODUCTION

Damage within deep grey matter structures (DGMS) is a major contributor to disability in multiple sclerosis (MS) (Trovar-Moll et al., 2009) with symptoms ranging from fatigue to sensorimotor and cognitive dysfunction (Finke et al., 2015; Schoonheim, Brandt, Barkhof, & Geurts, 2015). Both local tissue abnormalities and propagation of remote pathology sub-serve the clinical expression of DGMS damage (Ciccarelli et al., 2001) that can occur from the early stages of the disease (Rojas et al., 2018).

The involvement of DGMS in higher motor control and motivation can help to explain the clinical impact of DGMS damage in MS (Packard, 2001). However, DGMS play also a major role in motor learning, as they contribute to motor responses following encoding of motor sequences and to retrieval of learned sequences of movements (Doyon, Penhune, & Ungerleider, 2003; Lehéricy et al., 2005). The connectivity of DGMS to cortical regions and their "hubness" in the human connectome (Crossley et al., 2014), along with their well-characterised neurotransmitter system (Mcgeer, Staines, & Mcgeer, 1984), make them targets of therapeutic interventions aimed at regaining or adapting lost functions through selective pharmacological modulation or electrophysiological stimulation (Tomassini, Matthews, et al., 2012). However, a targeted modulation of DGMS function that can promote recovery in MS requires an improved understanding of the localised changes occurring in the DGMS as a consequence of MS damage and their impact on performance improvements with training. The aims of the present study are as follows. *Firstly*, we identify nuclei within the DGMS that are functionally relevant for task performance. *Secondly*, we investigate global and localised changes in the volume and shape of these DGMS in MS patients in comparison to healthy controls to characterise structural alterations. *Thirdly*, we relate these measures of tissue integrity to changes in visuomotor performance in the patients in order to identify specific areas

within the DGMS that are relevant for training. *Fourthly*, we localise these behaviourally relevant regions with respect to their structural connectivity to the cortex to find pathways and cortical areas whose function might be manipulated in future pharmacological or electrophysiological interventions.

2.2 METHODS

Participants. We recruited 29 patients with MS (Polman et al., 2011) and the following eligibility criteria: age between 18 and 60, right-handed, retained use of their right upper limb, no relapse or change in pharmacological and non-pharmacological treatment for at least 3 months before study entry, no other neurological or psychiatric conditions. Nineteen age- and sex-matched healthy volunteers acted as controls.

The study was approved by the NHS South-West Ethics (reference: 15/SW/0105) and the Cardiff and Vale University Health Board R&D (reference: 15-CMC-6190) committees. All participants provided written informed consent.

Demographic and clinical characteristics. Participants underwent a baseline assessment, where demographical and clinical measures were collected (**Table 2.1**). In the same session, they also underwent a multi-modal MRI scan. After this session, participants were instructed to perform SRT training programme at home, as described below.

Statistical analysis of demographic, clinical and behavioural data. To investigate between-group differences in age and behavioural measures, we used a two-tailed unpaired t-test. A chi-square test was used to assess sex differences between groups. For all the statistical tests, differences were considered significant at $p \leq 0.05$. Values are reported as mean±standard error (SE), unless stated otherwise. Tests investigating cognitive domains (i.e. SDMT, WLG and PASAT) were corrected for education.

SRT task and home training. We used a serial reaction time (SRT) task as a standardized experimental tool to induce visuomotor performance changes in the short-term (within session,

during the MRI scan) and in the longer-term (with home training) (Lipp, Foster, et al., 2020; Tacchino et al., 2014; Tomassini, Jbabdi, et al., 2011; Tomassini, Matthews, et al., 2012). Participants were asked to respond as quickly as possible to the location of visual stimuli presented on a computer screen by pressing the corresponding key on a keypad with one of four fingers (index to little finger) of their right hand. Stimuli were presented in a long repetitive sequence (16 stimuli for the home training and 8 stimuli for the MRI version). In the MRI version of SRT, 12 blocks (8 Sequence and 4 Random blocks – **Figure 2.1**) were interleaved with Rest blocks. Each home-training session was approximately 15-minutes long, consisted of 21 blocks (14 Sequence and 7 Random), separated by Rest blocks. Participants were asked to practice the SRT task at home on a laptop for 5 days/week for a total of 4 weeks. For each training session of the SRT task, the mean number (accuracy) and median latency (reaction time, RT) of responses were calculated. As RT can continuously decrease up to a point where participants anticipate the stimuli and respond before the onset, we allowed a time window for anticipation (up to 500ms before stimulus onset, during which at least 50% of the given responses corresponded to the subsequent stimulus). The changes in accuracy and RT over days of practice were quantified by the slope of Sequence-specific changes, with the Sequence specificity being defined by the contrast Sequence vs. Random condition.

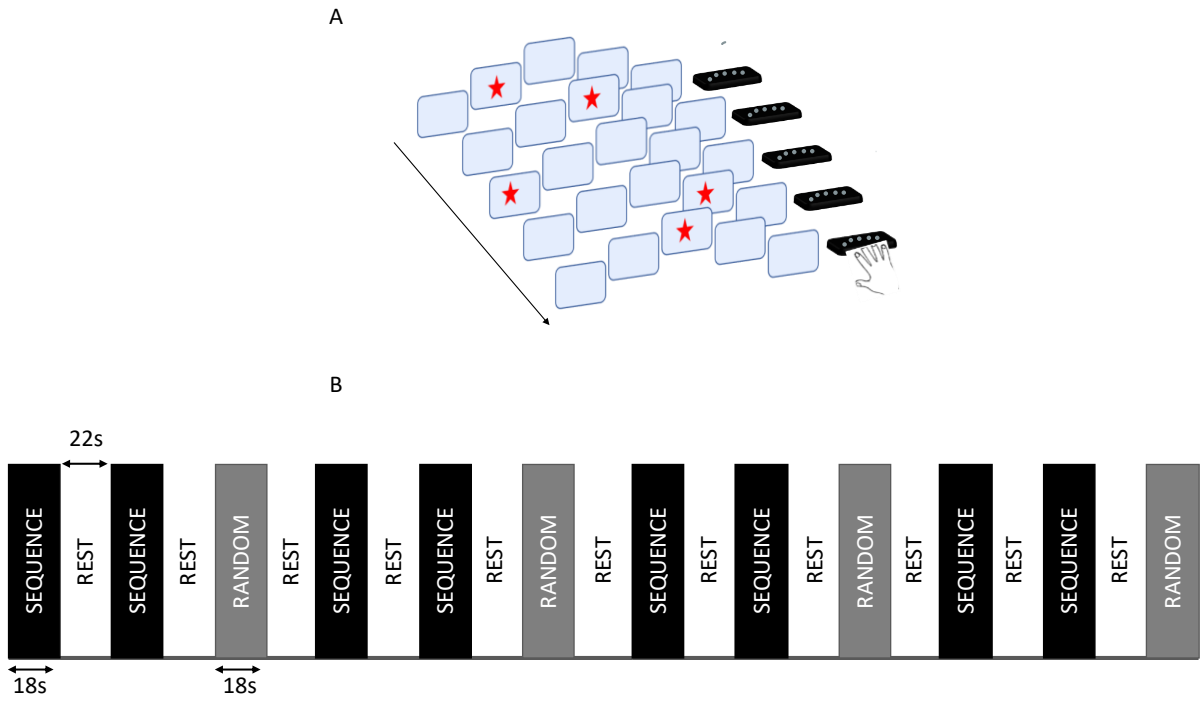

Figure 2.1. Serial Reaction Time (SRT) Task. *(A) Example of SRT task presented during in the scanner. Participants were asked to respond as quickly as possible to the location of visual stimuli presented on a computer screen by pressing the corresponding key on a keypad with one of four fingers (index to little finger) of their right hand. (B) Block design of the task. 12 blocks (8 Sequence and 4 Random blocks) were interleaved with rest blocks.*

MRI DATA ACQUISITION AND ANALYSIS

Functional MRI (fMRI). To identify brain regions relevant for the SRT task, the short version of the SRT task was presented in the scanner (3T General Electric HDx MRI system with an eight channel receive-only head RF coil - GE Medical Systems, Milwaukee, WI) while BOLD-weighted fMRI images were acquired (resolution= 3.4x3.4x3 mm, TR=3000 ms, TE=35 ms, FOV/slice=220 mm, flip angle=90°, 46 slices of 2 mm with a 1 mm slice gap acquired in AC-PC orientation and an interleaved order, 142 volumes, 7 min). Pre-processing and first level analyses were carried out using FEAT (FMRIB Expert Analysis Tool, v6, Oxford University, UK, (Woolrich, Ripley, Brady, & Smith, 2001)). Pre-processing steps included: high pass

filtering (100s temporal cut-off), skull stripping using BET (Smith, 2002), MCFLIRT motion correction (Jenkinson et al., 2002), spatial smoothing with a Gaussian kernel of full-width-half-maximum 5mm. Functional images were registered using boundary-based registration with simultaneous field-map correction (Greve & Fischl, 2010). To model the functional response to the task for the entire group (patients and controls), one event type was defined (SRT sequence condition > Rest). The model was convolved with the (Gamma) hemodynamic response and high-frequency temporal filtering was applied to the model. Temporal derivatives of the event type regressors were included as regressors of no interest. AtlasQuery (FSL tool) with the Harvard-Subcortical atlas was used to anatomically localize the subcortical regions functionally involved in the SRT task.

Structural MRI. We acquired T2-weighted images (proton-density/T2-weighted dual echo sequence, resolution= 0.94x0.94x4.5 mm, matrix size=256x256, 36 slices, 3 mm+1.5 mm gap, TEs= 9.0/80.6 ms, TR= 3000 ms, flip angle= 90°,2min) and T2-weighted fluid-attenuated inversion recovery sequence (resolution= 0.86x0.86x2.4 mm, matrix size=256x256, 36 slices, 3 mm+1.5 mm gap, TEs= 122.3 ms, TR= 9502 ms, TI=2,250,flip angle= 90°,3min) for identification of white matter lesions. High-resolution 3D Fast Spoiled Gradient-Recalled-Echo T1-weighted images were also acquired for GM volumetric analysis and for co-registration of all MRI modalities. (resolution=1x1x1mm, matrix size=256x256x172, TE=3ms, TR=7.5ms, flip angle=20°, 7.5min). Whole brain tissue volume was estimated with FSL tool SIENAX (Smith et al., 2002).

Lesion volume and filling. White matter lesions were segmented semi-automatically using the software package JIM (v.6, Xinapse System, Leicester, England) on T2-weighted images, also consulting the PD-weighted and the T2-weighted fluid-attenuated inversion recovery sequence.

For lesion filling of the T1-weighted image, the T2-weighted image was registered to the high-resolution T1-weighted image with an affine registration using FLIRT (Jenkinson, Bannister, Brady, & Smith, 2002). The resulting registration matrix was applied to the T2-derived lesion maps. The resulting interpolated lesion map was thresholded at 0.5 to approximately preserve the size of the original lesion map, but also to allow a small amount of inflation in order for the lesion map to better overlap with the lesions on the T1-image, in case of registration errors, and it was then binarized. Lesion volume was calculated for each patient (Battaglini, Jenkinson, & De Stefano, 2012; Gelineau-Morel et al., 2012). FSL FAST (Zhang, Brady, & Smith, 2001) was used to create a white matter probability map for the T1-weighted image. Using FSL's lesion filling tool ('lesion_filling' (Battaglini et al., 2012)), we filled the lesion areas with intensities similar to those in the non-lesion neighbourhood. FSL-FAST was then run again on the lesion-filled T1-image to produce a robust PVE of GM.

Volume and shape analysis. Automated segmentation of DGMS involved in SRT task was performed on T1-weighted images using FIRST (Patenaude, Smith, Kennedy, & Jenkinson, 2011) which uses mesh models trained with a large amount of hand-segmented training data to perform segmentation on subcortical structures (**Figure 2.2**). We quantified the volume of functionally-relevant DGMS and tested for differences in each DGMS volume between patients and healthy volunteers. We performed a vertex-wise analysis to investigate localised between-group differences in the shape of DGMS, assessed as the displacement on a per-vertex basis of each DGMS. Statistics were conducted with Randomise (Winkler, Ridgway, Webster, Smith, & Nichols, 2014 - http://fsl.fmrib.ox.ac.uk/fsl/fslwiki/Randomise). Correction for multiple comparisons was performed using threshold-free cluster enhancement (TFCE) (Smith & Nichols, 2009). Differences were considered significant if $p < 0.05$.

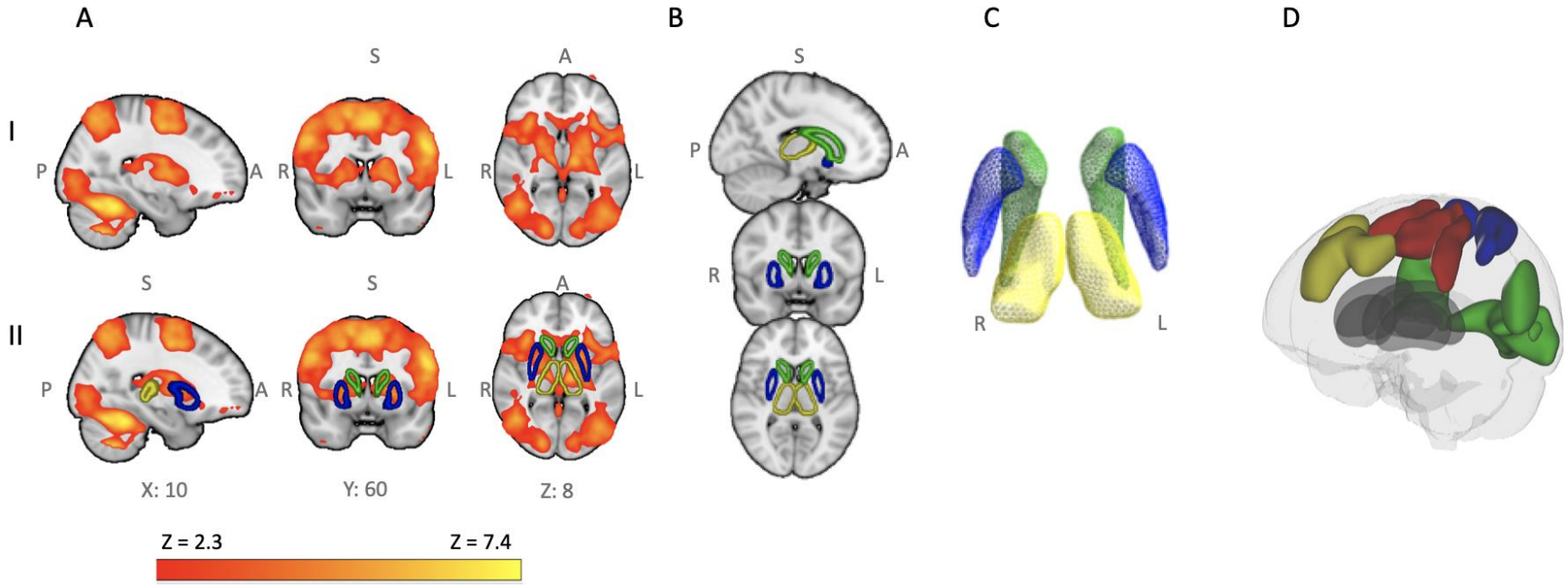

Figure 2.2. Data analysis flow.

A. *(I) Functional activation related to SRT task-response reported as z score. (II) Identification of DGMS involved in task response with Atlasquery (Green: Left and Right Caudate. Yellow: Left and Right Thalami. Blue: Right and Left Putamen).*
B. *Segmentation of DGMS involved in the task for each participant using FIRST. Volume was extracted to investigate between-group differences in volume.*
C. *Creation of the mesh (surface) in order to investigate differences in the shape of DGMS and to correlate the shape with performance improvement.*
D. *From each vertex of the mesh (grey), connectivity is run to cortical targets (Yellow: frontal areas, Red: motor areas, Blue: Parietal areas, Green: Visual areas) to obtain a diffusion based parcellation of the structure.*

Tractography-based parcellation of DGMS. Whole brain diffusion weighted images were acquired with a twice-refocussed diffusion-weighted sequence (40 uniformly distributed directions, b= 1200 s/mm^2). Fifty-seven contiguous axial slices were acquired with a field-of-view of 230 x 230 mm, acquisition matrix of 96 x 96, giving an isotropic acquisition voxel dimension of 1.8 mm. Data were pre-processed by using the FMRIB's Diffusion Toolbox (FDT) (Smith et al., 2004). After correction for head motion and image distortion due to eddy currents, a diffusion tensor model was fitted at each voxel and the three eigenvalues (lambda 1, 2 and 3) were calculated. DTI-derived maps were obtained and tractography analysis was carried out using FDT (https://fsl.fmrib.ox.ac.uk/fsl/fslwiki/FDT). Firstly, we ran BedpostX (Behrens et al., 2003) that performs Markov Chain Monte Carlo sampling to build distributions on diffusion parameters at each vertex. Then, tractography analysis was run for each subject using Probtrack-X (5000 streamline samples, 0.5 mm step lengths, curvature thresholds= 0.2, with distance correction) (Behrens, Berg, Jbabdi, Rushworth, & Woolrich, 2007). Each vertex of the DGMS was used as a seed. Target regions were chosen on the basis of their involvement in task execution using the "Harvard-Oxford Subcortical and Cortical Structural Atlas". For each DGMS, the output of the tractography algorithm was a probabilistic parcellation map that provided a connectivity value corresponding to the total number of samples running from the seed (vertex) to the cortical target region **(Figure 2.2).** For each parcellation map, a mean value of the probability of connection was calculated in patients and in controls. We then used an unpaired t-test to investigate between-group differences in connectivity. To test statistically whether the spatial distributions of the parcellation on the surface of individual DGMS were also different between groups, we used a permutation test with PALM (Winkler, Ridgway, Webster, Smith, & Nichols, 2014 - https://fsl.fmrib.ox.ac.uk/fsl/fslwiki/PALM). For all the statistical tests, differences were considered significant at $p \leq 0.05$.

In order to plot the results from permutation test, a set of pseudo-intensity matrices were

generated, each having geometric properties similar to the real matrices, and *p*-values as the intensity values.

Mean value of the probability of connection were also used to investigate the relationship between white matter and the slope performances improvement. Pearson correlation tests were carried out between white matter values and performances improvement using RStudio (http://www.rstudio.com/). Correlation were considered significant at $p < 0.05$

2.3 RESULTS

Demographic, clinical and MRI characteristics. Participants' characteristics are shown in **Table 2.1**. There was a significant difference in the level of education between groups. Patients differed from controls in hand dexterity (right: $t_{(29.286)} = -2.1883$; $p < 0.01$. left: $t_{(39.359)} = -3.7833$; $p < 0.01$) and walking ability ($t_{(30.417)} = -2.5481$; $p = 0.01$) and had lower normalised GM volume ($t_{(43.266)} = 2.5606$; $p = 0.01$)**.**

Table 2.1. Demographic, clinical and MRI characteristics. *Unless indicated otherwise, descriptive statistics are reported as means and standard deviations. For statistical comparisons between groups, chi-square was computed for categorical-variables, Kruskall-Wallis test for skewed variables (9-HPT, T25-FW), and unpaired t-test was used for the rest. p values were considered significant if p<0.05. PASAT, SDMT, WLG and normalised GM volume were adjusted for years of education. Normalised brain and grey matter volume were calculated with SIENAX.* ***Abbreviations:*** *EDSS = Extended Disability Status Scale; MSIS = Multiple Sclerosis Impact Scale; DMT = disease modifying treatment; BDI = Beck Depression Inventory; MFIS = Modified Fatigue Impact Scale; 9-HPT = 9-hole peg test; T25-FW = timed 25-foot walk; PASAT = paced auditory serial addition test; SDMT = Symbol Digit Modalities Test; WLG = World List Generation).*

	PATIENTS (29)	CONTROLS (19)	p
Age (years)	39.2±11.3	40.5±11.0	0.69
Sex (F/M)	17/12	12/7	0.75
Education (years)	15.9±3.9	19.8±4.9	**0.01**
Disease duration (years)	7.6±4.3	-	-
DMT (Yes/No)	13/16	-	-
EDSS (median/iqr)	2.4±1.1	-	-
MSIS-29 scale physical	31.6±12.4	-	-
MSIS-29 scale psychological	16.7±6.5	-	-
9-HPT (right) in sec. (across 2 trials) median/iqr	21.4±3.7	18.3±2.6	**<0.01**
9-HPT (left) in sec. (across 2 trials) median/iqr	22.1±3.3	19.5±2.9	**<0.01**
T25-FW in sec. (across 2 trials) median/iqr	5.0±1.6	4.3±0.9	**0.01**
No. correct responses PASAT 3s	44.5±12.2	51.0±6.4	0.14
No. correct responses PASAT 2s	31.1±8.6	33.9±7.1	0.69
Depression (BDI)	8.2±8.6	4.6±5.1	0.11
Fatigue (MFIS)	27.7±19.3	21.1±13.3	0.21
SDMT	57.1±11.1	61.4±8.3	0.77
WLG	24.4±7.3	28.3±7.1	0.69
Memory verbal delayed	8.9±2.5	9.8±2.0	0.19
Memory spatial delayed	7.2±2.3	7.8±2.1	0.35
Normalised GM volume (mm^3)	613.1±47.9	645.7±39.9	**0.01**
NBV (mm^3)	1196.4±109.5	1230±86.9	0.27
T2-hyperintense lesion volume (cm^3)	2.8±2.4	-	-

Performance improvement with home practice. All participants were able to complete the home training. Mean±SE number of days of practice was 18.9±0.23. Both accuracy (HC= $F_{(18, 342)}$: 2.34, $p < 0.01$; MS= $F_{(18, 532)}$: 4.17, $p < 0.01$) and RT (HC= $F_{(18, 342)}$: 4.73, $p < 0.01$; MS= $F_{(18, 53)}$: 6.53, $p < 0.01$) improved in both groups over time (**Figure 2.3**). There was a significant difference between patients and controls in the accuracy improvement ($t_{(45.79)}$: 2.43; $p = 0.02$), with no difference in RT improvement ($t_{(1.52)}$=1.52; $p = 0.14$).

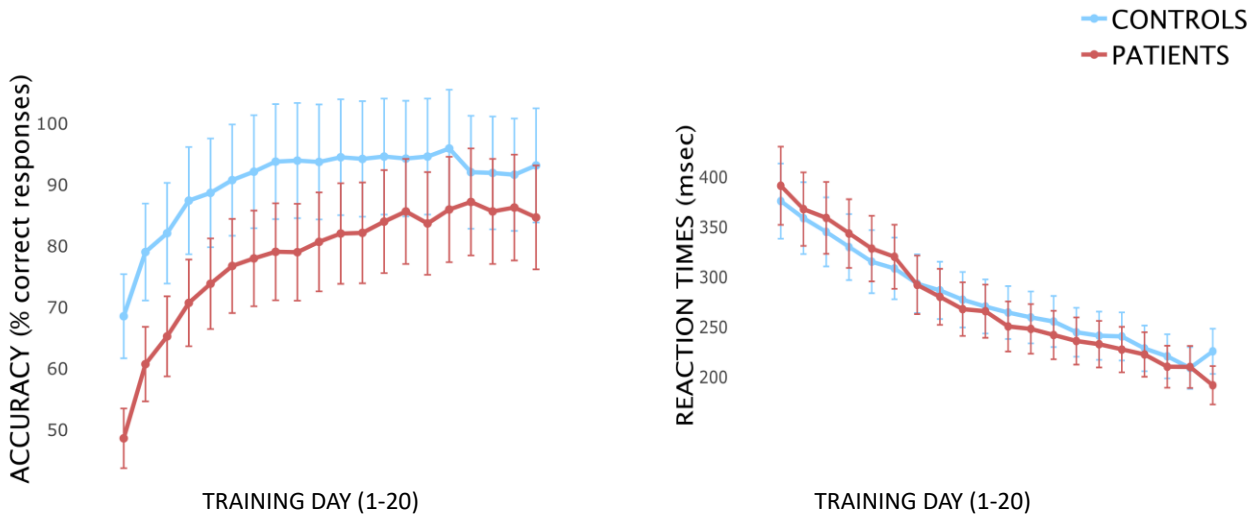

***Figure 2.3. Change in performance with practice**. There was an improvement in performance with practice in patients and controls for both accuracy and reaction time, with a significant between-group difference in accuracy improvement.*

Identification of functionally relevant DGMS through SRT-related fMRI changes. During SRT-task execution in the MRI scanner, controls showed higher accuracy than patients ($t_{(44.45)}$: 2.74; $p < 0.01$), with no between-group difference in RT ($t_{(38.67)}$:-1.5; $p = 0.14$).

From the group-combined analysis of the main effect of SRT task, clusters of activation were found bilaterally in the precentral gyrus (premotor, primary motor and somatosensory cortices), cerebellum (lobules V-VI on the right and VI left), in lower visual area and bilaterally in subcortical regions (caudate, putamen and thalamus) (**Figure 2.4**). These structures were defined as DGMS and used for further analysis.

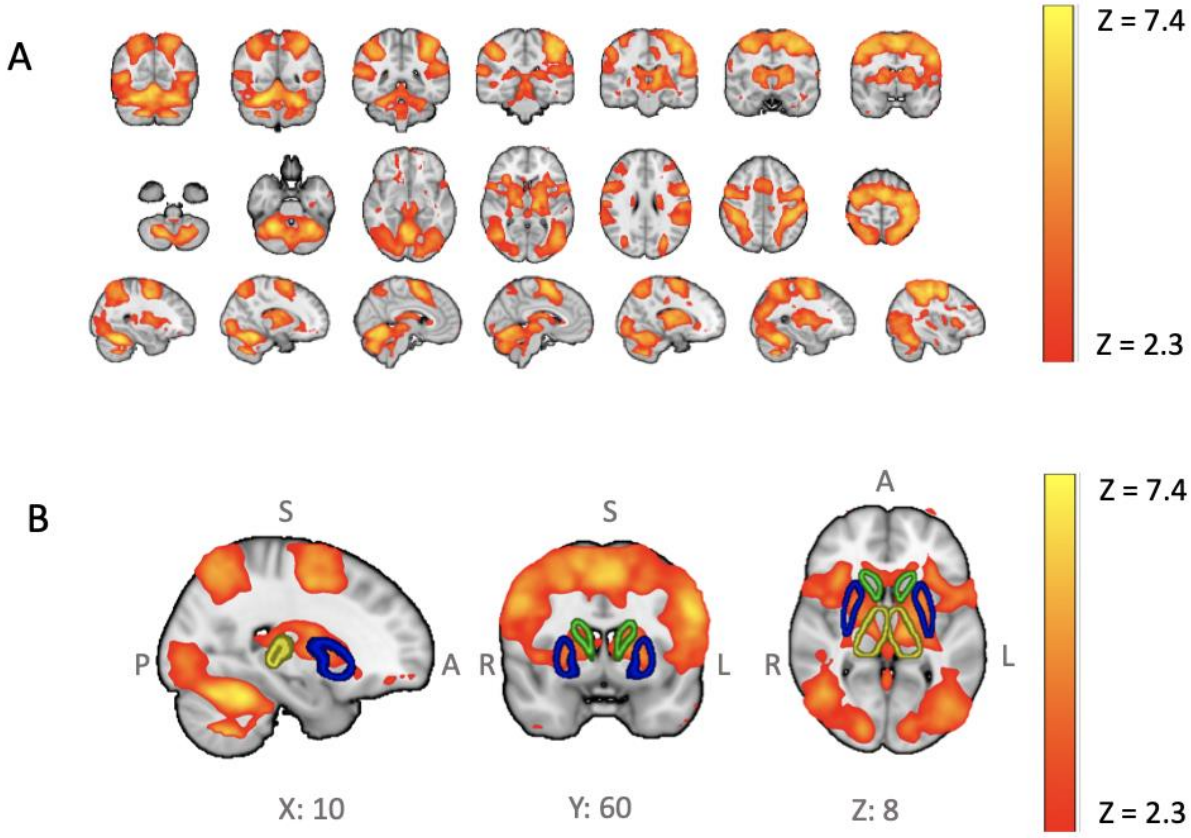

Figure 2.4. Main effect of the SRT task. *(A) Clusters involved in visuomotor integration and execution were identified in the two combined groups (z=2.3, p<0.05). (B) Boundaries of DGMS involved in SRT are indicated in green (caudate), blue (putamen) and yellow (thalamus). Abbreviations: SRT= serial reaction time.*

Differences between groups in volume and shape of functionally relevant DGMS. There was a significant difference between groups only in the volume of left thalamus ($t_{(42.83)}$=2.66; p=0.01) (Figure 2.5). However, group comparison of vertex displacement in the DGMS revealed a difference in the shape of both thalami indicating the pathological involvement of them (right thalamus: $t_{(45.79)}$=3.86; $p < 0.01$; left thalamus: $t_{(42.68)}$=4.32; $p < 0.01$) with localised

thinning (i.e., regional atrophy) in MS patients compared to controls (Figure 2.5).

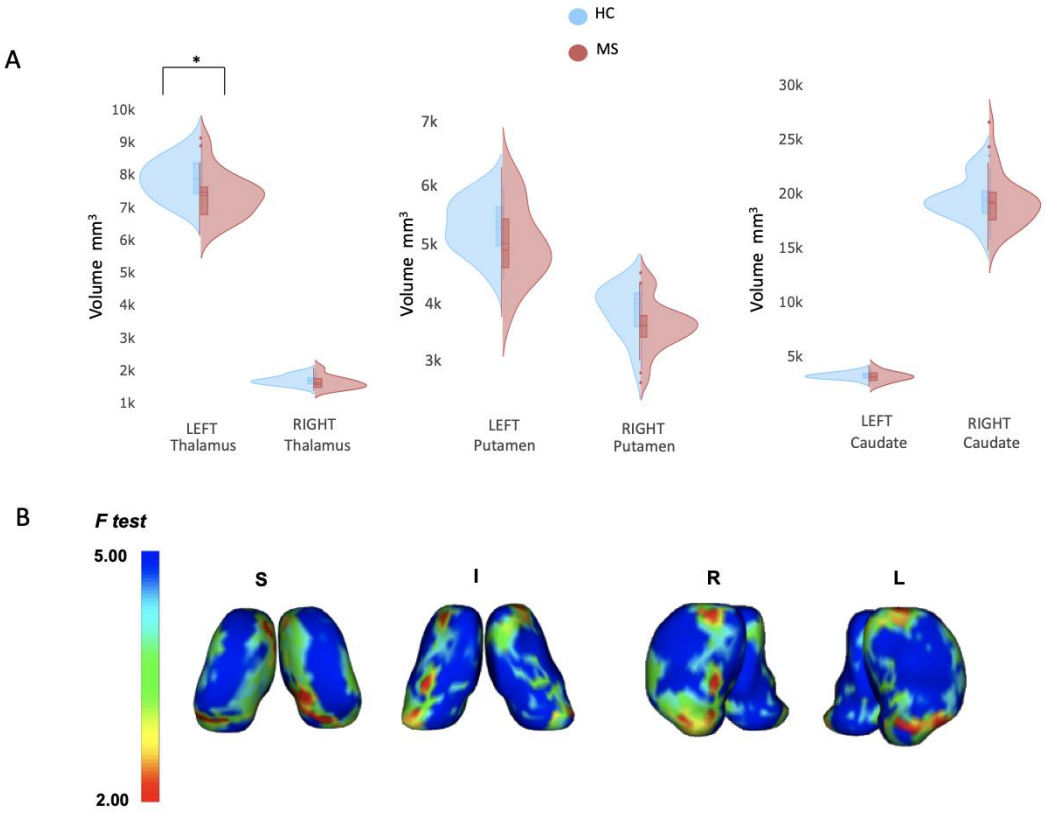

Figure 2.5. Between-group differences in volume and shape of DGMS. *(A) Volumetric differences in DGMS. MS patients showed smaller volume of the left thalamus compared to healthy controls. (B) Shape differences in DGMS. There was a significant difference between patients and controls in the shape of the thalami. Regions on the surface of the thalamus with greater differences between groups are shown in blue. In these regions, patients had an inward shift of grey/white matter boundaries, when compared to controls, indicating localized grey matter atrophy.* ***Abbreviations:*** *S= superior; I= inferior; R= right; L= left.*

Relationship between volume of DGM structures and improving performance. In controls, there were localised relationships between changes in performance and DGMS volumes: higher volume of the left caudate correlated with improving accuracy and RT (frontal/posterior caudate and central/medial caudate, respectively), whereas higher volume in right putamen (lateral) correlated only with accuracy. In MS patients, higher volume in right caudate (lateral) correlated with RT (Figure 2.6).

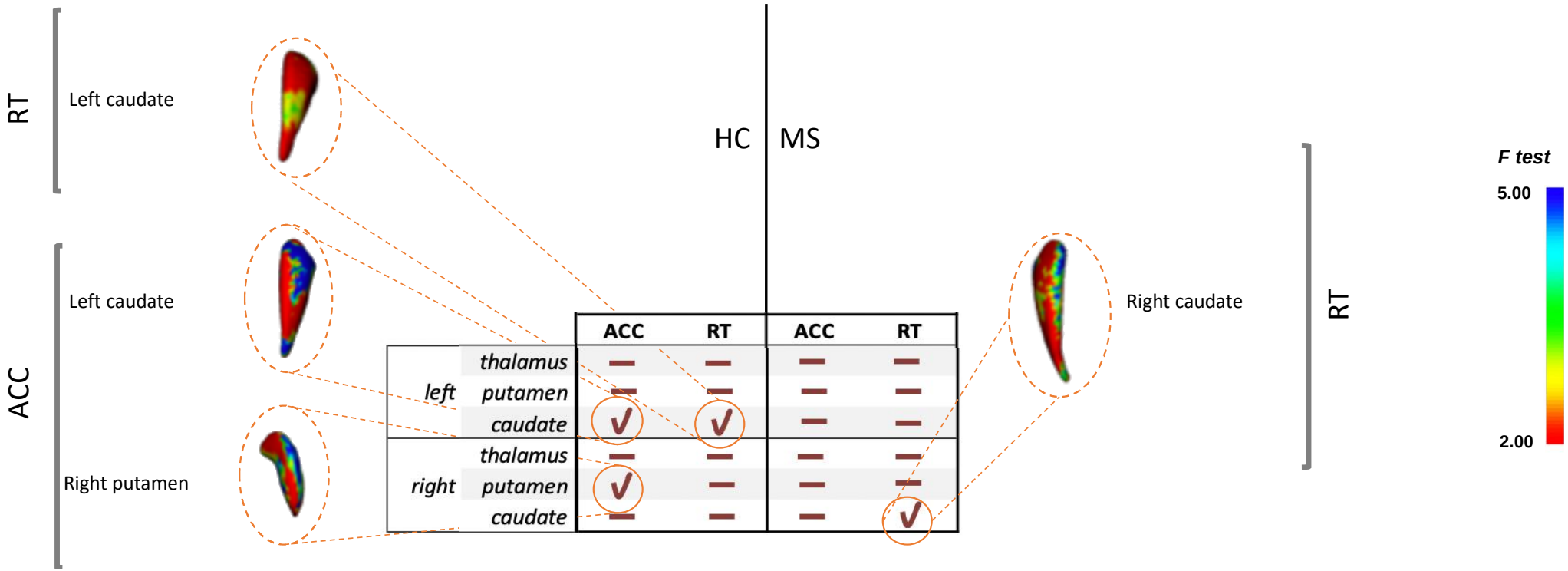

Figure 2.6. Relationship between shape of DGM structures and improving performance. *Healthy controls showed localised correlations between the shape of left caudate and accuracy and reaction times improvements; the shape of right putamen correlated only with accuracy improvement. MS patients showed a correlation between the shape of the right caudate and improvements in reaction times. Abbreviations: ACC = accuracy; RT = Reaction Times; HC = Controls; MS = Multiple sclerosis patients.*

A vertex-wise analysis was run to localise the group differences in the correlation between the volume of DGMS and improving performance with training (Figure 2.7). There was a difference between groups in the correlation between the volume of caudate and thalamus and improving accuracy and RT: the caudate (mainly medial, both anteriorly and posteriorly) showed this difference in the correlation with improving RT, whereas the thalami demonstrated a difference in the correlation with both accuracy (mainly posteriorly) and RT (anterior thalami, both superiorly and inferiorly).

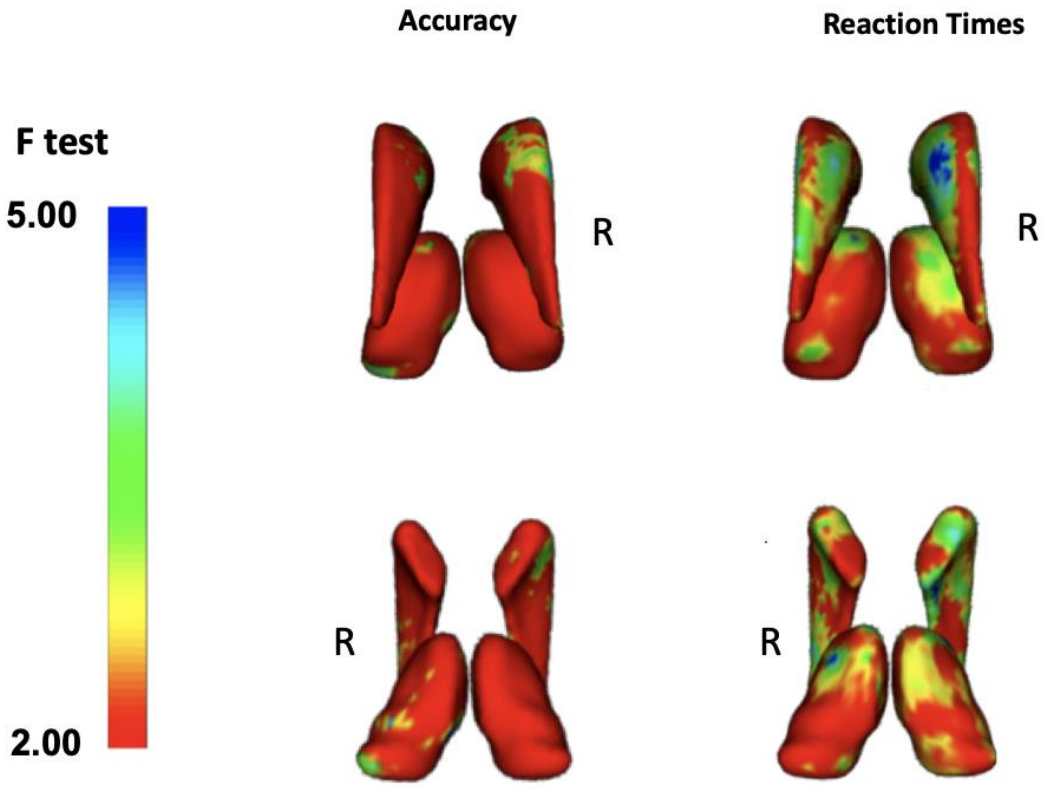

Figure 2.7. Between-group difference in brain-behaviour correlations*. The volume of the thalami correlated differently with improving accuracy and reaction times between groups. Similarly, there was a difference between patients and controls in the correlations between the volume of the caudate nuclei and improving reaction times only. Abbreviation: R=Right.*

Connectivity-based parcellation of behaviourally-relevant DGMS and between group differences. Figure 2.8 shows the connectivity-based parcellation of behaviourally-relevant DGMS to cortical targets involved in the main effect of SRT task. Between-group differences in the extent of DGMS areas connecting to cortical targets are also shown. We found between group differences in the extent of the right caudate areas connecting to frontal, motor and parietal areas. Differences between groups in the extent of subcortical areas connected from left caudate and left and right thalamus were found for each ROI (Figure 2.9). When compared to controls, patients had also a different spatial distribution of all the subcortical-cortical connections on their DGMS. Figure 2.10 shows results from permutation testing: each vertex has been replaced with the p-value of the permutation test in order to demonstrate the localisation of between-group difference in the spatial distribution of all the subcortical-cortical connections of DGMS.

Different correlation tests were run to investigate the association between white matter connection probability from each subcortical-cortical area and performances improvement (both accuracy and reaction time) and no significant correlation was found in any of the regions, in any group and in any performance parameter (accuracy and reaction times).

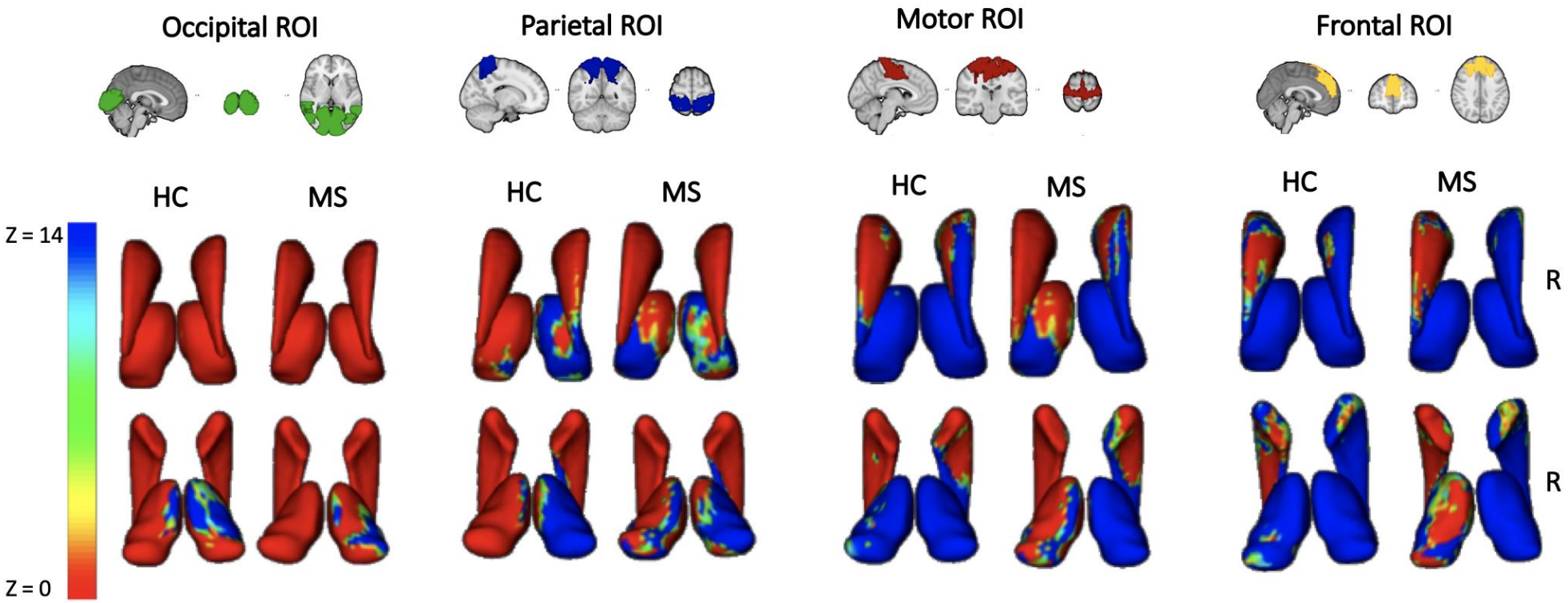

Figure 2.8. Connectivity-based parcellation of behaviourally-relevant DGMS reported for each group*. The figure shows the mean of connection probability based on parcellation of behaviourally-relevant DGMS to cortical targets involved in the main effect of SRT task for each group. HC = Healthy controls. MS = Multiple Sclerosis. Top row: dorsal view of DGMS. Bottom row: ventral view of DGMS. Values were transformed to Z scores for the purpose of displaying the connectivity mean on the top of subcortical structures.*

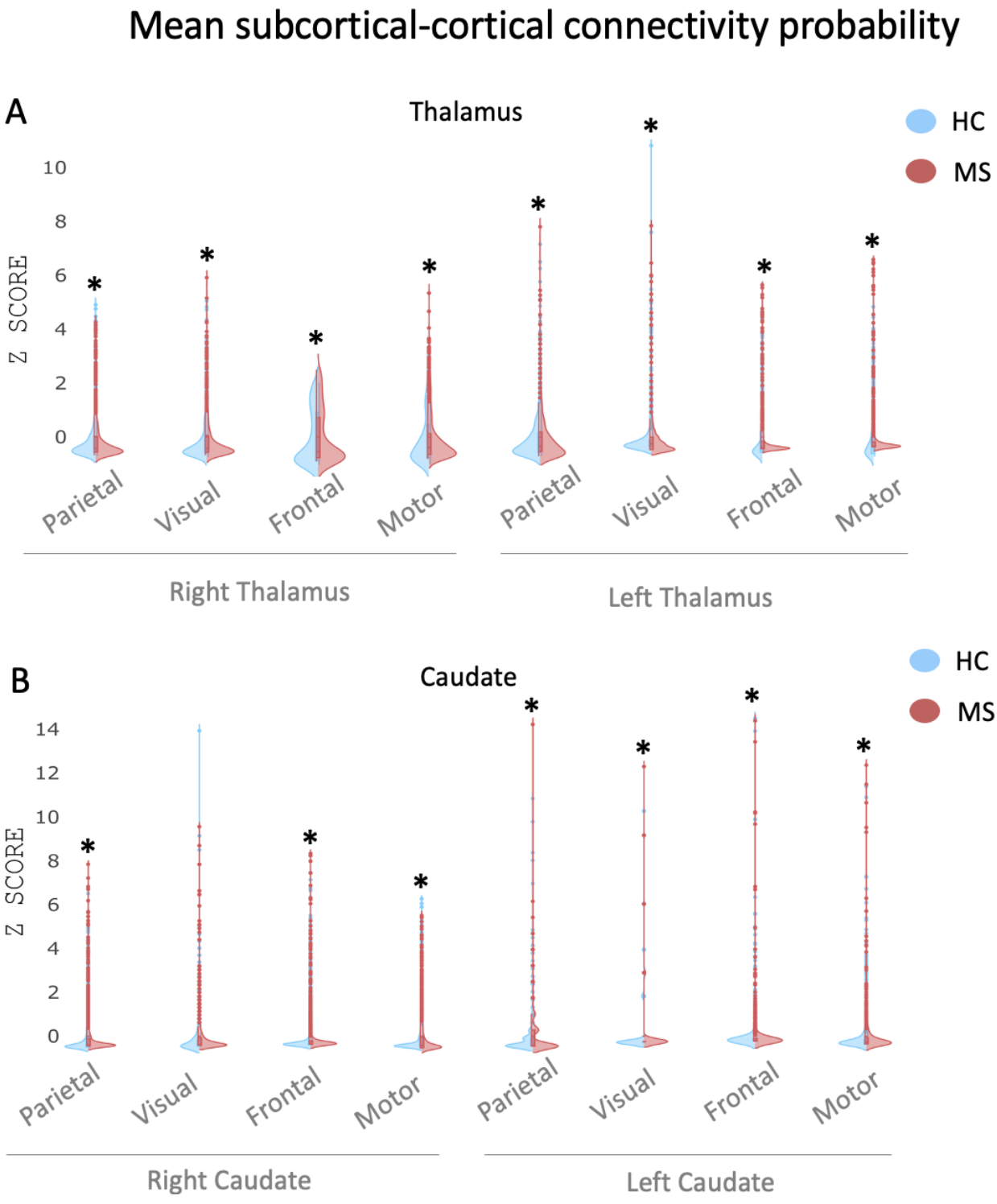

Figure 2.9. Mean subcortical-cortical connectivity probability. *The figure shows the mean of connection probability based on parcellation of behaviourally-relevant DGMS to cortical targets involved in the main effect of SRT task for each group. HC = Healthy controls (Blue). MS = Multiple Sclerosis (Red). Values were transformed to Z scores for the purpose of displaying the mean on the graph. Stars indicate a significant between-group difference in the amount of subcortical-cortical connectivity probability.*

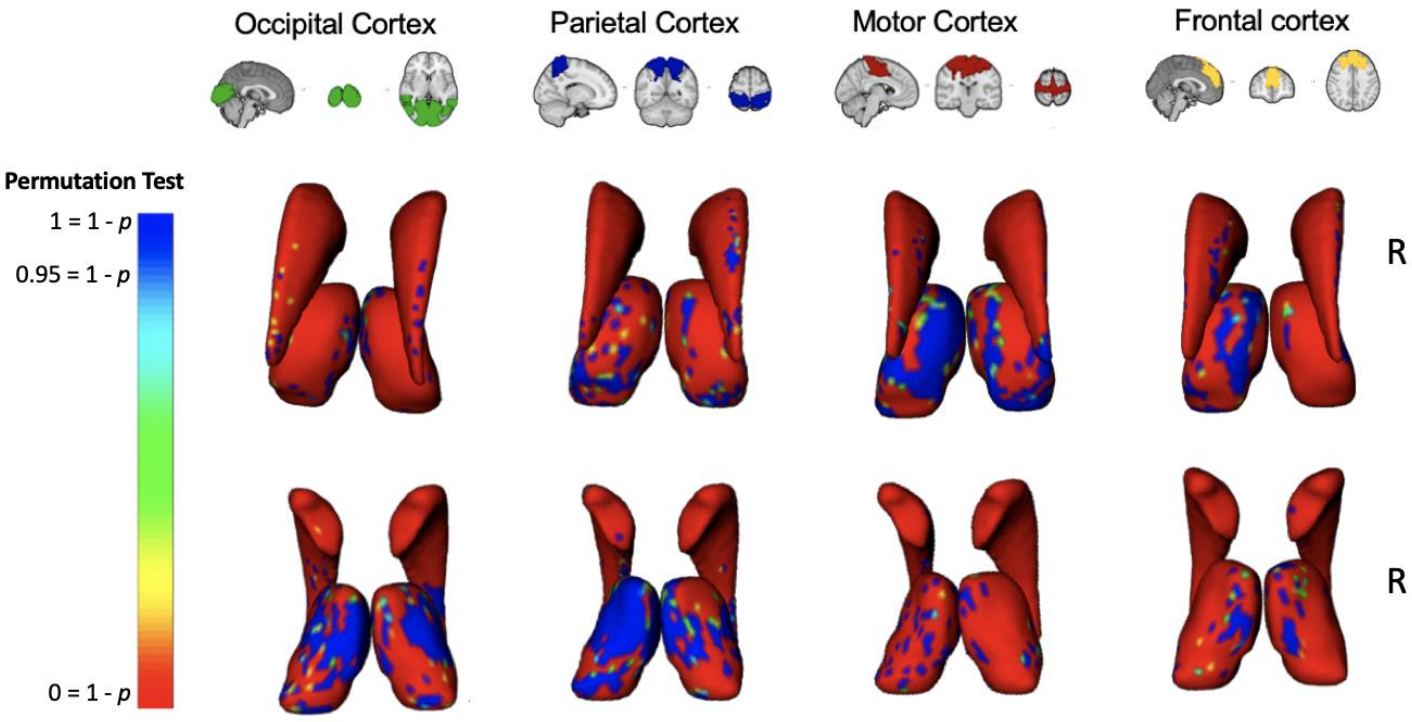

Figure 2.10. Between-group spatial difference in connectivity-based parcellation of behaviourally-relevant DGMS*. Between-group differences in the spatial distribution of DGMS-cortical connections on the thalamus and on the caudate surfaces Significant between-group differences in the extent of the DGMS regions connected to cortical areas are shown as blue area. Top row: dorsal view of DGMS. Bottom row: ventral view of DGMS*

Localising behaviourally relevant regions within DGMS with respect to long-range connectivity of DGMS. Comparisons of brain-behaviour (Figure 2.7) and connectivity (Figure 2.8 **and** 2.10) maps showed that regions of patient-specific brain-behaviour correlations were localised in DGMS areas connected to the prefrontal and motor cortices both in patients and in controls.

2.4 DISCUSSION

Our results suggest that MS inflammation alters the shape and volume of deep grey matter structures that are involved in the execution of a visuo-motor task. The dissimilarities in the shape are also associated with different improvement in task execution in MS patients compared to healthy controls. Furthermore, the connectivity based-parcellation of DGMS showed differences in the extent and in the spatial localization of subcortical-cortical connection in MS patients compared to healthy controls.

Alteration of thalamic shape and volume in MS patients. We tested for differences in the volume of the DGMS involved in SRT task execution and we found a reduction of the volume in the left thalamus in MS patients compared to healthy controls. Our results confirmed previous findings that showed how thalamus is frequently affected in the course of MS, as focal demyelinating lesions, atrophy and microstructural tissue changes. They all appear early in the disease and contribute to neurological and cognitive impairment (Hänninen et al., 2019; Rocca et al., 2010; Zivadinov et al., 2013). Thalamic lesions in MS are more frequent in the ventricular surface, therefore they may be influenced by CSF and be more susceptible to inflammatory cells and mediators, such as activated microglia and macrophages (Cifelli et al., 2002; Kipp et al., 2015; Vercellino et al., 2009).

However, it should be taken into account that we observed atrophy only in the left thalamus This result confirms previous findings of an asymmetric degeneration in the two hemispheres of MS brain as a result of local damage and long-range connectivity. Furthermore, we observed a change in the shape of both thalami, suggesting the hypothesis that the atrophy may happen in the near future; but further studies with more longitudinal data points are needed in order to test this.

It is also worth noting the high interconnectivity between thalamus and other brain structures, which makes the thalamus more vulnerable to the pathological process (Wagenknecht et al., 2016); therefore studies support the notion of thalamic degeneration as a predictor and/or marker of the disease progression (Wylezinska, Cifelli, Jezzard, Palace, & Alecci, 2003; Zivadinov et al., 2013). With our next analysis we made a step forward linking the thalamic degeneration to the prediction of behavioural training outcome in MS patients.

Reorganization of DGMS areas relevant for performing SRT. This study demonstrated that shape and volume of DGMS are associated with different performance improvements in MS patients compared to controls. An association between GM lesions in the primary cortex and the severity of motor impairment has been previously reported (Cohen-Adad et al., 2013). Overall, GM damage has been associated with general cognitive impairment (Calabrese et al., 2009) and hippocampal degeneration correlates with impaired visuospatial memory and processing speed (Roosendaal et al., 2009, 2008). However, none of the above studies correlated the shape of DGMS with behavioural outcome during training. We found that areas relevant for subsequent performance improvements differ between patients and controls indicating a reorganization of the behaviourally relevant DGMS in order to improve the performance during the training.

Specificity of loops within DGMS and their accessibility to promote recovery. Here we found that DGMS relevant for subsequent performance improvements differ between patients and controls, indicating that a compensatory mechanism within DGMS occur in MS to support functional recovery**.** The role of basal ganglia in motor control and reinforcement learning is widely accepted and previous studies have shown that direct pathway neurons mediate

movement, reinforcement, and reward, whereas indirect pathway neurons inhibit movement and mediate punishment and aversion (Kravitz & Kreitzer, 2012). But recent morphological studies have shown that direct and indirect pathway coexist in the striatum conferring a dual anatomical and physiological role to the basal ganglia (Fujiyama, Takahashi, & Karube, 2015). A disruption in the basal ganglia leads to the development of motor symptoms in neurodegenerative diseases (Wu et al., 2012). In particular, disruption of dopamine in putamen correlates with rigidity and bradykinesia and in caudate is associated with executive dysfunction (Brooks & Piccini, 2006) The well-known role of different DGMS in motor functions together with the known role of dopamine as a physiological mechanism that acts in both direct and indirect pathways could be exploited as pharmacological and physiological targets to promote functional recovery in patients with MS.

The connectivity-based parcellation of behaviourally-relevant DGMS showed a group difference in quantity and spatial distribution of subcortical-cortical connections. These results indicate a reorganization of connectivity and they can be interpreted as an expression of structural plasticity, where the extension and distribution likely reflect a remapping of DGMS circuits. Numerous studies have previously shown the reorganization mechanisms occurring in MS, and they are assumed to limit the negative effect of damage on behaviour (Filippi et al., 2012; Tomassini, Johansen-Berg, et al., 2012). Furthermore, previous local mapping has been shown in MS (Reddy, 2002) emphasizing the preserved mechanisms of brain reorganization as an expression of cortical adaptive plasticity. Taken together, we can speculate that observed structural reorganization is a response to inflammation and it may occur to keep the performance comparable to the healthy controls, despite the progression of the disease. It is worth noting that in this study we firstly assessed the grey matter damage and then we tracked the different white matter connectivity. Studies have investigated the relationship between grey

and white matter damage, and they found an association between white matter lesions and the structural disconnection between the cortex and the thalamus (Steenwijk et al., 2014). He et al. (He et al., 2009) showed that increasing white matter lesion volume in multiple sclerosis is significantly correlated with the impairment of both the global and local topological organization of the brain. But, again it is actually unknown whether grey and with matter damage are occurring at the same time, or one is causing the other. Further studies are needed to investigate the different role of these factors.

Methodological considerations and limitations. Limitations inherent to the imaging technique are a potential source of confounding. We used PROBTRACKX to assess for probability of connection, and although it takes into account crossing fibres, the detection of small fibre bundles perpendicular of major tracts is still a challenge (Honey et al., 2009).
These limitations increase when applied to multiple sclerosis population. The difference in connectivity density or strength in MS patients has previously led to methodological issues when studying networks topology (Fornito, Zalesky, & Breakspear, 2013; van Wijk, Stam, & Daffertshofer, 2010). Furthermore, it has been shown that probabilistic tractography can lead to erroneous results when fibre tracts are severely damaged (Squarcina, Bertoldo, Ham, Heckemann, & Sharp, 2012). But a recent study from Lipp et al. (Lipp, Parker, et al., 2020) revisited the challenging of tracking fibres in MS lesions and despite the disease effects on the fibre orientation reconstruction, they conclude that fibre tracking through MS lesion is possible even in areas with high lesion probability.

CONCLUSION

Localised or global differences between patients and controls in DGMS accompany remapping of DGMS functions. Together they subserve performance improvements with practice,

suggesting that compensatory mechanisms within DGMS occur in MS to support functional recovery. DGMS circuits can be identified through connectivity-based parcellation and they may potentially be targeted by selective pharmacological manipulation or cortical electrophysiological modulation in order to enhance functional recovery.

CHAPTER 3

Changes in brain perfusion with training-related visuomotor improvement in MS

ABSTRACT

Multiple sclerosis is a chronic inflammatory disease of central nervous system. Despite the inflammation, many studies have demonstrated the preserved neuroplastic ability of functional cortical reorganization in MS patients; but the mechanisms underlying functional reorganization are still incompletely understood. A better understanding of these mechanisms would help with targeted intervention to promote recovery. Here we employed a multi-modal MRI approach to explore longitudinal brain changes that could underlie and support brain reorganization in MS and are associated with a sequence learning task. Firstly, baseline differences between patients and controls during the executions of a sequence learning task, as well as structural, clinical and behavioural measures, were measured. Participants were then trained on a visuomotor task for 4 weeks, in order to investigate mechanisms supporting functional reorganization; longitudinal functional changes were then associated with improving performance, changes in the vascular state of the tissue, and structural and microstructural damage.

Right-handed relapsing-remitting MS patients and matched healthy volunteers underwent clinical assessment and multi-modal brain MRI acquisition at baseline and after 4 weeks of home training of a serial reaction time task (SRT), where accuracy and reaction time (RT) were recorded. At each testing session, we acquired functional MRI (fMRI) during SRT, diffusion-weighted images, T1-weighted images and arterial spin labelling measurement of cerebral blood flow (CBF). Functional reorganisation, grey matter (GM) volume, white matter (WM) microstructure and cerebral blood flow (CBF) were quantified, and they were associated with performance changes. Functional reorganization was observed in MS patients after 4 weeks of training, as shown by the reduction of the BOLD signal during task execution. In MS patients, the functional reorganization was also accompanied by a CBF increase in putamen bilaterally and a CBF decrease in the right superior temporal gyrus, parahippocampal gyri and amygdalae. Furthermore, increased perfusion in right angular gyrus, right inferior occipital cortex, right insular cortex was associated with behavioural improvements in accuracy.

No longitudinal changes in white matter microstructural measures and grey matter volume were observed in MS patients; and there was no correlation between performance improvement and structural changes with training.

Our results suggest that the functional reorganization observed in MS patients following a behavioural intervention is supported by increases in baseline perfusion; highlighting the importance of CBF as a biomarker for functional/behavioural changes and the potential benefits of interventions that exploit preserved plasticity mechanisms in MS.

KEY WORDS

Multiple Sclerosis, MRI, Perfusion, Training, Plasticity, Recovery

3.1 INTRODUCTION

In multiple sclerosis (MS), the modulation exerted by pro-inflammatory mediators on synaptic plasticity might negatively affect repair of brain damage, progressively exhausting the plastic potential of the brain (Di Filippo, Sarchielli, Picconi, & Calabresi, 2008). Nevertheless, Reddy et al. (2000) demonstrated that the ability for system-level functional reorganisation of the motor circuits is preserved in MS brains despite the presence of severe inflammation. Moreover, cortical reorganization has been associated with improvements in motor function (Tomassini, Matthews, et al., 2012).

MRI techniques have been employed to investigate neuroplasticity in MS. Specifically, structural MRI studies have demonstrated the effect of a motor training, such as motor rehabilitation (Bonzano et al., 2014), balance training (Prosperini et al., 2014) and physiotherapy (Ibrahim et al., 2011), on white matter microstructural damage. Moreover, fMRI has been able to detect brain functional reorganization (Roosendaal et al., 2009) and a shift in inter-hemispheric lateralisation and the recruitment of additional brain areas have been extensively shown (Pantano et al., 2002; Petsas et al., 2013; Rocca et al., 2005; Wegner et al., 2008). Furthermore, changes in activation patterns following a visuomotor training (Tomassini et al., 2016; Tomassini, Matthews, et al., 2012) and cognitive rehabilitation (Filippi et al., 2012) have also been reported in MS patients. Taken together, these studies show that the neuroinflammation does not seem to hinder neuroplasticity in general, but it may lead to the recruitment of different neuroplasticity mechanisms compared to healthy controls (Morgen et al., 2004). It is conceivable that these neuroplasticity mechanisms could be exploited to promote functional and structural reorganization through targeted training.

It is worth noting that fMRI BOLD signal is the most commonly used measure of brain activation patterns due to its high SNR and clinical feasibility, but it is an indirect measure of

neural activity because it also reflects changes in cerebral blood volume, cerebral blood flow and oxygen consumption (Logothetis & Wandell, 2004). The interaction between neural activity and vascular factors could be affected by the inflammation, since abnormal cerebral perfusion has been previously reported in MS (Absinta et al., 2015; Santarnecchi et al., 2015) and it has been observed that changes in brain vasculature can contribute to the pathophysiology (D'haeseleer, Cambron, Vanopdenbosch, & Keyser, 2011; Zlokovic, 2011). Previous studies have also reported that metabolic impairment can contribute to hypoxia, demyelination, neuronal loss, brain atrophy and disability progression (Debernard et al., 2014; Ge et al., 2005; Holland et al., 2012; Juurlink, 2013; Kappus et al., 2016; Lassmann, 2003; Lucchinetti et al., 2000; Marrie et al., 2010; Trapp & Stys, 2009; Wuerfel et al., 2004). Considering the evidence about CBF impairment in MS, standard BOLD MRI should therefore be carried out with the help of complementary approaches, such as quantitative MRI measures or physiological data recording, to enable better understanding of reorganization in functional activity in MS.

The present study employs a multi-modal MRI approach to explore longitudinal brain changes that could underlie and support brain reorganization in MS and are associated with a sequence learning task. These tasks have been extensively used in MS as standardized, experimental ways of probing functional recovery through the exploitation of neuroplasticity mechanisms (Ghilardi, Moisello, Silvestri, Ghez, & Krakauer, 2009; Zahiri et al., 2017; Zeller & Classen, 2014), given their capacity to probe strong changes of functional activation in brain areas engaged in computing the task, measurable through fMRI (Mancini et al., 2009)

Firstly, baseline differences between patients and controls during the execution of a sequence learning task, as well as structural, clinical and behavioural measures, were measured. Participants were then trained on a visuomotor task for 4 weeks, in order to investigate mechanisms supporting functional reorganization; longitudinal functional changes were then

associated with performance improvements, changes in the vascular state of the tissue (CBF), and structural and microstructural damage.

3.2 METHODS

Participants and study design. Participants and study design.

Participants' details and baseline assessment are explained in chapter 2.

Then, they were asked to practice a serial reaction time (SRT) task at home for 4 weeks and to subsequently return for the second behavioural and MRI assessment.

VISUOMOTOR TRAINING

SRT task. We used a SRT task to probe recovery experimentally (Lipp et al., 2020; Tacchino et al., 2014; Tomassini et al., 2011; Tomassini, Matthews, et al., 2012). (See chapter 2 for details).

A similar version of SRT task was also presented in the scanner, both at baseline and at week 4. (See chapter 2 for details).

Training measures. In order to establish whether participants' performance had changed with the training, for each of the two sessions, average accuracy and RT across all responses within a block were calculated for each participant. A two-way ANOVA was performed to investigate changes in accuracy and RT after the training and between-group differences.

In order to quantify the changes in performances over days of practice, the slope of sequence-specific improvement was calculated from the mean number (accuracy) and median latency (RT) for each subject and for each training session of the SRT task.

Brain MRI

Structural characteristics. MRI structural acquisitions details, as well as lesion fillings and brain tissue volume estimation, are explained in chapter 2.

To test for localised differences between groups in grey matter volume at both time points and longitudinal differences within the group, T1 weighted images were analysed with FSL-VBM (Douaud et al., 2007; Good et al., 2001 - http://fsl.fmrib.ox.ac.uk/fsl/fslwiki/FSLVBM). Voxel-wise GLM (General Linear Model) was applied using permutation-based non-parametric testing, correcting for multiple comparisons across space using threshold-free cluster enhancement (TFCE) (Smith & Nichols, 2009). Voxel-wise GLM was also applied using permutation-based non-parametric testing to investigate the correlation between changes in GM and the slope of improving of behavioural performance. Differences were considered significant if $p < 0.05$.

Diffusion weighted images acquisition and pre-processing are explained in chapter 2.

Fractional anisotropy (FA) maps were obtained from diffusion data, corrected for head motion, distortions induced by eddy currents and EPI-induced geometrical distortions (Lipp, Parker, et al., 2019). A voxel-wise statistical analysis of the FA data was carried out using tract-based spatial statistic (TBSS) (Smith et al., 2006) to investigate longitudinal changes in brain microstructure with training. For each participant we linearly registered the FA maps from both scanning sessions to a space mid-way, using the registration matrix from the respective T1-weighted image to the mid-space created by SIENA (Smith, De Stefano, Jenkinson, & Matthews, 2001; Smith et al., 2002), to avoid bias of the skeleton towards one of the two sessions. We then averaged the two co-registered maps for each participant to create a subject specific mid-space template. All the subject-specific templates were then aligned to the FSL standard template and averaged to create a study specific mid-space mean FA map. For each subject, we projected local tract centres onto the skeleton of the mid-space mean FA map and used these images in the statistical comparisons.

Functional changes. The short version of the SRT task was presented in the scanner while BOLD-weighted functional MRI (fMRI) images were acquired (Details of acquisitions and pre-processing are in chapter 2.) Analyses were carried out using FEAT (Woolrich, Ripley, Brady, & Smith, 2001 - FMRIB Expert Analysis Tool, v6, Oxford University, UK).

To model the task, two conditions (Sequence and Random) were defined, contrasting each condition to Rest. One main contrast of interest was defined (sequence>rest) reflecting activation during task performance.

To investigate between group within session differences in functional activity, we set up an unpaired *t*-test at session 1 for the contrast of interest (sequence>rest), using FSL FLAME1 with outlier de-weighting, a voxel-threshold of Z>2.3 and a two-sided statistical cluster threshold of $p<0.05$. Grey matter volume was used as regressor of no interest to account for potential effects of differing brain tissue volume. To investigate within group differences between sessions and the group*time interaction, we set up a repeated measure mixed model for the contrast sequence>rest, using FLAME1, with a voxel-threshold of Z>2.3 and a two-sided statistical cluster threshold of $p<0.05$. To investigate the correlation between changes in functional activity during the task and SRT task-related changes in performance, a voxel-wise GLM was applied using permutation-based non-parametric testing (Woolrich, Behrens, Beckmann, Jenkinson, & Smith, 2004). Differences were considered significant if $p<0.05$. Functional activation was constrained to grey matter regions to avoid any activation in white matter likely due to contamination from physiological parameters such as breathing.

Cerebral blood flow. To quantify resting cerebral blood flow (CBF) as an indicator of vascular health, we used multi-inversion time pulsed arterial spin labelling (ASL). We employed a PICORE QUIPSS II sequence with a dual-echo gradient-echo readout and spiral k-space acquisition (Warnert, Murphy, Hall, & Wise, 2015). Image resolution was 3x3x8 mm in 22

slices (7 mm+1 mm gap). A calibration image was acquired with the same parameters, except for TR=4000 ms and no labelling pulse; this was to obtain the equilibrium magnetization of cerebrospinal fluid, needed for the quantification of CBF. This image was also used to create an affine registration matrix from native space to high resolution T1-space, using FLIRT (Jenkinson, Bannister, Brady, & Smith, 2002) with 6 degrees of freedom. A minimal contrast image was acquired with TE=11 ms, TR=2000 ms to correct for the coil sensitivity profile.

CBF was estimated using *oxford_asl* with partial volume correction (Chappell et al., 2011), through the application of FAST-derived estimated GM probabilities (Zhang, Brady, & Smith, 2001). CBF maps were then registered to the structural scan using the registration matrix mentioned above. Voxel-wise GLM was applied using permutation-based non-parametric testing, correcting for multiple comparisons across space using threshold-free cluster enhancement (TFCE) (Smith & Nichols, 2009), to investigate longitudinal differences between groups, as well as the correlation between changes in CBF maps and the slope of improvements in behavioural performance. Differences were considered significant if $p < 0.05$.

3.3 RESULTS

Baseline demographic and clinical characteristics. Twenty-nine MS patients and 19 matched healthy volunteers were recruited (Table 2.1).

MRI results at baseline.

Structural damage**.** Results of the T2-hyperintense lesion volume are reported in (Table 2.1). At baseline, patients showed lower FA measures than controls in major white matter tracts, including the corpus callosum, the corticospinal tracts and the optic radiations (Figure 3.1 -A). There was a significant difference in GM volume between groups, with a significantly reduced volume in the patients in the fusiform gyri, intra-calcarine gyri, cingulate gyri, inferior temporal gyri, right parahippocampal gyri, thalami, caudate nuclei, right putamen and cerebellum. Patients also showed higher volume in brainstem, left frontal gyrus and left motor cortex (Figure 3.1 - B).

Perfusion and functional activation. No significant differences between groups were found in the resting perfusion of the brain. At baseline, patients showed higher task related BOLD signal change then controls in 4 clusters on the right hemisphere, mainly corresponding to the precuneal cortex, left cingulate gyrus and bilaterally the medial portion of pre/post central gyri (Figure 3.1 - C).

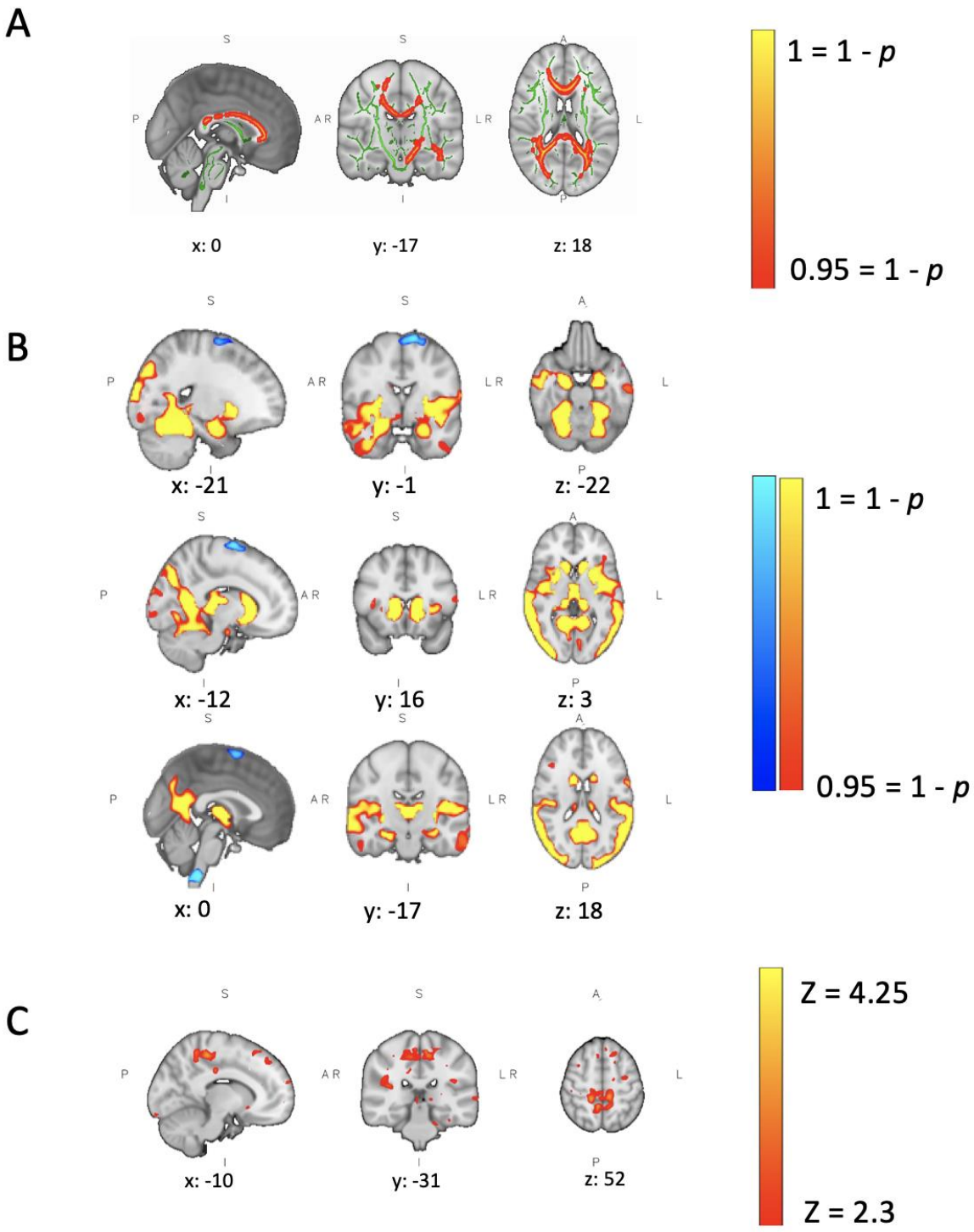

Figure 3.1. Between-group differences in brain structure and function. *(A) Patients showed lower WM fractional anisotropy (FA) at baseline compared to controls, indicating microstructural damage. Green defines the WM skeleton, in which the group-based statistical contrast was carried out; yellow-red indicates regions where patients show lower FA than controls (corpus callosum, left and right corticospinal tract, and left and right optic radiation).*

Differences were considered significant at p <0.05. (B) Patients showed reduced GM volume in yellow/red regions, including left/right fusiform gyrus, left/right intracalcarine gyrus, left/right cingulate gyrus, left/right inferior temporal gyrus, right parahippocampal gyrus, left/right thalamus, left/right caudate, right putamen and cerebellum. Patients also showed higher volume in brain stem, left frontal gyrus and left motor cortex. Differences were considered significant at p <0.05. (C) Higher cortical BOLD activation associated with SRT task were found in the patients in a widespread set of regions including right precuneal cortex, right inferior parietal lobule and right motor cortex. Results are reported as Z score. (Results are considered significant for Z > 2.3).

Behavioural and MRI changes with training

Behavioural changes. There was higher accuracy in controls than in patients in both sessions ($F_{(1,46)} = 8.3$, $p = 0.006$), with no significant group difference in RT ($F_{(1,46)} = 0.029$, $p = 0.863$). There was an increase in the number of correct responses ($F_{(1,46)} = 61.81$, $p < 0.01$) and a decrease in RT ($F_{(1,46)} = 118.81$, $p < 0.01$) from session 1 to session 2 in both groups, with no group*time interaction for accuracy ($F_{(1,46)} = 3.22$, $p = 0.08$) and for RT ($F_{(1,46)} = 1.34$, $p = 0.25$) **(Figure 3.2).**

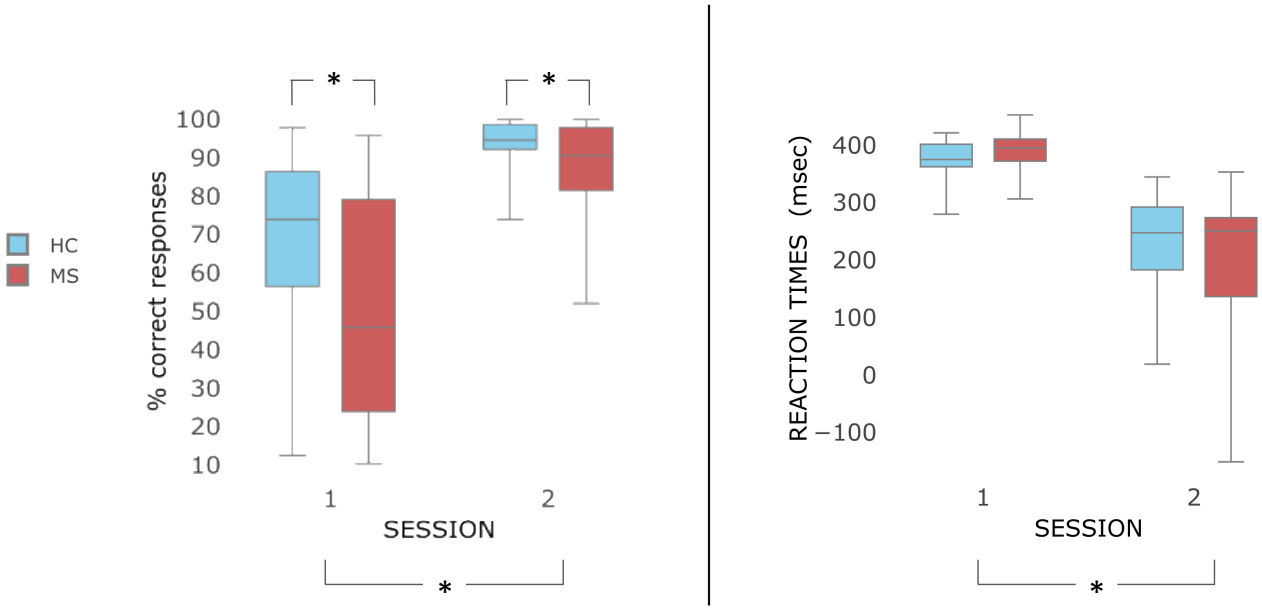

Figure 3.2. Behavioural performance during SRT task at session 1 and session 2*. Patients (red) and controls (blue) showed increased accuracy and decreased reaction time after the training. Higher accuracy was reported in HC compared to MS at both sessions. Values are reported as mean±SD.*

Functional changes. After 4 weeks of training a significant group*time interaction was found mainly in the right precentral gyrus and the right inferior temporal lobe (**Figure 3.3 - A**). This was due to reduced BOLD signal change in those regions in the patients. In both groups, behavioural changes did not correlate significantly with changes in task-related functional activity**.**

Perfusion changes. Voxel-wise analysis showed a significant change in resting perfusion maps after 4 weeks of training in the MS patients only. An increase in CBF was observed in the putamen bilaterally, whereas decreasing CBF was observed in the right superior temporal gyrus, parahippocampal gyri and amygdalae (**Figure 3.3 - B**). Also, in patients only, changes in accuracy (slope of changes) correlated with increased perfusion in right angular gyrus, right inferior occipital cortex, right insular cortex (**Figure 3.4**).

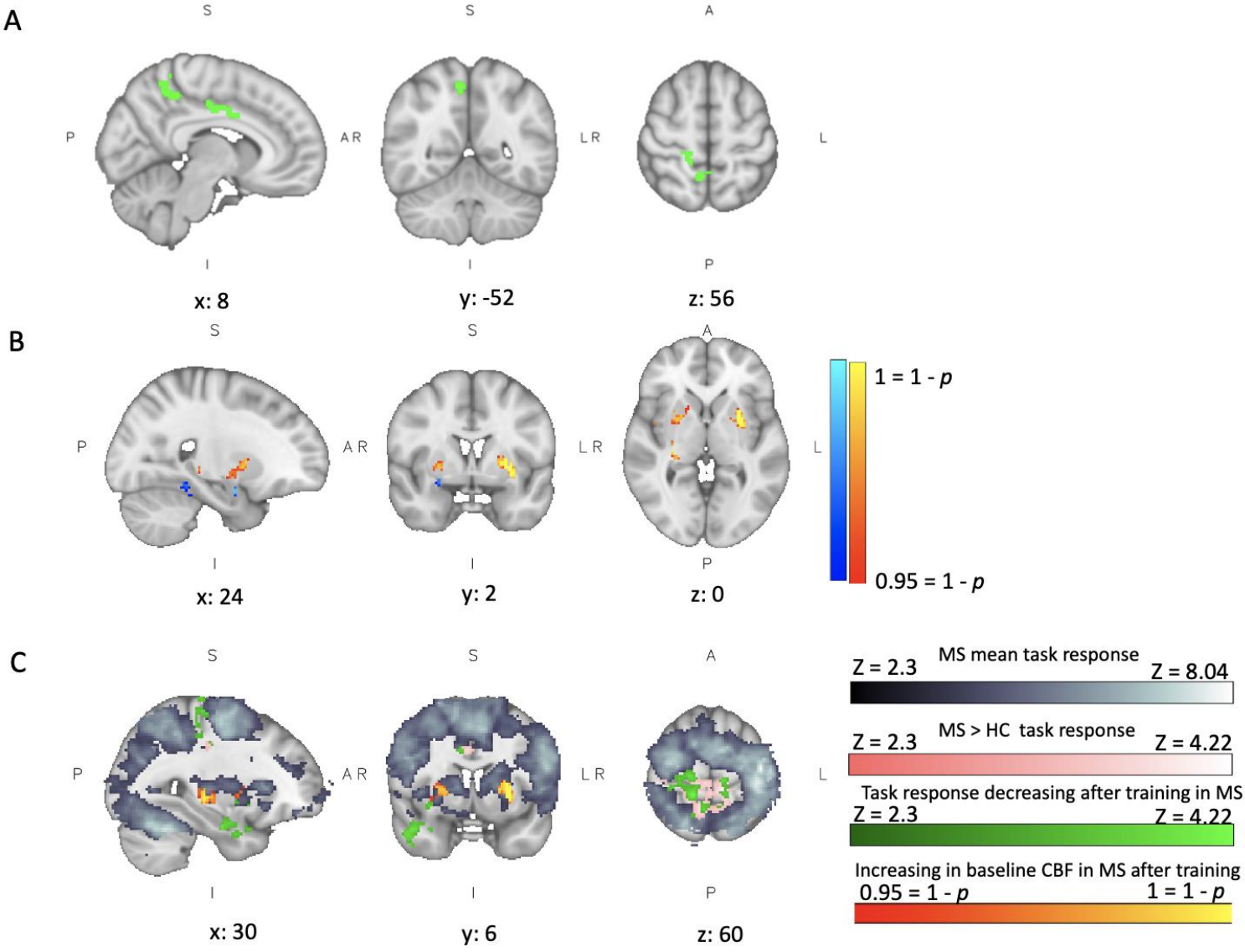

Figure 3.3. Changes in brain function and perfusion with training in patients. *(A) Reduction of functional activity in patients compared to controls after 4 weeks of SRT training were observed in the right precentral gyrus and in the right inferior temporal lobe. (B) Changes in brain resting perfusion in patients compared to controls with 4 weeks of training. Displayed in red: Increase of CBF in the putamen bilaterally. Displayed in blue: decrease of CBF in the right superior temporal gyrus, parahippocampal gyri and amygdalae. (C) Overlap among patients mean response to task at baseline (gray), higher to task in patients compared to healthy controls at baseline (pink), reduction of functional activity in patients compared to controls after 4 weeks of SRT training (green) and changes in resting perfusion in patients compared to controls after 4 weeks of training (red).*

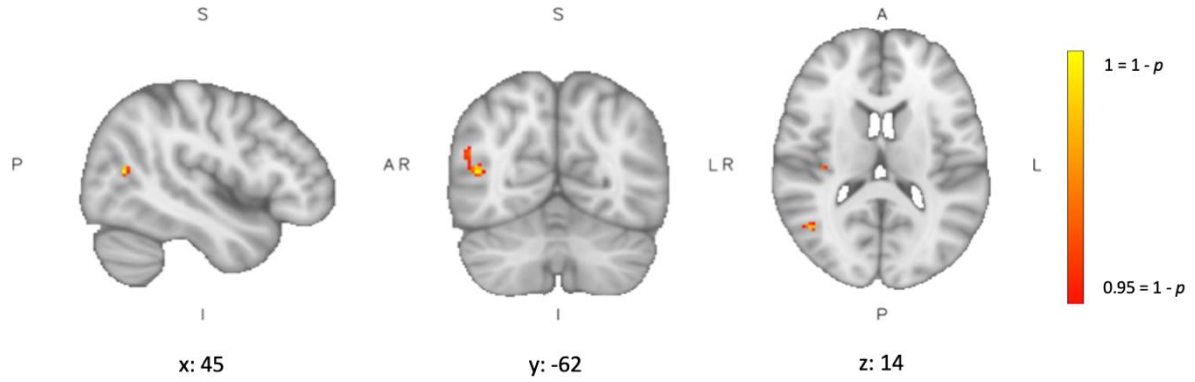

Figure 3.4. Relationship between perfusion changes and performance improvement*. Improvement in accuracy correlated with CBF increase in the right angular gyrus, right inferior occipital cortex and right insular cortex in patients only.*

Structural changes. Differences between sessions were found only in the GM volume of controls, who showed reduced GM volume in right amygdala and putamen. After 4 weeks of training, differences between groups in white matter microstructure and grey matter volume were still present. In both groups, there was no correlation between performance improvement and structural changes with training**.**

3.4 DISCUSSION

The aim of this study was to explore longitudinal brain and behavioural changes that are associated with 4 weeks of visuomotor training and that could underlie and support functional reorganization in MS patients. Functional reorganization was observed in MS patients after 4weeks of training, as shown by the reduction of the BOLD signal during task execution. In MS patients, the functional reorganization was also accompanied by changes in baseline CBF that were associated with behavioural improvements in accuracy.

Training leads to changes in CBF which are associated with improvement in accuracy. After 4 weeks of visuomotor training we observed a change in resting CBF maps in MS patients. We also observed a correlation with CBF increase and performance improvement in MS in areas related to SRT task execution. Specifically, we found the association between performance and angular gyrus, which is an attentive area involved in processing visual information, right inferior occipital cortex, where visual stimuli are processed, and right insular cortex, frequently associated with motor learning.

Previous studies have investigated the relationship between resting perfusion and cognitive and/or physical training. Particularly, increases in CBF of 20% have been found following exercise, accompanied by an increase in motor cortex CBF during a finger tapping task (Smith, Paulson, Cook, Verber, & Tian, 2010). This result was confirmed by Chapman et al. that reported higher resting CBF in the anterior cingulate region after 12 weeks of exercise training compared to a control group (Chapman et al., 2013). On the cognitive side, increase in resting regional CBF of the right lateral PFC has been reported after 4weeks of working memory

training (Takeuchi et al., 2012). These results support previous findings that linked exercise training with enhanced vascular health (Desouza et al., 2000; Whelton, Chin, Xin, & He, 2002), accompanied by improved cognitive performance (Colcombe et al., 2004; Erickson et al., 2011). Here we made a step forward showing a direct link between changes in resting CBF and performance improvement after 4weeks of visuomotor training. Our results corroborate the hypothesis of CBF as a promising neural marker of brain changes given a specific intervention (Mozolic, Hayasaka, & Laurienti, 2010; Vas, Spence, & Chapman, 2015), since the training may boost the energy consumption of neural components, like increases in cellular proteins, enzymes and neurotransmitter turnover (Attwell & Laughlin, 2001; Chapman et al., 2015). The lack of a third longitudinal point leaves open the question of how long increased CBF is sustained over time. Considering that Chapman et al. (Chapman et al., 2015) demonstrated that CBF increase is maintained higher after training stopped, we hypothesize a preserved CBF response in the long term, but further studies are needed to test this hypothesis.

Functional reorganization after training. A decrease of functional hyperactivation after 4 weeks of training was observed in the somatosensory network in MS patients, suggesting the occurrence of cortical plasticity as previous studies reported (Tomassini, Matthews, et al., 2012).

The hyperactivation observed at the first time point in patients confirms previous finding showing that MS patients differ from healthy volunteers in functional activation (Filippi et al., 2012; Rocca et al., 2005), specifically reporting hyperactivation in ipsi- and contra-lateral brain regions (Tomassini et al., 2016). Here, the hyperactivation was found in the somatosensory network, which is involved in higher-order processes, such as perception, attention, manual dexterity and coordination (Disbrow, Roberts, & Krubitzer, 2000; Hämäläinen, Hiltunen, & Titievskaja, 2000; Karhu & Tesche, 1999). Given the comparable RT between groups at the

first time point, the greater involvement of somatosensory network associated with task execution could be interpreted as a compensatory mechanism where higher level of integration is needed to perform the task in a similar manner to healthy controls. Further studies are needed to test this hypothesis.

After 4weeks of training, we observed a reduction of the hyperactivation, in parallel with an improving in accuracy and RT. Our results are in line with prior study showing a decreasing in functional activation following a long period of training in MS patients (Morgen et al., 2004). We can conclude that 4 weeks of visuomotor training leads to a normalization of brain activation, an expression of preserved brain plasticity in MS patients (Tomassini, Johansen-Berg, et al., 2012), supported by performance improvement.

Lack of changes in structural measures and study limitations. Despite the group differences in WM and GM observed at baseline, after 4weeks of visuomotor training, we did not observe an increasing in FA or in GM volume in MS patients. Fractional anisotropy (FA) is one of the most common MRI measures employed to assess WM integrity (Basser, Mattiello, & LeBihan, 1994). Reduced FA is thought to reflect underlying demyelination and axonal loss (Beaulieu, Does, Snyder, & Allen, 1996; Schmierer et al., 2007) and our results confirm previous findings reporting lower FA value in MS patients (Ciccarelli et al., 2001; Vrenken et al., 2006). Previous longitudinal studies observed structural changes after training, but, unlike our study, the training was longer than 4 weeks (Chapman et al., 2015; Scholz, Klein, Behrens, & Johansen-Berg, 2009). Particularly, Chapman et al. (Chapman et al., 2015) investigated structural changes after 6 weeks and 12 weeks of cognitive changes and they reported that the structural changes emerged only at the later assessment. Structural plasticity covers many different processes, such as changes in synapse numbers, axonal fibre densities, synaptic connectivity patterns and neuronal cell numbers (Butz, Wörgötter, & Ooyen, 2009), and they

all cost energy in the form of greater blood supply. Taken together with our lack of changes in DTI measures, these results support the hypothesis that structural changes take longer than functional and vascular changes to occur (Bruel-Jungerman, Davis, & Laroche, 2007). Therefore, the increased perfusion observed after the training will be likely reflected in structural changes in a longer term.

However, we should also consider the hypothesis that the training acted as a protector of the tissue and prevented further damage (Bonzano et al., 2014), but we were not able to test this hypothesis given the lack of a patient control group.

CONCLUSION

Our results suggest that the functional reorganization observed in MS patients following a behavioural intervention is supported by increased baseline perfusion; highlighting (i) the importance of CBF as a biomarker for functional/behavioural changes and (ii) the potential benefits of interventions that exploit preserved plasticity mechanisms in MS.

Due to the link between vascular and structural tissue, further studies are needed in order to better understand the relationship between vascular alteration and microstructural damage. Advanced neuroimaging techniques would allow the study of physiological mechanisms, such as metabolism and energy supply, sub-serving neuroplasticity phenomena.

CHAPTER 4

Quantitative fMRI to investigate the energetics of brain plasticity in the healthy and MS brain

ABSTRACT

The regulation of tissue metabolism in the brain is essential to maintain healthy functions. It can be assessed using calibrated fMRI, which employs a biophysical model to estimate relative changes of oxygen consumption ($CMRO_2$) from task-induced ASL and BOLD responses. The interaction between neural activity and the brain's vasculature could be affected by brain inflammation, such as that present in multiple sclerosis (MS). Despite the metabolic impairment shown in people with MS, studies have demonstrated neuroplasticity mechanisms are preserved in MS, although with differences from healthy volunteers. Whether these differences can be attributed to unusual energy consumption or usage, remains to be explored. Here we use calibrated fMRI to examine changes in brain energetics, indexed by blood flow and oxygenation, underlying task adaption in healthy and MS brain. We also examined the concordance between adaptation assessed through BOLD signal and by the CBF and $CMRO_2$, anticipated to be more representative of tissue physiology.

23 relapsing-remitting MS (35.6±7 years) patients and 22 matched healthy controls (HC, 34.2±6 years) underwent MRI that included dual-excitation pseudo-continuous arterial spin labelling and hypercapnic and hyperoxic calibration to map baseline brain oxygen consumption and its fractional changes during the performance of a serial reaction time task (SRT) and a visual checkerboard task (passive viewing). Brain regions showing task-related positive and negative BOLD signal changes were identified for each task. Cluster analysis was then performed to group regions on the basis of similarity in BOLD signal time-courses. From the resulting clusters, for each task block, we extracted % BOLD, CBF and $CMRO_2$ change relative to rest as well as resting baseline values for CBF and $CMRO_2$.

We found a lower baseline CBF and $CMRO_2$ in some of task-related areas in MS patients compared to healthy controls. However, during the task execution MS and HC showed similar fractional responses in CBF and $CMRO_2$, indicating that MS patients are able to recruit similar vascular and metabolic resources as healthy volunteers.

Task adaptation showed different trends over time among BOLD, CBF and $CMRO_2$, in particular, the CBF and relative $CMRO_2$ measures suggest a reduction of energy usage with time that was not evident in the BOLD signal during SRT task only, suggestive of adaptation. This points to the importance of quantitative fMRI, going beyond classical BOLD fMRI, to investigate physiological mechanisms underlying brain plasticity.

KEY WORDS

Quantitative fMRI – Neuroplasticity – Brain Metabolism – MS

4.1 INTRODUCTION

The brain accounts for over 20% of total oxygen metabolism in the human body, representing one of the highest levels of energy consumption for a single organ, as it is only a small fraction of our total body mass. It is estimated that neurons consume 75%-80% of this energy produced in the brain (Hyder, Rothman, & Bennett, 2013). Therefore, the regulation of cellular energy metabolism is essential to maintain healthy cellular and systemic function in the brain. Increased neuronal activity is associated with increased energy consumption and compensatory vasculature responses ensure sufficient supply of substrates for the release of energy in tissue (Roy & Sherrington, 1890).

Oxygen metabolism in the brain can be assessed using a family of techniques called calibrated fMRI. In order to relate the BOLD response to underlying changes in cerebral blood flow (CBF) and the cerebral rate of oxygen consumption ($CMRO_2$), these techniques use a calibration procedure that involves a breathing manipulation (such as hypercapnia and/or hyperoxia) simultaneously with the acquisition of BOLD and ASL signals. Biophysical models then permit the estimation of relative changes in oxidative metabolism from task-induced BOLD and ASL responses (Chiarelli, Bulte, Wise, Gallichan, & Jezzard, 2007; Davis, Kwong, Weisskoff, & Rosen, 1998; Gauthier & Hoge, 2012). Calibrated fMRI, with the use of both hypercapnia and hyperoxia calibration steps, has also been used for measuring baseline oxidative metabolism (Bulte et al., 2012; Gauthier & Hoge, 2012; Wise, Harris, Stone, & Murphy, 2013).

Energy requirements are not uniform throughout the brain as dynamically increased metabolism in localized regions can depend on neuronal demands and activity (Watts, Pocock, & Claudianos, 2018). Neuroimaging techniques have been used to detect metabolic and vascular signals that are coupled to changes in neuronal activity to identify brain areas that change their level of activity during particular tasks (Magistretti & Allaman, 2015).

Normal brain function requires metabolism to be tightly regulated both temporally and spatially in order to compute a task. The adjustments can be reflected simultaneously in different areas of the brain that work together to perform a task; with fMRI, it is possible to identify the degree to which different areas work together in a functional manner (Magistretti, 2016).

fMRI has also been widely employed to study neuroplasticity: the intrinsic characteristic of the nervous system to reorganize its structural and functional connections (Draganski & May, 2008). Especially BOLD signal has been used as a marker of changes in brain function due to its high SNR and clinical feasibility. But BOLD represents a relative change from an unknown baseline and as well as offering only an indirect measure of neural activity, it does not represent a single physiologically interpretable quantity. This is because BOLD signal changes result from a mixture of changes in blood flow, blood volume and the rate of oxygen consumption metabolism. These limitations reduce the strength of the inferences that can be made in assessing brain plasticity, this property being the brain's ability to adapt new experiences as well as to repair and reorganise functions following injuries (Krieger et al., 2014; Leontiev & Buxton, 2007; Logothetis & Wandell, 2004; Zeller & Classen, 2014). fMRI has been widely applied in understanding the above-mentioned changes in the brain. Previous studies reported decreasing BOLD signal associated with increasing performance (Albouy et al., 2012; Mackey, Miller Singley, & Bunge, 2013); although the underlying neurobiological mechanisms facilitating plasticity are still unknown.

Therefore, while BOLD signal decreases and increases indicate that some change has happened, with BOLD signal only, we do not know if this change is solely neural or vascular in nature or a mixture of the two. Because of the simultaneous measurement of various vascular parameters, calibrated fMRI would help understanding whether BOLD signal changes during plasticity tasks reflect the underlying changes in oxygen metabolism consumption and thus energy consumption (Tardif et al., 2016). Furthermore, calibrated fMRI techniques have been

shown to be highly reliable and more reproducible than BOLD, but they have not been applied in the study of neuroplasticity yet (Krieger et al., 2014; Leontiev & Buxton, 2007).

The interaction between neural activity and vascular factors could be affected by brain inflammation, such as in multiple sclerosis (MS) (Absinta et al., 2015; Santarnecchi et al., 2015), an inflammatory autoimmune disease of the central nervous system that causes demyelination and axonal loss leading to chronic disabilities with limited functional recovery (Trapp, Ransohoff, Fisher, & Rudick, 1999). MS is associated with vascular impairment; in particular cerebral hypoperfusion seems to be related to reduced axonal activity and astrocyte energy metabolism. Impaired cerebral perfusion appears to be correlated with cognitive impairment and daily living ability loss (D'haeseleer, Cambron, Vanopdenbosch, & Keyser, 2011) and metabolic dysfunction could play a central role in altered plasticity phenomena (Fan et al., 2015; Ge et al., 2012; Kidd et al., 1999), since it is thought that plasticity is highly dependent on the local environment; such as the underlying dynamic range of neuronal, vascular and metabolic resources. (Huang, Leu, & Zou, 2015; List et al., 2013; Murphy, Dias, & Thuret, 2014; Pearson-Fuhrhop & Cramer, 2010). Studies have demonstrated plasticity mechanisms are preserved in MS (Casadio, Sanguineti, Morasso, & Solaro, 2008; Leocani et al., 2007; Tomassini et al., 2011), although differently from healthy volunteers (Tomassini et al., 2011). The role of altered blood flow and energy consumption in these differences remains to be fully explored.

Here we use calibrated fMRI to examine changes in brain energetics, indexed by blood flow and oxygenation, underlying task adaption in healthy and MS brain. We also examine the concordance between adaptation assessed through BOLD signal and by the CBF and $CMRO_2$, anticipated to be more representative of tissue physiology. The same methods are applied to two different tasks; a motor task where we expect a higher adaptation and a visual passive stimulation task where we expect less adaptation.

4.2 METHODS

Participants. 23 relapsing-remitting MS patients according to McDonald criteria (Polman et al., 2011) and 22 age and gender matched controls were recruited. Eligibility criteria was age between 18 and 60 years old, retained use of the right upper limb, no relapse or change in pharmacological and non-pharmacological treatment for at least 3 months before the study, no other neurological or psychiatric conditions and no contraindications for MRI or for gas challenge. Out of the 23 patients, 17 were on disease modifying treatment (DMT) at the time of testing.

Participants all completed the MRI session, questionnaires and behavioural testing. Before the MRI scanning, we tested participants' tolerance of hypercapnic periods and breathing through a face-mask to ensure that they were comfortable with the procedures.

Written consent was obtained according to the protocol approved by NHS Research Ethics Committee, Wales, UK.

Behavioural Testing. All participants completed a socio-demographic and lifestyle questionnaire before the MRI session. This included age, height, weight, and years of education (from start of school onwards). Tests from the MS Functional Composite (Cutter, Baier, & Rudick, 1999) were carried out on all participants: 9-Hole Peg Test (9-HPT) for arm/hand function, the Timed 25-foot-walk (T25-FW) for leg function/ambulation, and the Paced Auditory Serial Addition Test (PASAT) 2 and 3 seconds as a measure of cognitive function. The Symbol Digit Modalities Test (SDMT) was also used to assess cognitive function (Benedict et al., 2017). Participants were tested with corrected-vision; matched to the correction that they had during the MRI scans.

For patients only, disability and disease impact was assessed with the self-reported Multiple Sclerosis Impact Scale (MSIS-29) (Hobart, Lamping, Fitzpatrick, Riazi, & Thompson, 2001)

and the Fatigue Scale for Motor and Cognitive Functions (FSMC) (Penner et al., 2009). Clinical records and a short interview on disease history and impact gave information on: disease onset, EDSS (Kurtzke, 1983), relapse history and impact of MS on occupation.

Magnetic Resonance Imaging. Data were acquired on Siemens Prisma 3T MRI scanner (Siemens Healthineers, Erlangen, Germany), using a 32-channel head coil. A magnetization prepared rapid acquisition with gradient echo (MPRAGE), T1-weighted scan was acquired for registration and brain segmentation purposes (1mm isotropic resolution, 200 slices, TR/TE = 2100/3.24ms). A 3D T2-weighted Fluid Attenuated Inversion Recovery (FLAIR) image (1mm isotropic resolution, 256 slices, slice thickness = 1mm, TR/TE = 5000/388ms) and T2/Proton Density dual-echo image (41 slices, slice thickness = 3mm, 0.8 x 0.8 x 3.9 mm, TR/TE1/TE2= 4050/11/90ms) were acquired for lesion identification.

A dual-calibrated fMRI scan was acquired with interleaved periods of hypercapnia, hyperoxia and medical air delivered through a facemask to the subjects, following the protocol previously described by (Germuska et al., 2016; Merola, Germuska, Murphy, & Wise, 2018). This acquisition sequence lasted 18 mins; three periods of hypercapnia (5% CO_2 in air) were given, interleaved with two periods of hyperoxia (50% O_2 in air, with short period (14secs) of 100% O_2 and 10% O_2 delivered in order to accelerate the transitions to the hyperoxic state and back to the baseline). Participant's heart rate and oxygen saturation were monitored with a pulse oximeter constantly throughout the scanning session. $P_{ET}CO_2$ and $P_{ET}O_2$ (partial pressure of end-tidal carbon dioxide or oxygen) were sampled from the facemask, using a rapidly responding gas analyser (AEI Technologies, Pittsburgh, PA, USA).

Calibrated fMRI data were acquired using a pCASL acquisition with pre-saturation and background suppression (Okell, Chappell, Kelly, & Jezzard, 2013) and a dual- excitation (DEXI) readout (Schmithorst et al., 2014). The labelling duration and post label delay (PLD)

were both set to 1.5s, GRAPPA acceleration (factor of 3) was used with TE1=10ms and TE2 = 30ms. An effective TR (the total TR including labelling and both readouts) of 4.4 seconds was used to acquire 16 slices, in-plane resolution 3.4 x 3.4 mm and slice thickness 7mm with a 20% slice gap. A calibration (M0 image) was acquired for ASL quantification with pCASL and background suppression switched off, with TR of 6 seconds, TE=10ms (Figure 4.1-D).

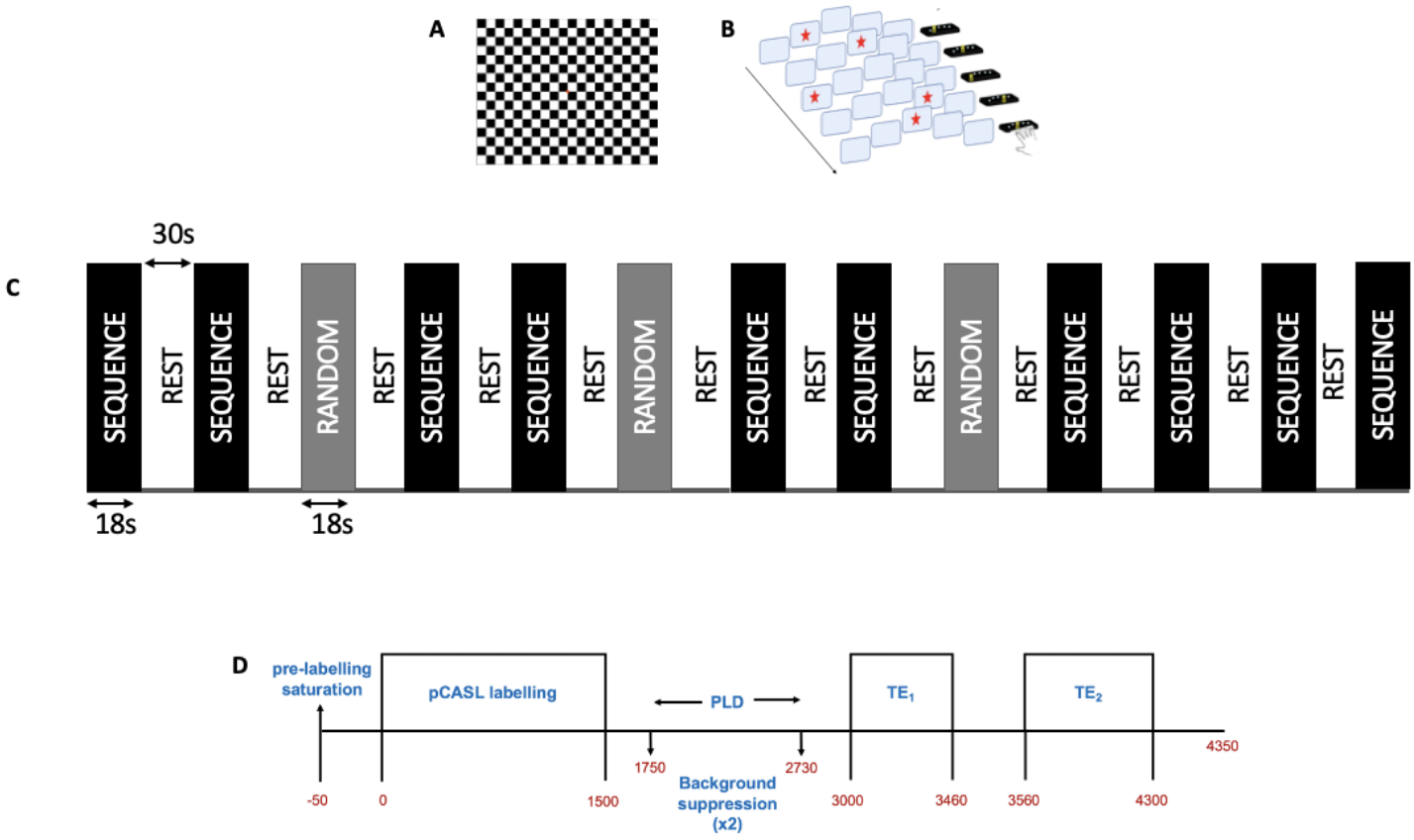

Figure 4.1. Experimental design. *(A) Reversing checkerboard pattern used during visual stimulation. (B) Example of SRT task presented during in the scanner. Participants were asked to respond as quickly as possible to the location of visual stimuli presented on a computer screen by pressing the corresponding key on a keypad with one of four fingers (index to little finger) of their right hand. (C) Block design of SRT task presented in the scanner. (D) Graphical representation of the sequence parameters and timings for dc-fMRI dual-excitation sequence. TE_1 represents ASL weighted signal, whereas TE_2 is BOLD weighted.*

Visual Task. The visual stimulus consisted of a reversing checkerboard (total size 8x8 degrees of visual angle, checks 3 cycles per degree, 100% contrast, checkerboard polarity reversing every 250ms). The design included a 30 second rest block followed by a 30 second stimulus block, repeated 8 times, then ending on rest block (total time 8.5 minutes). Participants were asked to focus on a red fixation square in the centre of the image, present during rest blocks and stimulus blocks. Functional data during visual task were also acquired using the above described DEXI pCASL acquisition yielding BOLD and CBF weighted data (**Figure 4.1-A).**

Motor task. A serial reaction time task (SRT) was employed as a motor task. Studies have shown that performance (measured with reaction time and accuracy) tends to improve with practice (Nissen & Bullemer, 1987).

The task requires the participant to respond as quickly as possible to the location of a visual cue (a dot in a box) presented in the scanner by pressing the corresponding key on a button box with one of four fingers (index to little finger) of the right hand. Stimuli were presented either in a predefined sequence (4 repetitions of the same sequence within a block with a variable inter-stimulus interval between 600-1000ms) or in a random order. 10 sequence blocks and 3 random blocks were presented in total ([S S R S S R S S R S S S S]). Control (random) blocks were intended to be used to separate activity due to simple motor activation from sequence-specific learning in order to identify networks involved in sequence learning. Each block was 18sec long alternated with 30sec rest blocks. The total length of the task was 661msec.

Functional data during the motor task were acquired using the above described DEXI pCASL acquisition yielding BOLD and CBF weighted data. (**Figure 4.1-B and C**)

DATA ANALYSIS

Demographic, clinical and MRI characteristics. To investigate between-group differences in age and behavioural measures we used a two-tailed unpaired t-test. A chi-square test was used to assess differences in the balance between sexes in the groups. For all the statistical tests, differences were considered significant at $p < 0.05$. Values are reported as mean±standard error (SE), unless stated otherwise (**Table 4.1**). Tests investigating cognitive domains (i.e. SDMT, WLG and PASAT) were corrected for education.

Motor performance improvement. For each sequence block of SRT task, the number (accuracy) and mean latency (reaction time, RT) of responses were calculated in order to establish whether participants' performance change during task execution. For each random block, accuracy and RT were also extracted, but the statistical analysis was performed only on sequence blocks as we were principally interested in changes during the repeated sequence.

Normalised Whole Brain Volume. Whole brain tissue volume was first normalised for subject head size and then it was estimated with FSL tool SIENAX (Smith et al., 2002). Brain and skull images were then extracted from the T1-weighted image (lesion-filled for the patients). The brain image was registered to MNI152 space using the skull image to determine the registration scaling, and to obtain the volumetric scaling factor. Three-class segmentation was carried out and whole brain volumes, normalized for head size, were calculated using the volumetric scaling factor.

Lesion Volumes, Lesion Filling and GM mask. T2, PD, and T2-FLAIR images were brain extracted. The T2-FLAIR image was transformed with a linear registration and 6 DOF to the same space as T2-PD image. JIM (Version 6.0) was used to draw lesions manually using the

contour ROI tool, without 3D propagation. All three image contrasts were then used to locate the lesions, and if in doubt a lesion was not drawn around. This lesion map was exported as a NIFTI file, with a pixel area threshold of 50% threshold, and a lesion volume was calculated for each patient. (Battaglini, Jenkinson, & De Stefano, 2012; Gelineau-Morel et al., 2012)

For the lesion filling of the T1 image, the PD image was registered to the T1 image in order to fill the lesions of the T1 image; the lesion map was then binarized, transformed to T1-space and thresholded at 0.4 to approximately preserve the size of the original lesion map after transformation and to allow a small amount of inflation, in case of registration errors. The function 'lesion_filling' (Battaglini et al., 2012) was used to fill the lesion area with intensities similar to those in the non-lesion neighbourhood (restricted to WM only – a WM PVE map was created with FAST (Zhang, Brady, & Smith, 2001) previous to this). FSL-FAST was run again on lesion-filled T1-image to produce a new PVE of GM.

Calibrated fMRI pre-processing and modelling. The first and second echo from the pCASL sequence's data were motion corrected using FSL tool MCFLIRT (Jenkinson, Bannister, Brady, & Smith, 2002) and then brain extracted using BET (Smith et al., 2002). Spatial smoothing (FWHM = 4.5mm) of the BOLD data (surround average of TE_2) was carried out with SUSAN (Smith & Brady, 1997), with high-pass temporal filter applied with a cut off of 90s. ASL data (surround subtraction of TE_1) and M_0 acquisition were spatially smoothed using a 3D Gaussian kernel (FWHM = 4.5mm). FSL tool FLIRT (Jenkinson et al., 2002; Jenkinson & Smith, 2001) was used to linearly register CBF data (first echo) and BOLD data (surround average of second echo) to individual T1-structural data (6 DOF) and then to linearly register it to MNI standard space (12 DOF). Most of MS studies use linear registration, as the know difficulty of brain with multiple sclerosis pathology during the registration process. (Eloyan et

al., 2014). However, the investigation of the best registration methods was not the scope of this chapter.

Functional DEXI data was registered to the structural T1-weighted image using FSL's epi-reg tool, and GM, WM and CSF PVE output were created through FAST (Zhang, Brady, & Smith, 2001) segmentation of the T1-weighted image. The T1-image and the GM-PVE image were transformed to DEXI space, using the inverse of this matrix. The GM-PVE image was thresholded at probability 0.5 and binarized and used as a GM mask for the parameter estimates. The model applied to this study, was the model already validated by our lab. Code for the pre-processing of physiological traces (end tidal oxygen and carbon dioxide) as well as code for modelling of dual-calibrated fMRI data were written by Michael Germuska (Germuska et al., 2019, 2016). It models how the ASL and BOLD signals change given the cerebral physiology, characteristics of the pCASL sequence, $P_{ET}O_2$ and $P_{ET}CO_2$. CBF, effective oxygen diffusivity (OD) and oxygen extraction fraction (OEF) are modelled with a compartmental model of oxygen exchange between capillaries and tissue. The final estimated parameters are needed to estimate the absolute (baseline) cerebral metabolic rate of O_2 ($CMRO_2$). A full description is provided in (Germuska et al., 2019).

Task Modelling. In order to create a map of areas involved in the tasks needed for defining our ROIs, BOLD responses for visual and motor tasks individually were first registered to the high resolution T1 weighted structural image using FLIRT (Jenkinson & Smith, 2001) with 6 degrees of freedom. The high-resolution images were then registered to the Montreal Neurological Institute (MNI) standard space with 12 degrees of freedom. Functional data (TASK > REST and REST > TASK) were then modelled in two separate FEAT designs and motion correction parameters were added as regressors (**Figure 4.2-A and 4.3-A**). A higher-level analysis was performed with FEAT (Woolrich, Behrens, Beckmann, Jenkinson, & Smith,

2004) using a mixed effects model (FLAME 1) to model the functional responses to the task across all participants (regardless of group). Z statistic images were thresholded at Z>2.3 and significance threshold of p = 0.05 was set.

In order to investigate changes in functional responses over time, a second model was set up to estimate the percentage change of BOLD signal and CBF, relative to rest, for each block of task execution (10 blocks for the motor task and 8 for the visual task, BlockN > REST). Parameters of the model are the same as for the previous model (**Figure 4.2-B and 4.3-B**).

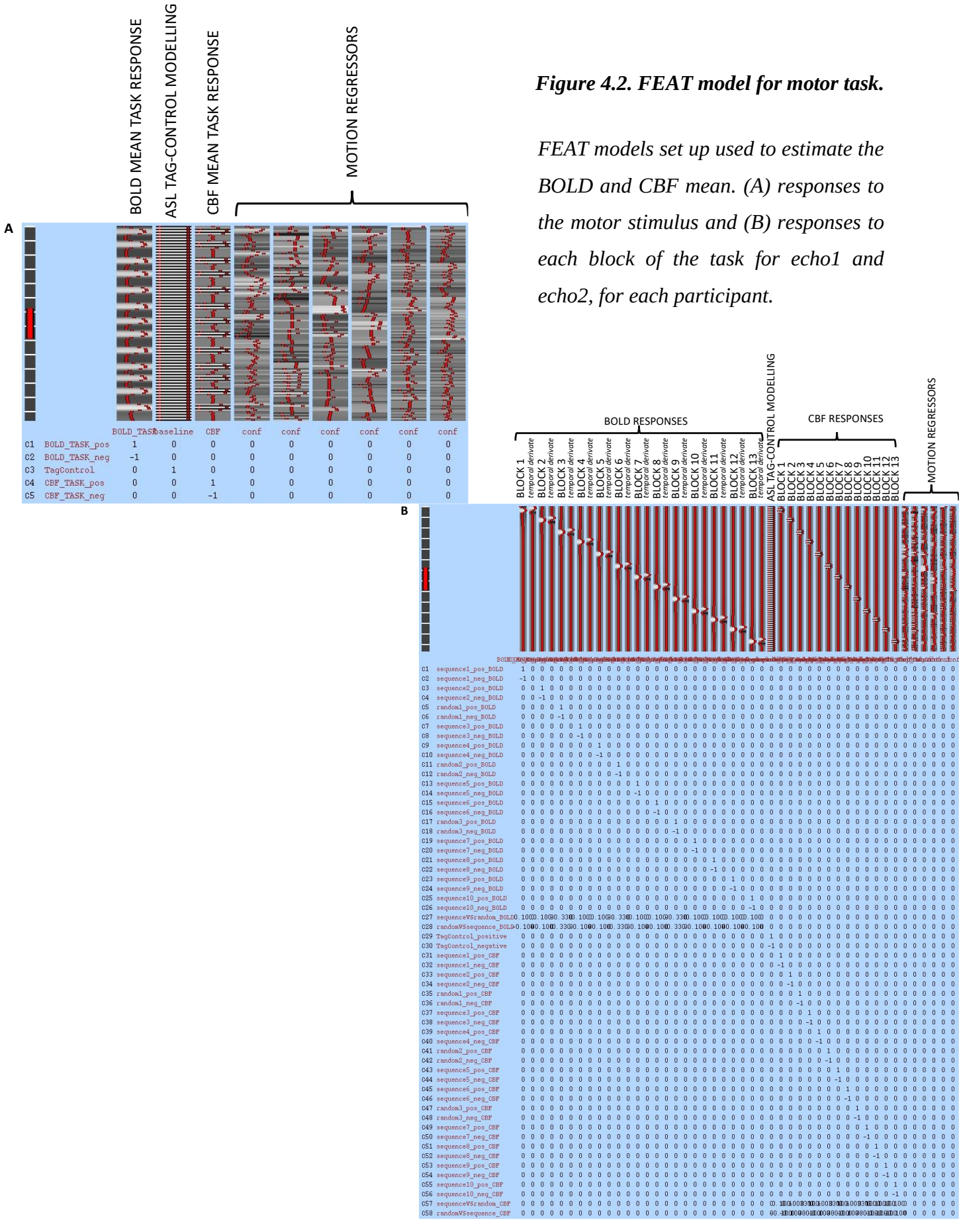

Figure 4.2. FEAT model for motor task.

FEAT models set up used to estimate the BOLD and CBF mean. (A) responses to the motor stimulus and (B) responses to each block of the task for echo1 and echo2, for each participant.

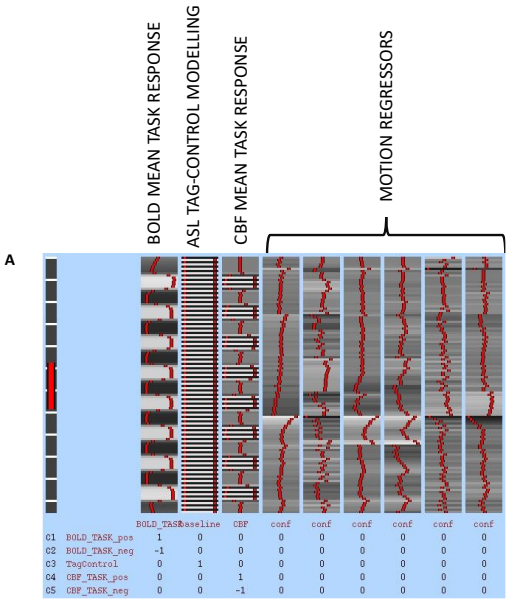

Figure 4.3. FEAT model for visual task.

FEAT models set up used to estimate the BOLD and CBF mean (A) responses to the visual stimulus and (B) responses to each block of the task for echo1 and echo2, for each participant.

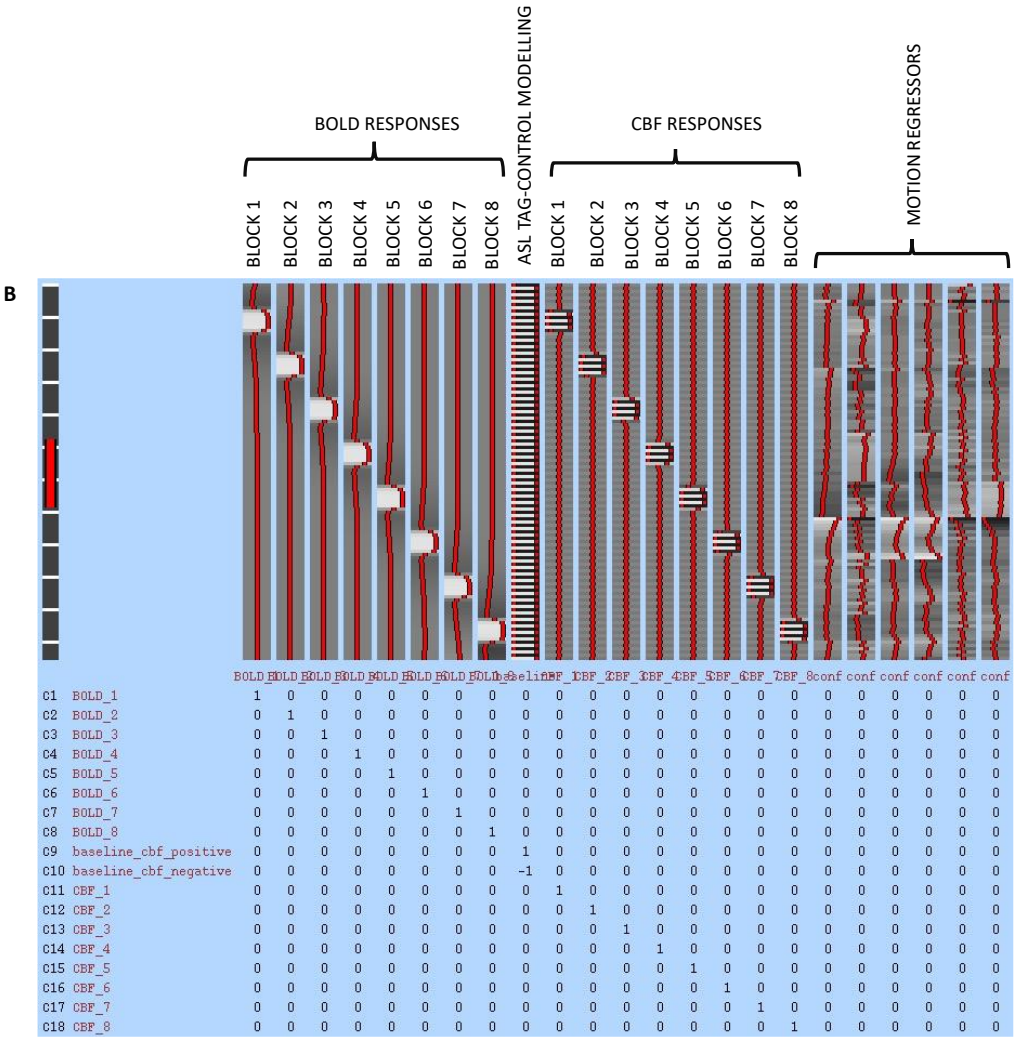

Cluster Analysis and functional ROI definition. BOLD task-response maps were obtained for visual and motor tasks respectively. All the analyses were performed separately for each task. The FSL tool (atlasquery) was used to identify the anatomical regions showing a significant (either positive or negative) BOLD response to the task. For each anatomical region involved in the task, BOLD signal was extracted for each participant. The mean across subjects in each anatomical region was calculated and then fed into a cluster analysis (K-mean) to group regions on the basis of their similarities in BOLD signal time course using RStudio (http://www.rstudio.com/). In order to decide the number of clusters to use in the K-mean analysis we used the elbow method. The elbow method looks at the percentage of variance explained as a function of the number of clusters. This method exists upon the idea that one should choose a number of clusters so that adding another cluster does not give better modelling of the data. The percentage of variance explained by the clusters is plotted against the number of clusters. The first cluster will add much information but at some point the marginal gain will drop dramatically and gives an angle or elbow in the graph, up to the point that the new cluster is very near to some of the already existing clusters (Purnima & Arvind, 2014). The clusters were then intersected with BOLD task-related response map and used as our functional regions of interests (ROIs). For every subject, BOLD and CBF signals were extracted from each ROI and for each block of the task as a fractional change from baseline for BOLD and relative value (CBF/CBF_0) for CBF.

$CMRO_2$ modelling. To model task-induced changes in relative $CMRO_2$ we need an estimation of the factor M in the same ROI, which it is usually computed with the equation proposed by Davis et al. (Davis et al., 1998) (**Equation 4.1**):

$$\frac{CMRO_2}{CMRO_{2_0}} = \left(\frac{CBF}{CBF_0}\right)^{1-\frac{\alpha}{\beta}} \cdot \left(1 - \frac{\frac{\Delta BOLD}{BOLD_0}}{M}\right)^{\frac{1}{\beta}}$$

Equation 4.1. $CMRO_2$ modelling by Davies et. al (1998).

Here, the Δ symbol means change from baseline and the 0 subscript refers to the baseline state. There is a power-law relationship between BOLD and de-oxyhaemoglobin concentration, represented by the β parameter. β varies with field strength and it is dependent on vessel size distribution. It is assumed to be 1.3 at 3T MRI scan (Kennan, Zhong, & Gore, 1994). α is the 'Grubb exponent' and relates the relative increase in CBF to CBV, and it is usually assumed to be 0.38, based on early animal work (Grubb, Raichle, Eichling, & Ter-Pogossian, 1974).
M is a parameter representing the theoretical maximum BOLD response, assuming a washout of de-oxyhemoglobin (dHb) for the baseline state and is estimated by the use of hypercapnic calibration. CO_2 inspiration leads to hypercapnia: blood flow is sensitive to changes in arterial CO_2, but cerebrovascular reactivity to CO_2 is assumed to be isometabolic (i.e., it elicits a purely vascular response through a reduction in dHb).

We actually used the following simplified version of this model for consistency between the model used to estimate absolute (baseline) $CMRO_2$ and that used to estimate task-induced relative changes in $CMRO_2$ (Merola et al., 2016) (**Equation 4.2**):

$$\frac{CMRO_2}{CMRO_{2_0}} = \left(\frac{CBF}{CBF_0}\right)^{1-\theta} \cdot \left(1 - \frac{\frac{\Delta BOLD}{BOLD_0}}{TE \cdot k \cdot [dHB]_0}\right)$$

Equation 4.2. Equation used for $CMRO_2$ modelling.

Where TE is the echo time of the acquisition, κ is a composite calibration parameter that represents the combination of the venous weighted blood volume and water diffusion effects, [dHb] is the de-oxyhemoglobin concentration and θ (assigned a value of 0.06, previously represented by both α and β) is an empirical parameter combining contributions from venous blood volume changes and extra-vascular water diffusion effects.

Absolute $CMRO_2$ was estimated using a forward physiological model using dual-calibrated fMRI data. OEF and CBF (and therefore $CMRO_2$) are quantified within a forward modelling framework (Germuska et al., 2016). End-tidal traces are aligned with the DEXI data via a cross-correlation between $PaCO_2$ (partial pressure of CO_2) and the mean GM ASL signal.

Haemoglobin concentration informs the relationship between the different physiological parameters and their fitting. A non-linear least squares minimisation routine is used to optimise voxel-wise estimates of baseline $D_{C,}$ OEF, CBF and CVR. Absolute baseline $CMRO_2$ is determined by multiplying OEF by O_2 delivery, which is the product of CBF_0 * $CaO_{2.}$ A constant $CMRO_2$ is assumed across periods of normocapnia/normoxia, hypercapnia and hyperoxia. The model development was not the focus of this chapter but the application of this model to investigate neuroplasticity, for a full explanation of the model see (Germuska et al., 2016).

All the calculations to model $CMRO_2$ were performed with SPM12 (www.fil.ion.ucl.ac.uk/spm) and MATLAB (R2015_a, Mathworks Inc., MA, USA). M values were extracted in each functional ROI, and $CMRO_2$ was then estimated both at rest and each task time points in each ROI.

We then performed an ANOVA for each of the parameter (BOLD, CBF and $CMRO_2$) in order to investigate between-group difference both at rest and during task execution, as well as differences in signal changes throughout the task across blocks. All results were corrected for multiple comparisons using Bonferroni correction. Statistical differences were considered significant at $p < 0.05$.

4.3 RESULTS

Demographic, clinical and MRI characteristics. Participants' characteristics are shown in Table 4.1. Patients differed from controls in walking ability only ($t_{(29.832)} = -2.8183$; $p < 0.001$).

TABLE COHORT CHARACTERISTICS			
	PATIENTS	CONTROLS	p
N	23	22	-
Age (years)	35.6±7	34.2±6	0.46
Sex (F/M)	18/5	16/6	0.7533
Education (years)	17.1±1.9	18.1±3.1	0.18
Disease duration (years)	8±4.8	-	-
EDSS (median/iqr)	3.0/1.5	-	-
MSIS-29 scale physical	35.3±15.7	-	-
MSIS-29 scale psychological	17.1±6.4	-	-
9-HPT (dominant) in sec. (across 2 trials) median/iqr	19.9/2.9	19.9/2.8	0.43
T25-FW in sec. (across 2 trials) median/iqr	4.58/0.8	4.1/0.8	0.001*
No. correct responses PASAT 2s	34.7±11.9	36.1±12.5	0.37
No. correct responses PASAT 3s	44.5±12.7	47.9±10.6	0.73
SDMT	59.5±7.3	62.8±9.5	0.22
Normalized GM volume (cm^3)	614.3±52.5	645.9±62.1	0.09
NBV (cm^3)	1133.2±94.1	1198.4±120.2	0.06
T2-hyperintense lesion volume (cm^3)	10.2±9.1	-	-

Table 4.1. Demographic, clinical and MRI characteristics*. Unless otherwise indicated, descriptive statistics are reported as means and standard deviations. For statistical comparisons between the two groups, chi-square was computed for categorical-variables, Kruskall-Wallis test for skewed variables (9-hole peg test, timed-25-foot walk), and unpaired t-tests were used for the rest. p values were considered significant if <0.05 (as highlighted by the stars) adjusted for years of education. Normalized brain and grey matter volume were calculated with SIENAX. Abbreviations: EDSS = Extended Disability Status Scale; MSIS = Multiple Sclerosis Impact Scale; 9-HPT = 9-hole peg test; T25-FW = timed 25-foot walk; PASAT = paced auditory serial addition test; SDMT = Symbol Digit Modalities Test; NBV = Normalised Brain Volume.*

Behavioural Response to Motor Task (Performances improvement). A 2-way ANOVA was performed in order to investigate differences in accuracy and reaction time between patients and controls during task execution. The analysis demonstrated a main effect of block (time) in both accuracy and reaction time ($F_{(8,288)} = 11.67$, $p < 0.001$; $F_{(8,288)} = 10.61$, $p < 0.001$), indicating increasing in performances in controls and patients during task execution. No significant group difference either in the reaction time ($F_{(1,8)} = 3.13$, $p = 0.08$) or in accuracy ($F_{(1,8)} = 0.67$, $p = 0.41$) was observed; as well as no interaction effect (time x group) in both measures was observed (rt: $F_{(8,288)} = 1.27$, $p = 0.25$; accuracy: $F_{(8,288)} = 1.23$, $p = 0.28$); indicating that patients and controls increased in their performances to a similar extent. (**Figure 4.4**).

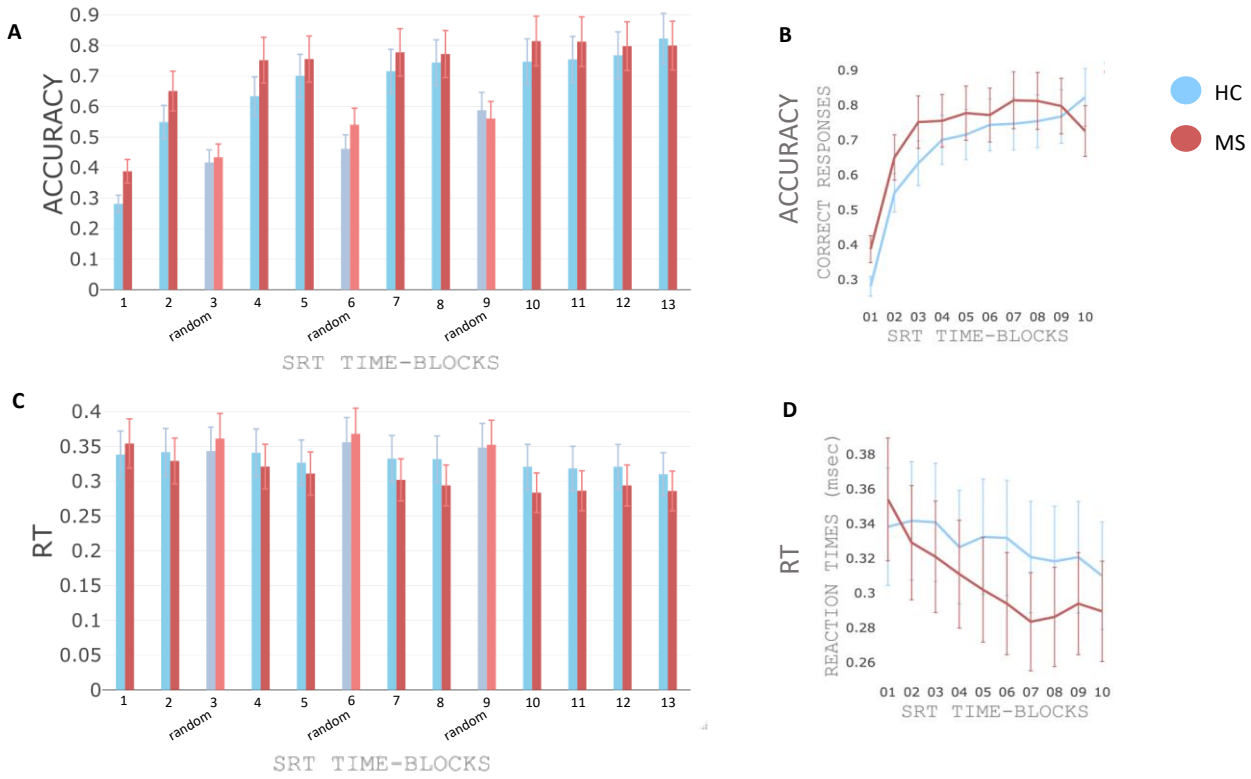

Figure 4.4. Behavioral results. *Performances (rt and accuracy) improve during SRT task execution in both groups (blue: HC; red: MS). (TOP) Increasing in accuracy block by block with (A) and without (B) random blocks. (BOTTOM) Decreasing in RT with (C) and without (D) random blocks.*

FUNCTIONAL ROI DEFINITION AND BOLD, CBF, $CMRO_2$ EXTRACTION

Motor Task. Main areas of positive BOLD activation were found in left/right postcentral gyri, precentral gyri angular gyri, supramarginal gyri, visual areas and insular cortex. De-activation of BOLD associated with task execution was found in left/right cingulate gyri, middle and superior frontal gyri and insular cortex.

'Atlasquery' identified 27 different anatomical areas involved in the task response on the base of the "Harvard-Oxford anatomical atlas". These areas were first thresholded to a probability of 0.40 with 'fslmaths' in order to avoid overlapping among regions and then grouped together on the basis of the similarities of their BOLD timeseries with K-means analysis. To identify the number of clusters required we used the elbow method, yielding 5 as the number of clusters (**Figure 4.5**).

Results from cluster analysis are shown in **Figure 4.5 and 4.6;** cluster 1 shows a positive response to the task and it is formed mainly by motor areas. Cluster 2 and 3 show a negative response to the task. Cluster 2 is formed by frontal medial cortex only. Cluster 3 is formed mainly by higher visual and frontal areas. Cluster 4 shows a positive response to task is formed mainly by lower visual areas and subcortical regions, while cluster 5 shows a negative response to the task and it is formed only by hippocampus. Each cluster constitutes a different region of interest (ROI) for the subsequent analysis.

From each ROI we extracted absolute CBF and $CMRO_2$ values at rest from the dual-calibrated acquisition. Lower CBF in patients compared to healthy controls was found in cluster 1 ($t_{(36)}$=2.45; p=0.03), cluster 3 ($t_{(35)}$=2.7; p=0.01) and cluster 4 ($t_{(35)}$=2.45; p=0.02). Patients

also reported lower baseline $CMRO_2$ compared to controls in the same clusters (cluster 1: $t_{(36)}$=2.7; p=0.01; cluster 3: $t_{(36)}$=2.4; p=0.02; cluster 4: $t_{(36)}$=2.1; p=0.04). **(Figure 4.7).**

We then extracted relative BOLD and CBF changes during task execution from each ROI and we computed the $CMRO_2$ response, relative to baseline. (**Figure 4.8**). We performed a 2way ANOVA in order to investigate between-group differences during adaptation of these measurements across time points (10 SRT blocks).

Results show reduction in activity (main effect of time) across blocks for BOLD, CBF and $CMRO_2$ in cluster 1 (respectively: $F_{(9,315)}$=2.17; p=0.02; $F_{(9,315)}$=5.05; p<0.001; $F_{(9,315)}$=4.62; p<0.001) and cluster 3 (respectively: $F_{(9,315)}$= 6.74; p<0.001; $F_{(9,315)}$=4.8; p<0.001; $F_{(9,315)}$=3.14; p<0.002). Cluster 2 presented a change across time only in BOLD signal ($F_{(9,315)}$=2.22; p= 0.02) but no changes across time was observed in CBF and $CMRO_2$ (respectively: $F_{(9,315)}$=1.22; p=0.27; $F_{(9,315)}$=0.29; p= 0.97). On the other hand, cluster 4 showed changes across time in CBF and $CMRO_2$ ($F_{(9,315)}$=5.19; p<0.001; $F_{(9,315)}$=5.44; p<0.001), but not in BOLD ($F_{(9,315)}$=1.83; p=0.1). Any change across time was reported in cluster 5 (BOLD: $F_{(9,315)}$= 1.28; p= 0.79; CBF: $F_{(9,315)}$= 0.74; p=0.67; $CMRO_2$: $F_{(9,315)}$= 1.28; p=0.24). **(Table 4.2).**

Cluster 3 was the only one which showed differences between group in changes across time (interaction effect) and only in the BOLD response. ($F_{(9,315)}$= 2.88; p=0.002).

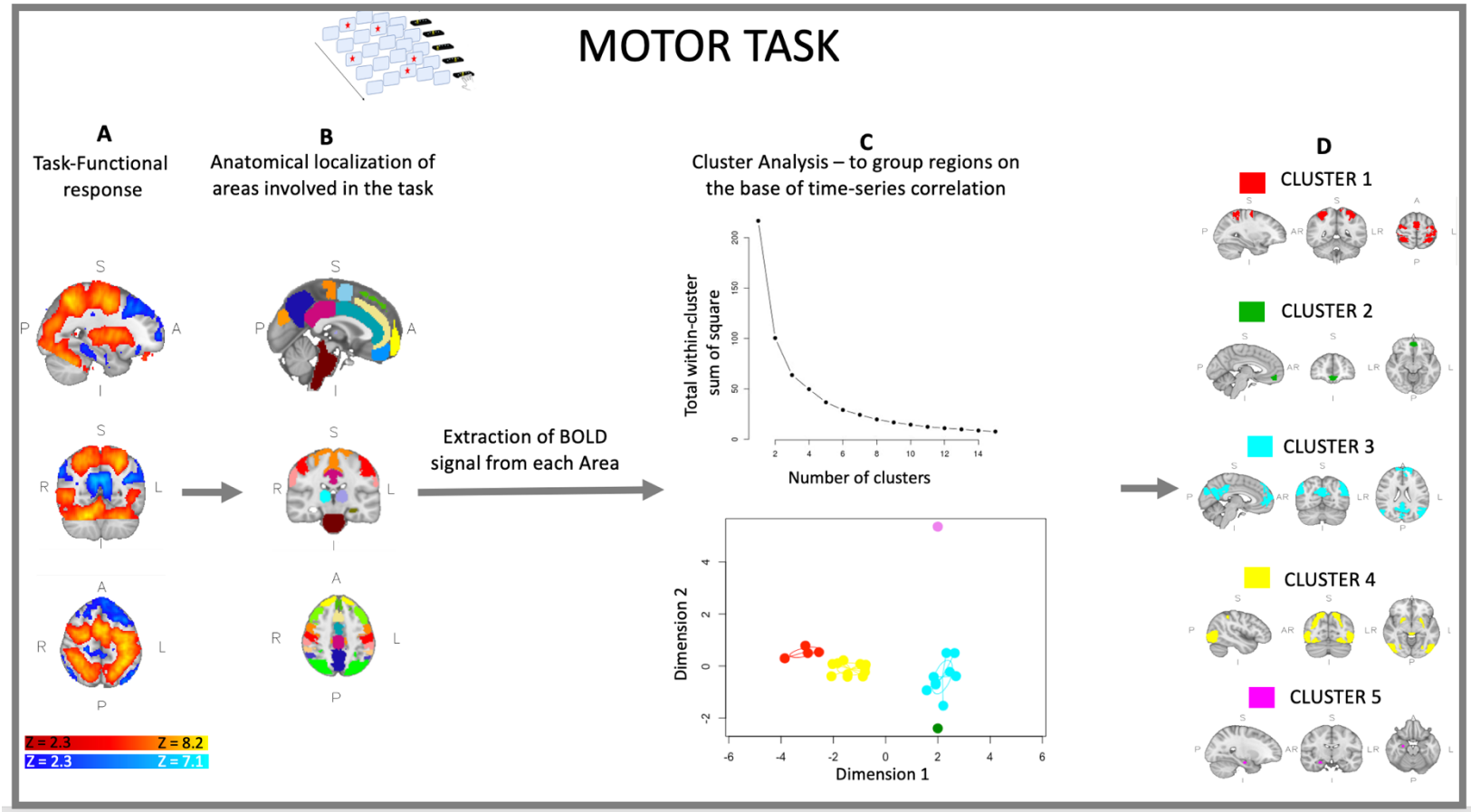

Figure 4.5. Motor task results. *(A) Regions with positive (red) and negative (blue) SRT-related BOLD signal change. (B) Anatomical mask of active regions according to Harvard-Oxford Structural Atlas. (C) Elbow method to pick the number of cluster and cluster analysis to group regions on the bases of their similarity in BOLD signal change throughout the task. Plot shows variance within cluster and distance between clusters. (D) Anatomical areas corresponding to each cluster.*

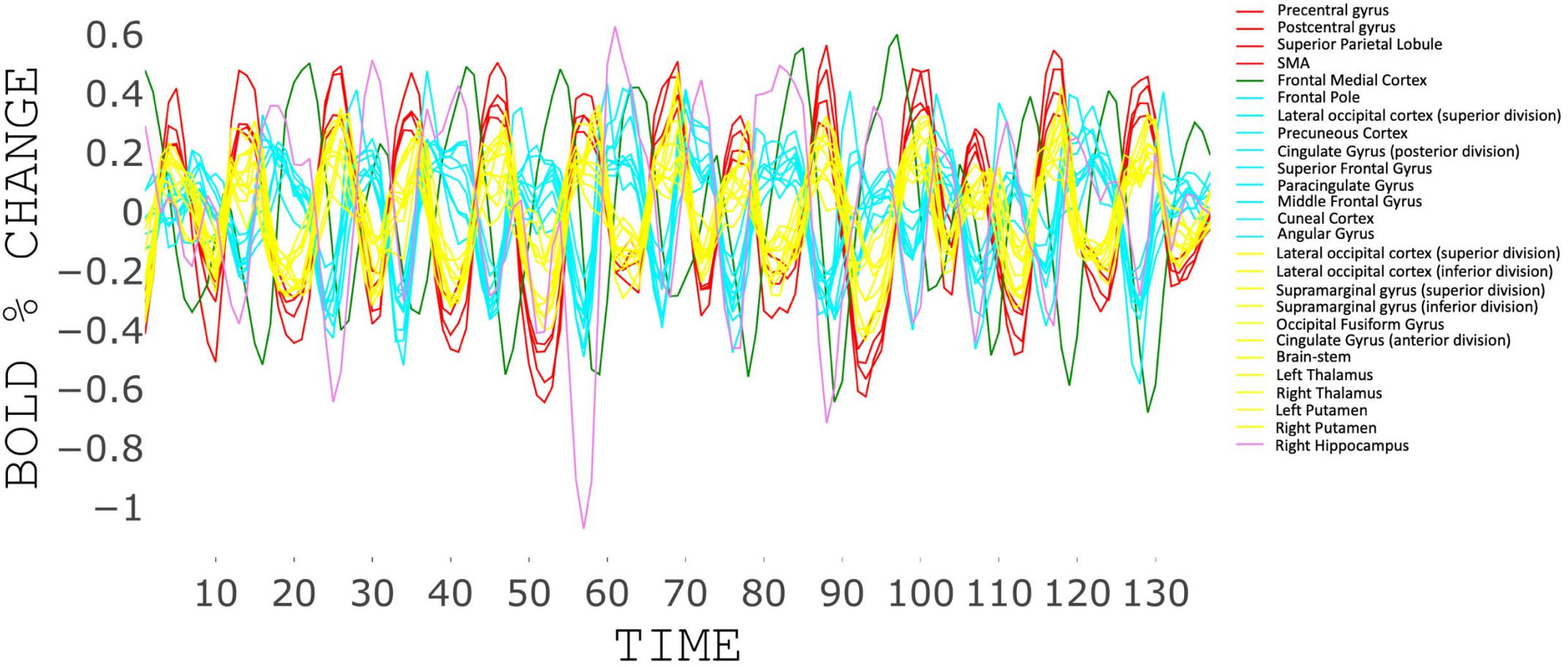

Figure 4.6. Motor task ROI Time Series. *BOLD signal was extracted from each anatomical region involved in SRT task. X axis represents time (1= TR). Y axis represents BOLD percentage change demeaned. Colours represent the outcome of the cluster analysis (red = cluster 1; green = cluster 2; light blue = cluster 3; yellow = cluster 4; violet = cluster 5).*

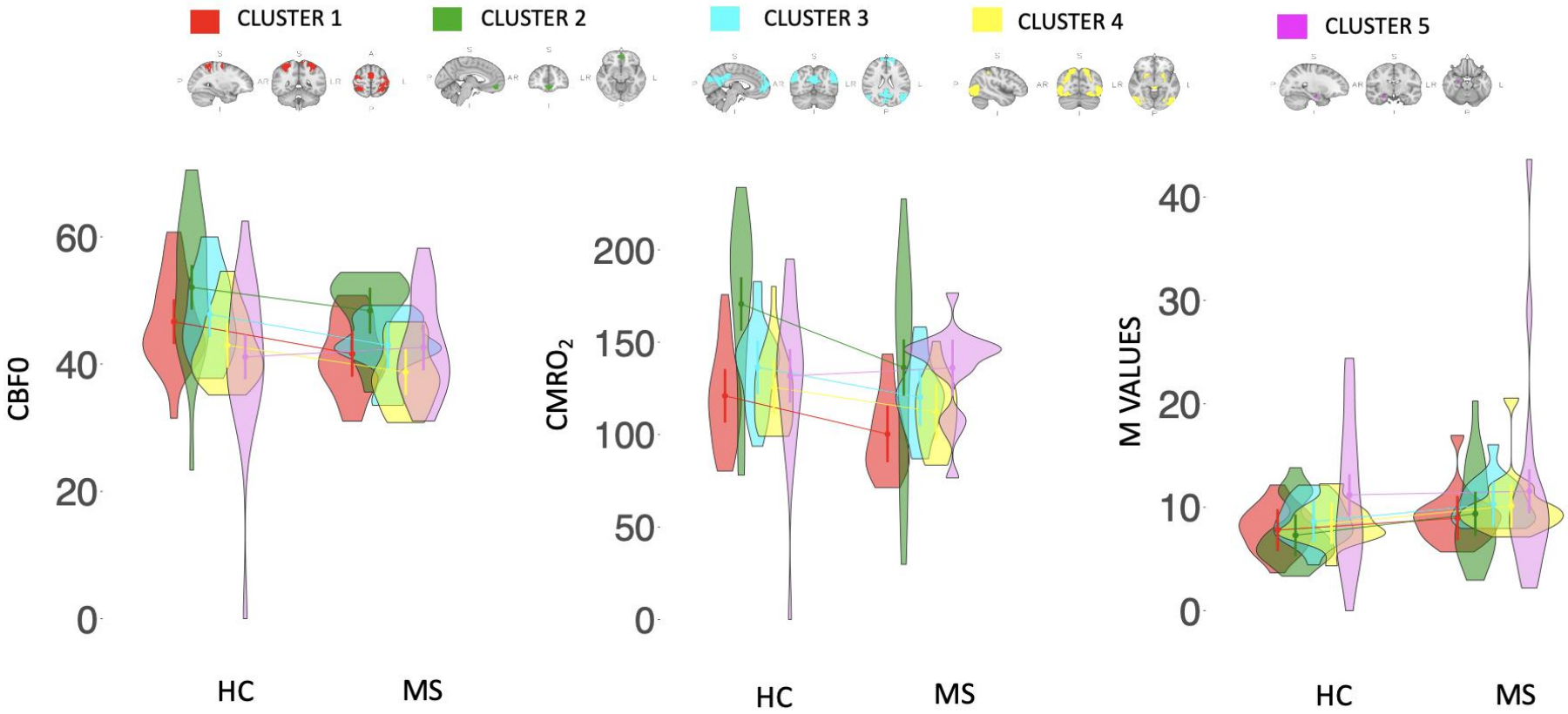

Figure 4.7. Baseline metabolic group differences. *For each ROI involved in SRT task execution, CBF0, $CMRO_2$ and M parameter (mean±sd) were extracted at baseline for both groups.*

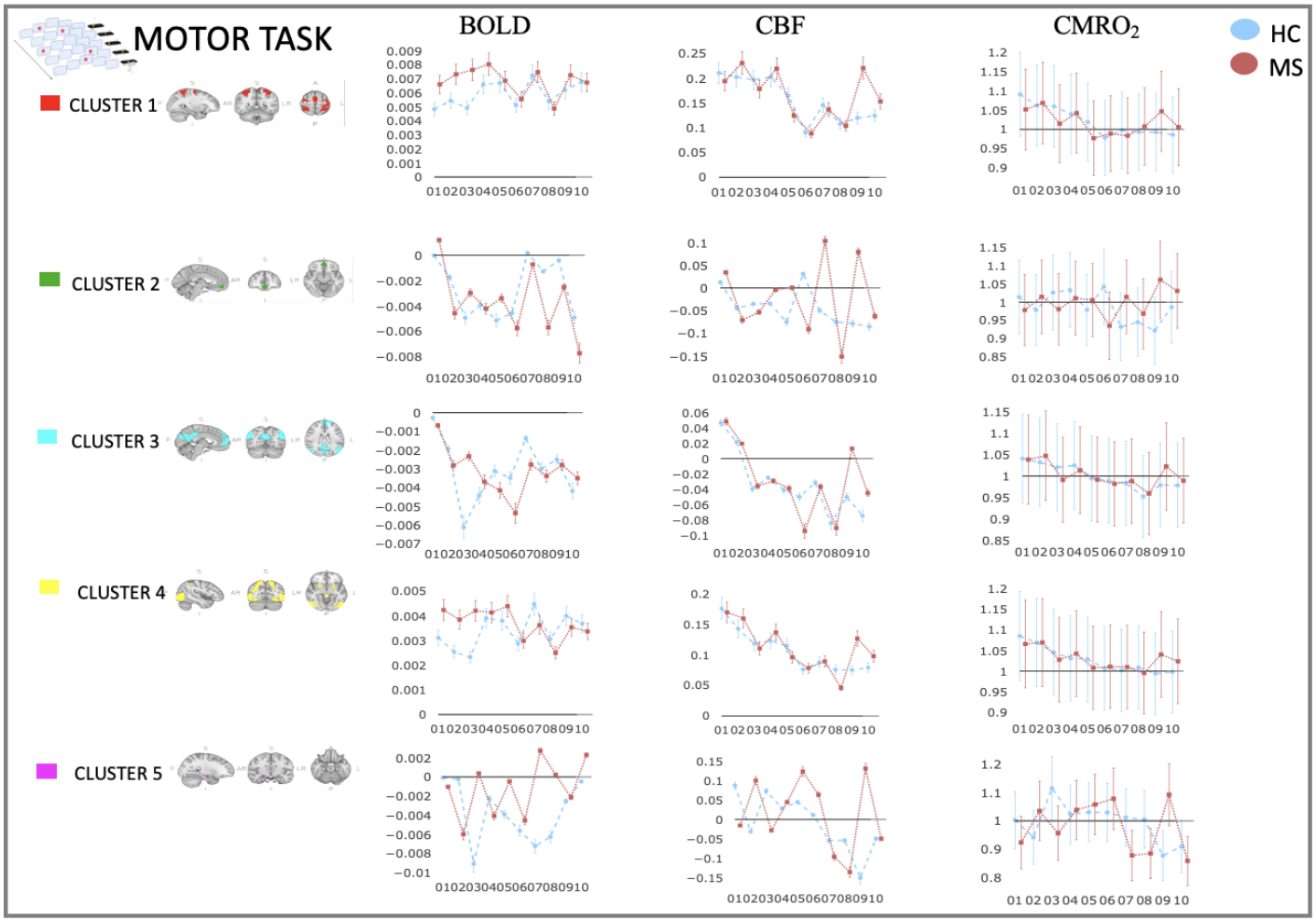

Figure 4.8. SRT Task adaptation. *For each cluster, BOLD, CBF and $CMRO_2$ signals during task execution are plotted. For each block of the experiment mean±sd of activation were extracted. (Blue: HC; Red: MS). Cluster 3 is an example of simultaneously adaptation (main effect of time) of functional, vascular and metabolic responses. On the other hand, Cluster 4 is an example of adaptation (main effect of time) of vascular and metabolic response, but not in the functional.*

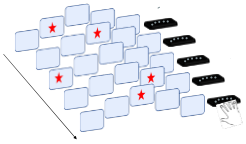

SRT

BOLD

	Main Effect Time	Main effect Group	Interaction Time*Group
CLUSTER 1	**$F_{(9,315)}$ = 2.17; p = 0.02**	$F_{(1,35)}$ = 0.71; p = 0.4	$F_{(9,315)}$ = 0.49; p = 0.48
CLUSTER 2	**$F_{(9,315)}$ = 2.22; p = 0.02**	$F_{(1,35)}$ = 0.11; p = 0.73	$F_{(9,315)}$ = 0.54; p = 0.84
CLUSTER 3	**$F_{(9,315)}$ = 2.88; p < 0.001**	$F_{(1,35)}$ = 0.02; p = 0.88	**$F_{(9,315)}$ = 2.88; p = 0.002**
CLUSTER 4	$F_{(9,315)}$ = 1.83; p = 0.06	$F_{(1,35)}$ = 0.15; p = 0.7	$F_{(9,315)}$ = 1.66; p = 0.1
CLUSTER 5	$F_{(9,315)}$ = 0.60; p = 0.78	$F_{(1,35)}$ = 0.75; p = 0.39	$F_{(9,315)}$ = 1.28; p = 0.24

CBF

	Main Effect Time	Main effect Group	Interaction Time*Group
CLUSTER 1	**$F_{(9,315)}$ = 5.05; p < 0.001**	$F_{(1,35)}$ = 0.13; p = 0.71	$F_{(9,315)}$ = 0.99; p = 0.44
CLUSTER 2	$F_{(9,315)}$ = 1.22; p = 0.27	$F_{(1,35)}$ = 0.51; p = 0.47	$F_{(9,315)}$ = 0.22; p = 1.32
CLUSTER 3	**$F_{(9,315)}$ = 4.8; p < 0.001**	$F_{(1,35)}$ = 0.04; p = 0.83	$F_{(9,315)}$ = 0.55; p = 0.83
CLUSTER 4	**$F_{(9,315)}$ = 5.19; p < 0.001**	$F_{(1,35)}$ = 0.05; p = 0.8	$F_{(9,315)}$ = 0.57; p = 0.82
CLUSTER 5	$F_{(9,315)}$ = 0.80; p = 0.67	$F_{(1,35)}$ = 0.16; p = 0.68	$F_{(9,315)}$ = 0.8; p = 0.61

$CMRO_2$

	Main Effect Time	Main effect Group	Interaction Time*Group
CLUSTER 1	**$F_{(9,315)}$ = 4.62; p < 0.001**	$F_{(1,35)}$ = 0.05; p = 0.82	$F_{(9,315)}$ = 1.16; p = 0.31
CLUSTER 2	$F_{(9,315)}$ = 0.29; p = 0.97	$F_{(1,35)}$ = 0.26; p = 0.61	$F_{(9,315)}$ = 1.1; p =0.36
CLUSTER 3	**$F_{(9,315)}$ = 3.14; p = 0.001**	$F_{(1,35)}$ = 0.04; p = 0.84	$F_{(9,315)}$ = 0.41; p = 0.92
CLUSTER 4	**$F_{(9,315)}$ = 5.44; p < 0.001**	$F_{(1,35)}$ = 0.07; p = 0.78	$F_{(9,315)}$ = 0.94; p = 0.48
CLUSTER 5	$F_{(9,315)}$ = 1.28; p = 0.24	$F_{(1,35)}$ = 0.09; p = 0.75	$F_{(9,315)}$ = 1.46; p = 0.15

Table 4.2. Adaptation of functional, vascular and metabolic response during SRT and between group difference*. Significant statistic is highlighted in bold. Results were corrected for multiple comparisons across regions.*

Visual Task. Main areas of positive BOLD activation were found in left/right postcentral gyri, precentral gyri and visual areas. De-activation of BOLD associated with task was found in left/right cuneal cortex, intracalcarine sulci and angular gyri.

Atlasquery identified 23 different anatomical areas involved in the task response on the base of the "Harvard-Oxford anatomical atlas". These areas were first thresholded to a probability of 0.40 with fslmaths in order to avoid overlapping among regions and then grouped together on the base of their functional similarities with K-means analysis. To identify the number of clusters required we used the elbow method yielding 5 as the number of clusters (**Figure 4.9**). Results from cluster analysis are shown in **Figure 4.9 and 4.10**; cluster 1 shows a negative response to task and it is formed by higher visual areas. Cluster 2, 3 and 4 show a positive response to task. Cluster 2 is formed only by fusiform gyrus. Cluster 3 is formed occipital areas. Cluster 4 is formed by frontal, temporal and parietal areas. Cluster 5 shows a negative response to task and it is formed by subcortical regions and areas involved in the attention processes. Each cluster constitutes a different region of interest (ROI) for the subsequent analysis

From each ROI we extracted absolute CBF and $CMRO_2$ values at rest and we found a reduction in resting CBF in cluster 4 ($t_{(42)}$=2.2; p=0.03) and cluster 5 ($t_{(42)}$=2.28; p=0.03) in patients compared to controls. No significant differences in resting $CMRO_2$ were observed (**Figure 4.11**).

We then extracted BOLD and CBF measurements during task execution from each ROI and we computed $CMRO_2$ response. (**Figure 4.12**). We performed a 2way ANOVA in order to investigate between-group differences during adaptation of these measurements across time points (8 blocks). None of the cluster shown significant changes across time in none of the measures. Furthermore, we did not observe any between-group differences. (**Table 4.3**).

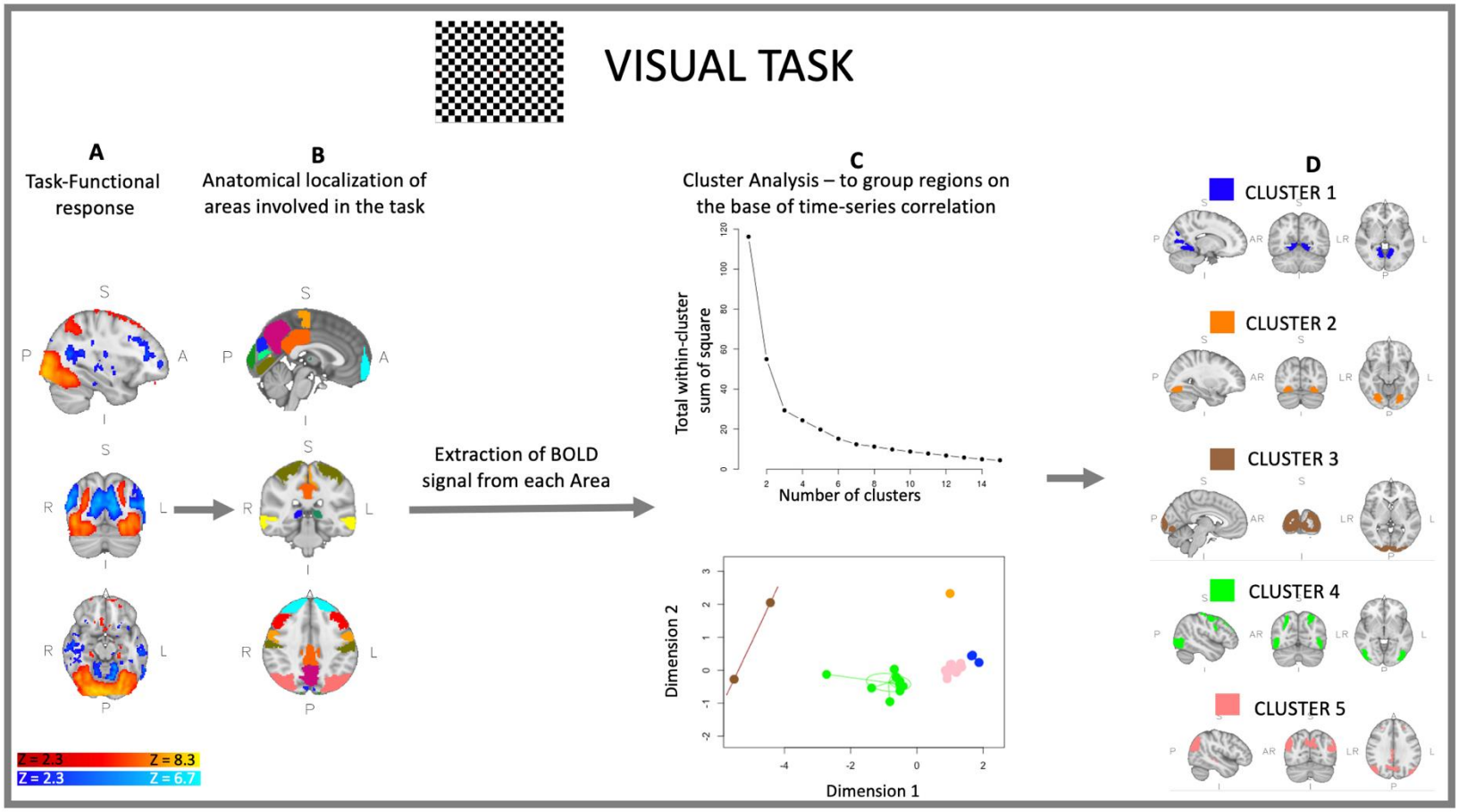

Figure 4.9. Visual task results. *(A). Regions with positive (red) and negative (blue) checkerboard stimulation BOLD signal change. (B). Anatomical mask of active regions according to Harvard-Oxford Structural Atlas. (C). Elbow method to pick the number of cluster and cluster analysis to group regions on the bases of their similarity in BOLD signal change throughout the task. Plot shows variance within cluster and distance between clusters. (D) Anatomical areas corresponding to each cluster.*

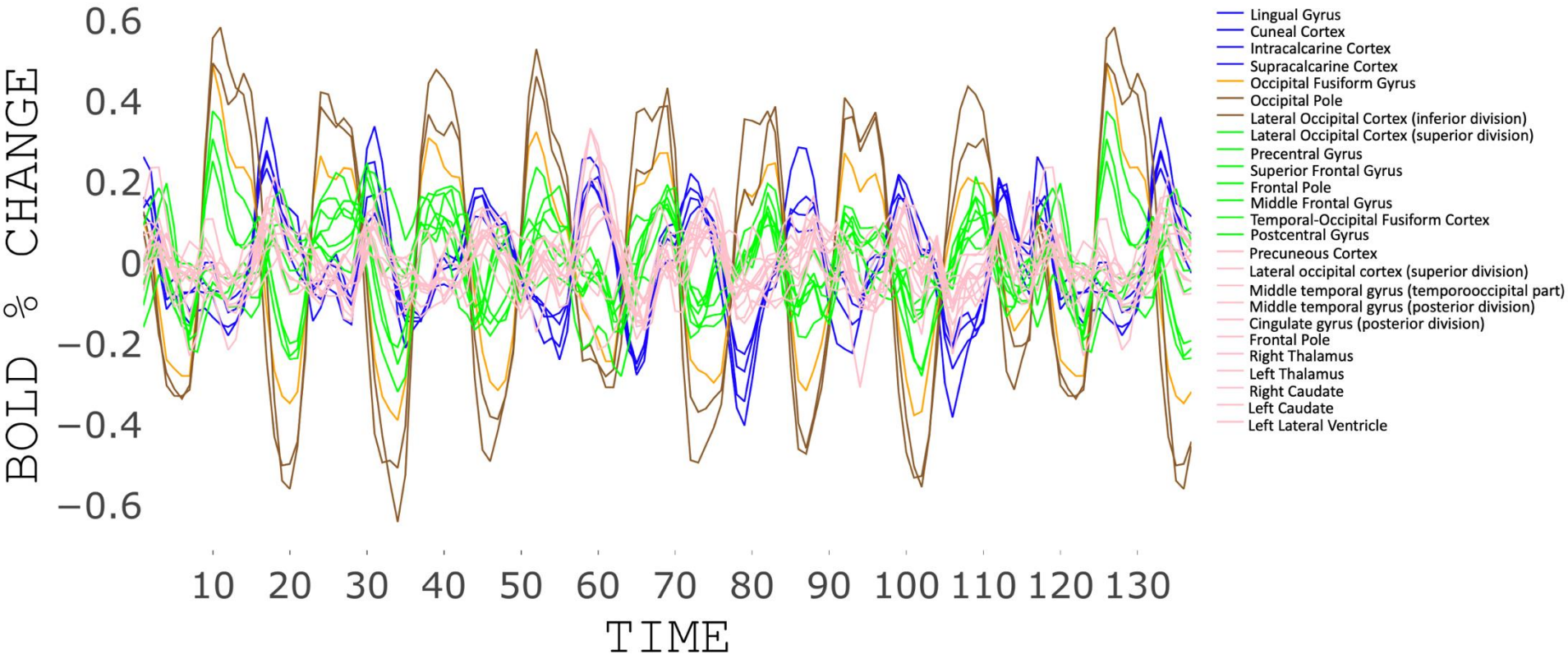

Figure 4.10. Visual task results. *BOLD signal was extracted from each anatomical region involved in SRT task. X axis represents time (1= TR). Y axis represents BOLD percentage change demeaned. Colours represent the outcome of the cluster analysis (red = cluster 1; green = cluster 2; light blue = cluster 3; yellow = cluster 4; violet = cluster 5)*

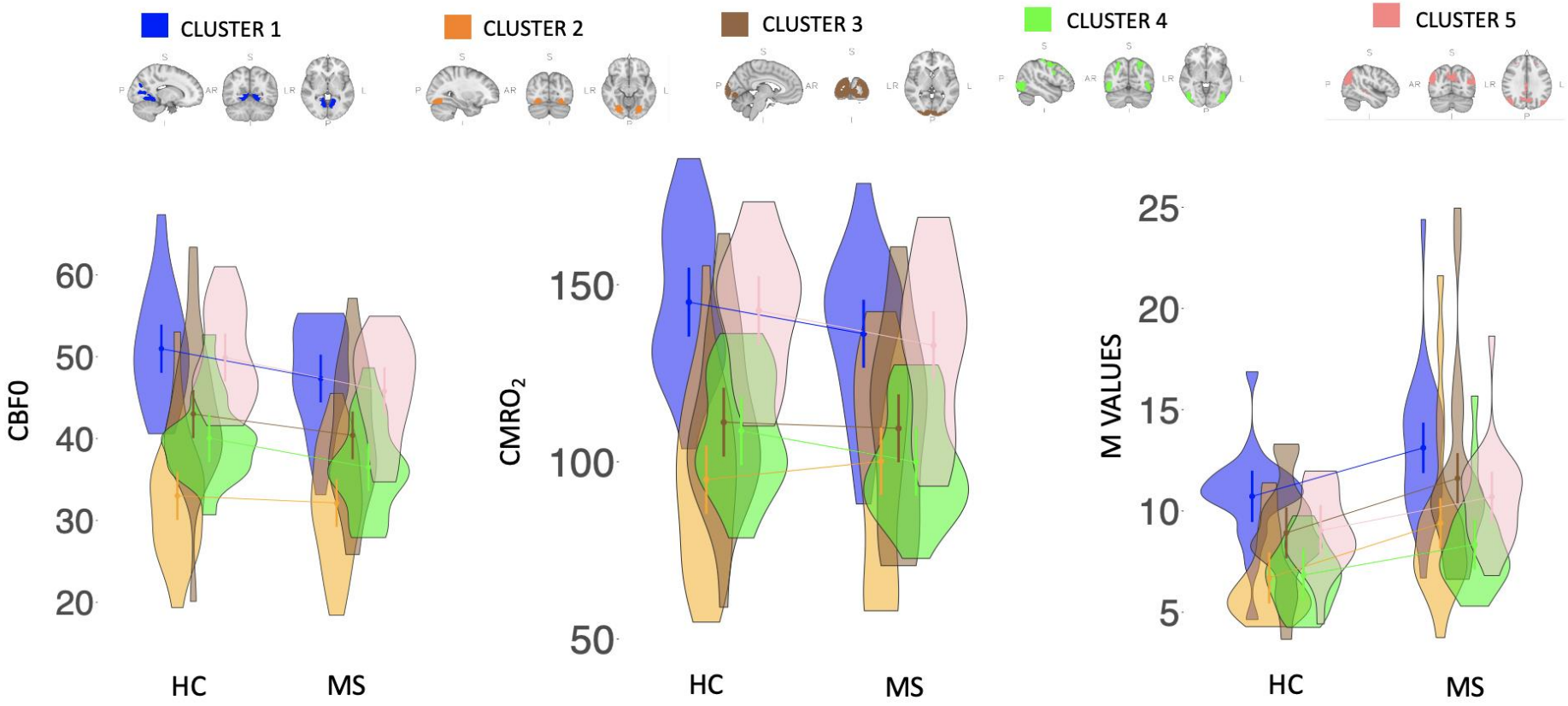

Figure 4.11. Baseline metabolic group differences. *For each ROI involved in checkerboard stimulation, CBF0 and $CMRO_2$ and M parameter (mean±sd) were extracted at baseline for both groups.*

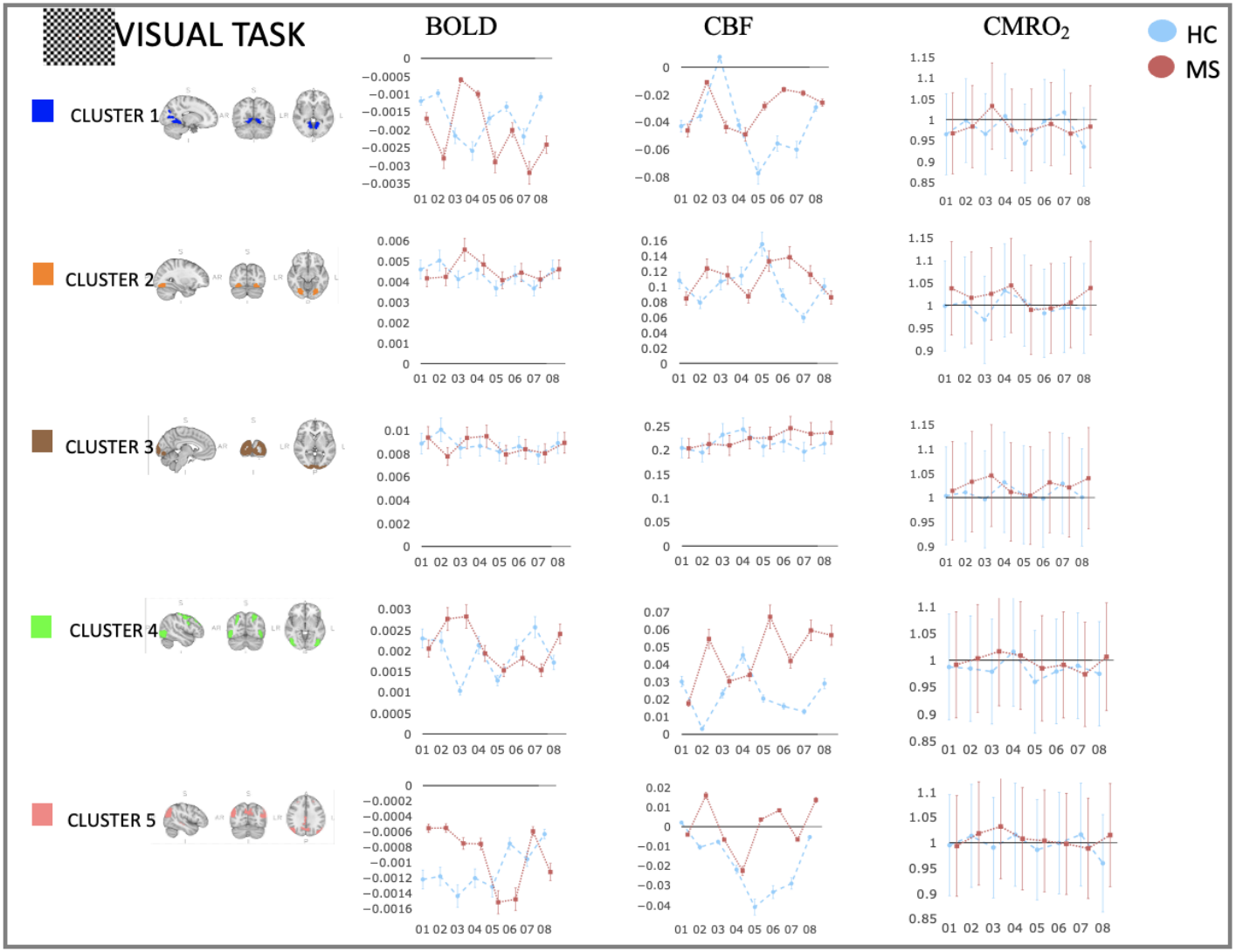

Figure 4.12. Visual task adaptation. *For each cluster, BOLD, CBF and $CMRO_2$ signals during task execution are plotted. (Blue: HC; Red: MS).*

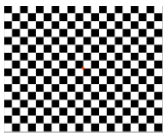

CHECKERBOARD

	Main Effect Time	Main effect Group	Interaction Time*Group
BOLD			
CLUSTER 1	$F_{(7,287)} = 0.93$; p = 0.47	$F_{(1,41)} = 0.53$; p = 0.46	**$F_{(7,287)} = 2.07$; p = 0.04**
CLUSTER 2	$F_{(7,287)} = 0.80$; p = 0.57	$F_{(1,41)} = 0.04$; p = 0.83	$F_{(7,287)} = 0.67$; p = 0.69
CLUSTER 3	$F_{(7,287)} = 0.82$; p = 0.56	$F_{(1,41)} = 0.001$; p = 0.96	$F_{(7,287)} = 0.98$; p = 0.44
CLUSTER 4	$F_{(7,287)} = 0.72$; p = 0.64	$F_{(1,41)} = 0.17$; p = 0.67	$F_{(7,287)} = 1.39$; p = 0.2
CLUSTER 5	$F_{(7,287)} = 0.43$; p = 0.87	$F_{(1,41)} = 0.24$; p = 0.62	$F_{(7,287)} = 0.82$; p = 0.57
CBF			
	Main Effect Time	Main effect Group	Interaction Time*Group
CLUSTER 1	$F_{(7,287)} = 0.52$; p = 0.81	$F_{(1,41)} = 0.4$; p = 0.52	$F_{(7,287)} = 1.01$; p = 0.42
CLUSTER 2	$F_{(7,287)} = 1.1$; p = 0.36	$F_{(1,41)} = 0.14$; p = 0.7	$F_{(7,287)} = 1.13$; p = 0.34
CLUSTER 3	$F_{(7,287)} = 0.84$; p = 0.54	$F_{(1,41)} = 0.1$; p = 0.74	$F_{(7,287)} = 0.77$; p = 0.61
CLUSTER 4	$F_{(7,287)} = 0.44$; p = 0.87	$F_{(1,41)} = 3.28$; p = 0.07	$F_{(7,287)} = 1.23$; p = 0.28
CLUSTER 5	$F_{(7,287)} = 0.82$; p = 0.56	$F_{(1,41)} = 1.81$; p = 0.18	$F_{(7,287)} = 0.72$; p = 0.65
$CMRO_2$			
	Main Effect Time	Main effect Group	Interaction Time*Group
CLUSTER 1	$F_{(7,287)} = 1.41$; p = 0.19	$F_{(1,41)} = 0.14$; p = 0.71	**$F_{(7,287)} = 2.07$; p = 0.04**
CLUSTER 2	$F_{(7,287)} = 1.74$; p = 0.09	$F_{(1,41)} = 3.4$; p = 0.07	$F_{(7,287)} = 1.07$; p = 0.37
CLUSTER 3	$F_{(7,287)} = 0.6$; p = 0.75	$F_{(1,41)} = 1.04$; p = 0.31	$F_{(7,287)} = 1.78$; p = 0.09
CLUSTER 4	$F_{(7,287)} = 1.61$; p = 0.13	$F_{(1,41)} = 2.64$; p = 0.11	$F_{(7,287)} = 1.02$; p = 0.41
CLUSTER 5	$F_{(7,287)} = 0.38$; p = 1.06	$F_{(1,41)} = 1.1$; p = 0.29	$F_{(7,287)} = 1.9$; p = 0.06

Table 4.3. Adaptation of functional, vascular and metabolic response during checkerboard stimulation and between group difference. *Significant statistic is highlighted in bold. Results were corrected for multiple comparisons across regions*

4.4 DISCUSSION

The aim of this study was to understand the changes in brain energetics underlying task adaptation and their alteration in MS, and to investigate physiological measures (such as blood flow and oxygen consumption) as methods to characterise brain metabolism sub-serving neuroplasticity by comparison to use of BOLD fMRI signal alone. Overall, despite baseline metabolic reductions shown at rest by MS patients, they were able to use a similar increase in oxygen consumption as healthy volunteers to perform the motor and visual tasks.

Brain networks performing visual and motor tasks. Here we developed a new pipeline, which involved the use of cluster analysis to group regions on the basis of their functional similarities, in order to treat the brain as a network. We ended up with clusters that represent different cognitive functions; moreover, areas might belong to the same cluster independently of their anatomical localizations, meaning that they may be working together to perform the task. Cluster 1 and 4, involved in motor task execution show a positive response to the task and this is in line with previous studies reporting a cortical/subcortical activation during the execution of sequence learning task, mainly motor and visual areas (Robertson, 2007).

The remain clusters are associated with negative response to task. Specifically, cluster 3 recalls the default mode network, which is known to be deactivated during the execution of a task (Raichle et al., 2001). In the visual task, cluster 4 recalls the dorsal attention network (Fox, Corbetta, Snyder, Vincent, & Raichle, 2006) indicating a main recruitment of attentive processes during checkerboard stimulation.

Despite the fact that most of the studies on brain plasticity have focused their attention on localised changes in the brain, it is widely known that the brain acts as a network in order to perform demanding tasks (Dayan & Cohen, 2011; Halsband & Lange, 2006; Tardif et al.,

2016); and this is consistent with our results. The employed analysis highlights the need of treating the brain as a network when studying neuroplasticity. Furthermore, our pipeline helps reduce the problem of multiple comparisons which is very often found in fMRI plasticity studies. It allows us to take into account a number of anatomical regions involved in task execution within a limited number of regions of interest.

Metabolic impairment in MS patients is masked by task-execution. We found a difference between MS patients and healthy controls in baseline CBF and $CMRO_2$ in some of task-involved areas, which suggests an underlying metabolic impairment in people with MS.

Motor, visual, frontal and subcortical areas involved in motor task execution showed between-group differences in baseline perfusion and oxygen metabolism; whereas frontal, parietal and subcortical regions stimulated by the visual task presented only perfusion reductions, without significant baseline reductions in oxygen consumption. These finding may suggest that oxygen metabolism impairment is not secondary to the blood flow disruption.

Previous studies have reported metabolic impairment in MS (Ge et al., 2012), but their method provides only one measurement for the entire brain. Here, we were able to estimate $CMRO_2$ separately for each ROI and also to investigate between-group differences within each ROI.

Furthermore, we observed between-group differences in some ROIs but not in others; indicating that the metabolism is not impaired in the entire brain to the same extent. An interesting hypothesis is that metabolic impairment follows the same pattern of the neurodegenerative process that leads to lesions in the brain: lesion genesis is heterogenous across patients with some part of the brain where lesions are visible and others completely healthy (Lee et al., 1999). Furthermore, it has been suggested that the metabolic impairment could happen before the neurodegeneration as a reflection of inflammation (Marshall et al., 2014). Marshall et al. found a global cerebrovascular reactivity (CVR) impairment in MS

patients, which is the capacity of cerebral circulation to match blood supply to metabolic demand, and they argued that inadequate blood flow to neurons due to impaired CVR can cause a chronic state of hypoxia leading to neurodegeneration. Also, reduced arterial reactivity leads to impaired perfusion, resulting in hypoxia, development of lesions, neurodegeneration and cognitive dysfunction. Moreover, evidence from MRI and histologic studies shows that lesions in MS are found in areas with the lowest blood perfusion, the so-called watershed zones (Haider et al., 2016; Holland et al., 2012; Narayana et al., 2014). Comparably, MS animal models tend to develop demyelinating lesions in areas with the worst blood supply (Desai et al., 2016). However, more longitudinal studies are needed to test the hypothesis of energy impairment as a trigger for neurodegeneration in MS.

We did not find between-group difference during task execution either in performances or in MRI related measures. The result indicates a preserved ability of our cohort of patients with MS to use energy in a similar way as healthy volunteers despite the inflammation and the initial metabolic impairment. This result could be explained by the non-severe cohort that we recruited for this study. Our group of patients was a relatively stable group (as shown by the inclusion criteria and the demographic/clinical table) meaning that MS patients are very similar to healthy controls and they could be in an early stage of disease, or at least have comparatively little accumulated damage. We speculate that our cohort is in a kind of transition phase to 'metabolic hypoxia', where the oxygen needed for computing the task may be available, but cells and tissues are unable to use it (Aboul-Enein & Lassmann, 2005; Trapp & Stys, 2009). Further studies should replicate our study including a more severe cohort. Additionally, this preserved ability could be exploited in training studies targeting to probing recovery and improving metabolic impairment with the aim of exploring the potential role of the training in

slowing down the degenerative process alongside with cerebral perfusion as a potential modulator of the pathogenic and/or reparative processes in inflammatory lesions.

SRT task shows adaptation processes as investigated with calibrated fMRI. The imaging results from SRT suggest adaptive processes, through a decreasing of signal throughout the execution of the task, principally in CBF and $CMRO_2$ and less evident with BOLD alone. Despite previous studies have shown a similar adaptation of the response also in a visual checkerboard task (Janz, Heinrich, Kornmayer, Bach, & Hennig, 2001), we were not able to detect it. This could be because the length of the stimulation was short, compared to previous studies (Janz et al., 2001). Furthermore, checkerboard stimulation is a less cognitive-demanding task compared to SRT (Engel, Glover, & Wandell, 1997; Grafton, Hazeltine, & Ivry, 1995); as confirmed from our cluster analysis, where a larger portion of the brain was actively involved to performed the motor task compared to the visual task. It is worth noting that the checkerboard is a passive stimulation of the visual system, whereas the SRT requires an active response from the subject along with evidence of behavioural adaptation. Further studies are needed in order to generalize our motor results to other cognitive domains.

Different physiological mechanisms contribute to neuroplasticity mechanisms. We investigated for the first time the vascular and metabolic correlates of task adaptation and we showed differences in signal adaptation among different physiological measurements. The result indicates that calibrated fMRI can be employed to study simultaneously different physiological aspects of neuroplasticity: the blood supply (CBF) and rate of oxygen consumption ($CMRO_2$).

As shown by **Figure 4.8**, we concurrently observed a negative BOLD response while CBF shows a positive response at the beginning of the task in cluster 3. Previous studies shown a concomitance among the negative BOLD and negative CBF responses (Shmuel et al., 2002). The exact physiological origin of the negative hemodynamic response is poorly understood and it can be described by many independent mechanisms: an increase in neuronal activity and oxygen consumption independently of CBF increase or a decrease in CBF due to neural inhibition caused by an adjacent activated cortical region. A reduction in CBF due to vasoconstriction without neural inhibition or due to a decrease in neuronal activity with a lesser reduction in $CMRO_2$, resulting in an increase of OEF. A decrease of CBF in the superficial cortical layers accompanied by an increase of CBV in deeper layers (Ma et al., 2016; Mullinger, Mayhew, Bagshaw, Bowtell, & Francis, 2014). Further studies are needed to discern among all the eventual physiological mechanisms that contribute to the observed discrepancy. Furthermore, the significant adaptation shown by CBF and $CMRO_2$ (**Figure 4.8 – Cluster 4**) but not by BOLD means a decreasing of vascular and metabolic response that is not detectable by BOLD alone. The opposite result was also observed in cluster 2 (**Figure 4.8 – Cluster 2**): a significant BOLD decreasing, but stable CBF and $CMRO_2$; that could be interpretable as a decreasing in the functional response that is not coupled with changes in vascular and metabolic responses. Given the complexity of the BOLD signal and tissue processes associated with brain activity, its temporal features, such as signal adaptation during stimulation or signal reduction after the stimulation, cannot be taken as a direct evidence of neuronal adaptation or post-stimulation deactivation (Havlicek, Ivanov, Roebroeck, & Uludağ, 2017). For the same reason, advanced MRI techniques could be more reliable in assessing functional changes observed during task execution (Tardif et al., 2016).

Strengths and limitations of methods. Here we presented one of the first application of calibrated fMRI in MS populations to investigate brain energy supporting neuroplasticity. It is worth noting that the validity of the modelling in patients groups is still under investigation, given that the modelling assumptions may need further validation (Germuska & Wise, 2018). Therefore, parameters estimation may not be accurate as for the healthy volunteers.

Furthermore, some noise in the data could lead to the big error bars observed in $CMRO_2$ measurement (**Figure 4.8** and **4.12**). Given the nature of the equation to estimate $CMRO_2$, the values in the error bars could be attributed to heterogenous M values, especially in the visual cortex. One hypothesis could also be a huge variability between the subjects, but since this variability is not observed in other MRI or behavioural measures, we feel confident to exclude this hypothesis.

Further studies are needed to better validate the application of calibrated fMRI in clinical populations, and different analysis approaches could cope with the noise of the data.

CONCLUSION

To the best of our knowledge, this is the first study investigating the neural energetics underlying brain plasticity. Despite the inflammation and the lower CBF and $CMRO_2$ reported at baseline, MS patients showed similar behavioural performance, functional, vascular and energetic adaptation as controls.

Furthermore, the functional, vascular and energetic changes during task execution was different in distinctive areas of the brain; highlighting the importance of treating the brain as a network.

In the end, we highlighted the importance of using calibrated MRI techniques, rather than BOLD fMRI alone, to study simultaneously different physiological mechanisms involved in brain plasticity.

CHAPTER 5

A pipeline to investigate the feasibility of mapping brain oxygen metabolism at a voxel-wise level during task execution in MS and healthy brain

ABSTRACT

Relative changes in the cerebral metabolic rate of oxygen consumption ($CMRO_2$) can be estimated using calibrated fMRI, which uses ASL and blood gas manipulation to assess the blood flow and metabolic contributions to the BOLD response. In neuroinflammatory conditions such as multiple sclerosis (MS), where the coupling between neural activity and the vascular signal may be affected, the quantification of $CMRO_2$ may offer more biologically-relevant information on the state of brain tissue than the BOLD signal alone. Previous studies investigated oxygen metabolism in response to tasks within BOLD signal defined regions of interests (ROIs). But changes in energy requirements may not be wholly detectable based on BOLD signal alone. Therefore, an estimation of $CMRO_2$ at a voxel-level would be advantageous. In the previous chapter a ROI-based analysis was performed; whereas this chapter aims to explore the feasibility of a voxel-wise approach with the same data.

Specifically, we aim to (I) build an approach to investigate $CMRO_2$ on a voxel-by-voxel basis during the execution of task in MS patients and healthy controls (HC) and (II) to map between-group differences in changes in oxygen metabolism in task-related regions.

23 MS patients and 22 matched controls underwent 3T MRI that included a multiparametric dual-calibrated fMRI method to map baseline (absolute) brain oxygen consumption and to provide the calibration parameter (M) for estimating relative changes in oxygen consumption. The same acquisition scheme was used during the performance of a serial reaction time task and the stimulation with a visual checkerboard.

In order to estimate relative $CMRO_2$ on a voxel-wise basis for each subject, BOLD, CBF and M maps were first registered to MNI standard space and then $CMRO_2$ was calculated with SPM. Permutation tests were used to (I) investigate changes of relative $CMRO_2$ during task execution and (II) localise differences at the group level between HC and MS patients.

Our results show a good anatomical correspondence between BOLD and CBF maps and mean $CMRO_2$ consumption during task-execution calculated with our new pipeline indicating the feasibility of estimating oxygen metabolism voxel-by-voxel. Furthermore, HC and MS showed a similar $CMRO_2$ response to the task; although we observed decrease over time of positive task-induced $CMRO_2$ response in healthy volunteers only, suggesting a block to block reduction of energy consumption. Our results need to take into account potential methodological confounders, but overall they represent a methodological step forward when seeking to understand functionality and dysfunctionality of tissue energetics by demonstrating feasibility of analysis at a voxel-wise level.

KEY WORDS

Quantitative fMRI - Brain Metabolism – $CMRO_2$ – MS – Brain physiology

5.1 INTRODUCTION

The brain depends mainly on oxygen and glucose to meet its energy needs and relative changes in the cerebral metabolic rate of oxygen consumption ($CMRO_2$) provide a direct, quantitative measure of the brain's energy utilization and represents an important marker of brain tissue viability and function. While the precise cellular mechanisms relating neuronal signalling and cerebral metabolism are still a topic of investigation, it is known that most of the brain energy is devoted to support ongoing signalling process and to preserve membrane potentials (Attwell & Laughlin, 2001; Fox & Raichle, 2007). Animal studies have shown that $CMRO_2$ response to stimuli exhibits closer spatiotemporal correlation with neuronal activation compared to BOLD signal (Malonek & Grinvald, 1996).

A number of magnetic resonance techniques for measurement and mapping of $CMRO_2$ have emerged during the past two decades. T_2-relaxation-under-spin-tagging (TRUST) (Lu & Ge, 2008) and susceptometry-based oximetry (SBO) (Jain, Langham, & Wehrli, 2010) have been successfully applied as whole-brain $CMRO_2$ quantification techniques, in both normal and altered human physiology; suggesting the potential of $CMRO_2$ as a biomarker of the brain's neurometabolic state (Bulte et al., 2012; Gauthier & Hoge, 2013; Wise, Harris, Stone, & Murphy, 2013).

However, the alterations in $CMRO_2$ with task execution are small and voxel-wise mapping techniques may be more informative compared to global $CMRO_2$ methods (Rodgers, Detre, & Wehrli, 2016). Voxel-wise oxidative metabolism can be estimated with calibrated fMRI (Davis, Kwong, Weisskoff, & Rosen, 1998); the technique uses a combination of BOLD, ASL and breathing manipulation (e.g. hypercapnia, where the participant breathes air mixed with low percentage of carbon dioxide) to estimate the vascular component of BOLD response. The

calibration procedure allows the extraction of the relative change in oxidative metabolism from task-induced BOLD and ASL responses using biophysical models (Chiarelli, Bulte, Wise, Gallichan, & Jezzard, 2007; Davis et al., 1998; Gauthier & Hoge, 2013) and previous studies have shown the higher reproducibility of this technique compared to BOLD (Leontiev & Buxton, 2007). Calibrated fMRI has recently been extended to allow measurement of baseline oxidative metabolism (Bulte et al., 2012; Gauthier & Hoge, 2012; Wise et al., 2013) and it could be highly relevant for the study of plasticity due to the association among synaptogenesis, neurogenesis, gliogenesis, and glial hypertrophy with local baseline metabolism.

Previous studies investigated oxygen metabolism in response to tasks within BOLD signal defined regions of interests (ROIs) (Foster, Steventon, Helme, Tomassini, & Wise, 2020; Tardif et al., 2016). But changes in energy requirements may not be wholly detectable based on BOLD signal alone. Therefore, an estimation of $CMRO_2$ at a voxel-level would be advantageous.

Modifications in $CMRO_2$ have been reported in cerebrovascular disease, where reductions in CBF limit the supply of adequate oxygen to satisfy metabolic needs, eventually resulting in cerebral infarction (Iadecola, 2004). Additionally, variations in $CMRO_2$ might occur due to mitochondrial dysfunction, which has been related to different neurodegenerative disorders (Lin & Beal, 2006), or due to changes in energy regulations such as in the Warburg effect reported in cancer (Warburg, 1956). Particularly, in neuroinflammatory conditions such as multiple sclerosis (MS), where the coupling between neural activity and the vascular signal may be affected (Marshall, Chawla, Lu, Pape, & Ge, 2016), the quantification of $CMRO_2$ may offer more biologically-relevant information on the state of brain tissue than the BOLD signal alone.

In the previous chapter BOLD signal was used to define ROIs, given the high signal to noise ratio (SNR) in BOLD, and a ROI-based analysis was performed. But a variation in how BOLD

indexes energy consumption (due to disease or task adaptation) could be masked by this approach. Consequently, $CMRO_2$ is expected to be a better marker of energetic changes during adaptation than BOLD.

Therefore, this chapter aims to explore the feasibility of a voxel-wise approach with the same data. Specifically, we aim to (I) build an approach to investigate relative $CMRO_2$ on a voxel-by-voxel basis during the execution of tasks in MS patients and healthy controls (HC) and (II) to map between-group differences in changes over time in oxygen metabolism in task-related regions.

5.2 METHODS

Participants, **behavioural testing, MRI details and tasks.** Participants' details are explained in chapter 4, as well as the behavioural testing, magnetic resonance imaging and tasks.

DATA ANALYSIS

Demographic, clinical and MRI characteristics. Demographic, clinical and MRI characteristics are explained in chapter 4.

Normalised Whole Brain Volume and Lesion Volumes, Lesion Filling and GM mask. Details are explained in chapter 4.

Calibrated fMRI pre-processing and modelling. Details are explained in chapter 4.

Task Modelling. Details are explained in chapter 4.

Voxel-by-voxel $CMRO_2$ modelling and statistical analysis. In order to model $CMRO_2$, we need an estimate of the calibration factor M for each participant (M corresponds to $TE \cdot k \cdot [dHb]_0$), which is made from the baseline data (DEXI pCASL) of the resting scan during gas challenges. Then for every subject, CBF and BOLD cope (contrast of parameter) images from each contrast of the FEAT model (corresponding to different task-blocks) were divided by their respective baseline in order to get the percentage change in the vascular and functional responses over the baseline at different time-points. They were then transformed to the standard space, along with the M map, using FLIRT (FSL tool) and converted to matrix using SPM12 (www.fil.ion.ucl.ac.uk/spm). Linear registration was employed for consistency with

pre-processing steps. $CMRO_2$ was calculated in MATLAB (R2015_a, Mathworks Inc., MA, USA) using a simplified version of the Davis model (Davis et al., 1998)(Merola et al., 2016) (see **equations 4.1** and **4.2** in chapter 4, as well as the explanation of the parameters) and the new matrix was converted to a new image in order to get a map of $CMRO_2$ relative changes during tasks execution for each individual subject.

GLM (fsl_glm) was used to fit the slope of $CMRO_2$ response linear decrease across each task-block during task execution for each participant (visual task [7 5 3 1 -1 -3 -5 -7]; motor task [9 7 5 3 1 -1 -3 -5 -7 -9]).

Permutation tests (FSL-Randomise) were used (5000 iterations) to (I) investigate changes of BOLD, CBF and $CMRO_2$ during task execution and (II) localise differences at the group level between HC and MS patients. All the analysis were constrained to grey matter only. Correction for multiple comparisons was performed using threshold-free cluster enhancement (TFCE) (Smith & Nichols, 2009). Decrease during task execution and between-group differences were considered significant if $p < 0.05$.

5.3 RESULTS

Demographic, clinical and MRI characteristics. Participants' characteristics are shown in Table 4.1 (Chapter 4).

Feasibility of mapping $CMRO_2$ at a voxel-wise level. The steps to register maps to standard space and to calculate $CMRO_2$ at a voxel-wise level are shown in Figure 5.1 indicating the feasibility of estimating oxygen metabolism voxel-by-voxel. Figure 5.2 shows the M maps for patients and controls, Figure 5.3 shows the anatomical correspondence among BOLD and CBF task-responses assessed with FEAT models and $CMRO_2$ mean responses to tasks computed voxel-wise.

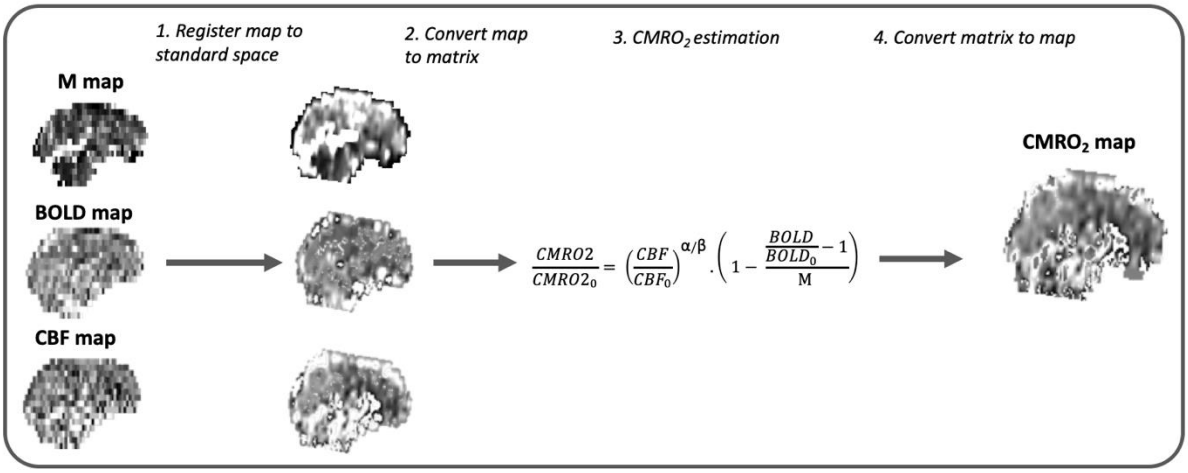

Figure 5.1*. *Analysis pipeline. *(I) For each participant M, BOLD and CBF maps were linearly registered to standard space and (II) then converted to matrix using SPM. (III) $CMRO_2$ was calculated using matlab. (IV) $CMRO_2$ matrix were converted to map using SPM.*

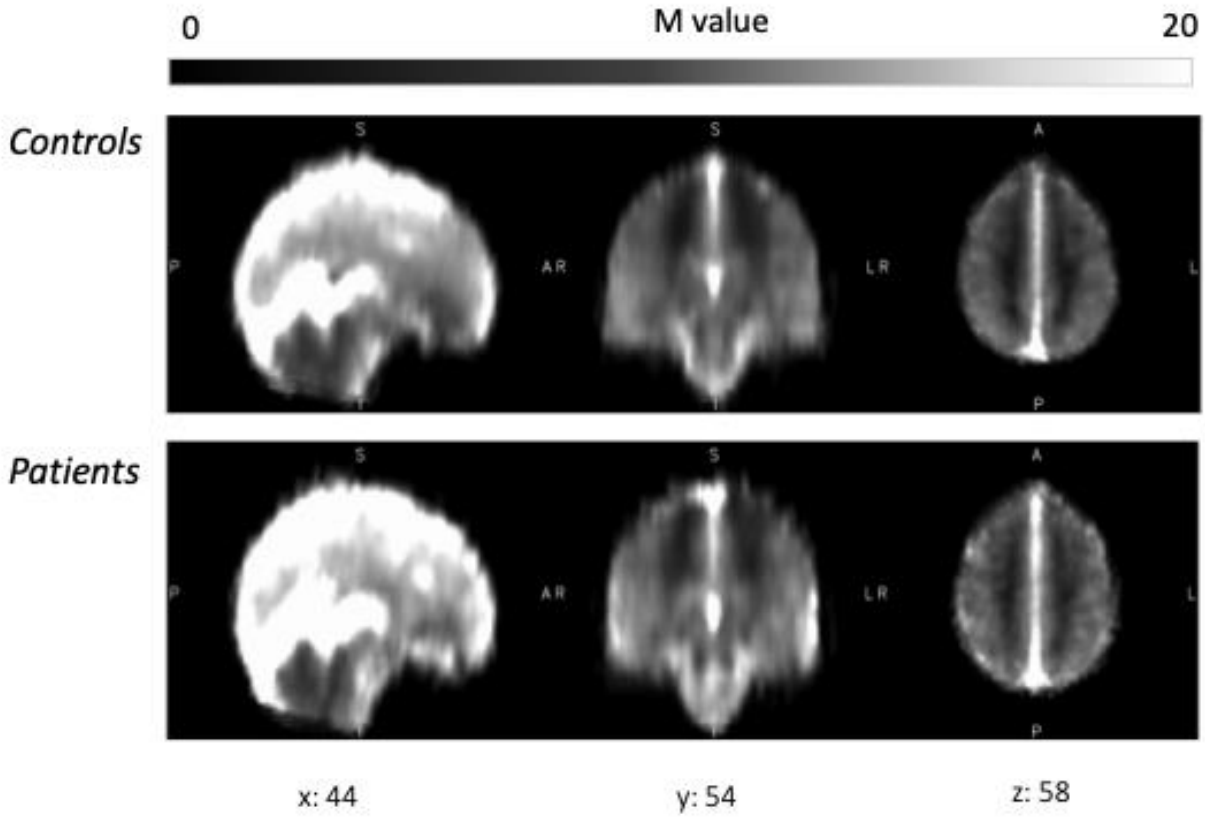

Figure 5.2. ***M maps.*** *M maps averaged for Controls (Top) and Patients. Upper threshold was set to 20, in order to reduce venous blood contamination from large veins.*

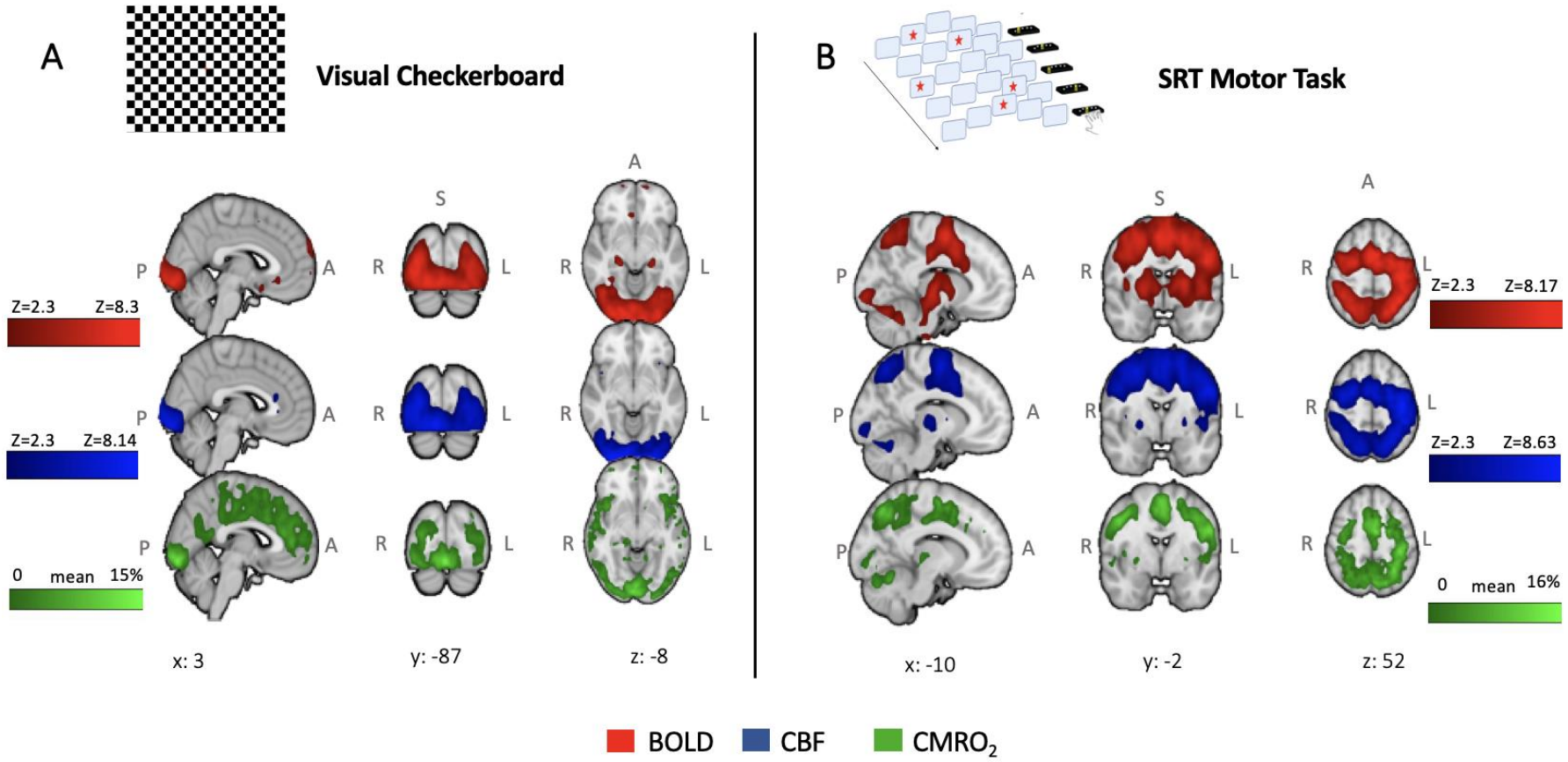

Figure 5.3. BOLD, CBF and $CMRO_2$ responses to tasks execution. *Good anatomical correspondence among BOLD and CBF maps calculated with FEAT (Z statistic images were thresholded a Z>2.3) and mean $CMRO_2$ consumption (Differences were considered significant for $p > 0.05$ and correction for multiple comparisons was performed using TFCE) during tasks-execution calculated with our new pipeline in both tasks, (A) visual and (B) motor.*

Between-group differences in $CMRO_2$ during task execution and signal adaptation. Mean positive relative $CMRO_2$ response was investigated in the whole brain. Mean (±SEM) response to motor task execution was 3.1±0.63% increasing from the baseline (mainly in left/right cerebellum, motor, visual and frontal areas); randomise was used to investigate between-groups difference at voxel-wise level and we did not find any between groups statistical differences in the mean relative $CMRO_2$ response to SRT (Mean±SEM = HC: 3.89±0.57%; MS: 2.18±1.17%). Similar results were found in the mean $CMRO_2$ response to visual stimulation; where the mean (±SEM) response was 1.63±0.56% (mainly activation was found in visual and temporal areas) with no statistical difference between groups (Mean±SEM = HC: 0.92±0.99%; MS: 2.25±0.6%).

Randomise was also used to investigate changes of BOLD, CBF and $CMRO_2$ response during task progression in regions showing a positive metabolic response to the task. Both tasks showed a significant decrease of CBF and $CMRO_2$ over time in controls only (Mean±SEM = $CMRO_2$ - *Motor*: HC: 7.99±1.51% - MS: 4.52±2.37%. *Visual:* HC:3.4±1.95% - MS: 1.17±1.75%); indicating an adaptation of CBF and $CMRO_2$ with task-progress in healthy people only (**Figure 5.4** and **5.5**), with no statistically significant changes in CBF response and oxygen metabolism response in people with MS throughout task execution. Main areas of CBF and $CMRO_2$ decreasing during checkerboard stimulation were found in precentral, postcentral, angular, frontal superior gyri, occipital cortex and parietal lobules. CBF and $CMRO_2$ decreases associated with motor task execution were found primarily in precuneous and occipital cortex, precentral, postcentral, angular, middle temporal and middle frontal gyri, and cerebellum.

A significant decrease in positive BOLD signal across blocks was found in MS patients only during visual task execution located in left and right occipital cortex (**Figure 5.6**), indicating a decrease of functional response in patients with MS but not accompanied by a decrease in CBF and $CMRO_2$ responses.

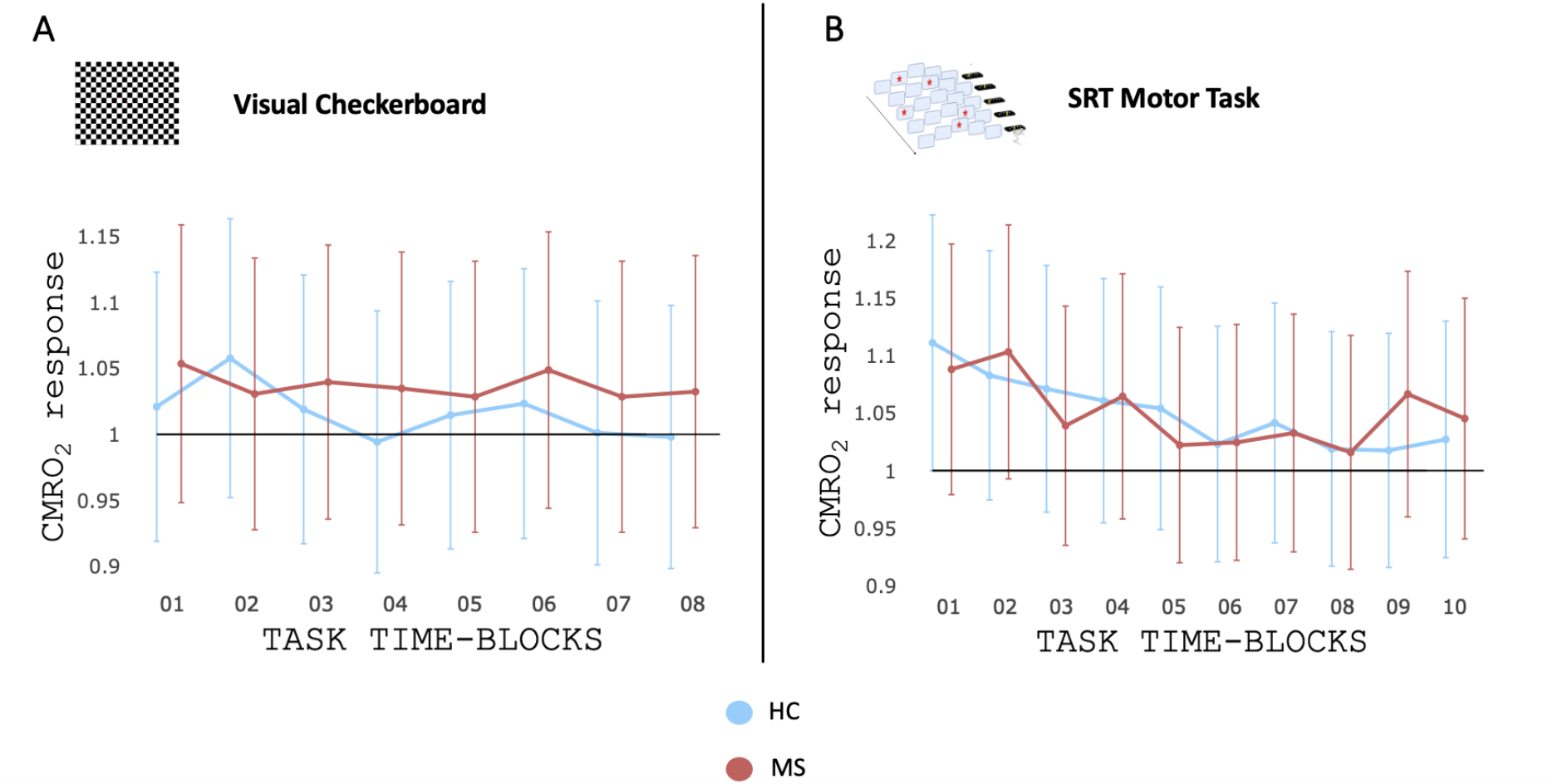

Figure 5.4. $CMRO_2$ tasks adaptation. *$CMRO_2$ response for (A) visual and (B) motor task in HC (blue) and MS patients (RED) for each block of the task*

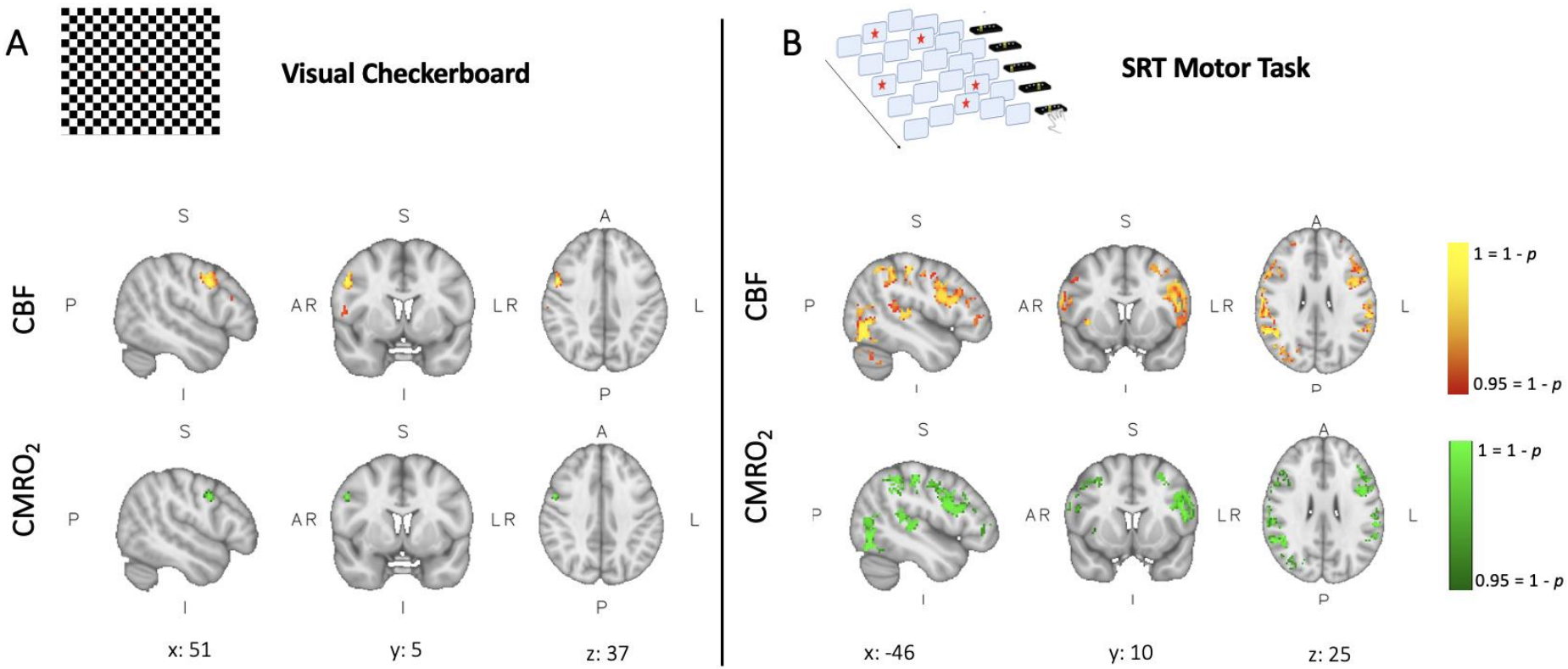

Figure 5.5. CBF and $CMRO_2$ decrease of responses during task execution. *CBF and $CMRO_2$ responses decreasing over task execution during (A) visual checkerboard stimulation and (B) SRT performing in HC only assessed with Randomise (Differences were considered significant for $p > 0.05$ and correction for multiple comparisons was performed using TFCE)*

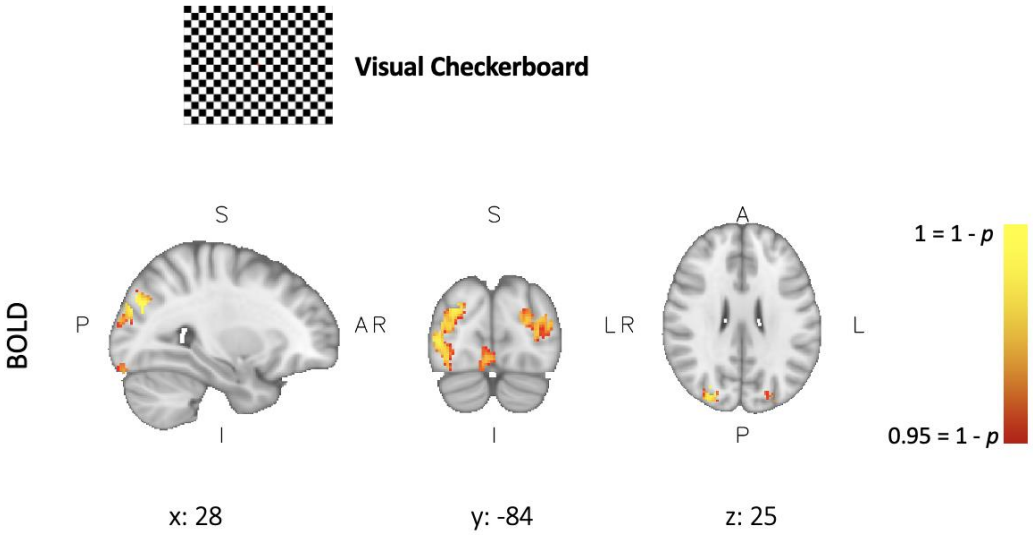

Figure 5.6. BOLD decrease of responses during visual task execution. *Bold response decreasing over visual checkerboard stimulation in MS only assessed with randomise (differences were considered significant for $p > 0.05$ and correction for multiple comparisons was performed using TFCE).*

5.4 DISCUSSION

Using quantitative fMRI we demonstrated the feasibility of mapping changes induced by motor and visual tasks in $CMRO_2$ on a voxel-by-voxel basis in MS patients and healthy controls. The use of calibrated fMRI for voxel-wise relative $CMRO_2$ estimation permits the mapping of the task in terms of oxygen consumption, going beyond earlier studies using either BOLD or CBF. We demonstrated a good anatomical correspondence among BOLD and CBF maps and mean $CMRO_2$ consumption during task-execution calculated with our new pipeline. Particularly, the identification of regional metabolic response to the task identified on $CMRO_2$ maps directly is of great interest considering that using ROIs defined from BOLD-response only could miss metabolic responses happening in parts of the brain where BOLD may under-represent the change in oxygen consumption, for example, where flow-metabolism coupling is altered.

Here, using calibrated fMRI we were able to detect a tissue oxygen consumption change, a marker of energy consumption, during task execution in healthy volunteers. Because of the brain's dependence on oxygen to meet its energy demands, $CMRO_2$ provides a direct, quantitative measure of the brain's energy utilization. It is likely that $CMRO_2$ simply responds as needed to match ATP production to ATP consumption; making $CMRO_2$ a more informative parameter of neural activity than BOLD signal (Blockley, Griffeth, Simon, & Buxton, 2013). Previous neuroplasticity studies have used BOLD to investigate brain changes during task execution (Albouy et al., 2012; Mackey, Miller Singley, & Bunge, 2013) reducing the strength of the inferences that can be made in assessing brain plasticity (Krieger et al., 2014; Leontiev & Buxton, 2007; Logothetis & Wandell, 2004).

Given the assumption that $CMRO_2$ is the parameter most closely related to neural activity (Buxton, 2013); we can conclude that a change of $CMRO_2$ reflects a change in the overall energy cost of the evoked neural activity.

Furthermore, our technique could be helpful in discerning the two physiological mechanisms underlying BOLD changes. BOLD changes over time has been widely observed as an adaptation in response to environment or lesions and it has been interpreted as recruitment of new/different neural networks (Fridman et al., 2004; Heuninckx, Wenderoth, & Swinnen, 2008; Johansen-berg et al., 2002; Lotze et al., 2006); but due to the contribution of both vascular and neural components, the physiological mechanisms underlying BOLD changes are difficult to interpret. In particular, our results show a main decreasing of $CMRO_2$ during both tasks execution in HC, that can be interpreted as a decreasing of neural activity, or energy utilisation, over time.

We did not find a statistically significant change in $CMRO_2$ in MS patients over time during task execution. The lack of significant change in $CMRO_2$ could be due to poor SNR for CBF signals. Although ASL sensitivity has considerably improved in the recent years, ASL still has lower SNR and lower temporal resolution than standard BOLD-fMRI; because both a label and a control image have to be acquired, as well as labelling of the blood. Therefore, with ASL is more complicated to detect very small changes, especially in populations where motion is difficult to minimise (i.e. patient groups). Despite the limitations, it is widely known that ASL is more closely coupled to neuronal activity than BOLD as it reflects capillary blood. Furthermore, we employed a PCASL sequence which has higher flow contrast compared to standard PASL sequence, providing increased temporal SNR (Tancredi et al., 2012), but the reduction of power needs to be taken into account when interpreting the data, as fewer images are acquired.

Our results could also be interpreted in the light of a hypothesis of mitochondrial dysfunction in MS. In recent years, it has become increasingly clear that dysfunctional mitochondria is a

key feature of common neurodegenerative diseases (Beal, 1995), in MS particularly they are important contributors to damage and loss of both axons and neurons (Witte, Mahad, Lassmann, & van Horssen, 2014). The prime function of mitochondria is to provide cells with energy, in the form of ATP, by oxidation of metabolic fuels, required for maintenance of sodium and calcium (Attwell & Laughlin, 2001) and the sodium/potassium pump consumes most of the ATP needed for recovery from excitatory neural signalling (Ames A III 2000 CNS energy metabolism as related to function Brain Res. Rev). In the MS cortex, neural mitochondrial dysfunction can happen because of production of reactive oxygen species (ROS) and nitric oxide (NO) by continuously activated microglia in the cortex that leads to inhibition of oxidative phosphorylation and damage to mitochondrial DNA. The damage will reduce ATP production, which may eventually fully compromise mitochondrial functional and lead to neuronal cell death (Witte, Geurts, de Vries, van der Valk, & van Horssen, 2010; Witte et al., 2014). Mitochondria have a main role in the modification of synaptic transmission and thus also related processes of functional plasticity, given their oxidative, metabolic, and calcium buffering functions (Todorova & Blokland, 2017). Many studies suggest that synaptic function and plasticity depend on mitochondria (Amaral & Pozzo-miller, 2012; Cheng, Hou, & Mattson, 2010; Su, Ji, Sun, Liu, & Chen, 2014); particularly, Verstreken et al. (Verstreken et al., 2005) demonstrated that during intense stimulation, neurons with impaired mitochondrial functions could not maintain normal neurotransmitter release like control neurons. The evidence suggests that this effect was due to lower mitochondrial ATP. Together, given the role that mitochondria play in process of plasticity by generating energy in the form of ATP (Cheng et al., 2010; Valenti, Bari, Filippis, Henrion-caude, & Anna, 2014), we speculate that mitochondrial dysfunction may stop MS patients undergoing brain energy changes that accompany tasks execution.

Quantitative fMRI is a promising method providing a more direct measure of neural activity ($CMRO_2$) (Blockley et al., 2013; Hoge, 2012) together with our voxel-wise investigation, it may provide a more sensitive method to investigate energy dysfunction in MS and physiologically relevant markers of tissue damage for the future evaluation of therapeutic strategies, particularly those aiming to promote plasticity.

Overall, our results represent a methodological step forward when seeking to understand tissue energetics, as they reduce the need to define regions of interest from the less physiologically interpretable BOLD response that may be confounded by disease-induced changes in vascular behaviour.

CHAPTER 6

Evidence for a sustained cerebrovascular response following motor practice

ABSTRACT

Motor tasks have been extensively used to probe neuroplasticity and the observed functional changes are often associated with improved performance. Studies have also demonstrated that in the absence of an overt task, fluctuations in the blood oxygenation-level dependent (BOLD) signal functionally correlate across brain regions and associations between altered resting activity and changes observed during task performance have been demonstrated. Specifically, changes in BOLD resting states following motor training have been reported. Although many studies have employed ASL techniques to study resting state fluctuations, few works have focused on the changes in resting cerebral blood flow (CBF) following motor tasks. Here we implemented a new motor task to probe neuroplasticity and investigated the changes in resting perfusion immediately after motor task execution. We hypothesized that motor learning would induce localised changes in blood flow sustained even after the execution of the task ceases.

20 healthy volunteers underwent two MRI sessions: a task session with a sequence learning task performed with a data glove and a control session where subjects were asked to do nothing.

During each session ASL (CBF) and BOLD signals were acquired during the task and during sustained periods of rest before and after execution of the sequence learning task.

BOLD and CBF responses to the motor task were seen to decrease as the task proceeded and performance improved, indicating that our task was well designed to probe neuroplasticity. Furthermore, we demonstrated a sustained localised increase in resting CBF after the completion of the motor learning task. The control session allowed us to exclude an effect of time on CBF changes, leading to an important connection between neuroplastic changes induced by learning and the perfusion in resting brain. It remains to be investigated whether the sustained increase in CBF for at least several minutes after the task is secondary to elevated neuronal activity or whether it represents a change in, and therefore plasticity of, the cerebrovascular system in response to task practice.

KEY WORDS

CBF – Resting State – Neuroplasticity – Motor Task

6.1 INTRODUCTION

The capacity of human brain for functional reorganization throughout life is now well recognized under the name of *neuroplasticity*. Developments in neuroimaging have enabled non-invasive investigation of the living human brain, while learning of new skills are used as paradigms to investigate different aspects of neuroplasticity. In particular, motor tasks have been extensively used as methods to probe neuroplasticity and the observed functional imaging changes are often associated with improved performance, suggesting that fMRI is a sensitive marker for experience-dependent plasticity (Mozolic, Hayasaka, & Laurienti, 2010; Thomas et al., 2009). Studies have also reported rapid neural adaptions across motor cortex and their functionally connected regions following motor training (Hardwick, Rottschy, Miall, & Eickhoff, 2013; Ungerleider, Doyon, & Karni, 2002).

fMRI has been employed to study baseline activity, in the form of resting state fluctuations of BOLD signal, and studies have demonstrated that in the absence of an overt task, such fluctuations functionally correlate in time across brain regions. (Gusnard & Raichle, 2001; Laird et al., 2011; Raichle & Mintun, 2006). Moreover, temporal correlations do not appear to be random as studies identified consistent resting state patterns across subjects. These are termed resting state networks (RSNs). (Damoiseaux & Greicius, 2009). RSNs correlate with neuroelectric activity and are influenced by structural connectivity. (Britz, Van De Ville, & Michel, 2010; Damoiseaux & Greicius, 2009; Mantini, Perrucci, Del Gratta, Romani, & Corbetta, 2007).

The neuronal circuitry underlying the observation of RSNs are thought to play an important role in supporting the execution of behaviour (Miall & Robertson, 2006). The association between altered resting activity and changes observed during task performance has been studied (Xiong et al., 2009). The strength of correlation within and between networks has

behavioural relevance (Guerra-Carrillo, MacKey, & Bunge, 2014) and resting state (RS) fMRI has been proposed as an effective measure of plasticity. Thus the study of RS is particularly adapted to highlight neuroplastic modification (Buckner & Vincent, 2007; Guerra-Carrillo et al., 2014) and changes in BOLD-RS have been reported following motor training (Albert, Robertson, Miall, & Hall, 2009).

RSNs identified from spontaneous BOLD fluctuations are very consistent across participants, but whether these fluctuations reflect real changes in neural activity is still largely unexplored; although it is well known that task-evoked BOLD responses are a mixture of changes in cerebral blood flow (CBF), cerebral metabolic rate of oxygen ($CMRO_2$) and venous blood volume (Blockley, Griffeth, Simon, & Buxton, 2013). A number of studies have explored functional connectivity based on RS-fluctuations in CBF, rather than BOLD signal, using the arterial-spin labelling (ASL) technique (Biswal, Kylen, & Hyde, 1997; Chuang et al., 2008; Fukunaga et al., 2008; Liang, Zou, He, & Yang, 2013; Viviani, Messina, & Walter, 2011; Zou, Wu, Stein, Zang, & Yang, 2009); however works have focused on short term fluctuations and not on the sustained changes in CBF following a motor task and their relation to that motor task.

Using ASL imaging it is possible to investigate the absolute level of perfusion, which is information that is not available in standard BOLD-EPI (Zou et al., 2009). Perfusion imaging is then a potential marker of individual differences in brain vasculature and provides the benefit of directly assessing mean CBF changes. Furthermore, CBF is a single parameter (vs. BOLD which is a composite of several parameters) and is more closely related to cerebral vasculature and metabolic demand than BOLD, therefore changes in CBF are more informative of the brain physiology. Under the assumption of stable neurovascular coupling (Iadecola, 2017), we expect CBF to reflect changes not only in underlying neuronal activity over short time-scales seen for stimulus responses and spontaneous fluctuations in neuronal activity, but also for

longer term changes in neuronal activity as a proxy of brain plasticity. Specifically, change in CBF, CBV, or capillary function, can happen to match energy supply to modified energy usage, leading to microvascular plasticity and, so, neuroplasticity. Together with the observation that altered resting state following motor learning tasks is an evidence of changes in neuronal behaviour (Guerra-carrillo, Mackey, & Bunge, 2014), we hypothesise that there are observable *sustained* changes in CBF, in a longer time-scale than few seconds of the end of the task, in motor-relevant brain regions following the execution of a motor learning task.

To investigate this hypothesis, we implement a new task to probe neuroplasticity. Motor tasks have been extensively used to probe neuroplasticity (Nissen & Bullemer, 1987), and the associated activity in the brain is reported to be mainly in the motor areas (Hikosaka, Nakamura, Sakai, & Nakahara, 2002; Robertson, 2007). Although they require learning of sequential motor patterns, they have minimal demand on motor execution, as participants respond through primarily isometric contractions of the finger muscles (Hardwick et al., 2013). We aim to create a new task in order to exploit the capacity of the brain to work as a network (Dayan & Cohen, 2011) that requires bigger hands movements to be performed. Therefore, we created a motor task where performance can be adjusted in real-time thanks to the visual feedback and we use it to study the voxel-wise changes in CBF over a period of 8 minutes following a motor task conducted over a period of 10 minutes.

6.2 METHODS

Participants. 20 healthy volunteers (age: 27.5±3.8 years; 11F/9M) underwent two MRI sessions a week apart. Before each session, participants gave written informed consent and they were screened for MRI compatibility. At the end of each session, they received 10£/hour for taking part. The study was approved by the Cardiff University School of Psychology ethics committee.

Experimental design and Motor task. At each of the two sessions participants underwent a structural and a functional scan. During the task session, participants underwent 8min resting state, followed by 10min of motor task and 8min of resting state. During the control session, participants underwent 8min resting state, followed by 10min where they did nothing apart from laying in the scanner and 8min of resting state again (**Figure 6.1**). During the rest scan in the task session and for the entire duration of the control session, a white fixation cross and the word 'REST' were presented on a black screen.

10 participants did the task session first, while the other 10 did the control session first.

For the present experiment we used an MRI-compatible right hand 5DT Data Glove 16 MRI (Fifth Dimension Technologies, 5DT Data Glove 16 MRI, https://5dt.com/5dt-data-glove-ultra/) with fibreoptic sensors to measure 14 joint angles of the hand. The data glove is metal free and safe to be used in an MRI environment. The data glove was worn by the subjects in the scanner and a set of fibreoptic cables (5 meters long) connected the glove to the control room, where the glove was plugged into the stimulus PC and motor responses were recorded with PsychoPy (Peirce, 2007). Before the beginning of the task the glove was calibrated for each participant. This was done in the scanner just before the first resting period. Participants were asked to extend and flex index, middle, ring and all fingers at different times in order to

assess maximum extension and flexion for each subject; this calibration was applied in real time to make virtual hand movements correspond to the subject's own movement.

During the task, a white circle presented on a black screen expanded and contracted in a fixed sequence. Participants were able to control the size of a green circle, presented on top of the white one, by squeezing their hand into a fist. Namely, the green circle changed diameter based on the participant's flexion and extension of all of their fingers. They were instructed to keep matching the two circles and they were not aware of the existence of a fixed sequence pattern. The task was split into 10 blocks, each block lasted for 30 sec and was followed by a 30sec rest period. During each block the prefixed sequence of size changes was presented 3 times. During the duration of the task, performance was recorded with PsychoPy.

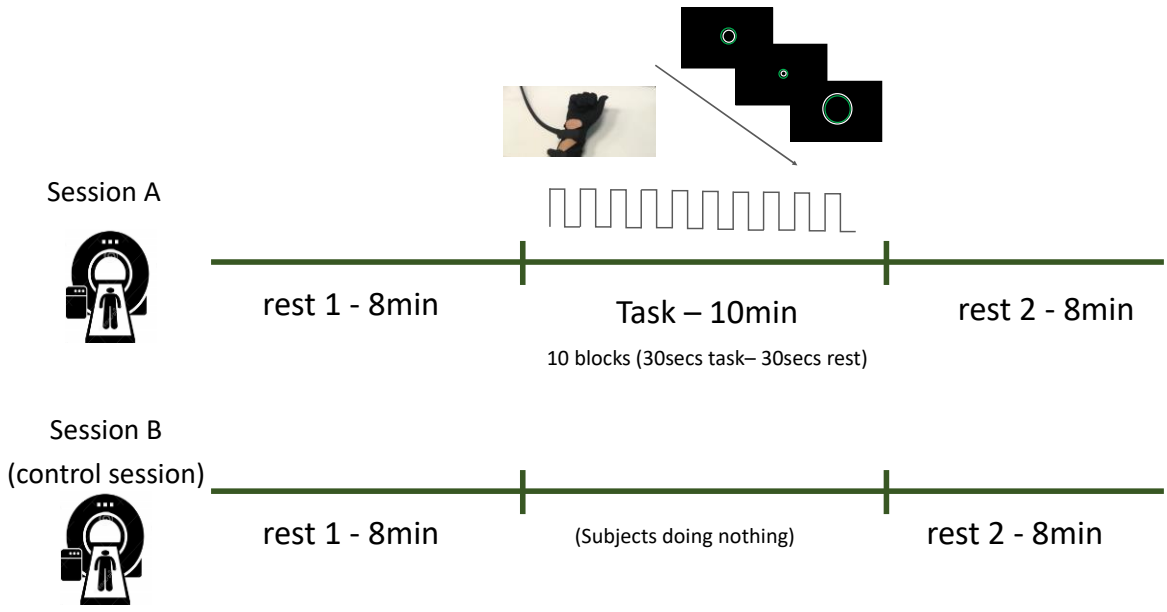

Figure 6.1. ***Experimental design***. *Participants were scanned twice. During the task session (A), participants underwent 8min resting state, followed by 10min of motor task and 8min of resting state. During the control session (B), participants underwent 8min resting state, followed by 10min where did nothing apart from laying in the scanner and 8min of resting state again. During the rest scans in the task session and for the entire duration of the control session, a white fixation cross and the word 'REST' were presented on a black screen. 10 participants randomly did the task session first, while the other 10 did the control session first.*

Magnetic Resonance Imaging. Data were acquired on Siemens Prisma 3T scanner (Siemens Healthineers, Erlangen, Germany), using a 32-channel head coil. A magnetization prepared rapid acquisition with gradient echo (MPRAGE), T1-weighted scan was acquired for registration (1mm isotropic resolution, 200 slices, TR/TE = 2100/3.24ms).

All the functional scans were acquired using a pCASL acquisition with pre-saturation and background suppression (Okell, Chappell, Kelly, & Jezzard, 2013) and a dual-excitation (DEXI) readout (Schmithorst et al., 2014) aimed at producing a good ASL signal from the short echo-time data and BOLD contrast from the longer echo-time data. The labelling duration and post label delay (PLD) were both set to 1.5s, GRAPPA acceleration (factor of 3) was used with TE1=10ms and TE2=30ms. An effective TR (the total TR including labelling and both readouts) of 4.4 seconds was used to acquire 16 slices, in-plane resolution 3.4 x 3.4 mm and slice thickness 7mm with a 20% slice gap. 351 tag-control pairs resulted in 702 volumes being acquired over the 26-min task, given that the scanner run continuously through the 'rests' and 'task' session.

A calibration (M0 image) was acquired for ASL quantification with pCASL and background suppression switched off, with TR of 6 seconds, TE=10ms.

During the entire scanning sessions, physiological monitoring was used to record CO_2 and O_2 end-tidal traces using a nasal cannula connected through a sampling to a gas analyser system (PowerLab®, ADInstruments, Sydney, Australia).

DATA ANALYSIS

Behavioural response to the task. For each participant, behavioural responses to the task were resampled to match the same number of time points as contained in the prefixed sequence. In order to investigate the correspondence between the size of the two circles, for each time point

of the prefixed sequence within the experimental blocks a Pearson's correlation between the diameter of the white circle (pre-fixed sequence) and the diameter of the green circle drawn by the participant's fist (behavioural response) was calculated. Then, to investigate the increase in performance during task execution, a one-way ANOVA was performed with the correlation index as the dependent variable and each block of the experiment as the independent variable. An increase of correlation over time is expected as an outcome of implicit learning of the pre-fixed sequence. All the analyses were conducted with an in-house built MATLAB (R2017_b, Mathworks Inc., MA, USA) script. Differences were considered significant at $p < 0.05$.

fMRI Analysis. The first and second echo from the pCASL sequence's data were motion corrected using FSL tool MCFLIRT (Jenkinson, Bannister, Brady, & Smith, 2002) and then brain extracted using BET (Smith et al., 2002). Spatial smoothing (FWHM = 4.5mm) of the BOLD data (surround average of TE_2) was carried out with SUSAN (Smith & Brady, 1997), with high-pass temporal filter applied with a cut off of 90s. ASL data (surround subtraction of TE_1) were spatially smoothed using a 3D Gaussian kernel (FWHM = 4.5mm). FSL tool FLIRT (Jenkinson et al., 2002; Jenkinson & Smith, 2001) was used to linearly register BOLD data (surround average of second echo) to individual T1-structural data (6 DOF) and then to linearly register it to MNI standard space (12 DOF). The resulting registration matrix were then used to transform CBF data (first echo) into T1 and MNI spaces using FLIRT. Given the voxelwise approach, linear registration was more appropriate for this study than non-linear one, as the latter has a higher degree of elasticity that can model local deformation.

Resting and task portions of the experiment were considered separately. The BOLD and CBF task responses were modelled for the middle 10 minute portion of data: TASK > REST, REST > TASK and linearly decreasing and increasing activations over time (linear adaptation over

10 blocks with the contrast [9 7 5 3 1 -1 -3 -5 -7 -9] and reverse) using two separate FEAT designs and motion correction parameters were added as regressors. (**Figure 6.2**)**.**

A higher-level analysis was performed with FEAT (Woolrich, Behrens, Beckmann, Jenkinson, & Smith, 2004) using a mixed effects model (FLAME 1) to model the functional responses to the task and decreasing of responses across all participants. Z statistic images were thresholded a $Z > 2.3$ and a cluster significance threshold of $p = 0.05$ was set.

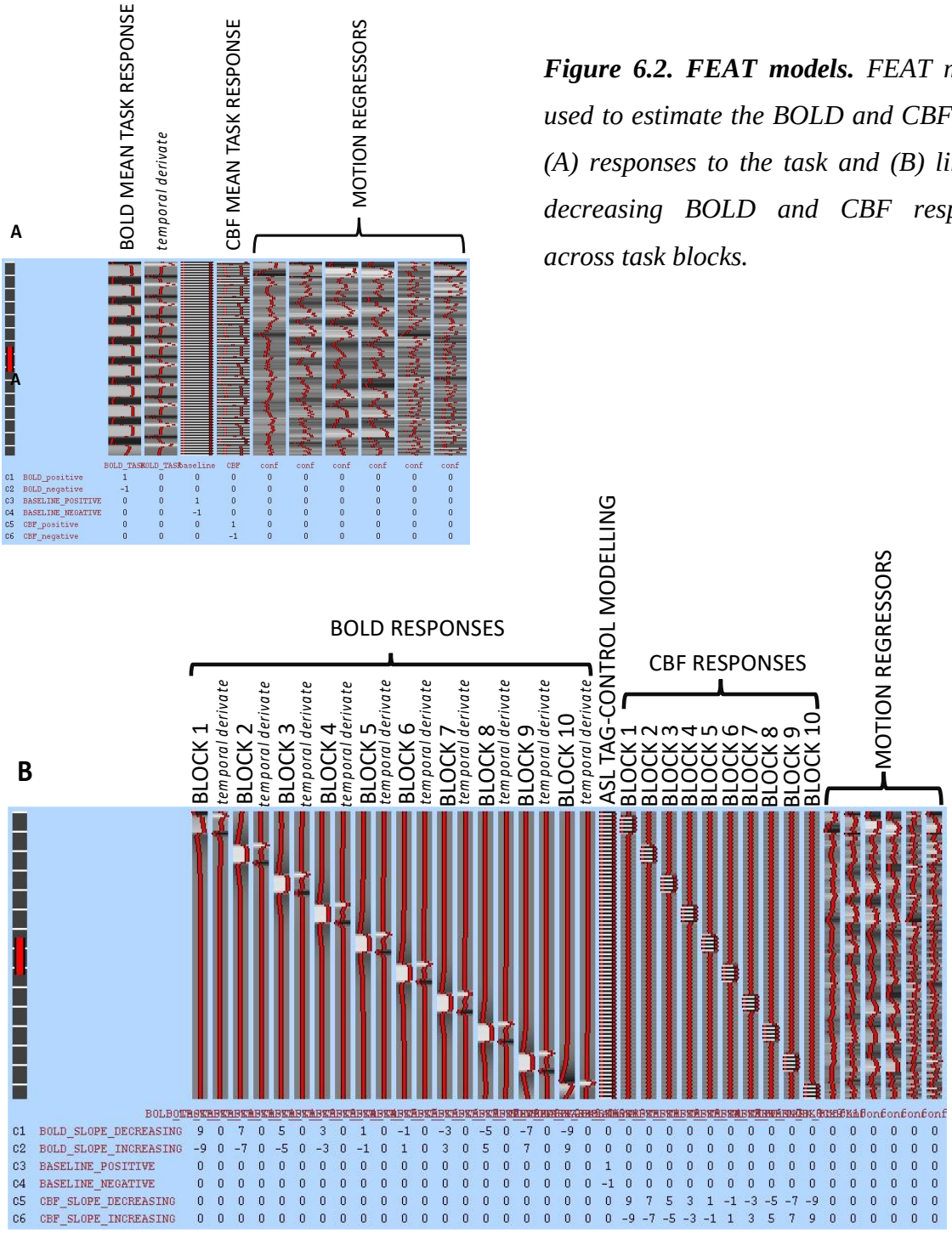

Figure 6.2. FEAT models. *FEAT models used to estimate the BOLD and CBF mean (A) responses to the task and (B) linearly decreasing BOLD and CBF responses across task blocks.*

Changes in resting CBF induced by the motor task. To investigate changes between the resting periods (before/after the tasks in both sessions) CBF maps from the resting periods were converted to units of ml/100g/min using BASIL toolbox (Chappell, Groves, Whitcher, & Woolrich, 2009); assuming a labelling efficiency of 0.85 and T1blood = 1.65s. After the conversion, for each subject separately, from each MRI session the perfusion map of the second resting state was subtracted from the perfusion map of the first resting state in order to obtain maps of perfusion changes for the two MRI conditions (respectively task and control). Data were then merged together in order to create a 4D image to be fed into the GLM model for which permutation testing (FSL-RANDOMISE; Winkler, Ridgway, Webster, Smith, & Nichols, 2014 - http://fsl.fmrib.ox.ac.uk/fsl/fslwiki/Randomise) was used to investigate difference between conditions (task vs control) in the resting perfusion change maps at a voxel-wise level. CO_2 differences between the two resting scans were calculated for each participant and they were included as regressors of no interest in the GLM model. Analysis were constrained to grey matter only. Correction for multiple comparisons was performed using threshold-free cluster enhancement (TFCE) (Smith & Nichols, 2009). Differences were considered significant if $p < 0.05$.

6.3 RESULTS

Motor Task. ANOVA was performed in order to investigate performance changes during task execution. The analysis demonstrated a main effect of block (time) ($F_{(1,9)} = 10.89$, $p < 0.001$), indicating an increasing in correlation among the size of the 2 circles block after block and so an improvement of performance with time. As shown by the **Figure 6.3**, most of the improvement happened in the first 3 blocks.

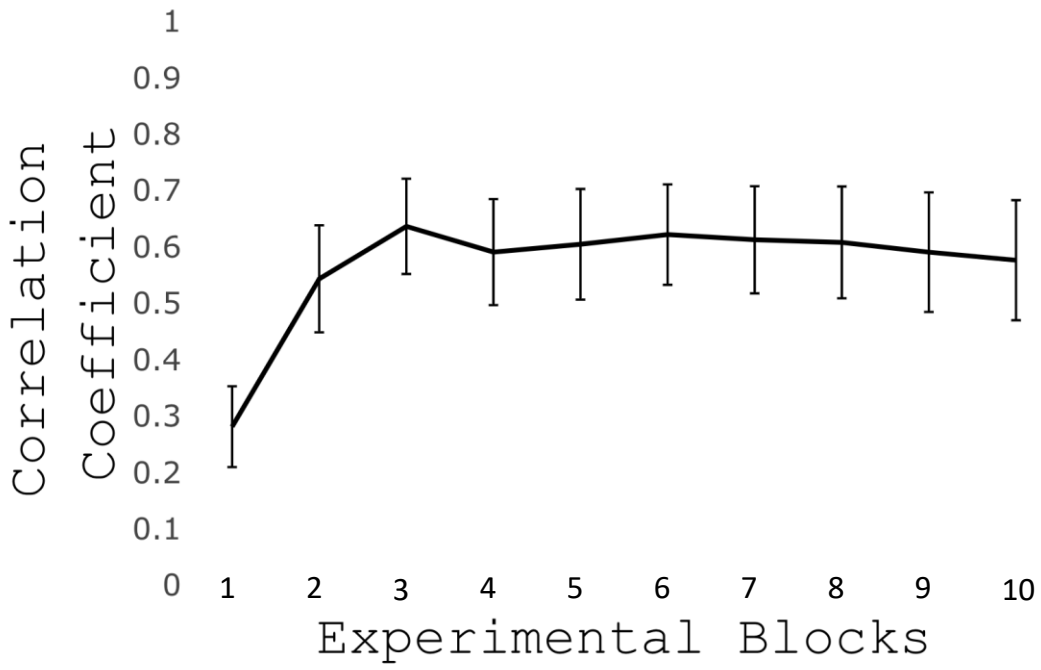

Figure 6.3. Behavioral results. *Increasing temporal correlation between the size of two circles throughout task performance (mean±sem across participants). This result suggests an improvement in performance especially over the first 3 blocks.*

Task-related functional response. Main areas of BOLD and CBF responses to the task were found bilaterally in postcentral gyri, inferior occipital cortex, superior parietal lobules, cerebellum (lobules V-VI) and left precentral gyrus. BOLD activation was also found in bilaterally in putamen and in left thalamus. (**Figure 6.4**).

A reduction of BOLD activity during task execution was found mainly bilaterally in precentral gyri; whereas a reduction of CBF activity was found mainly bilaterally in cerebellum (**Figure 6.5**). An increase of BOLD activity was found bilaterally in the orbital cortex, left precuneal cortex and medial cingulate gyrus.

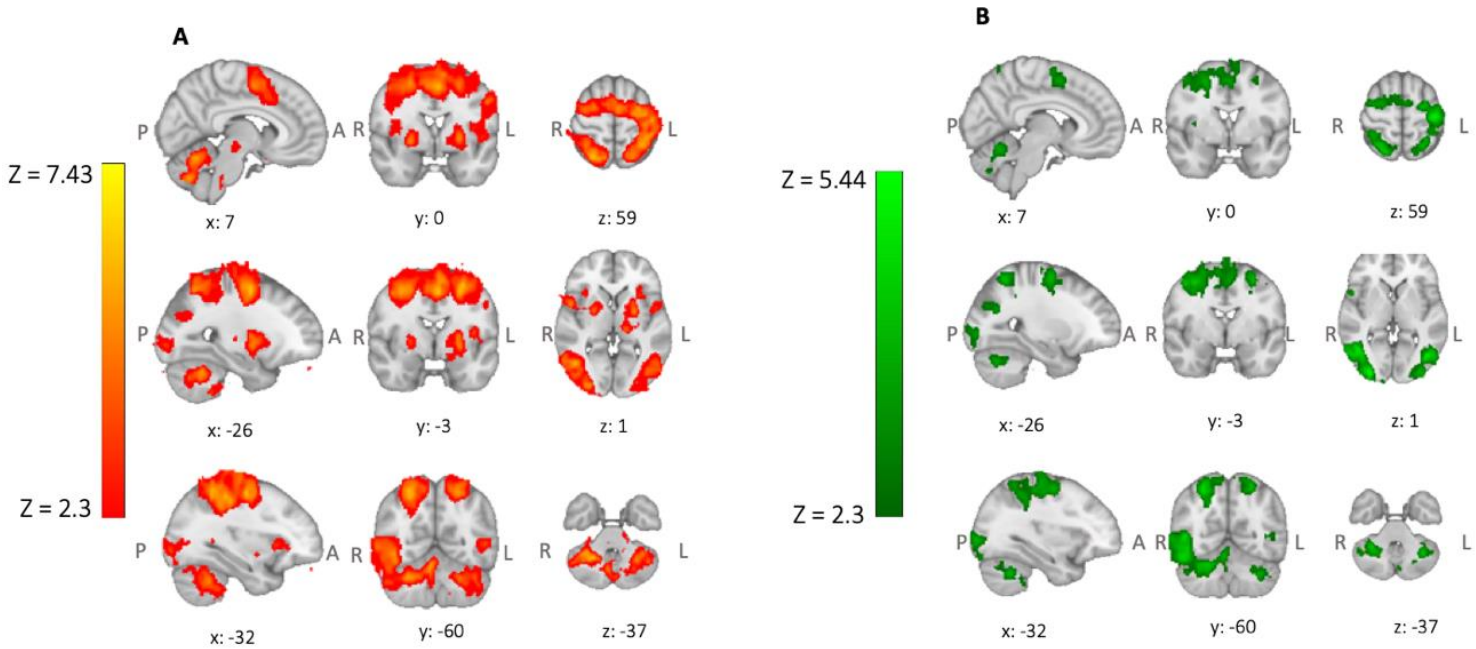

Figure 6.4. Task execution responses. *BOLD (A) and CBF (B) mean responses to task execution reported as z stats.*

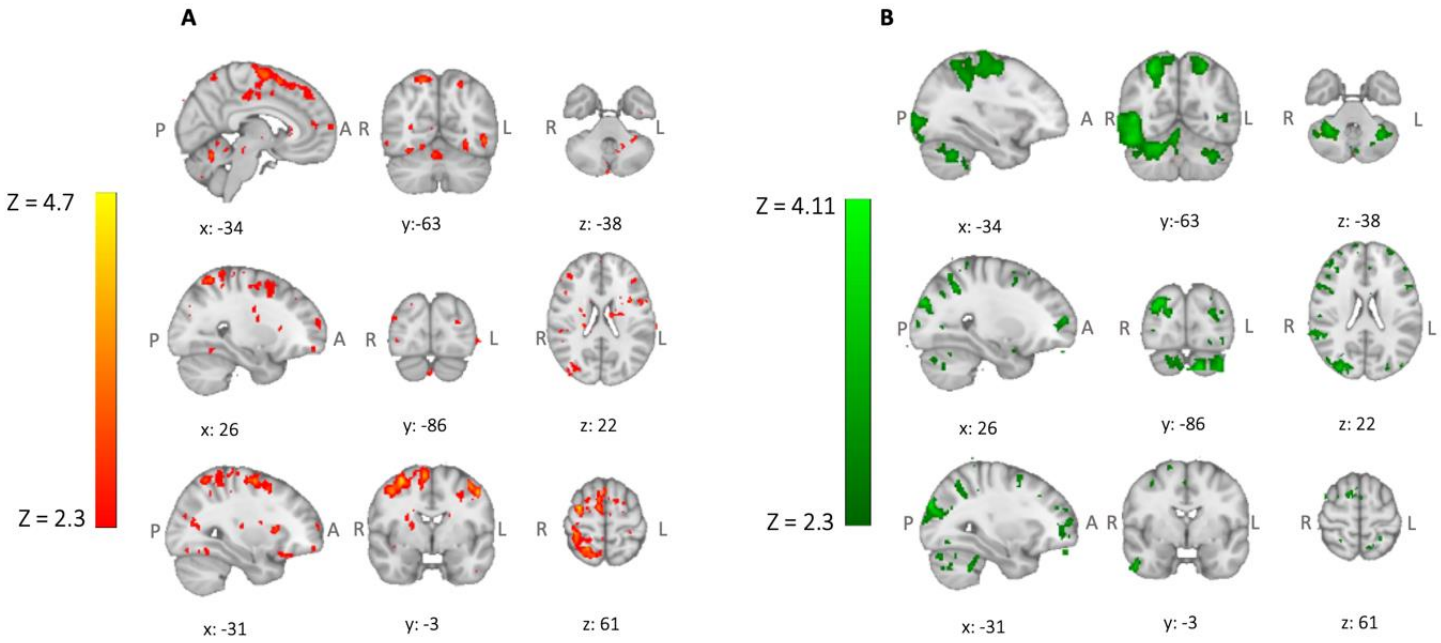

Figure 6.5. Task responses decrease. *BOLD (A) and CBF (B) areas of linearly decreasing task response across blocks reported as z stats.*

Sustained changes in CBF after task execution. Randomise results showed an increase in resting-state perfusion after task compared to the no-task session, indicating that the observed augmentation is due to the task and not to time passing. Area with significantly increased perfusion is extrastriate visual area MT (V5). (**Figure 6.6**).

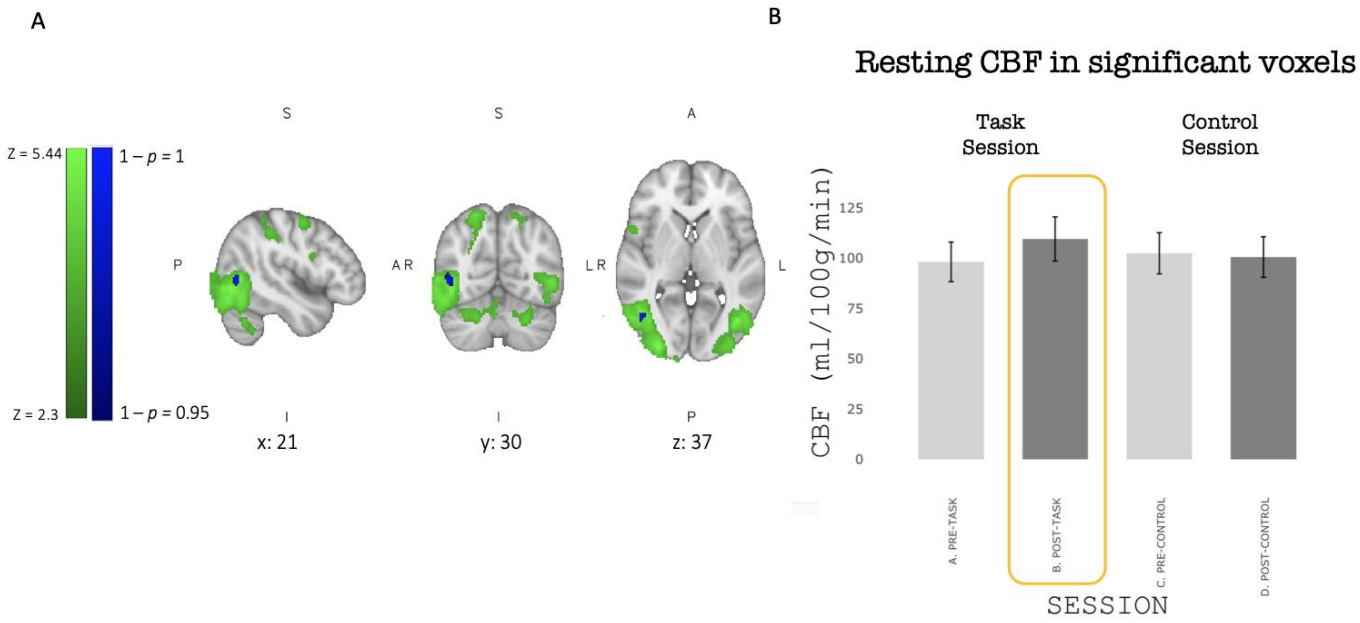

Figure 6.6. Baseline CBF increase. *(A) Significant areas (extrastriate visual area MT - V5) showing increase in resting CBF only after task execution reported as p value (blue) overlapped on task related activation areas (green). (B) Mean±sem resting CBF during the different resting periods (pre-/post- task/control) in the ROI.*

6.4 DISCUSSION

In the present study, we used an ASL technique to detect a sustained and localised CBF increase following 10 mins of motor task. We also showed decreasing BOLD and CBF signals during task execution, accompanied by an improvement in performance, indicating that our task was well designed to probe neuroplasticity.

A data glove as a new tool to study neuroplasticity. To the best of our knowledge, we used for the first time a data glove to probe neuroplasticity in healthy volunteers. Previous studies have used a data glove in the context of neurorehabilitation, brain recovery and assessment of functions in clinical populations (Bonzano et al., 2015; Limanowski, Kirilina, & Blankenburg, 2017; Ranganathan, 2017; Richards, Georgilas, & Dagnino, 2015); whereas we asked participants to perform a sequence learning task. Neuroimaging studies have largely employed variants of the serial reaction time task (SRTT) (Nissen & Bullemer, 1987) to study neural correlates and adaptations of sequential motor learning (Hardwick et al., 2013). The brain areas usually active to perform tasks similar to SRTT are the striatum, cerebellum and prefrontal areas (Robertson, 2007) and performance improvements have been associated with activation in premotor cortical regions, caudate and associative cerebellar regions (Hikosaka, Nakamura, Sakai, & Nakahara, 2002). Our results are coherent with the above studies, given that brain activation associated with task performance was found in similar areas.

We also observed a decrease of activation between blocks during task execution which is consistent with previous studies reporting that notion that motor training is associated with reduced excitability of the motor cortex (Pascual, Wassermann, Sadato, & Hallett, 1995;

Shadmehr & Holcomb, 1997). Learning new tasks requires plastic changes to accommodate the neural network involved in the execution of the demands. Therefore, it is widely accepted that decreasing activity revealed during fMRI studies reflects changes due to increased efficiency, reduced errors and consolidation of learning (Hardwick et al., 2013); rendering this technique a reliable methods for assessing local biological processing (Álvarez-Salvado, Pallarés, Moreno, & Canals, 2014). We found a decrease in both BOLD and CBF signals indicating a change in the recruitment of neural resources (Reber, 2013). These changes are often attributed to the unmasking of latent connections leading to more efficient neural networks work to ensure performances. However, it is worth noting the medium sample size recruited for this study. In order to generalize the results to different populations further studies are needed.

Baseline perfusion increases following 10mins of motor task. With the use of ASL technique combined with an advanced data glove system, we showed that the amount of perfusion in specific areas of the resting brain increases, for at least 8 mins, following the execution of the motor task. Furthermore, the control condition allowed us to exclude the hypothesis that changes in perfusion are caused by the simple time passing, making an important connection between neuroplastic changes induced by the motor task and perfusion changes in the resting brain.

To the best of our knowledge, the present study is the first to investigate CBF resting state immediately after the execution of a motor task. Previous studies have used BOLD to assess functional changes following tasks execution and they demonstrated that experience-dependent sensorimotor plasticity can induce changes in BOLD resting state (Amad et al., 2017; Ge, Zhang, Yao, & Long, 2015; Taubert, Lohmann, Margulies, Villringer, & Ragert, 2011; Zhang et al., 2014), thus functional resting state can be a valuable index of the functional changes that

support sensorimotor adaptive processes (Guerra-Carrillo et al., 2014). In particular, motor training studies show that the changes in BOLD resting state networks are not confined to canonical regions supporting motor functions (Guerra-Carrillo et al., 2014). Therefore, motor learning can induce changes in the resting state functional connectivity and this is suggestive of a functional reorganization of the brain networks supporting the offline consolidation of new motor skills (Sami, Robertson, & Miall, 2014). Furthermore, changes in spontaneous brain fluctuations have been associated with the performance improvement (Vahdat, Darainy, Milner, & Ostry, 2011). We observed changes in perfusion in V5, which is an area involved in processes of visual attention, specifically its function is to detect the presence of motion. Our results are in line with previous reports that used BOLD signal to investigate changes after tasks/trainings and reported an involvement of areas related to attentive processes (Albert et al., 2009; Amad et al., 2017; Zhang et al., 2014). Taken together, we suggest that our observed changes in perfusion, sustained after the completion of the task, are a proxy of the underlying reorganization that support motor skill acquisition.

Additionally, our results contribute to understanding the vascular nature of the changes observed in previous studies, considering that we detected changes directly on CBF maps, without relying on BOLD signal. Given the close coupling between CBF and glucose utilization/oxygen consumption (Raichle et al., 2001; Vaishnavi, Vlassenko, Rundle, Snyder, & Mintun, 2010), we can suggest that increased in perfusion maps at rest reflect a higher needed of metabolic demand in that area. CBF changes are thought to be prompted by activation of specific neural networks and release of messengers (Lecrux, Bourourou, & Hamel, 2019), suggesting the existence of multiple neural pathways influencing the hemodynamic output (Mathias, Kenny, Plank, & David, 2018). Although the identification of the precise neural correlates of hemodynamic responses is complex, it has been observed that changes in hemodynamics correlate with changes in gamma band (Harris et al., 2014; Niessing et al.,

2005; Shmuel & Leopold, 2008), which are a signature of engaged neuronal networks (Jia & Kohn, 2011). Overall, we can speculate that a sustained CBF responses in specific areas could be attributed to a larger engagement of the underlying networks.

Cerebrovascular plasticity is observed at many hierarchic levels and the time scale of these different processes span a wide range. Changes in CBF in response to increases in neural activity occur with a time constant on the order of seconds, whereas changes in cerebrovascular architecture can be due to sensory deprivation, aerobic exercise or hypoxia and they can occur with time constants of several weeks (Bogorad, Destefano, Linville, Wong, & Searson, 2019). Given the small time-window in which we observed changes in CBF, we may interpret the increasing in CBF after the task as an increase in the neural activity in those specific areas.

ASL signal encodes the time course of a single physiological parameter (CBF) and it can detect changes in a lower frequency range (Borogovac, Habeck, Small, & Asllani, 2010) compared to BOLD signal which is dominated by noise at low frequency. Furthermore, CBF measurements are highly reproducible across time and scanners (Jann et al., 2015). Together with our results we can conclude that resting CBF can be an important imaging marker for characterizing resting brain function and to better understand the neurovascular mechanisms underlying resting states.

Overall, we were able to demonstrate resting CBF increases after the end of the motor learning task. The control session allowed us to exclude an effect of time on CBF changes, leading to an important connection between neuroplastic changes induced by learning and the perfusion in the resting brain. Further studies are needed to better investigate the physiological meaning of the oscillatory patterns found in the post-task resting period. An increased sample size, as well as clinical populations, would be indispensable in order to generalise the use of a data glove to probe neuroplasticity.

CHAPTER 7

Investigating the role of cortical myelin on brain function and neuroplasticity

ABSTRACT

Myelination of grey matter is variable across the cortex and is subject to changes during brain development. MRI methods have been recently developed to investigate the myelin content of cerebral cortex by exploiting the sensitivity of the MR longitudinal relaxation time (T1) to myelin content. Despite the fact that grey matter myelination has been studied in recent years, its general functions and its role in adult neuroplasticity are still not well known.

Here we aim to study the relationship between GM myelination and the functional activity during a motor task aimed at probing plasticity; respectively assessed with T1-sensitive MP2RAGE and ASL-BOLD sequences. We hypothesised that higher cortical GM myelination, represented by T1, would be associated with higher functional and vascular task-responses in predefined regions of interest (ROIs). We also explored whether the amount of GM myelination is associated with the degree of change of functional BOLD and CBF signals during task learning.

20 healthy volunteers underwent one 3T MRI session involving: (I) a sequence motor learning task session performed with a data glove with simultaneously acquisition of ASL (CBF) and BOLD signals and (II) a structural scan to extract R1 maps (1/T1) acquired with a MP2RAGE sequence.

We showed a positive correlation between R1, assumed to represent the amount of GM myelination, and BOLD signal during the motor task in both occipital cortices. We also showed an association between the amount of GM myelination, indexed by R1, and the reduction of functional signal during task execution, in some of the ROIs. Despite the lack of correlation between R1 maps and behavioural changes to the task, these results provide a link between the structural morphology and the functional characteristic of the brain, as well as a window on the role of cortical myelination in neuroplasticity.

KEY WORDS

Cortical Myelination – BOLD – CBF – Neuroplasticity

7.1 INTRODUCTION

Myelin is a mixture of proteins and phospholipids forming an insulating sheath wrapped around axons to provide electrical insulation and metabolic support (Simons & Nave, 2016). The mechanisms and functions of white matter myelin have been extensively studied, but less is known about grey matter (GM) myelination. Myelination of GM axons is variable (Tomassy et al., 2014) and cortical areas responsible for higher cognitive function contain less myelin and require more time to become myelinated during brain development (Glasser, Goyal, Preuss, Raichle, & Van Essen, 2014). Recent findings suggest GM myelination to have an active role in the synchronization of conduction velocity of the entire network (Timmler & Simons, 2019), indicating that cortical myelination could be informative of the communication in a specific neural network. Nevertheless, the exact function of GM myelination is still under debate.

Cortical myelination is subject to plasticity mechanisms throughout development and it is not completely established until 30 years of age (Deoni, Dean, Remer, Dirks, & Muircheartaigh, 2015; Shafee, Buckner, & Fischl, 2015). Swire et al. (Swire et al., 2019) showed an indirect control of adaptive myelination by vascular response and neural activity, indicating that endothelin signalling may be employed in the coupling between the metabolic support of function and myelin demand, representing a novel mechanism for adaptive myelination. Furthermore, an association between myelination and learning has been shown in animals (McKenzie et al., 2014) thanks to the main role of oligodendrocytes in the adaptation of myelin structure (Xiao et al., 2016). However, no studies have yet investigated the role of GM myelination in adaptation and plasticity in vivo and in humans, particularly during adulthood.

Despite GM myelination having been widely studied in the recent years, its functions are still not well known (Timmler & Simons, 2019). Recent animal works have demonstrated the

connection between cortical myelination and electrical activity (Fields, 2015; Pajevic, Basser, & Fields, 2014), suggesting that the amount of cortical myelin in a region predicts the magnitude of electrophysiological responses. In humans, Hunt et al. (Hunt et al., 2016) showed a positive relationship between GM myelination and electrophysiological networks assessed with MEG, suggesting that myelin supports functional networks. Whether these relations are also observable in functional MRI has not been explored yet.

MRI-based methods have been recently developed to investigate the myelin content of cerebral cortex (Shams, Norris, & Marques, 2019) and in recent years progress has been made in mapping individual cortical areas in-vivo, exploiting the sensitivity of the MR longitudinal relaxation time (T1) to myelin content (Dick et al., 2012; Fischl et al., 2004; Geyer, Weiss, Reimann, Lohmann, & Turner, 2011; Marques & Gruetter, 2013; Sereno, Lutti, Weiskopf, & Dick, 2013; Stüber et al., 2014). Previous works have demonstrated a direct relationship between longitudinal relaxation rate (R1 - the inverse of T1) and myelin content (Mottershead et al., 2003; Schmierer, Scaravilli, Altmann, Barker, & Miller, 2004). Studies have also reported a good correspondence between histological data and myelin patterns in the cortex observed with MRI (Eickhoff et al., 2005) and the ability to detect distinct myelination patterns across the cortex (Walters et al., 2003).

Approaches to investigate myelination in the GM have been developed based on MPRAGE acquisition (Mugler & Brookeman, 1990), such as MP2RAGE implemented by Marques et al. (Marques, Kober, Krueger, & Zwaag, 2010). They extracted quantitative R1 maps from the ratio of two MPRAGE images acquired with different excitation flip angles and inversion times. R1 maps were then corrected for the effects of the radio-frequency receive field B_1 and R2*. Since then, the MP2RAGE technique has been widely used to detect variation in myelination across the cortex (Marques & Gruetter, 2013; Waehnert et al., 2014).

Given the assumed role of GM myelination in network efficiency, here we aim to study the relationship between cortical GM myelination, represented by R1, and the functional activity during a motor task; respectively assessed with MP2RAGE and ASL-BOLD sequences. We hypothesised that in a cross-sectional study across participants higher GM myelination would be associated with higher functional and vascular task-responses in predefined regions of interest (ROIs). We also explored whether the amount of GM myelination is associated with the degree of change of functional and vascular signals that index adaptation during motor task execution.

7.2 METHODS

Participants. Participants' details are explained in chapter 6.

Magnetic Resonance Imaging and the motor task. During the MRI session participants underwent a functional and a structural scan.

Details of the functional scan are described in the previous chapter (chapter 6), together with the description of the motor task they executed in the scanner.

Participants also underwent MP2RAGE sequence (Marques et al., 2010) to obtained in-vivo whole-brain quantitative T1 maps at 1mm isotropic resolution (TI_1 = 700 ms, TI_2 = 1500 ms, TR = 5 s, TE = 2.36 ms, GRAPPA = 2, scan time = 7:55 min).

DATA ANALYSIS

Behavioural response to the task. Behavioural analysis details are explained in chapter 6.

MRI analysis. Details of the functional MRI analysis to model the functional responses to the task and decreasing of responses during repeated task execution are reported in the previous chapter (chapter 6).

T1w images were first brain extracted using AFNI software (Analysis of Functional NeuroImages - afni.nimh.nih.gov/afni) and then FreeSurfer 'recon-all' function (v 6.0.0; http://surfer.nmr.mgh.harvard.edu/fswiki/recon-all) was used for cortical reconstruction and brain segmentation. Participant's individual quantitative R1 maps (1/T1) were generated during reconstruction on the scanner (Marques et al., 2010) and they were then mapped onto the cortical surface at a specific cortical depth (with a 1 projection fraction) using FreeSurfer function 'mri_vol2surf'.

Correlation analysis between cortical myelin and functional activity. Occipital and motor cortex bilaterally were defined as regions of interest (ROIs) on the basis of the "Harvard-Oxford anatomical atlas", given their role in the execution of the motor task (**Figure 7.1**). For each subject, each of the cope images (BOLD and CBF) from the task responses contrast were transformed to the Montreal Neurological Institute (MNI) standard space with 12 degrees of freedom using the registration matrix previously defined on EPI volume (chapter 6). The resulting images were then masked by each ROI and thresholded at the 95th percentile in order to retain only the voxels responding most strongly to task execution and individually masked for GM, the GM having previously been identified with FSL FAST (Zhang, Brady, & Smith, 2001). The resulted areas (intersection between functional peaks and ROIs) were then transformed to the space of the R1 brain. The mean R1 in these areas was extracted using FreeSurfer 'mris_calc' tool. CBF and BOLD mean responses were also respectively extracted in each area.

Pearson correlation tests were carried out between R1 values and CBF, and R1 maps and BOLD using RStudio (http://www.rstudio.com/). Correlation were considered significant at $p < 0.05$. Bonferroni correction was used to correct for multiple comparisons across the ROIs; setting the new pvalue for considering significant the differences at 0.0125.

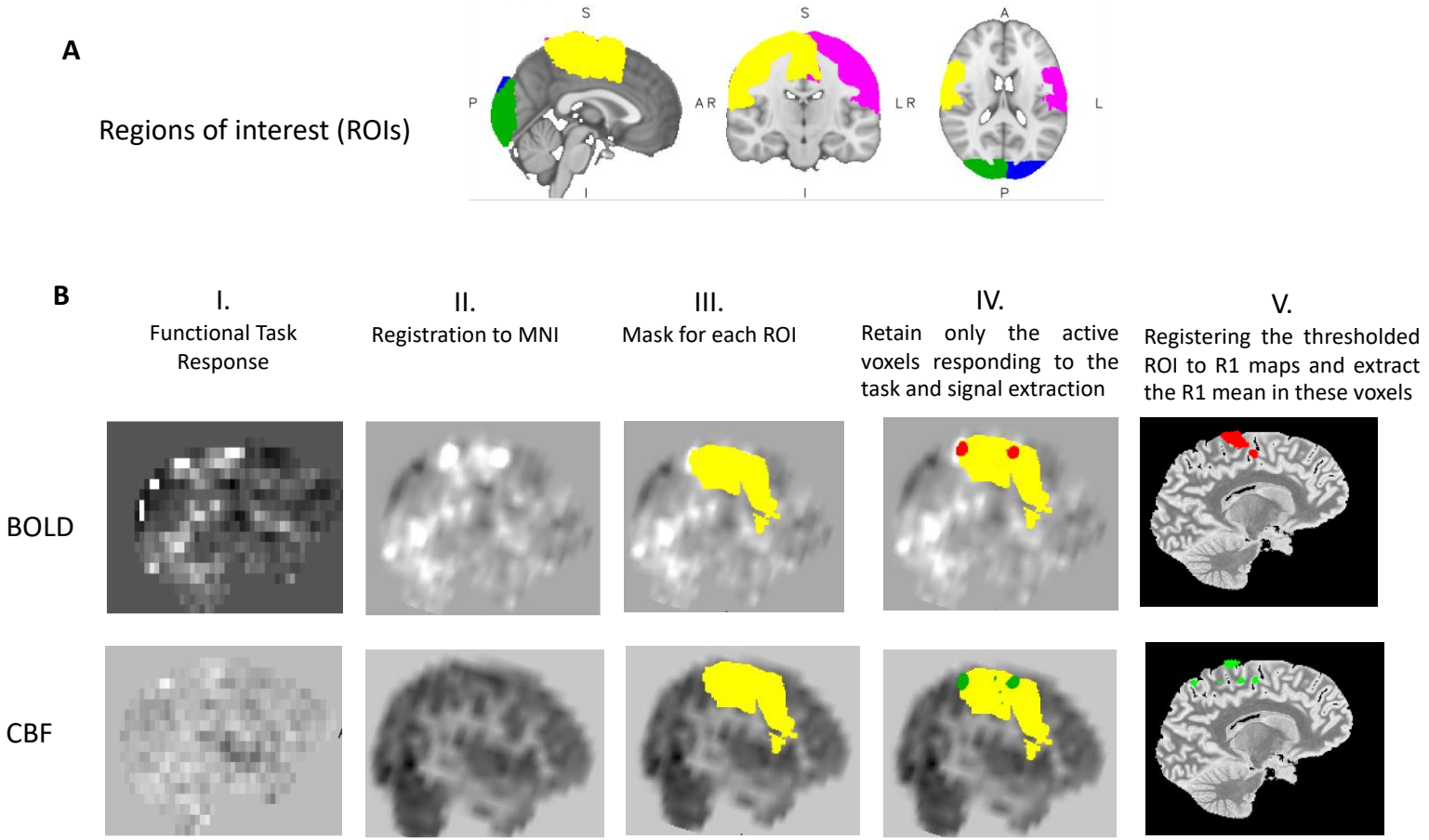

Figure 7.1. Analysis pipeline. *(A) Bilateral motor cortex and bilateral occipital cortex were defined as regions of interest (ROIs) on the base of the 'Harvard-Oxford Atlas'. (B) Pipeline of the analysis: (I) COPE images of task responses from the FEAT model are (II) transformed to standard space. (III) The image is then masked for each ROI. (IV) The image is thresholded at the 95th percentile in order to retain only the voxels responding to task execution and mean signal change is extracted, and then masked for GM. (V) The resulted areas (intersection between functional peaks and ROIs) are transformed to the space of the R1 map and R1 mean (s^{-1}) in those voxels is calculated.*

Correlation analysis between cortical myelin and changes in functional activity. The same pipeline described in the previous paragraph was also applied to investigate the effect of cortical myelination on functional and vascular signals decreasing during task execution, using the cope images (BOLD and CBF) from the decrease of responses during task execution from block to block (Picture of the model: Chapter 6 – Figure 6.2-B).

Pearson correlation tests were carried out between R1 values and change in CBF, and R1 maps and change in BOLD using RStudio (http://www.rstudio.com/). Correlation were considered significant at $p < 0.05$. Bonferroni correction was used to correct for multiple comparisons across the ROIs; setting the new pvalue for considering significant the differences at 0.0125.

Correlation between cortical myelin and performance improvement. The changes in performance during task execution were quantified by the slope of improvement (calculated as the mean of the differences in the correlation between the size of the two circles block after block), for each individual subject. In order to investigate the association between performance improvement and cortical myelin, Pearson correlation tests were carried out between R1 values in each intersected area and the slope of behavioural changes using RStudio (http://www.rstudio.com/). Correlation were considered significant at $p < 0.05$. Bonferroni correction was used to correct for multiple comparisons across the ROIs; setting the new pvalue for considering significant the differences at 0.0125.

Partial volume effects (PVE). Functional data voxel size is much bigger than the structural data voxel size, therefore the functional MRI acquisition could be more affected than the structural acquisition by differences of functional signal across the cortical thickness and the presence of extra-cortical tissue within the voxel. To investigate the potential confound of cortical thickness on functional activation, firstly, cortical thickness was calculated for each

subject using FreeSurfer (v 6.0.0; http://surfer.nmr.mgh.harvard.edu/fswiki/recon-all)). The entire pipeline is fully explained online (http://surfer.nmr.mgh.harvard.edu/fswiki/FreeSurferAnalysisPipelineOverview). In summary cortical thickness maps are calculated as the closest distance between GM/WM surface to the pial surface at each vertex of the tessellated surface (Fischl & Dale, 2000). Secondly, a Pearson correlation test between cortical thickness and CBF/BOLD task-response in each intersected area using RStudio was run to investigate the association between cortical thickness and functional activation (http://www.rstudio.com/). Correlation were considered significant at $p < 0.05$. Bonferroni correction was used to correct for multiple comparisons across the ROIs; setting the new pvalue for considering significant the differences at 0.0125.

7.3 RESULTS

Task responses and decreasing of responses during task execution. These results are reported in the previous chapter (Chapter 6. Task related Functional response – **Figures 6.4 and 6.5**).

Correlation between R1 maps and functional activity. Different correlation tests were run to investigate the association between R1 maps (our indicator of cortical myelination) and functional activation. We found a significant positive correlation between BOLD task response and R1 in the areas intersected with both of occipital cortices (right: R=0.69, p=0.001 (statistical difference is still significant after Bonferroni correction); left: R=0.48, p=0.04). We did not observe a significant correlation between BOLD task response and R1 the areas intersected with the motor cortices (right: R=0.14, p=0.53; left: R=0.24, p=0.30). CBF task response did not correlate with R1 in any of our intersected areas. (Right occipital cortex: R=0.28, p=0.24; Left occipital cortex: R=0.20, p=0.40; Right motor cortex: R=-0.01, p=0.97; Left motor cortex: R=-0.1, p=0.67). (**Figure 7.2**).

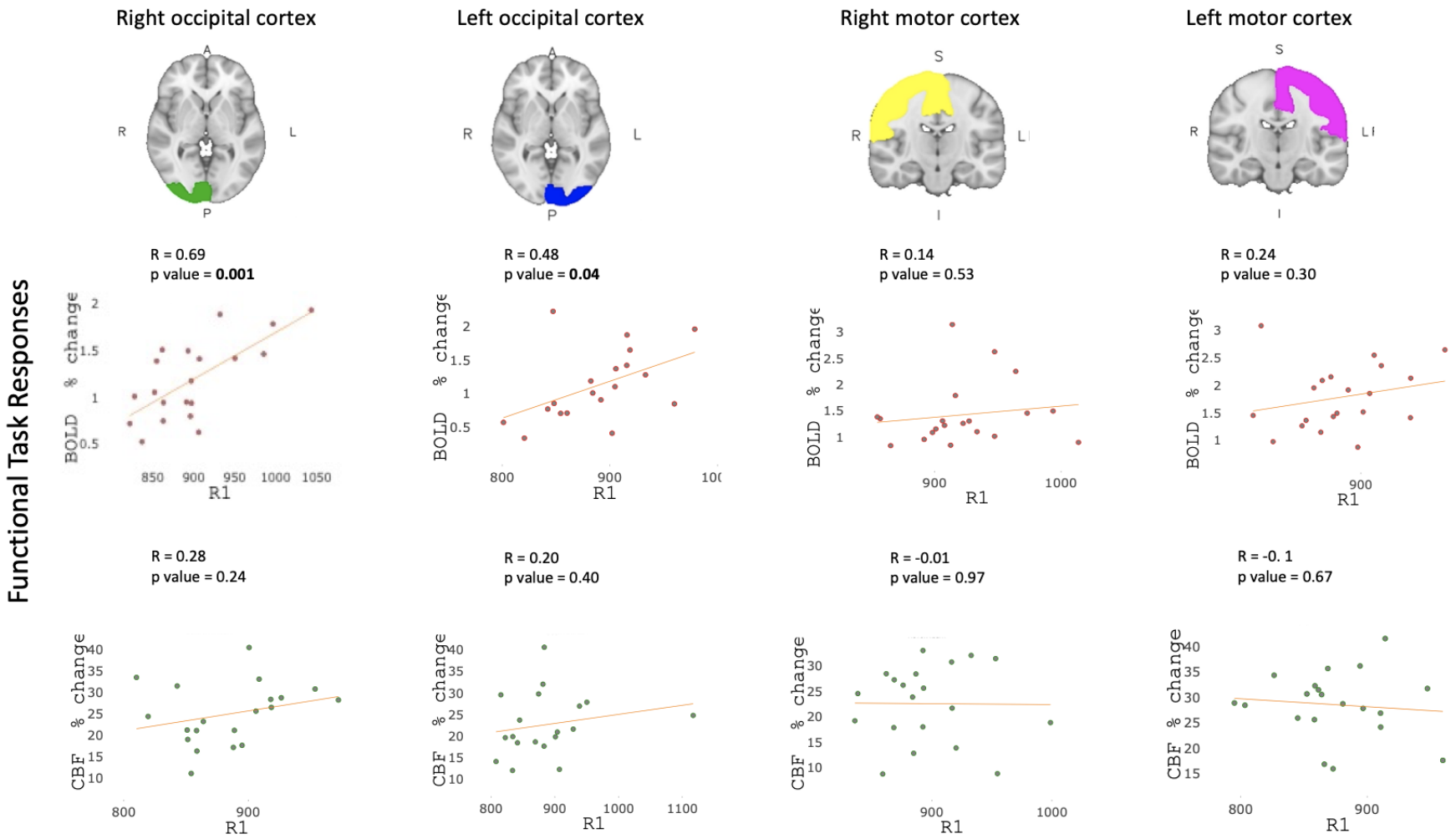

Figure 7.2. Functional task responses and R1 maps. *Correlation plots for each ROI. X axis: R1 values (s^{-1}). Y axis: Functional Task responses for BOLD (top) and CBF (bottom). Each point represents one participant.*

Correlation between R1 maps and changes in BOLD and CBF signals during task execution. Correlation tests were also used to investigate the association between R1 values and functional and vascular signals decreasing during task execution. We found a significant positive correlation between the amount of BOLD signal decrease (expressed as percentage change) during task execution and R1 values in areas intersected with occipital cortex bilaterally (right: R=0.61, p=0.003 (statistical difference is still significant after Bonferroni correction); left: R=0.53, p=0.01) and in areas intersected with the left motor cortex (R=0.77, p<0.001. When the outlier is removed, the correlation is still present (R=0.5, p=0.04)) (Outlier was defined on the criterion of being 3 standard deviations away from the mean) . No significant correlation was found in the areas intersected with right motor cortex (R=-0.06, p=0.79). CBF decreasing during task execution did not correlate with R1 in any of the areas intersected with our ROIs (Right occipital cortex: R=0.26, p=0.27; Left occipital cortex: R= -0.27, p=0.24; Right motor cortex: R= -0.06, p=0.81; Left motor cortex: R= -0.01, p=0.99). (**Figure 7.3**).

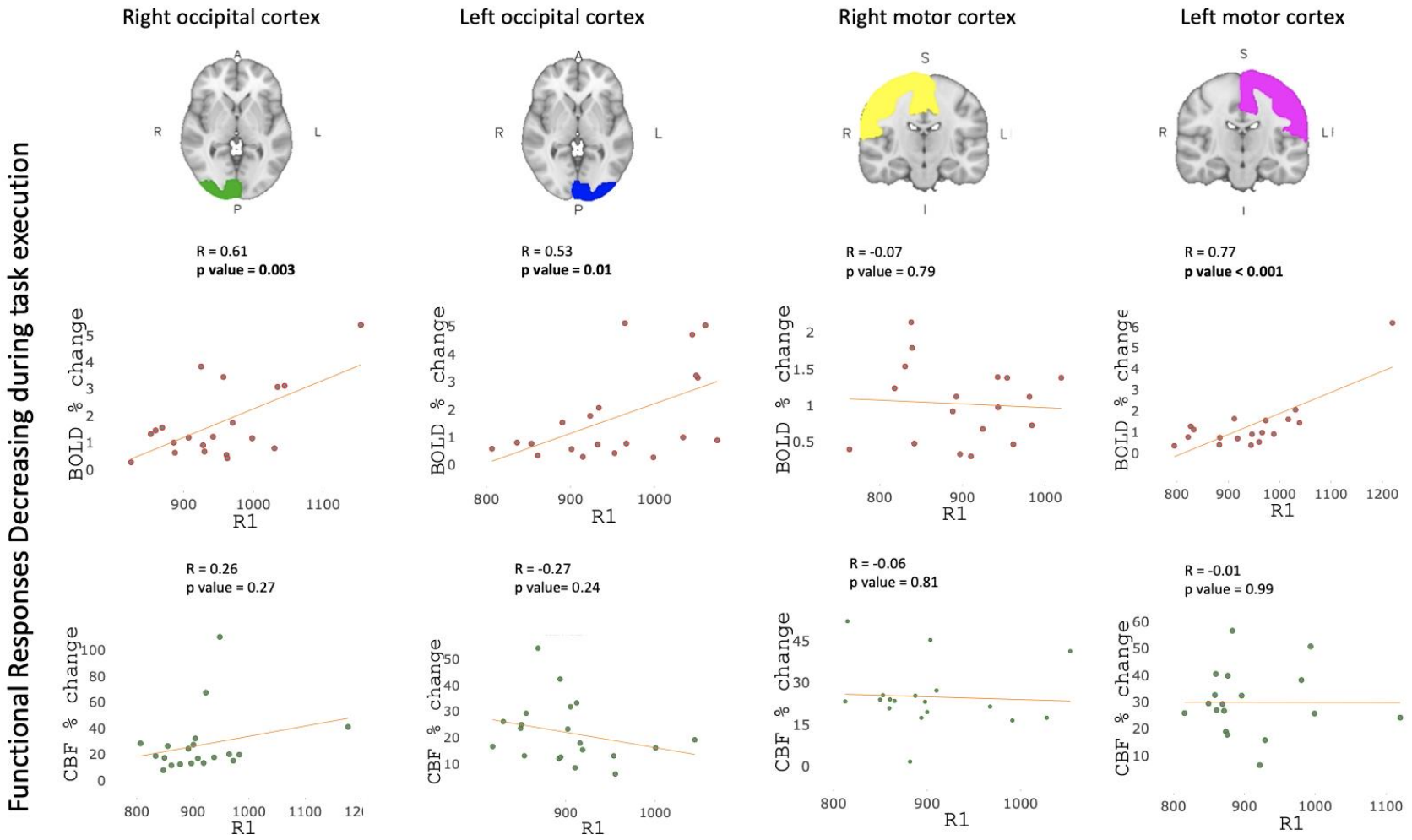

Figure 7.3. Functional task responses decrease and R1 maps. *Correlation plots for each ROI. X axis: R1 values (s^{-1}). Y axis: Functional response decreasing during task execution for BOLD (top) and CBF (bottom).*

Correlation between R1 maps and performance improving. No significant correlation between R1 values and slope of changes in task performance was found in any of the areas intersected with our ROIs. (BOLD - Right occipital cortex: R=0.04, *p*=0.86; Left occipital cortex: R=0.01, *p*=0.96; Right motor cortex: R=-0.16, *p*=0.5; Left motor cortex: R=-0.13, *p*=0.58. CBF - Right occipital cortex: R=0.18, *p*=0.44; Left occipital cortex: R=-0.17, *p*=0.48; Right motor cortex: R=-0.26, *p*=0.26; Left motor cortex: R=-0.21, *p*=0.36).

PVE problem. No significant correlation between the task functional responses and cortical thickness was found in any of the areas intersected with our ROIs (**Figure 7.4**); indicating that any effect of cortical thickness on the amount of functional and vascular activation observed is likely to be weak (BOLD - Right occipital cortex: R=0.31, *p*=0.18; Left occipital cortex: R= -0.13, *p*=0.58; Right motor cortex: R=0.20, *p*=0.40; Left motor cortex: R=0.03, *p*=0.89. CBF - Right occipital cortex: R= -0.02, *p*=0.91; Left occipital cortex: R= -0.14, *p*=0.55; Right motor cortex: R=0.1 *p*=0.95; Left motor cortex: R=-0.17, *p*=0.45).

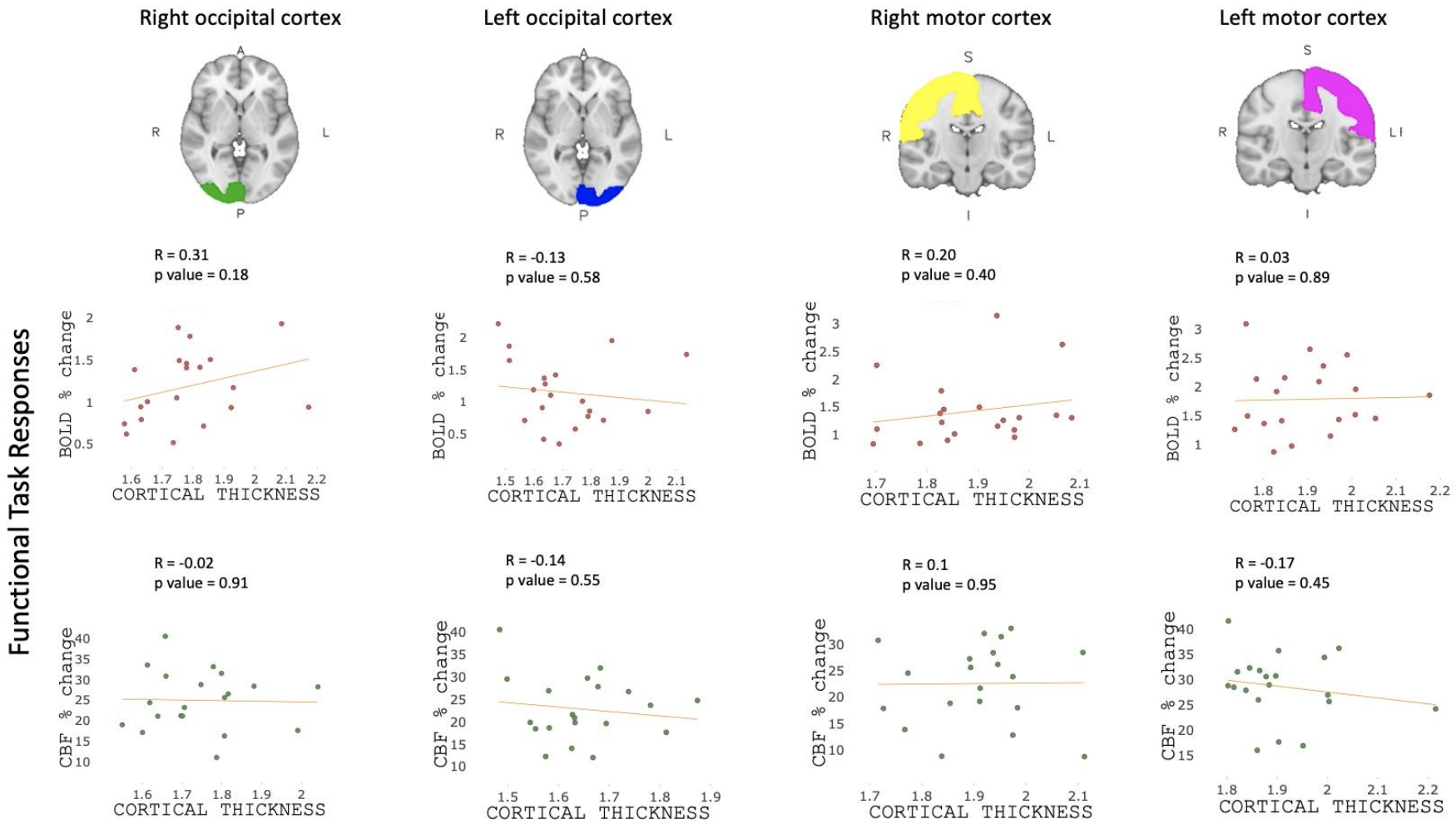

Figure 7.4. Functional task responses and cortical thickness. *Correlation plots for each ROI to investigate the association between cortical thickness and measured activation. X axis: Cortical thickness. Y axis: Functional task responses for BOLD (top) and CBF (bottom).*

7.4 DISCUSSION

In the present study, we showed a correlation between cortical R1 values, as an indicator of GM myelination, and BOLD signal during a motor task in bilateral occipital cortex. We also showed an association between R1 values and the decrease in size of functional responses during task execution, in some of the areas intersected with predefined ROIs in both motor and visual cortex.

MP2RAGE as a method to map cortical myelination. The methods used in this study to investigate myelination in the GM rely on the MP2RAGE acquisition (Marques et al., 2010) which creates maps based on the longitudinal relaxation rate R1 (Dick et al., 2012; Fischl et al., 2004; Geyer et al., 2011; Marques & Gruetter, 2013; Sereno et al., 2013; Stüber et al., 2014). R1 variations reflect water mobility (Bock, Kocharyan, Liu, & Silva, 2009; Sigalovsky, Fischl, & Melcher, 2006), but it is worth noting the impact of iron content on R1 tissue contrast (Rooney et al., 2007). Iron and myelin often colocalize within the cortex (Fukunaga et al., 2010), therefore it can be assumed that cortical T1 contrast is partly caused by iron. But the literature regarding iron and T1 contrast is controversial with data showing either a clear correlation or no significant correlation between the two (Ogg & Steen, 1998; Steen, Reddick, & Ogg, 2000). Further studies with the use of different methods to investigate myelination in the GM would be ideal to discern between the myelin and iron contents in the brain. Other methods to investigate cortical GM myelination are the apparent transverse relaxation rate R2* (the inverse of the apparent transverse relaxation time T2*) (Cohen-Adad et al., 2013; Sanchez-Panchuelo, Francis, Schluppeck, & Bowtell, 2012) and T1w/T2*w mapping (Glasser & Van Essen, 2011; Martino et al., 2015).

Myelin water fraction imaging using multi-compartment T2 fitting approaches (Mackay et al., 1994) and magnetisation transfer included in multi-compartment relaxometry (Deoni & Kolind, 2015; Stanisz, Kecojevic, Bronskill, & Henkelman, 1999) are known to be the most specific methods to detect myelin concentration; but the higher specificity leads to a decrease in sensitivity which does not permit entire brain acquisitions at the resolution required to map cortical myelin distribution (Shams et al., 2019). Taken together, R1 maps are then more reproducible and ex-vivo studies have shown a direct relationship between R1 and myelin content (Mottershead et al., 2003; Schmierer et al., 2004).

Cortical myelination predicts functional activity. We observed a positive correlation between the amount of cortical myelination (R1 values) in both the occipital cortices and the BOLD signal during task execution, indicating that the amount of cortical myelination, detected with R1 maps, predicts the functional activation during motor task execution.

In recent years, studies have raised the hypothesis that the function of myelination in the grey matter is not to speed up nerve conduction to maximal values, but to synchronize conduction velocity of the entire network (Timmler & Simons, 2019). This hypothesis is supported by the well-known model where the precision of spike timing is a critical parameter in neuronal network function and myelination can affect the absolute time that it takes for a spike to arrive (Pajevic et al., 2014). Furthermore, the frequency, propagation and coupling of the neural activity is strongly influenced by conduction delays and thus by myelin (Nunez, Srinivasan, & Fields, 2015). Therefore, cortical myelination could be informative of the communication in a specific neural network. We can then speculate that cortical myelination could be a proxy of efficiency in a specific brain network.

The lack of significant correlation observed in the motor cortex could be attributed to the small variability in R1 values reported in our sample. Therefore, we are not able to conclude whether it could be interpreted as a less efficient network compared to the occipital one.

We did not observe significant correlation between cortical myelination and CBF measurements of task response. Given that CBF is arguably a more reliable measurement of neural activity than BOLD (Blockley, Griffeth, Simon, & Buxton, 2013) and that myelin maps correlate with the density of neurons per unit cortical volume where lightly myelinated areas tend to have lower neuronal densities (Collins, Airey, Young, Leitch, & Kaas, 2010; Glasser & Van Essen, 2011), we would expect a strong positive correlation between CBF signal and myelin content. The lack of correlation could be due to a methodological issue, such as lower contrast-to-noise in the CBF acquisition compared to BOLD. It is worth considering the hypothesis of an opposite effect, where less energy is needed for a given function because of higher myelination that makes the area more efficient. In order to better understand the source of the issues, further studies are needed with a pipeline more focused on CBF acquisitions.

Cortical myelination is associated with short-term plasticity. We found a positive correlation between cortical myelination and the decreasing of BOLD task-related signals during task execution in some of the areas intersected with our ROIs.

As discussed in the previous chapter (chapter 6), the decrease of positive functional and vascular signals that accompany motor task execution is widely accepted to be a reflection of changes ascribable to neuroplasticity mechanisms (Pascual, Wassermann, Sadato, & Hallett, 1995; Shadmehr & Holcomb, 1997).

It has been shown that myelination has a role in plasticity and learning. McKenzie et al. (McKenzie et al., 2014) have shown that the loss of MyrF transcription factor, essential for oligodendrocyte differentiation, causes a deficit in learning a skilled motor task despite no other

observed behavioural deficits, concluding that the production of new oligodendrocytes and new myelin is essential for learning a new motor task. These results were broadened by Xiao et al. (Xiao et al., 2016) showing that the maturation of new oligodendrocytes is essential to learning on a time scale of hours, indicating that oligodendrocytes may have a role in adaptation of myelin structure. Current studies are focusing on the role of myelin on axons sprouting and synapse formation in organizing the connectivity of neural networks in GM through an inhibitory process (Fields, 2014; Schwab & Strittmatter, 2014; Tomassy et al., 2014). The process is explained as backpropagating action potentials that reduce synaptic strength and couple neurones into transient functional assemblies during learning (Bukalo, Campanac, Hoffman, & Fields, 2013). Human studies have also shown a positive correlation between cortical myelination, cognitive abilities and improvement in performance (Grydeland, Walhovd, Tamnes, Westlye, & Fjell, 2013; Kwon, Pfefferbaum, Sullivan, & Pohl, 2020).

Our results support the notion that cortical myelin plays a role in plasticity mechanisms, despite the lack of significant correlation between R1 maps and behavioural changes during task execution. GM myelination correlates with a decreasing of BOLD signal in both occipital cortices and in the left motor cortex only (**Figure 7.3**), indicating that GM myelin very likely has an effect on adaptation and plasticity, but further studies are needed to clarify the role of GM myelin in BOLD and CBF measures of plasticity.

Overall, we were able to demonstrate a relationship between cortical myelination and functional activity, as well as with functional adaptations during the execution of a motor adaptation task. These results provide a strong link between the structural morphology and the functional characteristics of the brain. Further studies are needed in order to better understand the physiological mechanisms by which cortical myelin is acting on functional activity. For

this purpose, studies that allowed the contemporary record of the neural and vascular activity would be essential; such as EEG-fMRI studies in humans or two-photon imaging studies in animals.

CHAPTER 8

General Discussion

This thesis had two main aims. Neuroscientifically, it aimed to better understand mechanisms supporting brain plasticity in MS and healthy brain. Methodologically, it aimed to explore new approaches to study neuroplasticity. Chapters 2 and 3 investigated the mechanisms underlying long-term neuroplasticity in MS. Specifically, different MRI techniques have been employed to predict the outcome of a visuomotor training and to explore the changes underlying the BOLD adaptations. Given that the interpretation of BOLD is not straightforward because of the coexistence of many contributing physiological parameters, the other experimental chapters have employed advanced neuroimaging techniques to study neuroplasticity. Specifically, chapter 4 aimed to study the changes in brain energetics underlying adaptation in healthy and MS brain using calibrated fMRI. The results highlight the importance of using quantitative MRI techniques, rather than BOLD fMRI alone, to study simultaneously different physiological mechanisms involved in brain plasticity. In chapter 5 the same data from chapter 4 have been used and a further step forward has been made, showing the feasibility of estimating relative oxygen consumption voxel-by-voxel without relying on BOLD-defined ROI.

In chapter 6 a new task to study short-term neuroplasticity has been validated and it has been used to probe changes in vascular baseline, assessed with quantitative measurements of blood flow. The same task was then used in chapter 7 to investigate the relationship between grey matter myelination and functional/vascular activity during task execution, highlighting the importance of integrating structural and functional MRI.

In this chapter the main findings of this thesis are brought together in order to integrate the results, discuss the strength and limitations of the methods, and consider future plans.

8.1 MULTIPLE SCLEROSIS

The first four experimental chapters of the thesis investigated neuroplasticity in MS patients. In chapter 2, we found that MS inflammation alters the shape and volume of basal ganglia and the dissimilarities are associated with different improvements of performance during a visuomotor task. These results support the idea that deep grey matter degeneration can be a predictor and/or a marker of disease progression (Wylezinska, Cifelli, Jezzard, Palace, & Alecci, 2003; Zivadinov et al., 2013). Furthermore, we also showed a reorganization of the subcortical-cortical connection compared to healthy volunteers, indicating that structural brain plasticity is still preserved in people with MS. This result was extended in chapter 3: despite the structural impairment observed in chapter 2, we showed that also the functional neuroplasticity mechanisms are preserved in MS patients. Particularly, the reduction observed in BOLD after 4weeks of a visuomotor training task, was accompanied by an increase in CBF baseline, supporting the role of CBF as a biomarker for functional/behavioural changes (Mozolic, Hayasaka, & Laurienti, 2010; Vas, Spence, & Chapman, 2015). A third longitudinal point, together with a control-patients group, would have helped in understanding whether the perfusional and behavioural changes are sustained over time and whether the changes observed are due to the task and not to the time passing.

In chapter 4, we employed advanced neuroimaging techniques to study short-term neuroplasticity. We showed that MS patients present a metabolic impairment at rest in task-related regions; but they were then able to recruit a similar amount of energy when compared to healthy volunteers to perform the tasks. Indicating that the metabolic impairment in MS

patients is masked by the task execution; our results are in line with previous studies reporting a metabolic impairment in MS (Ge et al., 2012; Marshall et al., 2014). Furthermore, in chapter 5 we observed a lack of adaptation in oxygen consumption during task execution in MS patients compared to healthy volunteers.

Taken together our results lead to the idea that the investigation of metabolism in MS brain could be an early detector of disease. Given that patients recruited in chapter 4 and 5 were very stable, as reported in table 4.1, we could not draw conclusion on the later stage of disease. Previous work has already suggested that the metabolic impairment could happen before the neurodegeneration as a reflection of inflammation (Marshall et al., 2014). It is widely known that energy in the brain is provided by mitochondria in the form of ATP and that mitochondrial dysfunction is common in neurodegenerative disease (Beal, 1995). The subsequent hypothesis is that an initial impairment in metabolism would lead to impaired perfusion and then to hypoxia; prolonged hypoxia could then lead to inadequate fuel to neurons resulting in neurodegeneration and subsequentially to cognitive dysfunction. Further studies are needed to test these hypotheses and cohorts at different stage of disease would permit the investigation of the temporal relationship of events. Furthermore, longitudinal studies would be useful to monitor the progression of the disease and they would help in the validation of new biomarkers to investigate disease outcomes and to design targeted interventions aimed at metabolic or perfusion dysfunction.

8.2 ADVANCED NEUROIMAGING TECHNIQUES TO STUDY NEUROPLASTICITY

The metabolic demand supporting neuroplasticity mechanisms was investigated in chapter 4, 5 and 6.

In chapter 4, we showed that the functional, vascular and energetic changes during task execution were different in distinctive areas of the brain, highlighting the importance of studying simultaneously different physiological mechanisms involved in brain plasticity. In chapter 5, we demonstrated the feasibility of mapping changes induced by tasks in $CMRO_2$ on a voxel-by-voxel basis; furthermore, the identification of regional metabolic response to the task identified on $CMRO_2$ maps directly is of great interest considering that using ROIs defined from BOLD-response only could miss metabolic responses happening in parts of the brain where BOLD may under-represent the change in oxygen consumption. These two chapters together, stress the importance of employing quantitative fMRI when studying neuroplasticity as a more informative method of brain adaptation, given the contribution of vascular and neural components to the BOLD signal (Blockley, Griffeth, Simon, & Buxton, 2013; Hoge, 2012; Tardif et al., 2016).

In chapter 6, we employed advanced CBF sequence to detect a sustained and localised CBF increase following 10 mins of motor task, investigated with a voxel-wise method. Previous studies have used BOLD signal to show baseline changes after new motor skills acquisition (Guerra-Carrillo, MacKey, & Bunge, 2014; Sami, Robertson, & Miall, 2014), whereas we were able to detect perfusion increasing directly on CBF maps. Considering the different nature of the two signals, as BOLD reflects a signal detected in the veins and CBF reflects a signal detected in the capillaries, we can easily understand the added value of multiparametric fMRI approach. Where resting CBF can be an important imaging marker for characterizing resting brain function and to better understand the neurovascular mechanisms underlying changes in resting states.

In chapter 7, the MP2RAGE sequence was employed to reveal a relationship between R1 values and functional/vascular adaptions during the execution of a motor task. Given the high reproducibility of R1 maps and the relationship between R1 and myelin content (Mottershead

et al., 2003; Schmierer, Scaravilli, Altmann, Barker, & Miller, 2004), our results in-vivo in humans corroborate previous hypothesis that myelination has a main role in plasticity and learning (McKenzie et al., 2014; Xiao et al., 2016).

In order to generalize the findings to different cognitive domains, further studies employing tasks involving different systems are needed. Furthermore, the same methods could be applied to different clinical populations to better understand the healthy as well as dysfunctional biological mechanisms supporting brain adaptions. Taken together, advanced neuroimaging techniques would contribute to the study of neuroplasticity given their more biologically specificity as methods and a more objective interpretability.

8.3 INTEGRATING STRUCTURAL AND FUNCTIONAL IMAGING

Different chapters of this thesis aimed to integrate the functional characteristics and the structural morphology of the brain. In chapter 2, the definition and the further structural investigation of the deep grey matter involved in the task was detected on the base of functional activation during task execution. A similar approach was used in chapter 7, where the functional task-related response was used to define ROIs, where R1 values were extracted. We demonstrated a relationship between R1 values and functional activity.

In chapter 3, functional and structural reorganization were investigated in parallel. We did not observe changes in brain structure, but we hypothesize that the observed changes in functional activity and perfusion could be reflected in structural changes in longer term.

Taken together, these chapters showed how different MRI measurements can be integrated to allow in-vivo detection of physiological processes sub-serving neuroplasticity in humans and the importance of treating the brain as a network when studying neuroplasticity.

Previous works investigated functional and structural changes in parallel (Keller & Just, 2016) and linked the observed changes with training and learning (Chapman et al., 2015; Tomassini et al., 2011). Further studies are needed in order to better understand the physiological mechanisms by which structure and functions of the brain interact together, hypothesising that the functional properties of the brain are mainly defined by the structural features of the neurons, their synaptic connections and brain networks. The integration of different methods, together with the higher interpretability of quantitative MRI, would help addressing the questions of how the physiology and micro-/macro-structure of the brain act together to code the information between neurons and their flow through synapses in order to promote optimal brain adaptation.

CONCLUSION

New approaches and analysis pipelines to investigate neuroplasticity have been explored in this thesis; results highlight the importance of treating the brain as a network and the advantages of integrating different MRI modalities. Advanced neuroimaging techniques have been employed to investigate in-vivo the physiological mechanisms and morphological characteristics supporting neuroplasticity. Our results emphasize the feasibility of using quantitative methods to study neuroplasticity, encouraging their application in this field given their higher biological interpretation. We also showed that the same methods are applicable to clinical populations, such as MS, despite the observed metabolic impairment. Our methods can contribute to the study of disease progression and to the building of targeted interventions. It is worth noting that not all the works presented in this thesis have been validated in MS patients,

additional studies in this direction are needed in order to generalize our results to different populations.

TAKE-HOME MESSAGE

This thesis is the culmination of a four-year journey; where I continuously had the chance to learn and to understand my own mistakes. If I had the opportunity to go back and redo part of the early chapters work, I would apply a data dimension reduction from the beginning, to group and select task-related regions in a more efficient way. I would also re-think about some analysis on the base of the statistical knowledge acquired in the later chapters. In the end, I would try to employ advanced MRI sequences used in later chapters, also in the first chapters, given their specificity and their ability to detect simultaneously multiple parameters, describing brain activity changes. Overall, this thesis reflects the learning process behind my PhD, and being able to discuss some of my early choices can be considered part of the personal development undertaken during this journey.

REFERENCES

Aboul-Enein, F., & Lassmann, H. (2005, January 11). Mitochondrial damage and histotoxic hypoxia: A pathway of tissue injury in inflammatory brain disease? *Acta Neuropathologica*. Springer. https://doi.org/10.1007/s00401-004-0954-8

Absinta, M., Nair, G., Sati, P., Cortese, I. C. M., Filippi, M., & Reich, D. S. (2015). Direct MRI detection of impending plaque development in multiple sclerosis. *Neurology: Neuroimmunology and NeuroInflammation*, *2*(5), e145. https://doi.org/10.1212/NXI.0000000000000145

Albensi, B. C. (2001). Models of Brain Injury and Alterations in Synaptic Plasticity. *Journal of Neuroscience Research*, *65*, 279–283.

Albert, N. B., Robertson, E. M., Miall, R. C., & Hall, G. (2009). The Resting Human Brain and Motor Learning. *Current Biology*, *19*(12), 1023–1027. https://doi.org/10.1016/j.cub.2009.04.028

Albouy, G., Sterpenich, V., Vandewalle, G., Darsaud, A., Gais, S., Rauchs, G., … Maquet, P. (2012). Neural correlates of performance variability during motor sequence acquisition. *NeuroImage*, *60*(1), 324–331. https://doi.org/10.1016/j.neuroimage.2011.12.049

Álvarez-Salvado, E., Pallarés, V., Moreno, A., & Canals, S. (2014). Functional MRI of long-term potentiation: Imaging network plasticity. *Philosophical Transactions of the Royal Society B: Biological Sciences*, *369*(1633). https://doi.org/10.1098/rstb.2013.0152

Amad, A., Seidman, J., Draper, S. B., Bruchhage, M. M. K., Lowry, R. G., Wheeler, J., … Smith, M. S. (2017). Motor Learning Induces Plasticity in the Resting Brain — Drumming Up a Connection. *Cerebral Cortex*, (March), 2010–2021. https://doi.org/10.1093/cercor/bhw048

Amaral, M. D., & Pozzo-miller, L. (2012). Intracellular Ca 2 + Stores and Ca 2 + Influx Are Both Required for BDNF to Rapidly Increase Quantal Vesicular Transmitter Release, *2012*. https://doi.org/10.1155/2012/203536

Assaf, Y., Johansen-Berg, H., & Thiebaut de Schotten, M. (2019). The role of diffusion MRI in neuroscience. *NMR in Biomedicine*, *32*(4), 1–16. https://doi.org/10.1002/nbm.3762

Attwell, D, & Laughlin, S. B. (2001). An energy budget for signaling in the grey matter of the brain. *Journal of Cerebral Blood Flow and Metabolism : Official Journal of the International Society of Cerebral Blood Flow and Metabolism*, *21*(10), 1133–1145. https://doi.org/10.1097/00004647-200110000-00001

Attwell, David, & Iadecola, C. (2002). The neural basis of functional brain imaging signals. *Trends in Neurosciences*, *25*(12), 621–625. https://doi.org/10.1016/S0166-2236(02)02264-6

Barghi, A., Allendorfer, J. B., Taub, E., Womble, B., Hicks, J. M., Uswatte, G., … Mark, V. W. (2018). Phase II Randomized Controlled Trial of Constraint-Induced Movement Therapy in Multiple Sclerosis . Part 2 : Effect on White Matter Integrity. *Neurorehabilitation and Neural Repair*, *32*(3), 233–241. https://doi.org/10.1177/1545968317753073

Basser, P. J., Mattiello, J., & LeBihan, D. (1994). MR diffusion tensor spectroscopy and imaging. *Biophysical Journal*, *66*(1), 259–267. https://doi.org/10.1016/S0006-3495(94)80775-1

Battaglini, M., Jenkinson, M., & De Stefano, N. (2012). Evaluating and reducing the impact of white matter lesions on brain volume measurements. *Human Brain Mapping*, *33*(9), 2062–2071. https://doi.org/10.1002/hbm.21344

Beal, M. F. (1995). Aging, energy, and oxidative stress in neurodegenerative diseases. *Annals of Neurology*, *38*(3), 357–366. https://doi.org/10.1002/ana.410380304

Beaulieu, C., Does, M. D., Snyder, R. E., & Allen, P. S. (1996). Changes in water diffusion due to Wallerian degeneration in peripheral nerve. *Magnetic Resonance in Medicine*, *36*(4), 627–631. https://doi.org/10.1002/mrm.1910360419

Behrens, T E J, Berg, H. J., Jbabdi, S., Rushworth, M. F. S., & Woolrich, M. W. (2007). Probabilistic diffusion tractography with multiple fibre orientations : What can we gain ?, *34*, 144–155. https://doi.org/10.1016/j.neuroimage.2006.09.018

Behrens, Timothy E.J., Woolrich, M. W., Jenkinson, M., Johansen-Berg, H., Nunes, R. G., Clare, S., … Smith, S. M. (2003). Characterization and Propagation of Uncertainty in Diffusion-Weighted MR Imaging. *Magnetic Resonance in Medicine*, *50*(5), 1077–1088. https://doi.org/10.1002/mrm.10609

Benedict, R. H., DeLuca, J., Phillips, G., LaRocca, N., Hudson, L. D., Rudick, R., & Multiple Sclerosis Outcome Assessments Consortium. (2017). Validity of the Symbol Digit Modalities Test as a cognition performance outcome measure for multiple sclerosis. *Multiple Sclerosis (Houndmills, Basingstoke, England)*, *23*(5), 721–733. https://doi.org/10.1177/1352458517690821

Bengtsson, S. L., Nagy, Z., Skare, S., Forsman, L., Forssberg, H., & Ullén, F. (2005). Extensive piano practicing has regionally specific effects on white matter development. *Nature*

Neuroscience, *8*(9), 1148–1150. https://doi.org/10.1038/nn1516

Biswal, B. B., Kylen, J. Van, & Hyde, J. S. (1997). Simultaneous Assessment of Flow and BOLD Signals in Resting-State Functional Connectivity Maps. *NMR in Biomedicine*, *10*, 165–170.

Black, J. E., Zelazny, A. M., & Greenough, W. T. (1991). Capillary and Mitochondrial Support of Neural Plasticity in Adult Rat Visual Cortex. *Experimental Neurology*, *111*, 204–209.

Blockley, N. P., Griffeth, V. E. M., Simon, A. B., & Buxton, R. B. (2013). A review of calibrated blood oxygenation level-dependent (BOLD) methods for the measurement of task-induced changes in brain oxygen metabolism. *NMR in Biomedicine*, *26*(8), 987–1003. https://doi.org/10.1002/nbm.2847

Blumenfeld-katzir, T., Pasternak, O., Dagan, M., & Assaf, Y. (2011). Diffusion MRI of Structural Brain Plasticity Induced by a Learning and Memory Task. *PLoS ONE*, *6*(6). https://doi.org/10.1371/journal.pone.0020678

Bock, N. A., Kocharyan, A., Liu, J. V, & Silva, A. C. (2009). Visualizing the entire cortical myelination pattern in marmosets with magnetic resonance imaging. *Journal of Neuroscience Methods*, *185*, 15–22. https://doi.org/10.1016/j.jneumeth.2009.08.022

Bogorad, M. I., Destefano, J. G., Linville, R. M., Wong, A. D., & Searson, P. C. (2019). Cerebrovascular plasticity : Processes that lead to changes in the architecture of brain microvessels. https://doi.org/10.1177/0271678X19855875

Bonzano, L., Tacchino, A., Brichetto, G., Roccatagliata, L., Dessypris, A., Feraco, P., … Bove, M. (2014). Upper limb motor rehabilitation impacts white matter microstructure in multiple sclerosis. *NeuroImage*, *90*, 107–116. https://doi.org/10.1016/j.neuroimage.2013.12.025

Bonzano, L., Tacchino, A., Roccatagliata, L., Inglese, M., Mancardi, G. L., Novellino, A., & Bove, M. (2015). An engineered glove for investigating the neural correlates of finger movements using functional magnetic resonance imaging. *Frontiers in Human Neuroscience*, *9*(September), 1–12. https://doi.org/10.3389/fnhum.2015.00503

Borogovac, A., Habeck, C., Small, S. A., & Asllani, I. (2010). Mapping brain function using a 30-day interval between baseline and activation : a novel arterial spin labeling fMRI approach. *Journal of Cerebral Blood Flow & Metabolism*, *30*(10), 1721–1733. https://doi.org/10.1038/jcbfm.2010.89

Bosnell, R. A., Kincses, T., Stagg, C. J., Tomassini, V., Kischka, U., Jbabdi, S., … Johansen-berg, H. (2011). Motor Practice Promotes Increased Activity in Brain Regions Structurally

Disconnected After Subcortical Stroke. *Neurorehabilitation and Neural Repair*. https://doi.org/10.1177/1545968311405675

Britz, J., Van De Ville, D., & Michel, C. M. (2010). BOLD correlates of EEG topography reveal rapid resting-state network dynamics. *NeuroImage*, *52*(4), 1162–1170. https://doi.org/10.1016/j.neuroimage.2010.02.052

Brooks, D. J., & Piccini, P. (2006). Imaging in Parkinson's Disease: The Role of Monoamines in Behavior. *Biological Psychiatry*, *59*, 908–918. https://doi.org/10.1016/j.biopsych.2005.12.017

Brown, J. A. (2006). Recovery of motor function after stroke. *Progress in Brain Research*, *157*, 223–228. https://doi.org/10.1016/S0079-6123(06)57015-3

Bruel-Jungerman, E., Davis, S., & Laroche, S. (2007). Brain plasticity mechanisms and memory: A party of four. *Neuroscientist*, *13*(5), 492–505. https://doi.org/10.1177/1073858407302725

Buckner, R. L., & Vincent, J. L. (2007). Unrest at rest : Default activity and spontaneous network correlations. *NeuroImage*, *37*, 1091–1096. https://doi.org/10.1016/j.neuroimage.2007.01.010

Bukalo, O., Campanac, E., Hoffman, D. A., & Fields, R. D. (2013). Synaptic plasticity by antidromic fi ring during hippocampal network oscillations OS, *110*(13). https://doi.org/10.1073/pnas.1210735110

Bullmore, E., & Sporns, O. (2009). Complex brain networks : graph theoretical analysis of structural and functional systems. *Nature*, *10*, 186–198. https://doi.org/10.1038/nrn2575

Bulte, D. P., Kelly, M., Germuska, M., Xie, J., Chappell, M. A., Okell, T. W., … Jezzard, P. (2012). Quantitative measurement of cerebral physiology using respiratory-calibrated MRI. *NeuroImage*, *60*(1), 582–591. https://doi.org/10.1016/j.neuroimage.2011.12.017

Butz, M., Wörgötter, F., & Ooyen, A. Van. (2009). Activity-dependent structural plasticity. *Brain Research Reviews*, *60*(2), 287–305. https://doi.org/10.1016/j.brainresrev.2008.12.023

Buxton, R. B. (2010). Interpreting oxygenation-based neuroimaging signals: the importance and the challenge of understanding brain oxygen metabolism. *Frontiers in Neuroenergetics*, *2*. https://doi.org/10.3389/fnene.2010.00008

Buxton, R. B. (2013). The physics of functional magnetic resonance imaging (fMRI). *Reports on Progress in Physics*, *76*(9). https://doi.org/10.1088/0034-4885/76/9/096601

Buxton, R. B., Frank, L. R., Wong, E. C., Siewert, B., Warach, S., & Edelman, R. R. (1998).

A General Kinetic Model for Quantitative Perhsion Imaging with Arterial Spin Labeling. *Magnetic Resonance in Medicine*, (19), 383–396.

Calabrese, M., Agosta, F., Rinaldi, F., Mattisi, I., Grossi, P., Favaretto, A., … Filippi, M. (2009). Cortical lesions and atrophy associated with cognitive impairment in relapsing-remitting multiple sclerosis. *Archives of Neurology*, *66*(9), 1144–1150. https://doi.org/10.1001/archneurol.2009.174

Camandola, S., & Mattson, M. P. (2017). Brain metabolism in health, aging, and neurodegeneration. *The EMBO Journal*, *36*(11), 1474–1492. https://doi.org/10.15252/embj.201695810

Casadio, M., Sanguineti, V., Morasso, P., & Solaro, C. (2008). Abnormal sensorimotor control , but intact force field adaptation , in multiple sclerosis subjects, (July 2007), 330–342.

Chapman, S. B., Aslan, S., Spence, J. S., Defina, L. F., Keebler, M. W., Didehbani, N., & Lu, H. (2013). Shorter term aerobic exercise improves brain, cognition, and cardiovascular fitness in aging. *Frontiers in Aging Neuroscience*, *5*(November), 1–9. https://doi.org/10.3389/fnagi.2013.00075

Chapman, S. B., Aslan, S., Spence, J. S., Hart, J. J., Bartz, E. K., Didehbani, N., … Lu, H. (2015). Neural mechanisms of brain plasticity with complex cognitive training in healthy seniors. *Cerebral Cortex*, *25*(2), 396–405. https://doi.org/10.1093/cercor/bht234

Chappell, M A, Groves, A. R., Macintosh, B. J., Donahue, M. J., Jezzard, P., & Woolrich, M. W. (2011). Partial Volume Correction of Multiple Inversion Time Arterial Spin Labeling MRI Data. *Magnetic Resonance in Medicine*, *C*(65), 1173–1183. https://doi.org/10.1002/mrm.22641

Chappell, Michael A, Groves, A. R., Whitcher, B., & Woolrich, M. W. (2009). Variational Bayesian Inference for a Nonlinear Forward Model. *IEEE Transactions on Signal Processing*, *57*(1), 223–236.

Chen, J, Zacharek, A., Li, Y., Li, A., Wang, L., Katakowski, M., … Chopp, M. (2009). N-CADHERIN MEDIATES NITRIC OXIDE-INDUCED NEUROGENESIS IN YOUNG AND RETIRED BREEDER NEUROSPHERES. *Neuroscience*, *140*(2), 377–388. https://doi.org/10.1016/j.neuroscience.2006.02.064.N-CADHERIN

Chen, Jieli, Zhang, Z. G., Li, Y., Wang, Y., Wang, L., Jiang, H., … Chopp, M. (2003). Statins Induce Angiogenesis, Neurogenesis, and Synaptogenesis after Stroke. *Ann Neurol*, (53), 743–751.

Cheng, A., Hou, Y., & Mattson, M. P. (2010). Mitochondria and neuroplasticity, *2*(5), 243–

256. https://doi.org/10.1042/AN20100019

Chiarelli, P. A., Bulte, D. P., Wise, R., Gallichan, D., & Jezzard, P. (2007). A calibration method for quantitative BOLD fMRI based on hyperoxia. *NeuroImage*, *37*(3), 808–820. https://doi.org/10.1016/j.neuroimage.2007.05.033

Chuang, K., Gelderen, P. Van, Merkle, H., Bodurka, J., Ikonomidou, V. N., Koretsky, A. P., … Talagala, S. L. (2008). Mapping resting-state functional connectivity using perfusion MRI, *40*, 1595–1605. https://doi.org/10.1016/j.neuroimage.2008.01.006

Ciccarelli, O., Werring, D. J., Wheeler-Kingshott, C. A. M., Barker, G. J., Parker, G. J. M., Thompson, A. J., & Miller, D. H. (2001). Investigation of MS normal-appearing brain using diffusion tensor MRI with. *Neurology*, *56(7)*, 926–933.

Cifelli, A., Arridge, M., Jezzard, P., Esiri, M., Palace, J., & Matthews, P. M. (2002). Thalamic Neurodegeneration in Multiple Sclerosis. *Ann Neurol*, *52*, 250–252. https://doi.org/10.1002/ana.10326

Clarke, D. D., & Sokoloff, L. (1999). Circulation and energy metabolism in the brain. In G. J. Siegel, B. W. Agranoff, D. S. Albers, S. K. Fisher & M. D. Uhler (Eds.). In *Basic Neurochemistry (6th ed.)*.

Cohen-Adad, J., Benner, T., Greve, D. N., Kinkel, R. P., Radding, A., Fischl, B., … Mainero, C. (2013). In vivo evidence of disseminated subpial T2* signal changes in multiple sclerosis at 7T: a surface-based analysis. *NeuroImage*, *57*(1), 1–20. https://doi.org/10.1016/j.neuroimage.2011.04.009.In

Colcombe, S. J., Kramer, A. F., Erickson, K. I., Scalf, P., Mcauley, E., Cohen, N. J., … Elavsky, S. (2004). Cardiovascular fitness, cortical plasticity, and aging. *Pnas*, *101*(9), 3316–3321.

Collins, C. E., Airey, D. C., Young, N. A., Leitch, D. B., & Kaas, J. H. (2010). Neuron densities vary across and within cortical areas in primates. *Pnas*, *107*(36), 15927–15932. https://doi.org/10.1073/pnas.1010356107

Cramer, S. C. (2008). Repairing the Human Brain after Stroke : I . Mechanisms of Spontaneous Recovery. *Ann Neurol*, (63), 272–287. https://doi.org/10.1002/ana.21393

Crossley, N. A., Mechelli, A., Scott, J., Carletti, F., Fox, P. T., Mcguire, P., & Bullmore, E. T. (2014). The hubs of the human connectome are generally implicated in the anatomy of brain disorders. *Brain*, *137*, 2382–2395. https://doi.org/10.1093/brain/awu132

Cruz-gómez, Á. J., Ventura-campos, N., Belenguer, A., Ávila, C., & Forn, C. (2014). The link between resting-state functional connectivity and cognition in MS patients. *MULTIPLE SCLEROSIS JOURNAL*, *20*(3), 338–348. https://doi.org/10.1177/1352458513495584

Cutter, G., Baier, M., & Rudick, R. (1999). Development of a multiple sclerosis functional composite as a clinical trial outcome measure. *Brain*, *122*(5), 871–882. https://doi.org/10.1093/brain/122.5.871

D'haeseleer, M., Cambron, M., Vanopdenbosch, L., & Keyser, J. De. (2011). Vascular aspects of multiple sclerosis. *The Lancet Neurology*, *10*(7), 657–666. https://doi.org/10.1016/S1474-4422(11)70105-3

Dai, W., Garcia, D., Bazelaire, C. De, & Alsop, D. C. (2008). Continuous Flow-Driven Inversion for Arterial Spin Labeling Using Pulsed Radio Frequency and Gradient. *Magnetic Resonance in Medicine*, *1497*(July), 1488–1497. https://doi.org/10.1002/mrm.21790

Damoiseaux, J. S., & Greicius, M. D. (2009). Greater than the sum of its parts: a review of studies combining structural connectivity and resting-state functional connectivity. *Brain Structure and Function*, *213*(6), 525–533. https://doi.org/10.1007/s00429-009-0208-6

Davis, T. L., Kwong, K. K., Weisskoff, R. M., & Rosen, B. R. (1998). Calibrated functional MRI: Mapping the dynamics of oxidative metabolism. *Proceedings of the National Academy of Sciences*, *95*(4), 1834–1839. https://doi.org/10.1073/pnas.95.4.1834

Dayan, E., & Cohen, L. G. (2011). Neuroplasticity subserving motor skill learning. *Neuron*, *72*(3), 443–454. https://doi.org/10.1016/j.neuron.2011.10.008

Debernard, L., Melzer, T. R., Van Stockum, S., Graham, C., Wheeler-Kingshott, C. A. M., Dalrymple-Alford, J. C., … Mason, D. F. (2014). Reduced grey matter perfusion without volume loss in early relapsing-remitting multiple sclerosis. *Journal of Neurology, Neurosurgery and Psychiatry*, *85*(5), 544–551. https://doi.org/10.1136/jnnp-2013-305612

Deoni, S. C. L., Dean, D. C., Remer, J., Dirks, H., & Muircheartaigh, J. O. (2015). Cortical maturation and myelination in healthy toddlers and young children. *NeuroImage*, *115*, 147–161. https://doi.org/10.1016/j.neuroimage.2015.04.058

Deoni, S. C. L., & Kolind, S. H. (2015). Investigating the Stability of mcDESPOT Myelin Water Fraction Values Derived Using a Stochastic Region Contraction Approach. *Magnetic Resonance in Medicine*, *169*, 161–169. https://doi.org/10.1002/mrm.25108

Deroost, N., Smetcoren, S., Vandenbossche, J., Hooghe, M. D., & Kerckhofs, E. (2014). Implicit And Explicit Learning of Sequential Motor Skill in Multiple Sclerosis : Directions for Rehabilitation. *Journal of Neuroscience and Rehabilitation*, *1*(1), 1–13.

Desai, R. A., Davies, A. L., Tachrount, M., Kasti, M., Laulund, F., Golay, X., & Smith, K. J. (2016). Cause and prevention of demyelination in a model multiple sclerosis lesion.

Annals of Neurology, *79*(4), 591–604. https://doi.org/10.1002/ana.24607

Desouza, C. A., Shapiro, L. F., Clevenger, C. M., Dinenno, F. A., Monahan, K. D., Tanaka, H., & Seals, D. R. (2000). Regular Aerobic Exercise Prevents and Restores Age-Related Declines in Endothelium-Dependent Vasodilation in Healthy Men. *Circulation*, (102), 1351–1357.

Di Filippo, M., Chiasserini, D., Gardoni, F., Viviani, B., Tozzi, A., Giampà, C., … Calabresi, P. (2013). Neurobiology of Disease Effects of central and peripheral in fl ammation on hippocampal synaptic plasticity. *Neurobiology of Disease*, *52*, 229–236. https://doi.org/10.1016/j.nbd.2012.12.009

Di Filippo, M., Sarchielli, P., Picconi, B., & Calabresi, P. (2008). Neuroinflammation and synaptic plasticity: theoretical basis for a novel, immune-centred, therapeutic approach to neurological disorders. *Trends in Pharmacological Sciences*, *29*(8), 402–412. https://doi.org/10.1016/j.tips.2008.06.005

Di Pasquale, O., Cooper, E. A., Tibble, J., Voon, V., Baglio, F., Baselli, G., … Harrison, N. A. (2016). Interferon- a acutely impairs whole-brain functional connectivity network architecture – A preliminary study. *Brain Behavior and Immunity*, *58*, 31–39. https://doi.org/10.1016/j.bbi.2015.12.011

Dick, F., Tierney, A. T., Lutti, A., Josephs, O., Sereno, M. I., & Weiskopf, N. (2012). In Vivo Functional and Myeloarchitectonic Mapping of Human Primary Auditory Areas, *32*(46), 16095–16105. https://doi.org/10.1523/JNEUROSCI.1712-12.2012

Disbrow, E., Roberts, T., & Krubitzer, L. (2000). Somatotopic organization of cortical fields in the lateral sulcus ofHomo sapiens: Evidence for SII and PV. *The Journal of Comparative Neurology*, *418*(1), 1–21. https://doi.org/10.1002/(SICI)1096-9861(20000228)418:1<1::AID-CNE1>3.0.CO;2-P

Dong, W. K., & Greenough, W. T. (2004). Plasticity of nonneuronal brain tissue: roles in developmental disorders. *Mental Retardation and Developmental Disabilities*, *90*(10), 85–90. https://doi.org/10.1002/mrdd.20016

Douaud, G., Smith, S., Jenkinson, M., Behrens, T., Johansen-berg, H., Vickers, J., … James, A. (2007). Anatomically related grey and white matter abnormalities in adolescent-onset schizophrenia. *Brain*, *130*, 2375–2386. https://doi.org/10.1093/brain/awm184

Doyon, J., & Benali, H. (2005). Reorganization and plasticity in the adult brain during learning of motor skills. *Current Opinion in Neurobiology*, (15), 161–167.

https://doi.org/10.1016/j.conb.2005.03.004

Doyon, J., Penhune, V., & Ungerleider, L. G. (2003). Distinct contribution of the cortico-striatal and cortico-cerebellar systems to motor skill learning. *Neuropsychologia*, *41*(3), 252–262. https://doi.org/10.1016/S0028-3932(02)00158-6

Draganski, B., Gaser, C., Busch, V., Schuierer, G., Bogdahn, U., & May, A. (2004). Changes in grey matter induced by training. *Nature*, *427*, 311–312. https://doi.org/10.1038/427311a

Draganski, B., Gaser, C., Kempermann, G., Kuhn, H. G., Winkler, J., Buchel, C., & May, A. (2006). Temporal and Spatial Dynamics of Brain Structure Changes during Extensive Learning. *Journal of Neuroscience*, *26*(23), 6314–6317. https://doi.org/10.1523/JNEUROSCI.4628-05.2006

Draganski, B., & May, A. (2008). Training-induced structural changes in the adult human brain. *Behavioural Brain Research*, *192*(1), 137–142. https://doi.org/10.1016/j.bbr.2008.02.015

Eickhoff, S., Walters, N. B., Schleicher, A., Kril, J., Egan, G. F., Zilles, K., … Amunts, K. (2005). High-Resolution MRI Reflects Myeloarchitecture and Cytoarchitecture of Human Cerebral Cortex. *Human Brain Mapping*, *215*(January 2004), 206–215. https://doi.org/10.1002/hbm.20082

Eloyan, A., Shou, H., Shinohara, R. T., Sweeney, E. M., Nebel, M. B., Cuzzocreo, J. L., … Crainiceanu, C. M. (2014). Health Effects of Lesion Localization in Multiple Sclerosis : Spatial Registration and Confounding Adjustment. PLoS ONE, 9(9).

Engel, S. A., Glover, G. H., & Wandell, B. A. (1997). Retinotopic Organization in Human Visual Cortex and the Spatial Precision of Functional MRI, 181–192.

Erickson, K. I., Voss, M. W., Prakash, S. R., Basak, C., Szabo, A., Chaddock, L., … Kramer, A. (2011). Exercise training increases size of hippocampus and improves memory. *PNAS*, *108*(7), 3017–3022. https://doi.org/10.1073/pnas.1015950108

Faivre, A., Rico, A., Zaaraoui, W., Crespy, L., Reuter, F., Wybrecht, D., … Audoin, B. (2012). Assessing brain connectivity at rest is clinically relevant in early multiple sclerosis. *MULTIPLE SCLEROSIS JOURNAL*, *18*(9), 1251–1258. https://doi.org/10.1177/1352458511435930

Fan, A. P., Govindarajan, S. T., Kinkel, R. P., Madigan, N. K., Nielsen, A. S., Benner, T., … Mainero, C. (2015). Quantitative oxygen extraction fraction from 7-Tesla MRI phase: Reproducibility and application in multiple sclerosis. *Journal of Cerebral Blood Flow and*

Metabolism, *35*(1), 131–139. https://doi.org/10.1038/jcbfm.2014.187

Fernández-Seara, M. A., Aznárez-Sanado, M., Mengual, E., Loayza, F. R., & Pastor, M. A. (2009). Continuous performance of a novel motor sequence leads to highly correlated striatal and hippocampal perfusion increases. *NeuroImage*, *47*(4), 1797–1808. https://doi.org/10.1016/j.neuroimage.2009.05.061

Fields, R. D. (2010). Change in the Brain's White Matter. *Neuroscience*, *330*(November), 768–770.

Fields, R. D. (2014). Myelin — More than Insulation. *Science*, *344*(April), 264–267.

Fields, R. D. (2015). A new mechanism of nervous system plasticity: activity-dependent myelination. *Nature Reviews Neuroscience*, *16*(12), 756–767. https://doi.org/10.1038/nrn4023

Filippi, M., Riccitelli, G., Mattioli, F., Capra, R., Stampatori, C., Pagani, E., … Rocca, M. A. (2012). Multiple Sclerosis: Effects of Cognitive Rehabilitation on Structural and Functional MR Imaging Measures—An Explorative Study. *Radiology*, *262*(3), 932–940. https://doi.org/10.1148/radiol.11111299

Finke, C., Schlichting, J., Papazoglou, S., Scheel, M., Freing, A., Soemmer, C., … Brandt, A. U. (2015). Altered basal ganglia functional connectivity in multiple sclerosis patients with fatigue. *Mult Scler*, (21 (7)), 925–934. https://doi.org/10.1177/1352458514555784

Fischl, B., & Dale, A. M. (2000). Measuring the thickness of the human cerebral cortex from magnetic resonance images. *PNAS*, *97*(20), 11050–11055.

Fischl, B., Salat, D. H., Kouwe, J. W. Van Der, Makris, N., Quinn, B. T., & Dale, A. M. (2004). Sequence-independent segmentation of magnetic resonance images. *NeuroImage*, *23*, 69–84. https://doi.org/10.1016/j.neuroimage.2004.07.016

Floyer-Lea, A., & Matthews, P. M. (2005). Distinguishable Brain Activation Networks for Short- and Long-Term Motor Skill Learning. *Journal of Neurophysiology*, *94*(1), 512–518. https://doi.org/10.1152/jn.00717.2004

Fornito, A., Zalesky, A., & Breakspear, M. (2013). Graph analysis of the human connectome: Promise , progress , and pitfalls. *NeuroImage*, *80*, 426–444. https://doi.org/10.1016/j.neuroimage.2013.04.087

Foster, C., Steventon, J. J., Helme, D., Tomassini, V., & Wise, R. G. (2020). Cerebral Metabolic Changes During Visuomotor Adaptation Assessed Using Quantitative fMRI. *Frontiers in Physiology*, *11*(May), 1–12. https://doi.org/10.3389/fphys.2020.00428

Fox, M. D., & Raichle, M. E. (2007). Spontaneous fluctuations in brain activity observed with

functional magnetic resonance imaging. *Nature Reviews Neuroscience*, *8*(9), 700–711. https://doi.org/10.1038/nrn2201

Fox, M. D., Corbetta, M., Snyder, A. Z., Vincent, J. L., & Raichle, M. E. (2006). Spontaneous neuronal activity distinguishes human dorsal and ventral attention system. *Pnas*, *103*(25), 9381–9386.

Fridman, E. A., Hanakawa, T., Chung, M., Hummel, F., Leiguarda, R. C., & Cohen, L. G. (2004). Reorganization of the human ipsilesional premotor cortex after stroke. https://doi.org/10.1093/brain/awh082

Fujiyama, F., Takahashi, S., & Karube, F. (2015). Morphological elucidation of basal ganglia circuits contributing reward prediction. *Frontiers in Neuroscience*, *9*(FEB), 1–8. https://doi.org/10.3389/fnins.2015.00006

Fukunaga, M., Horovitz, S. G., Zwart, J. A. De, Gelderen, P. Van, Balkin, T. J., Braun, A. R., & Duyn, J. H. (2008). Metabolic origin of BOLD signal fluctuations in the absence of stimuli, 1377–1387. https://doi.org/10.1038/jcbfm.2008.25

Fukunaga, M., Li, T., Gelderen, P. Van, Zwart, J. A. De, Shmueli, K., Yao, B., & Lee, J. (2010). Layer-speci fi c variation of iron content in cerebral cortex as a source of MRI contrast. *Pnas*, 1–6. https://doi.org/10.1073/pnas.0911177107

Gauthier, C. J., & Hoge, R. D. (2012). Magnetic resonance imaging of resting OEF and CMRO 2 using a generalized calibration model for hypercapnia and hyperoxia. *NeuroImage*, *60*(2), 1212–1225. https://doi.org/10.1016/j.neuroimage.2011.12.056

Gauthier, Claudine J, & Hoge, R. D. (2013). A Generalized Procedure for Calibrated MRI Incorporating Hyperoxia and Hypercapnia, *1069*(May 2011), 1053–1069. https://doi.org/10.1002/hbm.21495

Ge, R., Zhang, H., Yao, L., & Long, Z. (2015). Motor Imagery Learning Induced Changes in Functional Connectivity of the Default Mode Network. *IEEE Transactions on Neural Systems and Rehabilitation Engineering*, *23*(1), 138–148.

Ge, Y., Law, M., Johnson, G., Herbert, J., Babb, J. S., Mannon, L. J., & Grossman, R. I. (2005). Dynamic Susceptibility Contrast Perfusion MR Imaging of Multiple Sclerosis Lesions : Characterizing Hemodynamic Impairment and Inflammatory Activity. *AJNR. American Journal of Neuroradiology*, (July), 1539–1547.

Ge, Y., Zhang, Z., Lu, H., Tang, L., Jaggi, H., Herbert, J., … Grossman, R. I. (2012). Characterizing brain oxygen metabolism in patients with multiple sclerosis with. *Journal of Cerebral Blood Flow & Metabolism*, *32*(3), 403–412.

https://doi.org/10.1038/jcbfm.2011.191

Gelineau-Morel, R., Tomassini, V., Jenkinson, M., Johansen-Berg, H., Matthews, P. M., & Palace, J. (2012). The effect of hypointense white matter lesions on automated gray matter segmentation in multiple sclerosis. *Human Brain Mapping*, *33*(12), 2802–2814. https://doi.org/10.1002/hbm.21402

Germuska, M., Chandler, H. L., Stickland, R. C., Foster, C., Fasano, F., Okell, T. W., … Wise, R. G. (2019). Dual-calibrated fMRI measurement of absolute cerebral metabolic rate of oxygen consumption and effective oxygen diffusivity. *NeuroImage*, *184*(September 2018), 717–728. https://doi.org/10.1016/j.neuroimage.2018.09.035

Germuska, M., Merola, A., Murphy, K., Babic, A., Richmond, L., Khot, S., … Wise, R. G. (2016). A forward modelling approach for the estimation of oxygen extraction fraction by calibrated fMRI. *NeuroImage*, *139*, 313–323. https://doi.org/10.1016/J.NEUROIMAGE.2016.06.004

Germuska, M., & Wise, R. G. (2018). Calibrated fMRI for mapping absolute CMRO2: Practicalities and prospects. *NeuroImage*, (March), 1–9. https://doi.org/10.1016/j.neuroimage.2018.03.068

Geyer, S., Weiss, M., Reimann, K., Lohmann, G., & Turner, R. (2011). Microstructural parcellation of the human cerebral cortex – from Brodmann ' s post-mortem map to in vivo mapping with high-field magnetic resonance imaging, *5*(February), 1–7. https://doi.org/10.3389/fnhum.2011.00019

Ghilardi, M. F., Moisello, C., Silvestri, G., Ghez, C., & Krakauer, J. W. (2009). Learning of a Sequential Motor Skill Comprises Explicit and Implicit Components That Consolidate Differently. *Journal of Neurophysiology*, *101*(5), 2218–2229. https://doi.org/10.1152/jn.01138.2007

Gibson, E. M., Purger, D., Mount, C. W., Goldstein, A. K., Lin, G. L., Wood, L. S., … Monje, M. (2014). Neuronal Activity Promotes Oligodendrogenesis and Adaptive Myelination in the Mammalian Brain. *Science*, *344*(May). https://doi.org/10.1126/science.1254446

Girouard, H., & Iadecola, C. (2006). Neurovascular coupling in the normal brain and in hypertension, stroke, and Alzheimer disease. *J Appl Physiol*, *10021*, 328–335. https://doi.org/10.1152/japplphysiol.00966.2005.

Glasser, M. F., & Van Essen, D. C. (2011). Mapping Human Cortical Areas In Vivo Based on Myelin Content as Revealed by T1- and T2-Weighted MRI. *Journal of Neuroscience*, *31*(32), 11597–11616. https://doi.org/10.1523/jneurosci.2180-11.2011

Glasser, Matthew F., Goyal, M. S., Preuss, T. M., Raichle, M. E., & Van Essen, D. C. (2014). Trends and properties of human cerebral cortex: Correlations with cortical myelin content. *NeuroImage*, *93*, 165–175. https://doi.org/10.1016/j.neuroimage.2013.03.060

Good, C. D., Johnsrude, I. S., Ashburner, J., Henson, R. N. A., Friston, K. J., & Frackowiak, R. S. J. (2001). A Voxel-Based Morphometric Study of Ageing in 465 Normal Adult Human Brains, *36*, 21–36. https://doi.org/10.1006/nimg.2001.0786

Gould, E., Beylin, A., Tanapat, P., Reeves, A., & Shors, T. J. (1999). Learning enhances adult neurogenesis in the hippocampal formation. *Nature Neuroscience*, *2*(3).

Grafton, S. T., Hazeltine, E., & Ivry, R. (1995a). Functional mapping of sequence learning in normal humans. *Journal of Cognitive Neuroscience*, *7*(4), 497–510. https://doi.org/10.1162/jocn.1995.7.4.497

Grafton, S. T., Hazeltine, E., & Ivry, R. (1995b). Functional mapping of sequence learning in normal humans. *Journal of Cognitive Neuroscience*, *7*(4), 497–510. https://doi.org/10.1162/jocn.1995.7.4.497

Greve, D. N., & Fischl, B. (2010). Accurate and Robust Brain Image Alignment using Boundary-based Registration. *Neuroimage*, *48*(1), 63–72. https://doi.org/10.1016/j.neuroimage.2009.06.060.Accurate

Grigg, O., & Grady, C. L. (2010). Task-Related Effects on the Temporal and Spatial Dynamics of Resting-State Functional Connectivity in the Default Network, *5*(10), 1–12. https://doi.org/10.1371/journal.pone.0013311

Grubb, R. L., Raichle, M. E., Eichling, J. O., & Ter-Pogossian, M. M. (1974). The effects of changes in paco2on cerebral blood volume, blood flow, and vascular mean transit time. *Stroke*, *5*(5), 630–639. https://doi.org/10.1161/01.STR.5.5.630

Grydeland, H., Walhovd, K. B., Tamnes, C. K., Westlye, L. T., & Fjell, A. M. (2013). Intracortical Myelin Links with Performance Variability across the Human Lifespan : Results from T1- and T2- Weighted MRI Myelin Mapping and Diffusion Tensor Imaging. *The Journal of Neuroscience*, *33*(47), 18618–18630. https://doi.org/10.1523/JNEUROSCI.2811-13.2013

Guerra-carrillo, B., Mackey, A. P., & Bunge, S. A. (2014). Resting-State fMRI : A Window into Human Brain Plasticity. https://doi.org/10.1177/1073858414524442

Guerra-Carrillo, B., MacKey, A. P., & Bunge, S. A. (2014). Resting-state fMRI: A window into human brain plasticity. *Neuroscientist*, *20*(5), 522–533. https://doi.org/10.1177/1073858414524442

Gusnard, D. A., & Raichle, M. E. (2001). Gusnard and Raichle 2001 Searching for a Baseline, *2*(October).

Haider, L., Zrzavy, T., Hametner, S., Höftberger, R., Bagnato, F., Grabner, G., … Lassmann, H. (2016). The topograpy of demyelination and neurodegeneration in the multiple sclerosis brain. *Brain*, *139*(3), 807–815. https://doi.org/10.1093/brain/awv398

Haller, S., Zaharchuk, G., Thomas, D. L., Lovblad, K.-O., Barkhof, F., & Golay, X. (2016). Arterial Spin Labeling Perfusion of the Brain : Emerging Clinical Applications. *Radiology*, *281*(2).

Halsband, U., & Lange, R. K. (2006). Motor learning in man : A review of functional and clinical studies, *99*, 414–424. https://doi.org/10.1016/j.jphysparis.2006.03.007

Hämäläinen, H., Hiltunen, J., & Titievskaja, I. (2000). fMRI activations of SI and SII cortices during tactile stimulation depend on attention. *Neuroreport*, *11*(8), 1673–1676. Retrieved from http://www.ncbi.nlm.nih.gov/pubmed/10852223

Hannestad, J., Gallezot, J., Schafbauer, T., Lim, K., Kloczynski, T., Morris, E. D., … Cosgrove, K. P. (2012). Endotoxin-induced systemic in fl ammation activates microglia : [11 C] PBR28 positron emission tomography in nonhuman primates. *NeuroImage*, *63*(1), 232–239. https://doi.org/10.1016/j.neuroimage.2012.06.055

Hänninen, K., Viitala, M., Paavilainen, T., Karhu, J. O., Rinne, J., Koikkalainen, J., … Solilu-Hannine, M. (2019). Thalamic Atrophy Without Whole Brain Atrophy Is Associated With Absence of 2-Year NEDA in Multiple Sclerosis. *Frontiers in Neurology*, *10*(May), 1–9. https://doi.org/10.3389/fneur.2019.00459

Hardwick, R. M., Rottschy, C., Miall, R. C., & Eickhoff, S. B. (2013). A quantitative meta-analysis and review of motor learning in the human brain. *NeuroImage*, *67*, 283–297. https://doi.org/10.1016/j.neuroimage.2012.11.020

Haroutunian, V., Katsel, P., Roussos, P., Davis, K. L., Altshuler, L. L., & Bartzokis, G. (2014). Myelination, oligodendrocytes, and serious mental illness. *Glia*, *62*(11), 1856–1877. https://doi.org/10.1002/glia.22716

Harris, S., Ma, H., Zhao, M., Boorman, L., Zheng, Y., Kennerley, A., … Schwartz, T. H. (2014). Coupling between gamma-band power and cerebral blood volume during recurrent acute neocortical seizures. *NeuroImage*, *97*, 62–70. https://doi.org/10.1016/j.neuroimage.2014.04.014

Hasson, U., Nusbaum, H. C., & Small, S. L. (2009). Task-dependent organization of brain regions active during rest, *106*(26), 10841–10846.

Havlicek, M., Ivanov, D., Roebroeck, A., & Uludağ, K. (2017). Determining excitatory and inhibitory neuronal activity from multimodal fMRI data using a generative hemodynamic model. *Frontiers in Neuroscience*, *11*(NOV), 616. https://doi.org/10.3389/fnins.2017.00616

Hawellek, D. J., Hipp, J. F., Lewis, C. M., Corbetta, M., & Engel, A. K. (2011). Increased functional connectivity indicates the severity of cognitive impairment in multiple sclerosis. *Pnas*, *108*(47), 19066–19071. https://doi.org/10.1073/pnas.1110024108/-/DCSupplemental.www.pnas.org/cgi/doi/10.1073/pnas.1110024108

He, Y., Dagher, A., Chen, Z., Charil, A., Zijdenbos, A., Worsley, K., & Evans, A. (2009). Impaired small-world efficiency in structural cortical networks in multiple sclerosis associated with white matter lesion load, 3366–3379. https://doi.org/10.1093/brain/awp089

Heuninckx, S., Wenderoth, N., & Swinnen, S. P. (2008). Systems Neuroplasticity in the Aging Brain : Recruiting Additional Neural Resources for Successful Motor Performance in Elderly Persons, *28*(1), 91–99. https://doi.org/10.1523/JNEUROSCI.3300-07.2008

Hikosaka, O., Nakamura, K., Sakai, K., & Nakahara, H. (2002). Central mechanisms of motor skill learning. *Current Opinion in Neurobiology*, *12*, 217–222.

Hobart, J., Lamping, D., Fitzpatrick, R., Riazi, A., & Thompson, A. (2001). The multiple sclerosis impact scale (MSIS-29). *Brain (2001) 124, 962-973*, 1–12. https://doi.org/papers3://publication/uuid/E0443A9D-5E2B-452C-B5A0-40C7920F8B76

Hoge, R. D. (2012, August 15). Calibrated fMRI. *NeuroImage*. Academic Press. https://doi.org/10.1016/j.neuroimage.2012.02.022

Holland, C. M., Charil, A., Csapo, I., Liptak, Z., Ichise, M., Khoury, S. J., … Guttmann, C. R. G. (2012). The Relationship between Normal Cerebral Perfusion Patterns and White Matter Lesion Distribution in 1,249 Patients with Multiple Sclerosis. *Journal of Neuroimaging*, *22*(2), 129–136. https://doi.org/10.1111/j.1552-6569.2011.00585.x

Holtmaat, A., & Svoboda, K. (2009). Experience-dependent structural synaptic plasticity in the mammalian brain. *Nature Reviews Neuroscience*, *10*(9), 647–658. https://doi.org/10.1038/nrn2699

Honda, M., Deiber, M. P., Ibáñez, V., Pascual-Leone, A., Zhuang, P., & Hallett, M. (1998). Dynamic cortical involvement in implicit and explicit motor sequence learning. A PET study. *Brain*, *121*(11), 2159–2173. https://doi.org/10.1093/brain/121.11.2159

Honey, C. J., Sporns, O., Cammoun, L., Gigandet, X., Thiran, J. P., Meuli, R., & Hagmann, P. (2009). Predicting human resting-state functional connectivity. *Pnas*, *106*(6), 1–6.

Huang, T. T., Leu, D., & Zou, Y. (2015, June 2). Oxidative stress and redox regulation on hippocampal-dependent cognitive functions. *Archives of Biochemistry and Biophysics*. Academic Press Inc. https://doi.org/10.1016/j.abb.2015.03.014

Hunt, B. A. E., Tewarie, P. K., Mougin, O. E., Geades, N., Jones, D. K., Singh, K. D., … Brookes, M. J. (2016). Relationships between cortical myeloarchitecture and electrophysiological networks. *Proceedings of the National Academy of Sciences of the United States of America*, *113*(47), 13510–13515. https://doi.org/10.1073/pnas.1608587113

Hyder, F., Rothman, D. L., & Bennett, M. R. (2013, February 26). Cortical energy demands of signaling and nonsignaling components in brain are conserved across mammalian species and activity levels. *Proceedings of the National Academy of Sciences of the United States of America*. https://doi.org/10.1073/pnas.1214912110

Iadecola, C. (2004). Neurovascular regulation in the normal brain and in Alzheimer's disease. *Nature Reviews Neuroscience*, *5*(5), 347–360. https://doi.org/10.1038/nrn1387

Iadecola, C. (2017). The Neurovascular Unit Coming of Age: A Journey through Neurovascular Coupling in Health and Disease. *Neuron*, *96*(1), 17–42. https://doi.org/10.1016/J.NEURON.2017.07.030

Iannetti, G. D., & Wise, R. G. (2007). BOLD functional MRI in disease and pharmacological studies: room for improvement? *Magnetic Resonance Imaging*, *25*(6), 978–988. https://doi.org/10.1016/j.mri.2007.03.018

Ibrahim, I., Tintera, J., Skoch, A., Jirů, F., Hlustik, P., Martinkova, P., … Rasova, K. (2011). Fractional anisotropy and mean diffusivity in the corpus callosum of patients with multiple sclerosis: The effect of physiotherapy. *Neuroradiology*, *53*(11), 917–926. https://doi.org/10.1007/s00234-011-0879-6

Jain, V., Langham, M. C., & Wehrli, F. W. (2010). MRI estimation of global brain oxygen consumption rate. *Journal of Cerebral Blood Flow & Metabolism*, *30*(9), 1598–1607. https://doi.org/10.1038/jcbfm.2010.49

Jann, K., Gee, D. G., Kilroy, E., Schwab, S., Smith, R. X., Cannon, T. D., & Wang, D. J. J. (2015). Functional connectivity in BOLD and CBF data: Similarity and reliability of resting brain networks. *NeuroImage*, *106*, 111–122. https://doi.org/10.1016/j.neuroimage.2014.11.028.Functional

Jann, K., Orosz, A., Dierks, T., Wang, D. J. J., Wiest, R., & Federspiel, A. (2013). Quantification of Network Perfusion in ASL Cerebral Blood Flow Data with Seed Based and ICA Approaches, 569–580. https://doi.org/10.1007/s10548-013-0280-3

Janz, C., Heinrich, S. P., Kornmayer, J., Bach, M., & Hennig, J. (2001). Coupling of Neural Activity and BOLD fMRI Response : New Insights by Combination of fMRI and VEP Experiments in Transition From Single Events to Continuous Stimulation, *486*(December 2000), 482–486.

Jenkinson, M., Bannister, P., Brady, M., & Smith, S. (2002). Improved Optimization for the Robust and Accurate Linear Registration and Motion Correction of Brain Images, *841*, 825–841. https://doi.org/10.1006/nimg.2002.1132

Jenkinson, M., & Smith, S. (2001). A global optimisation method for robust affine registration of brain images, *5*, 143–156.

Jia, X., & Kohn, A. (2011). Gamma Rhythms in the Brain. *PLoS Biology*, *9*(4), 2–5. https://doi.org/10.1371/journal.pbio.1001045

Johansen-Berg, H. (2007). Structural Plasticity: Rewiring the Brain. *Current Biology*, *17*(4), 141–144. https://doi.org/10.1016/j.cub.2006.12.007

Johansen-berg, H., Rushworth, M. F. S., Bogdanovic, M. D., Kischka, U., Wimalaratna, S., & Matthews, P. M. (2002). The role of ipsilateral premotor cortex in hand movement after stroke.

Johansen-Berg, Heidi, Della-Maggiore, V., Behrens, T. E. J., Smith, S. M., & Paus, T. (2007). Integrity of white matter in the corpus callosum correlates with bimanual co-ordination skills. *NeuroImage*, *36*(SUPPL. 2), 16–21. https://doi.org/10.1016/j.neuroimage.2007.03.041

Juurlink, B. H. J. (2013). The Evidence for Hypoperfusion as a Factor in Multiple Sclerosis Lesion Development. *Multiple Sclerosis International*, *2013*(598093).

Kappus, N., Weinstock-guttman, B., Hagemeier, J., Kennedy, C., Melia, R., Carl, E., … Zivadinov, R. (2016). Cardiovascular risk factors are associated with increased lesion burden and brain atrophy in multiple sclerosis. *Journal of Neurology, Neurosurgery and Psychiatry*, (87), 181–187. https://doi.org/10.1136/jnnp-2014-310051

Karhu, J., & Tesche, C. D. (1999). Simultaneous Early Processing of Sensory Input in Human Primary (SI) and Secondary (SII) Somatosensory Cortices. *Journal of Neurophysiology*, *81*(5), 2017–2025. https://doi.org/10.1152/jn.1999.81.5.2017

Karni, A., Meyer, G., Jezzard, P., Adams, M. M., Turner, R., & Ungerleider, L. G. (1995).

Functional MRI evidence for adult motor cortex plasticity during motor skill learning. *Nature*, *377*(6545), 155.

Keller, T. A., & Just, M. A. (2016). Structural and functional neuroplasticity in human learning of spatial routes. *NeuroImage*, *125*, 256–266. https://doi.org/10.1016/j.neuroimage.2015.10.015

Kennan, R. P., Zhong, J., & Gore, J. C. (1994). Intravascular susceptibility contrast mechanisms in tissues. *Magnetic Resonance in Medicine*, *31*(1), 9–21. https://doi.org/10.1002/mrm.1910310103

Kerr, A. L., Steuer, E. L., Pochtarev, V., & Swain, R. A. (2010). Angiogenesis but not neurogenesis is critical for normal learning and memory acquisition. *Neuroscience*, *171*(1), 214–226. https://doi.org/10.1016/j.neuroscience.2010.08.008

Kettenmann, H., Kirchhoff, F., & Verkhratsky, A. (2013). Microglia: New Roles for the Synaptic Stripper. *Neuron*, *77*(1), 10–18. https://doi.org/10.1016/j.neuron.2012.12.023

Kidd, D., Barkhof, F., Mcconnell, R., Algra, P. R., Allen, I. V, & Revesz, T. (1999). Cortical lesions in multiple sclerosis, 17–26.

Kipp, M., Wagenknecht, N., Beyer, C., Samer, S., Wuerfel, J., & Nikoubashman, O. (2015). Thalamus pathology in multiple sclerosis : from biology to clinical application. *Cell. Mol. Life Sci.*, 1127–1147. https://doi.org/10.1007/s00018-014-1787-9

Kleim, J. A., Hogg, T. M., Vandenberg, P. M., Cooper, N. R., Bruneau, R., & Remple, M. (2004). Cortical Synaptogenesis and Motor Map Reorganization Occur during Late , But Not Early , Phase of Motor Skill Learning. *The Journal of Neuropsychiatry and Clinical Neurosciences*, *24*(3), 628–633. https://doi.org/10.1523/JNEUROSCI.3440-03.2004

Korman, M., Raz, N., Flash, T., & Karni, A. (2003). Multiple shifts in the representation of a motor sequence during the acquisition of skilled performance. *Pnas*, *100*(21), 12492–12497.

Kravitz, A. V., & Kreitzer, A. C. (2012). Striatal Mechanisms Underlying Movement, Reinforcement, and Punishment. *Physiology.*, *27*(3). https://doi.org/10.1152/physiol.00004.2012.Striatal

Krieger, S. N., Gauthier, C. J., Ivanov, D., Huber, L., Roggenhofer, E., Sehm, B., … Egan, G. F. (2014). Regional reproducibility of calibrated BOLD functional MRI: Implications for the study of cognition and plasticity. *NeuroImage*, *101*, 8–20. https://doi.org/10.1016/j.neuroimage.2014.06.072

Kurtzke, J. F. (1983). Rating neurologic impairment in multiple sclerosis: An expanded

disability status scale (EDSS). *Neurology*, *33*(11), 1444–1444. https://doi.org/10.1212/WNL.33.11.1444

Kwon, D., Pfefferbaum, A., Sullivan, E. V., & Pohl, K. M. (2020). Regional Growth Trajectories of Cortical Myelination in Adolescents and Young Adults: Longitudinal Validation and Functional Correlates. *Brain Imaging and Behavior*, (831).

Laird, A. R., Fox, P. M., Eickhoff, S. B., Turner, J. A., Ray, K. L., McKay, D. R., … Fox, P. T. (2011). Behavioral Interpretations of Intrinsic Connectivity Networks. *Journal of Cognitive Neuroscience*, *23*(12), 4022–4037. https://doi.org/10.1162/jocn_a_00077

Lassmann, H. (2003). Hypoxia-like tissue injury as a component of multiple sclerosis lesions. *Journal of Neurological Sciences*, *206*, 187–191.

Le Bihan, D. (2003). Looking into the functional architecture of the brain with diffusion MRI. *Nature*, *4*(June). https://doi.org/10.1038/nrn1119

Le Bihan, D. (2012). Diffusion, confusion and functional MRI. *NeuroImage*, *62*(2), 1131–1136. https://doi.org/10.1016/j.neuroimage.2011.09.058

Lecrux, C., Bourourou, M., & Hamel, E. (2019). Autonomic Neuroscience : Basic and Clinical How reliable is cerebral blood fl ow to map changes in neuronal activity ? *Autonomic Neuroscience: Basic and Clinical*, *217*(December 2018), 71–79. https://doi.org/10.1016/j.autneu.2019.01.005

Lee, M. A., Smith, S., Palace, J., Narayanan, S., Silver, N., Minicucci, L., … Matthews, P. M. (1999). Spatial mapping of T2 and gadolinium-enhancing T1 lesion volumes in multiple sclerosis: Evidence for distinct mechanisms of lesion genesis? *Brain*, *122*(7), 1261–1270. https://doi.org/10.1093/brain/122.7.1261

Lee, M., Reddy, H., Pendlebury, S., Jenkinson, M., Smith, S., Palace, J., & Matthews, P. M. (2000). The Motor Cortex Shows Adaptive Functional Changes to Brain Injury from Multiple Sclerosis. *Annals of Neurology*, *47*, 606–613. https://doi.org/10.1002/1531-8249(200005)47:5<606::AID-ANA8>3.0.CO;2-L

Lehéricy, S., Benali, H., Van de Moortele, P.-F., Pélégrini-Issac, M., Waechter, T., Ugurbil, K., & Doyon, J. (2005). Distinct basal ganglia territories are engaged in early and advanced motor sequence learning. *Proceedings of the National Academy of Sciences of the United States of America*, *102*(35), 12566–12571. https://doi.org/10.1073/pnas.0502762102

Leocani, L., Comi, E., Annovazzi, P., Rovaris, M., Rossi, P., Cursi, M., … Comi, G. (2007). Impaired Short-term Motor Learning in Multiple Sclerosis: Evidence From Virtual

Reality, 273–278. https://doi.org/10.1177/1545968306294913

Leontiev, O., & Buxton, R. B. (2007a). Reproducibility of BOLD, perfusion, and CMRO2 measurements with calibrated-BOLD fMRI. *NeuroImage*, *35*(1), 175–184. https://doi.org/10.1016/j.neuroimage.2006.10.044

Leontiev, O., & Buxton, R. B. (2007b). Reproducibility of BOLD, perfusion, and CMRO2measurements with calibrated-BOLD fMRI. *NeuroImage*, *35*(1), 175–184. https://doi.org/10.1016/j.neuroimage.2006.10.044

Lerch, J. P., Yiu, A. P., Martinez-Canabal, A., Pekar, T., Bohbot, V. D., Frankland, P. W., … Sled, J. G. (2011). Maze training in mice induces MRI-detectable brain shape changes specific to the type of learning. *NeuroImage*, *54*(3), 2086–2095. https://doi.org/10.1016/j.neuroimage.2010.09.086

Lewis, C. M., Baldassarre, A., Committeri, G., Luca, G., & Corbetta, M. (2009). Learning sculpts the spontaneous activity of the resting human brain, 1–6.

Li, Y., Chen, J., Zhang, C. L., Wang, L., Lu, D., Katakowski, M., … Chopp, M. (2005). Gliosis and Brain Remodeling After Treatment of Stroke in Rats With Marrow Stromal Cells. *Glia*, *417*(49), 407–417. https://doi.org/10.1002/glia.20126

Li, Y., & Chopp, M. (1999). Temporal profile of nestin expression after focal cerebral ischemia in adult rat. *Brain Research*, *838*, 1–10.

Liang, X., Zou, Q., He, Y., & Yang, Y. (2013). Coupling of functional connectivity and regional cerebral blood fl ow reveals a physiological basis for network hubs of the human brain, *110*(5), 1929–1934. https://doi.org/10.1073/pnas.1214900110

Limanowski, J., Kirilina, E., & Blankenburg, F. (2017). Neuronal correlates of continuous manual tracking under varying visual movement feedback in a virtual reality environment. *NeuroImage*, *146*(June 2016), 81–89. https://doi.org/10.1016/j.neuroimage.2016.11.009

Lin, M. T., & Beal, M. F. (2006). Mitochondrial dysfunction and oxidative stress in neurodegenerative disease. *Nature*, *443*, 787–795.

Lipp, I., Foster, C., Stickland, R., Davidson, A., Robertson, N., Jones, D., … Tomassini, V. (2016). Brain imaging of short-term functional plasticity predicts performance improvement with longer-term motor sequence training in multiple sclerosis. *MULTIPLE SCLEROSIS JOURNAL*, *22*, 32–32.

Lipp, I., Foster, C., Stickland, R., Sgarlata, E., Tallantyre, E. C., Davidson, A. E., … Tomassini, V. (2020). Predictors of training-related improvement in visuomotor performance in patients with multiple sclerosis : A behavioural and MRI study. *Multiple Sclerosis*

Journal, *1352458520*, 1–14. https://doi.org/10.1177/1352458520943788

Lipp, I., Parker, G. D., Tallantyre, E. C., Goodall, A., Grama, S., Patitucci, E., … Jones, D. K. (2020). Tractography in the presence of multiple sclerosis lesions. *NeuroImage*, *209*, 116471. https://doi.org/10.1016/j.neuroimage.2019.116471

Lipp, I., Parker, G. D., Tallantyre, E., Goodall, A., Grama, S., Patitucci, E., … Jones, D. (2019). Tractography in the presence of white matter lesions in multiple sclerosis. *BioRxiv*, 559708. https://doi.org/10.1101/559708

List, J., Kübke, J. C., Lindenberg, R., Külzow, N., Kerti, L., Witte, V., & Flöel, A. (2013). Relationship between excitability, plasticity and thickness of the motor cortex in older adults. *NeuroImage*, *83*, 809–816. https://doi.org/10.1016/j.neuroimage.2013.07.033

Liu, T., & Brown, G. (2007). Measurement of cerebral perfusion with arterial sping labeling: Part 2. Applications. *Journal of the International Neuropsychological Society*, *13*(5), 517–525. https://doi.org/10.1016/j.bbi.2008.05.010

Liu, Y., Wang, H., Duan, Y., Huang, J., Ren, Z., Ye, J., … Wang, J. (2017). Functional Brain Network Syndrome and Multiple Sclerosis: A graph-based connectome study. *Radiology*, *282*(2), 534–541.

Logothetis, N. K., Pauls, J., Augath, M., Trinath, T., & Oeltermann, A. (2001). Neurophysiological investigation of the basis of the fMRI signal. *Nature*, *412*.

Logothetis, N. K., & Wandell, B. A. (2004a). Interpreting the BOLD Signal. *Annual Review of Physiology*, *66*(1), 735–769. https://doi.org/10.1146/annurev.physiol.66.082602.092845

Logothetis, N. K., & Wandell, B. A. (2004b). INTERPRETING THE BOLD SIGNAL. *Annu. Rev. Physiol.*, *132*(66), 735–769. https://doi.org/10.1146/annurev.physiol.66.082602.092845

Lotze, M., Markert, J., Sauseng, P., Hoppe, J., Plewnia, C., & Gerloff, C. (2006). The Role of Multiple Contralesional Motor Areas for Complex Hand Movements after Internal Capsular Lesion, *26*(22), 6096–6102. https://doi.org/10.1523/JNEUROSCI.4564-05.2006

Lu, H., & Ge, Y. (2008). Quantitative Evaluation of Oxygenation in Venous Vessels Using T2-Relaxation-Under-Spin-Tagging MRI, *363*, 357–363. https://doi.org/10.1002/mrm.21627

Lucchinetti, C., Bruck, W., Parisi, J., Scheithauer, B., Rodrigues, M., & Lassmann, H. (2000). Heterogeneity of Multiple Sclerosis Lesions : Implications for the Pathogenesis of Demyelination. *Ann Neurol*, *47*, 707–717.

Ma, L., Narayana, S., Robin, D. A., Fox, P. T., & Xiong, J. (2011). Changes occur in resting

state network of motor system during 4 weeks of motor skill learning. *NeuroImage*, *58*(1), 226–233. https://doi.org/10.1016/j.neuroimage.2011.06.014

Ma, Z., Cao, P., Sun, P., Zhao, L., Li, L., Tong, S., … Chai, X. (2016). Inverted optical intrinsic response accompanied by decreased cerebral blood flow are related to both neuronal inhibition and excitation. *Scientific Reports*, *6*(1), 1–14. https://doi.org/10.1038/srep21627

Mackay, A., Whittall, K., Adler, J., Li, D., Paty, D., & Graeb, D. (1994). In vivo visualization of myelin water in brain by magnetic resonance. *Magnetic Resonance in Medicine*, *31*(6), 673–677. https://doi.org/10.1002/mrm.1910310614

Mackey, A. P., Miller Singley, A. T., & Bunge, S. A. (2013). Intensive Reasoning Training Alters Patterns of Brain Connectivity at Rest. *Journal of Neuroscience*, *33*(11), 4796–4803. https://doi.org/10.1523/JNEUROSCI.4141-12.2013

Magistretti, P. J. (2016). Imaging brain aerobic glycolysis as a marker of synaptic plasticity. *Proceedings of the National Academy of Sciences of the United States of America*, *113*(26), 7015–7016. https://doi.org/10.1073/pnas.1607423113

Magistretti, P. J., & Allaman, I. (2015). A Cellular Perspective on Brain Energy Metabolism and Functional Imaging. *Neuron*, *86*(4), 883–901. https://doi.org/10.1016/j.neuron.2015.03.035

Maguire, E. A., Gadian, D. G., Johnsrude, I. S., Good, C. D., Ashburner, J., Frackowiak, R. S. J., & Frith, C. D. (2000). Navigation-related structural change in the hippocampi of taxi drivers. *Proceedings of the National Academy of Sciences*, *97*(8), 4398–4403. https://doi.org/10.1073/pnas.070039597

Malonek, D., & Grinvald, A. (1996). Interactions between electrical activity and cortical microcirculation revealed by imaging spectroscopy: Implications for functional brain mapping. *Science*, *272*(5261), 551–554. https://doi.org/10.1126/science.272.5261.551

Mancini, L., Ciccarelli, O., Manfredonia, F., Thornton, J. S., Agosta, F., Barkhof, F., … Yousry, T. (2009). Short-term adaptation to a simple motor task: A physiological process preserved in multiple sclerosis. *NeuroImage*, *45*(2), 500–511. https://doi.org/10.1016/j.neuroimage.2008.12.006

Mantini, D., Perrucci, M. G., Del Gratta, C., Romani, G. L., & Corbetta, M. (2007). Electrophysiological signatures of resting state networks in the human brain. *Proceedings of the National Academy of Sciences*, *104*(32), 13170–13175. https://doi.org/10.1073/pnas.0700668104

Marques, J. P., Kober, T., Krueger, G., & Zwaag, W. Van Der. (2010). MP2RAGE, a self bias-field corrected sequence for improved segmentation and T1-mapping at high field. *NeuroImage*, *49*(2), 1271–1281. https://doi.org/10.1016/j.neuroimage.2009.10.002

Marques, P., & Gruetter, R. (2013). New Developments and Applications of the MP2RAGE Sequence - Focusing the Contrast and High Spatial Resolution R 1 Mapping. *PLoS ONE*, *8*(7). https://doi.org/10.1371/journal.pone.0069294

Marrie, R. A., Rudick, R., Horwitz, R., Cutter, G., Tyry, T., Campagnolo, D., & Vollmer, T. (2010). Vascular comorbidity is associated with more rapid disability progression in multiple sclerosis. *Neurology*, *74*, 1041–1047.

Marshall, O., Chawla, S., Lu, H., Pape, L., & Ge, Y. (2016). Cerebral blood flow modulation insufficiency in brain networks in multiple sclerosis : A hypercapnia MRI study. https://doi.org/10.1177/0271678X16654922

Marshall, O., Lu, H., Brisset, J. C., Xu, F., Liu, P., Herbert, J., … Ge, Y. (2014). Impaired cerebrovascular reactivity in multiple sclerosis. *JAMA Neurology*, *71*(10), 1275–1281. https://doi.org/10.1001/jamaneurol.2014.1668

Martino, F. De, Moerel, M., Xu, J., Moortele, P. Van De, Ugurbil, K., Goebel, R., … Formisano, E. (2015). High-Resolution Mapping of Myeloarchitecture In Vivo : Localization of Auditory Areas in the Human Brain. *Cerebral Cortex*, (October), 3394–3405. https://doi.org/10.1093/cercor/bhu150

Mathias, E. J., Kenny, A., Plank, M. J., & David, T. (2018). Integrated models of neurovascular coupling and BOLD signals: Responses for varying neural activations. *NeuroImage*, *174*(December 2017), 69–86. https://doi.org/10.1016/j.neuroimage.2018.03.010

May, A. (2011). Experience-dependent structural plasticity in the adult human brain. *Trends in Cognitive Sciences*, *15*(10), 475–482. https://doi.org/10.1016/j.tics.2011.08.002

Mcgeer, E. G., Staines, W. A., & Mcgeer, P. L. (1984). Neurotransmitters in the Basal Ganglia. *Can. j. Neurol. Science*, *11*(1), 89–99.

Mckenna, M. C., Dienel, G. A., Sonnewald, U., Waagepetersen, H. S., & Schousboe, A. (2012). Energy Metabolism of the Brain, 200–231. https://doi.org/10.1016/B978-0-12-374947-5.00011-0

McKenzie, I. A., Ohayon, D., Li, H., De Faria, J. P., Emery, B., Tohyama, K., & Richardson, W. D. (2014). Motor skill learning requires active central myelination. *Science*, *346*(6207), 318–322. https://doi.org/10.1126/science.1254960

Merola, A., Germuska, M. A., Murphy, K., & Wise, R. G. (2018). Assessing the repeatability

of absolute CMRO2, OEF and haemodynamic measurements from calibrated fMRI. *NeuroImage*, *173*, 113–126. https://doi.org/10.1016/J.NEUROIMAGE.2018.02.020

Merola, A., Murphy, K., Stone, A. J., Germuska, M. A., Griffeth, V. E. M., Blockley, N. P., … Wise, R. G. (2016). Measurement of oxygen extraction fraction (OEF): An optimized BOLD signal model for use with hypercapnic and hyperoxic calibration. *NeuroImage*, *129*, 159–174. https://doi.org/10.1016/j.neuroimage.2016.01.021

Mezzapesa, D. M., Rocca, M. A., Rodegher, M., Comi, G., & Filippi, M. (2008). Functional cortical changes of the sensorimotor network are associated with clinical recovery in multiple sclerosis. *Human Brain Mapping*, *29*(5), 562–573. https://doi.org/10.1002/hbm.20418

Miall, C. R., & Robertson, E. M. (2006). Functional Imaging : Is the Resting Brain Resting ? *Current Biology*, *16*(23), 998–1000.

Morgen, K., Kadom, N., Sawaki, L., Tessitore, A., Ohayon, J., McFarland, H., … Cohen, L. G. (2004). Training-dependent plasticity in patients with multiple sclerosis. *Brain*, *127*(11), 2506–2517. https://doi.org/10.1093/brain/awh266

Mori, F., Nisticò, R., Mandolesi, G., Piccinin, S., Mango, D., Kusayanagi, H., … Centonze, D. (2014). Interleukin-1 b Promotes Long-Term Potentiation in Patients with Multiple Sclerosis. *Neuromol Med*, (16), 38–51. https://doi.org/10.1007/s12017-013-8249-7

Mottershead, J. P., Schmierer, K., Clemence, M., Thornton, J. S., Scaravilli, F., Barker, G. J., … Miller, D. H. (2003). High field MRI correlates of myelin content and axonal density in multiple sclerosis. *Journal of Neurology*, *250*(11), 1293–1301. https://doi.org/10.1007/s00415-003-0192-3

Mozolic, J. L., Hayasaka, S., & Laurienti, P. J. (2010a). A cognitive training intervention increases resting cerebral blood flow in healthy older adults. *Frontiers in Human Neuroscience*, *4*, 16. https://doi.org/10.3389/neuro.09.016.2010

Mozolic, J. L., Hayasaka, S., & Laurienti, P. J. (2010b). A cognitive training intervention increases resting cerebral blood flow in healthy older adults. *Frontiers in Human Neuroscience*, *4*(March), 1–10. https://doi.org/10.3389/neuro.09.016.2010

Mugler III, J. P., & Brookeman, J. R. (1990). Three-Dimensional Magnetization-Prepared Rapid Gradient-Echo Imaging (3D MP RAGE). *Magnetic Resonance in Medicine*, *157*, 152–157.

Mullinger, K. J., Mayhew, S. D., Bagshaw, A. P., Bowtell, R., & Francis, S. T. (2014). Evidence that the negative BOLD response is neuronal in origin: A simultaneous EEG–

BOLD–CBF study in humans. *NeuroImage*, *94*, 263–274. https://doi.org/10.1016/j.neuroimage.2014.02.029

Muoio, V., Persson, P. B., & Sendeski, M. M. (2014). The neurovascular unit – concept review, 790–798. https://doi.org/10.1111/apha.12250

Muraskin, J., Dodhia, S., Lieberman, G., Garcia, J. O., Verstynen, T., Vettel, J. M., … Sajda, P. (2016). Brain Dynamics of Post-Task Resting State are Influenced by Expertise : Insights From Baseball Players, *4471*(July), 4454–4471. https://doi.org/10.1002/hbm.23321

Murphy, T., Dias, G. P., & Thuret, S. (2014). Effects of diet on brain plasticity in animal and human studies: Mind the gap. *Neural Plasticity*. Hindawi Publishing Corporation. https://doi.org/10.1155/2014/563160

Nagy, C., & Turecki, G. (2012). Sensitive Periods in Epigenetics : bringing us closer to complex behavioral phenotypes. *Epigenomics*, *4*(4), 445–457. https://doi.org/10.2217/epi.12.37.Sensitive

Narayana, P. A., Zhou, Y., Hasan, K. M., Datta, S., Sun, X., & Wolinsky, J. S. (2014). Hypoperfusion and T1-hypointense lesions in white matter in multiple sclerosis. *Multiple Sclerosis (Houndmills, Basingstoke, England)*, *20*(3), 365–373. https://doi.org/10.1177/1352458513495936

Niessing, J., Ebisch, B., Schmidt, K. E., Niessing, M., Singer, W., & Galuske, R. A. W. (2005). Hemodynamic Signals Correlate Tightly with Synchronized Gamma Oscillations. *Science*, *309*(August), 948–952.

Nissen, M. J., & Bullemer, P. (1987a). Attentional Requirements of Learning : Performance Measures Evidence from, *32*.

Nissen, M. J., & Bullemer, P. (1987b). Attentional requirements of learning: Evidence from performance measures. *Cognitive Psychology*, *19*(1), 1–32. https://doi.org/10.1016/0010-0285(87)90002-8

Nudo, R. J. (2003). ADAPTIVE PLASTICITY IN MOTOR CORTEX : IMPLICATIONS FOR REHABILITATION AFTER BRAIN INJURY. *Jorunal Rehabilitation Medicine*, (41), 7–10. https://doi.org/10.1080/16501960310010070

Nudo, R. J. (2006). Plasticity. *NeuroRx*, *3*, 420–427.

Nunez, P. L., Srinivasan, R., & Fields, R. D. (2015). Clinical Neurophysiology EEG functional connectivity , axon delays and white matter disease. *Clinical Neurophysiology*, *126*(1), 110–120. https://doi.org/10.1016/j.clinph.2014.04.003

Ogawa, S., Lee, T. M., Kay, A. R., & Tank, D. W. (1990). Brain magnetic resonance imaging with contrast dependent on blood oxygenation. *Proceedings of the National Academy of Sciences of the United States of America*, *87*(24), 9868–9872. https://doi.org/10.1073/pnas.87.24.9868

Ogg, R. J., & Steen, R. G. (1998). Age-Related Changes in Brain TI Are Correlated with Iron Concentration. *Magnetic Resonance in Medicine*, (24).

Okell, T. W., Chappell, M. A., Kelly, M. E., & Jezzard, P. (2013). Cerebral Blood Flow Quantification Using Vessel-Encoded Arterial Spin Labeling. *Journal of Cerebral Blood Flow & Metabolism*, *33*(11), 1716–1724. https://doi.org/10.1038/jcbfm.2013.129

Packard, M. G. (2001). Basal Ganglia. In N. J. Smelser & P. B. B. T.-I. E. of the S. & B. S. Baltes (Eds.) (pp. 1044–1048). Oxford: Pergamon. https://doi.org/https://doi.org/10.1016/B0-08-043076-7/03463-X

Pajevic, S., Basser, P. J., & Fields, R. D. (2014). Role of myelin plasticity in oscillations and synchrony of neuronal activity. *Neuroscience*, *276*, 135–147. https://doi.org/10.1016/J.NEUROSCIENCE.2013.11.007

Pantano, P., Mainero, C., Domenico Iannetti, G., Caramia, F., Di Legge, S., Piattella, M. C., … Lenzi, G. L. (2002). Contribution of corticospinal tract damage to cortical motor reorganization after a single clinical attack of multiple sclerosis. *NeuroImage*, *17*(4), 1837–1843. https://doi.org/10.1006/nimg.2002.1313

Pascual, A., Wassermann, E. M., Sadato, N., & Hallett, M. (1995). The role of reading activity on the modulation of motor cortical outputs to the reading hand in braille readers. *Annals of Neurology*, *38*(6), 910–915. https://doi.org/10.1002/ana.410380611

Patenaude, B., Smith, S. M., Kennedy, D. N., & Jenkinson, M. (2011). A Bayesian model of shape and appearance for subcortical brain segmentation. *NeuroImage*, *56*(3), 907–922. https://doi.org/10.1016/j.neuroimage.2011.02.046

Pearson-Fuhrhop, K. M., & Cramer, S. C. (2010). Genetic Influences on Neural Plasticity. *PM&R*, *2*, S227–S240. https://doi.org/10.1016/j.pmrj.2010.09.011

Peirce, J. W. (2007). PsychoPy-Psychophysics software in Python. *Journal of Neuroscience Methods*, *162*(1–2), 8–13. https://doi.org/10.1016/j.jneumeth.2006.11.017

Penner, I., Raselli, C., Stöcklin, M., Opwis, K., Kappos, L., & Calabrese, P. (2009). The Fatigue Scale for Motor and Cognitive Functions (FSMC): validation of a new instrument to assess multiple sclerosis-related fatigue. *Multiple Sclerosis Journal*, *15*(12), 1509–1517. https://doi.org/10.1177/1352458509348519

Petsas, N., Tinelli, E., Lenzi, D., Tomassini, V., Sbardella, E., Tona, F., … Pantano, P. (2013). Evidence of Impaired Brain Activity Balance after Passive Sensorimotor Stimulation in Multiple Sclerosis. *PLoS ONE*, *8*(6), 1–10. https://doi.org/10.1371/journal.pone.0065315

Petzold, G. C., & Murthy, V. N. (2011). Review Role of Astrocytes in Neurovascular Coupling. *Neuron*, *71*(5), 782–797. https://doi.org/10.1016/j.neuron.2011.08.009

Polman, C. H., Reingold, S. C., Banwell, B., Clanet, M., Cohen, J. A., Filippi, M., … Wolinsky, J. S. (2011). Diagnostic criteria for multiple sclerosis: 2010 Revisions to the McDonald criteria. *Annals of Neurology*, *69*(2), 292–302. https://doi.org/10.1002/ana.22366

Prosperini, L., Fanelli, F., Pestas, N., Sbardella, E., Tona, F., Raz, E., … Pantano, P. (2014). Changes in Microarchitecture of White Matter Tracts after training with a video game balance board. *Radiology*, *273*(2), 529–538. https://doi.org/10.1148/radiol.14140168

Purnima, B., & Arvind, K. (2014). EBK-Means: A Clustering Technique based on Elbow Method and K-Means in WSN. *International Journal of Computer Applications*, *105*(9), 17–24. Retrieved from https://www.ijcaonline.org/archives/volume105/number9/18405-9674

Raichle, M E, MacLeod, A. M., Snyder, A. Z., Powers, W. J., Gusnard, D. A., & Shulman, G. L. (2001). A default mode of brain function. *Proceedings of the National Academy of Sciences of the United States of America*, *98*(2), 676–682. https://doi.org/10.1073/pnas.98.2.676

Raichle, Marcus E., & Mintun, M. A. (2006). Brain Work and Brain Imaging. *Annual Review of Neuroscience*, *29*(1), 449–476. https://doi.org/10.1146/annurev.neuro.29.051605.112819

Ranganathan, R. (2017). Reorganization of finger coordination patterns through motor exploration in individuals after stroke, 1–12. https://doi.org/10.1186/s12984-017-0300-8

Reber, P. J. (2013). The neural basis of implicit learning and memory : A review of neuropsychological and neuroimaging research. *Neuropsychologia*, *51*(10), 2026–2042. https://doi.org/10.1016/j.neuropsychologia.2013.06.019

Reddy, H. (2002). Functional brain reorganization for hand movement in patients with multiple sclerosis: defining distinct effects of injury and disability. *Brain*, *125*(12), 2646–2657. https://doi.org/10.1093/brain/awf283

Reddy, H., Narayanan, S., Matthews, P. M., Hoge, R. D., Pike, G. B., Duquette, P., … Arnold, D. L. (2000). Relating axonal injury to functional recovery in MS. *Neurology*, *54*(1), 236–239. https://doi.org/10.1212/WNL.54.1.236

Richards, D. S., Georgilas, I., & Dagnino, G. (2015). Powered Exoskeleton with Palm Degrees of Freedom for Hand Rehabilitation, 4635–4638.

Rioult-Pedotti, M.-S., Friedman, D., & Donoghue, J. P. (2000). Learning-Induced LTP in Neocortex. *Science*, *290*(October), 533–537.

Robertson, E. M. (2007). The Serial Reaction Time Task: Implicit Motor Skill Learning? *Journal of Neuroscience*, *27*(38), 10073–10075. https://doi.org/10.1523/JNEUROSCI.2747-07.2007

Rocca, M. A., Absinta, M., Valsasina, P., Ciccarelli, O., Marino, S., Rovira, A., … Filippi, M. (2009). Abnormal Connectivity of the Sensorimotor Network in Patients With MS : A MultiCenter fMRI Study. *Human Brain Mapping*, *30*, 2412–2425. https://doi.org/10.1002/hbm.20679

Rocca, M. A., Colombo, B., Falini, A., Ghezzi, A., Martinelli, V., Scotti, G., … Filippi, M. (2005). Cortical adaptation in patients with MS: A cross-sectional functional MRI study of disease phenotypes. *Lancet Neurology*, *4*(10), 618–626. https://doi.org/10.1016/S1474-4422(05)70171-X

Rocca, M. A., Gallo, A., Colombo, B., Falini, A., Scotti, G., Comi, G., & Filippi, M. (2004). Pyramidal tract lesions and movement-associated cortical recruitment in patients with MS. *Neuroimage*, *23*, 141–147. https://doi.org/10.1016/j.neuroimage.2004.05.005

Rocca, M. A., Mesaros, S., Pagani, E., Sormani, M. P., Comi, G., & Filippi, M. (2010). Thalamic Damage and Long- in Multiple Sclerosis 1 Methods : Results : Conclusion : *Radiology*, *257*(2), 463–469.

Rocca, M. A., Valsasina, P., Leavitt, V. M., Rodegher, M., Radaelli, M., Riccitelli, G. C., … Filippi, M. (2018). Functional network connectivity abnormalities in multiple sclerosis : Correlations with disability and cognitive impairment. *MULTIPLE SCLEROSIS JOURNAL*, *24*(4), 459–471. https://doi.org/10.1177/1352458517699875

Rocca, M. A., Valsasina, P., Martinelli, V., Misci, P., & Falini, A. (2012). Large-scale neuronal network dysfunction in relapsing-remitting multiple sclerosis. *Neurology*, *79*, 1449–1457.

Rodgers, Z. B., Detre, J. A., & Wehrli, F. W. (2016). MRI-based methods for quantification of the cerebral metabolic rate of oxygen. *Journal of Cerebral Blood Flow and Metabolism*, *36*(7), 1165–1185. https://doi.org/10.1177/0271678X16643090

Rojas, J. I., Murphy, G., Sanchez, F., Patrucco, L., Fernandez, M. C., Miguez, J., … Cristiano, E. (2018). Thalamus volume change and cognitive impairment in early relapsing – remitting multiple sclerosis patients. *Neuroradiology Journal*, *31*, 3–8.

https://doi.org/10.1177/1971400918781977

Rooney, W. D., Johnson, G., Li, X., Cohen, E. R., Kim, S., Ugurbil, K., & Springer, C. S. (2007). Magnetic Field and Tissue Dependencies of Human Brain Longitudinal 1 H 2 O Relaxation in Vivo. *Magnetic Resonance in Medicine*, *318*, 308–318. https://doi.org/10.1002/mrm.21122

Roosendaal, S. D., Moraal, B., Pouwels, P. J. W., Vrenken, H., Castelijns, J. A., Barkhof, F., & Geurts, J. J. G. (2009). Accumulation of cortical lesions in MS: Relation with cognitive impairment. *Multiple Sclerosis*, *15*(6), 708–714. https://doi.org/10.1177/1352458509102907

Roosendaal, S. D., Moraal, B., Vrenken, H., Castelijns, J. A., Pouwels, P. J. W., Barkhof, F., & Geurts, J. J. G. (2008). In Vivo MR Imaging of Hippocampal Lesions in Multiple Sclerosis, *731*, 726–731. https://doi.org/10.1002/jmri.21294

Roosendaal, S. D., Schoonheim, M. M., Hulst, H. E., Sanz-arigita, E. J., Smith, S. M., Geurts, J. J. G., & Barkhof, F. (2010). Resting state networks change in clinically isolated syndrome. *Brain*, (133), 1612–1621. https://doi.org/10.1093/brain/awq058

Roy, C. S., & Sherrington, C. S. (1890). On the regulation of the blood supply of the brain. *Journal of Physiology*, *11*(5), 85–108. https://doi.org/10.1113/jphysiol.1890.sp000321

Sami, S., Robertson, E. M., & Miall, R. C. (2014). The Time Course of Task-Specific Memory Consolidation Effects in Resting State Networks, *34*(11), 3982–3992. https://doi.org/10.1523/JNEUROSCI.4341-13.2014

Sanchez-Panchuelo, R. M., Francis, S. T., Schluppeck, D., & Bowtell, R. W. (2012). Correspondence of Human Visual Areas Identified Using Functional and Anatomical MRI In Vivo at 7 T. *Journal of Magnetic Resonance Imaging*, *299*, 287–299. https://doi.org/10.1002/jmri.22822

Santarnecchi, E., Morbidelli, L., Severi, S., Galluzzi, P., Burroni, L., Menci, E., … Casasco, A. (2015). Cerebral Circulation Time is Prolonged and Not Correlated with EDSS in Multiple Sclerosis Patients: A Study Using Digital Subtracted Angiography. *Plos One*, *10*(2), e0116681. https://doi.org/10.1371/journal.pone.0116681

Schmierer, K., Scaravilli, F., Altmann, D. R., Barker, G. J., & Miller, D. H. (2004). Magnetization transfer ratio and myelin in postmortem multiple sclerosis brain. *Annals of Neurology*, *56*(3), 407–415. https://doi.org/10.1002/ana.20202

Schmierer, K., Wheeler-Kingshott, C. A. M., Boulby, P. A., Scaravilli, F., Altmann, D. R., Barker, G. J., … Miller, D. H. (2007). Diffusion tensor imaging of post mortem multiple

sclerosis brain. *NeuroImage*, *35*(2), 467–477. https://doi.org/10.1016/J.NEUROIMAGE.2006.12.010

Schmithorst, V. J., Hernandez-Garcia, L., Vannest, J., Rajagopal, A., Lee, G., & Holland, S. K. (2014). Optimized simultaneous ASL and BOLD functional imaging of the whole brain. *Journal of Magnetic Resonance Imaging*, *39*(5), 1104–1117. https://doi.org/10.1002/jmri.24273

Scholz, J., Klein, M. C., Behrens, T. E. J., & Johansen-Berg, H. (2009). Training induces changes in white-matter architecture. *Nature Neuroscience*, *12*(11), 1370–1371. https://doi.org/10.1038/nn.2412

Schoonheim, M. M., Brandt, R. B., Barkhof, F., & Geurts, J. J. G. (2015). Thalamus structure and function determine severity of cognitive impairment in multiple sclerosis. *Neurology*, *21 (7)*, 925–934.

Schwab, M. E., & Strittmatter, S. M. (2014). Nogo limits neural plasticity and recovery from injury. *Current Opinion in Neurobiology*, *27*, 53–60. https://doi.org/10.1016/j.conb.2014.02.011

Seitz, R. J., & Roland, P. E. (1992). Learning of Sequential Finger Movements in Man: A Combined Kinematic and Positron Emission Tomography (PET) Study. *European Journal of Neuroscience*, *4*(2), 154–165. https://doi.org/10.1111/j.1460-9568.1992.tb00862.x

Sereno, M. I., Lutti, A., Weiskopf, N., & Dick, F. (2013). Mapping the Human Cortical Surface by Combining Quantitative T 1 with Retinotopy †. *Cerebral Cortex*, (September), 2261–2268. https://doi.org/10.1093/cercor/bhs213

Shadmehr, R., & Holcomb, H. H. (1997). Neural Correlates of Motor Memory Consolidation, *277*(AUGUST), 821–826.

Shafee, R., Buckner, R. L., & Fischl, B. (2015). Gray matter myelination of 1555 human brains using partial volume corrected MRI images. *NeuroImage*, *105*, 473–485. https://doi.org/10.1016/j.neuroimage.2014.10.054

Shams, Z., Norris, D. G., & Marques, J. P. (2019). A comparison of in vivo MRI based cortical myelin mapping using T1w / T2w and R1 mapping at 3T. *PLoS ONE*, *1*, 1–22.

Shannon, B. J., Vaishnavi, S. N., Vlassenko, A. G., Shimony, J. S., Rutlin, J., & Raichle, M. E. (2016). Brain aerobic glycolysis and motor adaptation learning. *Proceedings of the National Academy of Sciences*, *113*(26), E3782–E3791. https://doi.org/10.1073/pnas.1604977113

Shmuel, A., & Leopold, D. A. (2008). Neuronal Correlates of Spontaneous Fluctuations in fMRI Signals in Monkey Visual Cortex : Implications for Functional Connectivity at Rest. *Human Brain Mapping*, *761*, 751–761. https://doi.org/10.1002/hbm.20580

Shmuel, A., Yacoub, E., Pfeuffer, J., Van de Moortele, P. F., Adriany, G., Hu, X., & Ugurbil, K. (2002). Sustained negative BOLD, blood flow and oxygen consumption response and its coupling to the positive response in the human brain. *Neuron*, *36*(6), 1195–1210. https://doi.org/10.1016/S0896-6273(02)01061-9

Shu, N., Duan, Y., Xia, M., Schoonheim, M. M., Huang, J., Ren, Z., … Liu, Y. (2016). Disrupted topological organization of structural and functional brain connectomes in clinically isolated syndrome and multiple sclerosis. *Nature Publishing Group*, (July), 1–11. https://doi.org/10.1038/srep29383

Sigalovsky, I. S., Fischl, B., & Melcher, J. R. (2006). Mapping an intrinsic MR property of gray matter in auditory cortex of living humans : A possible marker for primary cortex and hemispheric differences i. *NeuroImage*, *32*, 1524–1537. https://doi.org/10.1016/j.neuroimage.2006.05.023

Simons, M., & Nave, K. (2016). Oligodendrocytes : Myelination and Axonal. *Cold Spring Harbor Perspectives in Biology*, (a020479), 1–16.

Sluming, V., Barrick, T., Howard, M., Cezayirli, E., Mayes, A., & Roberts, N. (2002). Voxel-based morphometry reveals increased gray matter density in Broca's area in male symphony orchestra musicians. *NeuroImage*, *17*(3), 1613–1622. https://doi.org/10.1006/nimg.2002.1288

Smith, J. C., Paulson, E. S., Cook, D. B., Verber, M. D., & Tian, Q. (2010). Detecting changes in human cerebral blood flow after acute exercise using arterial spin labeling: Implications for fMRI. *Journal of Neuroscience Methods*, *191*(2), 258–262. https://doi.org/10.1016/j.jneumeth.2010.06.028

Smith, S. M., & Brady, J. M. (1997). SUSAN - A new approach to low level image processing. *International Journal of Computer Vision*, *23*(1), 45–78. https://doi.org/10.1023/A:1007963824710

Smith, S. M., De Stefano, N., Jenkinson, M., & Matthews, P. M. (2001). Normalized accurate measurement of longitudinal brain change. *Journal of Computer Assisted Tomography*, *25*(3), 466–475. https://doi.org/10.1097/00004728-200105000-00022

Smith, S. M., Jenkinson, M., Johansen-Berg, H., Rueckert, D., Nichols, T. E., Mackay, C. E., … Behrens, T. E. J. (2006). Tract-based spatial statistics: Voxelwise analysis of multi-

subject diffusion data. *NeuroImage*. https://doi.org/10.1016/j.neuroimage.2006.02.024

Smith, S. M., Jenkinson, M., Woolrich, M. W., Beckmann, C. F., Behrens, T. E. J., Johansen-Berg, H., … Matthews, P. M. (2004). Advances in functional and structural MR image analysis and implementation as FSL. *NeuroImage*, *23*(SUPPL. 1), 208–219. https://doi.org/10.1016/j.neuroimage.2004.07.051

Smith, S. M., & Nichols, T. E. (2009). Threshold-free cluster enhancement : Addressing problems of smoothing , threshold dependence and localisation in cluster inference. *NeuroImage*, *44*(1), 83–98. https://doi.org/10.1016/j.neuroimage.2008.03.061

Smith, S. M., Zhang, Y., Jenkinson, M., Chen, J., Matthews, P. M., Federico, A., & De Stefano, N. (2002). Accurate, Robust, and Automated Longitudinal and Cross-Sectional Brain Change Analysis. *NeuroImage*, *17*(1), 479–489. https://doi.org/10.1006/NIMG.2002.1040

Smith, S. M. (2002). Fast robust automated brain extraction. *Human Brain Mapping*, *17*(3), 143–155. https://doi.org/10.1002/hbm.10062

Squarcina, L., Bertoldo, A., Ham, T. E., Heckemann, R., & Sharp, D. J. (2012). A robust method for investigating thalamic white matter tracts after traumatic brain injury. *NeuroImage*, *63*(2), 779–788. https://doi.org/10.1016/j.neuroimage.2012.07.016

Stampanoni, M., Mori, F., Buttari, F., Marfia, G. A., Sancesario, A., Centonze, D., & Iezzi, E. (2017). Clinical Neurophysiology Neurophysiology of synaptic functioning in multiple sclerosis. *Clinical Neurophysiology*, *128*(7), 1148–1157. https://doi.org/10.1016/j.clinph.2017.04.006

Stanisz, G. J., Kecojevic, A., Bronskill, M. J., & Henkelman, R. M. (1999). Transfer and T 2. *Magnetic Resonance in Medicine*, *1136*(March), 1128–1136.

Steele, C. J., & Penhune, V. B. (2010). Specific Increases within Global Decreases: A Functional Magnetic Resonance Imaging Investigation of Five Days of Motor Sequence Learning. *Journal of Neuroscience*, *30*(24), 8332–8341. https://doi.org/10.1523/JNEUROSCI.5569-09.2010

Steen, R. G., Reddick, W. E., & Ogg, J. (2000). More than meets the eye : significant regional heterogeneity in human cortical T 1 *. *Magnetic Resonance Imaging*, *18*, 361–368.

Steenwijk, M. D., Daams, M., Pouwels, P. J. W., Balk, L. J., Tewarie, P. K., Killiestein, J., … Geurts, J. J. G. (2014). What Explains Gray Matter Atrophy in Long-standing Multiple Sclerosis? *Radiology*, *272*(3).

Stüber, C., Morawski, M., Schäfer, A., Labadie, C., Wähnert, M., Leuze, C., … Turner, R.

(2014). Myelin and iron concentration in the human brain : A quantitative study of MRI contrast. *NeuroImage*, *93*, 95–106. https://doi.org/10.1016/j.neuroimage.2014.02.026

Su, B., Ji, Y., Sun, X., Liu, X., & Chen, Z. (2014). Brain-derived Neurotrophic Factor (BDNF) -induced Mitochondrial Motility Arrest and Presynaptic Docking Contribute to BDNF-enhanced Synaptic Transmission *, *289*(3), 1213–1226. https://doi.org/10.1074/jbc.M113.526129

Swire, M., Kotelevtsev, Y., Webb, D. J., Lyons, D. A., Kingdom, U., Kingdom, U., … Kingdom, U. (2019). Endothelin signalling mediates experience-dependent myelination in the CNS. *ELife*, 1–23.

Tacchino, A., Bove, M., Roccatagliata, L., Luigi Mancardi, G., Uccelli, A., & Bonzano, L. (2014). Selective impairments of motor sequence learning in multiple sclerosis patients with minimal disability. *Brain Research*, *1585*, 91–98. https://doi.org/10.1016/j.brainres.2014.08.031

Takeuchi, H., Taki, Y., Nouchi, R., Hashizume, H., Sekiguchi, A., Kotozaki, Y., … Kawashima, R. (2012). Effects of working memory training on functional connectivity and cerebral blood flow during rest. *CORTEX*, *49*(8), 2106–2125. https://doi.org/10.1016/j.cortex.2012.09.007

Tancredi, F. B., Gauthier, C. J., Madjar, C., Bolar, D. S., Fisher, J. A., Wang, D. J. J., & Hoge, R. D. (2012). Comparison of pulsed and pseudocontinuous arterial spin-labeling for measuring CO2-induced cerebrovascular reactivity. *Journal of Magnetic Resonance Imaging*, *36*(2), 312–321. https://doi.org/10.1002/jmri.23658

Tardif, C. L., Gauthier, C. J., Steele, C. J., Bazin, P.-L., Schäfer, A., Schaefer, A., … Villringer, A. (2016a). Advanced MRI techniques to improve our understanding of experience-induced neuroplasticity. *NeuroImage*, *131*, 55–72. https://doi.org/10.1016/J.NEUROIMAGE.2015.08.047

Tardif, C. L., Gauthier, C. J., Steele, C. J., Bazin, P. L., Schäfer, A., Schaefer, A., … Villringer, A. (2016b). Advanced MRI techniques to improve our understanding of experience-induced neuroplasticity. *NeuroImage*. https://doi.org/10.1016/j.neuroimage.2015.08.047

Tardif, C. L., Gauthier, C. J., Steele, C. J., Bazin, P. L., Schäfer, A., Schaefer, A., … Villringer, A. (2016c). Advanced MRI techniques to improve our understanding of experience-induced neuroplasticity. *NeuroImage*, *131*, 55–72. https://doi.org/10.1016/j.neuroimage.2015.08.047

Taubert, M., Draganski, B., Anwander, A., Muller, K., Horstmann, A., Villringer, A., & Ragert,

P. (2010). Dynamic Properties of Human Brain Structure: Learning-Related Changes in Cortical Areas and Associated Fiber Connections. *Journal of Neuroscience*, *30*(35), 11670–11677. https://doi.org/10.1523/JNEUROSCI.2567-10.2010

Taubert, Marco, Lohmann, G., Margulies, D. S., Villringer, A., & Ragert, P. (2011). Long-term effects of motor training on resting-state networks and underlying brain structure. *NeuroImage*, *57*(4), 1492–1498. https://doi.org/10.1016/j.neuroimage.2011.05.078

Thiebaut De Schotten, M., Cohen, L., Amemiya, E., Braga, L. W., Dehaene, S., Yvette, G., & Paris-sud, F. U. (2014). Learning to Read Improves the Structure of the Arcuate Fasciculus. *Cerebral Cortex*, (April), 989–995. https://doi.org/10.1093/cercor/bhs383

Thomas, A. G., Marrett, S., Saad, Z. S., Ruff, D. A., Martin, A., & Bandettini, P. A. (2009). Functional but not structural changes associated with learning: An exploration of longitudinal Voxel-Based Morphometry (VBM). *NeuroImage*, *48*(1), 117–125. https://doi.org/10.1038/jid.2014.371

Timmler, S., & Simons, M. (2019). Grey matter myelination. *Glia*, (January), 2063–2070. https://doi.org/10.1002/glia.23614

Todorova, V., & Blokland, A. (2017). Mitochondria and Synaptic Plasticity in the Mature and Aging Nervous System, 166–173. https://doi.org/10.2174/1570159X14666160414111

Tomassini, V., d'Ambrosio, A., Petsas, N., Wise, R. G., Sbardella, E., Allen, M., … Pozzilli, C. (2016). The effect of inflammation and its reduction on brain plasticity in multiple sclerosis: MRI evidence. *Human Brain Mapping*, *37*(7), 2431–2445. https://doi.org/10.1002/hbm.23184

Tomassini, V., Jbabdi, S., Kincses, Z. T., Bosnell, R., Douaud, G., Pozzilli, C., … Johansen-berg, H. (2011). Structural and Functional Bases for Individual Differences in Motor Learning. *Human Brain Mapping*, *32*(3), 494–508. https://doi.org/10.1002/hbm.21037

Tomassini, V., Johansen-Berg, H., Jbabdi, S., Wise, R. G., Pozzilli, C., Palace, J., & Matthews, P. M. (2012). Relating brain damage to brain plasticity in patients with multiple sclerosis. *Neurorehabilitation and Neural Repair*, *26*(6), 581–593. https://doi.org/10.1177/1545968311433208

Tomassini, V., Johansen-Berg, H., Leonardi, L., Paixão, L., Jbabdi, S., Palace, J., … Matthews, P. M. (2011). Preservation of motor skill learning in patients with multiple sclerosis. *Multiple Sclerosis Journal*, *17*(1), 103–115. https://doi.org/10.1177/1352458510381257

Tomassini, V., Matthews, P. M., Thompson, A. J., Fuglø, D., Geurts, J. J., Johansen-berg, H., … Barkhof, F. (2012). Neuroplasticity and functional recovery in multiple sclerosis.

Nature Publishing Group, *8*(11), 635–646. https://doi.org/10.1038/nrneurol.2012.179

Tomassini, V., Johansen-Berg, H., Jbabdi, S., Wise, R. G., Pozzilli, C., Palace, J., & Matthews, P. M. (2012). Relating brain damage to brain plasticity in patients with multiple sclerosis. *Neurorehabilitation and Neural Repair*, *26*(6), 581–593. https://doi.org/10.1177/1545968311433208

Tomassy, G. S., Berger, D. R., Chen, H., Kasthuri, N., Hayworth, K. J., Vercelli, A., … Arlotta, P. (2014). Distinct profiles of myelin distribution along single axons of pyramidal neurons in the neocortex. *Science*, *344*(6181), 319–324. https://doi.org/10.1126/science.1249766.Distinct

Trapp, B. D., Ransohoff, R. M., Fisher, E., & Rudick, R. A. (1999). Neurodegeneration in multiple sclerosis: Relationship to neurological disability. *Neuroscientist*, *5*(1), 48–57. https://doi.org/10.1177/107385849900500107

Trapp, B. D., & Stys, P. K. (2009a). Virtual hypoxia and chronic necrosis of demyelinated axons in multiple sclerosis. *The Lancet Neurology*, *8*(3), 280–291. https://doi.org/10.1016/S1474-4422(09)70043-2

Trapp, B. D., & Stys, P. K. (2009b, March 1). Virtual hypoxia and chronic necrosis of demyelinated axons in multiple sclerosis. *The Lancet Neurology*. Elsevier. https://doi.org/10.1016/S1474-4422(09)70043-2

Tronel, S., Fabre, A., Charrier, V., Oliet, S. H. R., & Gage, F. H. (2010). Spatial learning sculpts the dendritic arbor of adult-born hippocampal neurons. *Pnas*, *107*(12), 7963–7968. https://doi.org/10.1073/pnas.0914613107

Trovar-Moll, F., Evangelou, I. E., Chiu, A. W., Richert, N. D., Ostuni, J. L., Ohayon, J. M., … Bagnato, F. (2009). Thalamic Involvement and Its Impact on Clinical Disability in Patients with Multiple Sclerosis : A Diffusion Tensor Imaging Study at 3T. *Neuroradiology*, *30 (7)*, 1380–1386. https://doi.org/10.3174/ajnr.A1564

Ungerleider, L. G., Doyon, J., & Karni, A. (2002). Imaging brain plasticity during motor skill learning. *Neurobiology of Learning and Memory*, *78*(3), 553–564. https://doi.org/10.1006/nlme.2002.4091

Vafaee, M. S., & Gjedde, A. (2004). Spatially dissociated flow-metabolism coupling in brain activation. *NeuroImage*, *21*(2), 507–515. https://doi.org/10.1016/j.neuroimage.2003.10.003

Vahdat, S., Darainy, M., Milner, T. E., & Ostry, D. J. (2011). Functionally Specific Changes in Resting-State Sensorimotor Networks after Motor Learning, *31*(47), 16907–16915.

https://doi.org/10.1523/JNEUROSCI.2737-11.2011

Vaishnavi, S. N., Vlassenko, A. G., Rundle, M. M., Snyder, A. Z., & Mintun, M. A. (2010). Regional aerobic glycolysis in the human brain, *107*(41), 17757–17762. https://doi.org/10.1073/pnas.1010459107

Valenti, D., Bari, L. De, Filippis, B. De, Henrion-caude, A., & Anna, R. (2014). Neuroscience and Biobehavioral Reviews Mitochondrial dysfunction as a central actor in intellectual disability-related diseases : An overview of Down syndrome , autism , Fragile X and Rett syndrome. *Neuroscience and Biobehavioral Reviews*, *46*, 202–217. https://doi.org/10.1016/j.neubiorev.2014.01.012

van Wijk, B. C. M. Van, Stam, C. J., & Daffertshofer, A. (2010). Comparing Brain Networks of Different Size and Connectivity Density Using Graph Theory. *PLoS ONE*, *5*(10). https://doi.org/10.1371/journal.pone.0013701

Vas, A. K., Spence, J., & Chapman, S. B. (2015). Abstracting meaning from complex information (gist reasoning) in adult traumatic brain injury. *Journal of Clinical and Experimental Neuropsychology*, *37*(2), 152–161. https://doi.org/10.1080/13803395.2014.994478

Vercellino, M., Masera, S., Lorenzatti, M., Condello, C., Merola, A., Mattioda, A., … Cavalla, P. (2009). Demyelination , Inflammation , and Neurodegeneration in Multiple Sclerosis Deep Gray Matter. *Journal of Neuropathology & Experimental Neurology*, *68*(5), 489–502.

Verstreken, P., Ly, C. V, Venken, K. J. T., Koh, T., Zhou, Y., & Bellen, H. J. (2005). for Mobilization of Reserve Pool Vesicles at Drosophila Neuromuscular Junctions, *47*, 365–378. https://doi.org/10.1016/j.neuron.2005.06.018

Vincent, J. L. (2009). Learning and Memory : While You Rest , Your Brain Keeps Working. *Current Biology*, *19*(12), R484–R486. https://doi.org/10.1016/j.cub.2009.05.024

Viviani, R., Messina, I., & Walter, M. (2011). Resting State Functional Connectivity in Perfusion Imaging : Correlation Maps with BOLD Connectivity and Resting State Perfusion. *PLoS ONE*, *6*(11). https://doi.org/10.1371/journal.pone.0027050

Vrenken, H., Pouwels, P. J. W., Geurts, J. J. G., Knol, D. L., Polman, C. H., Barkhof, F., & Castelijns, J. A. (2006). Altered diffusion tensor in multiple sclerosis normal-appearing brain tissue: Cortical diffusion changes seem related to clinical deterioration. *Journal of Magnetic Resonance Imaging*, *23*(5), 628–636. https://doi.org/10.1002/jmri.20564

Waehnert, M. D., Dinse, J., Weiss, M., Streicher, M. N., Waehnert, P., Geyer, S., … Bazin, P.-

L. (2014). Anatomically motivated modeling of cortical laminae. *NeuroImage*, *93*, 210–220. https://doi.org/10.1016/J.NEUROIMAGE.2013.03.078

Wagenknecht, N., Becker, B., Scheld, M., Beyer, C., Clarner, T., Hochstrasser, T., & Kipp, M. (2016). Thalamus Degeneration and Inflammation in Two Distinct Multiple Sclerosis Animal Models. *Journal of Molecular Neuroscience*, (60), 102–114. https://doi.org/10.1007/s12031-016-0790-z

Waites, A. B., Stanislavsky, A., Abbott, D. F., & Jackson, G. D. (2005). Effect of Prior Cognitive State on Resting State Networks Measured With Functional Connectivity, *68*, 59–68. https://doi.org/10.1002/hbm.20069

Walters, N. B., Egan, G. F., Kril, J. J., Kean, M., Waley, P., Jenkinson, M., & Watson, J. D. G. (2003). In vivo identification of human cortical areas using high-resolution MRI : An approach to cerebral structure – function correlation. *Pnas*, *1*(5), 193–196.

Wang, L., Zhang, Z., Wang, Y., Zhang, R., & Chopp, M. (2004). Treatment of Stroke With Erythropoietin Enhances Neurogenesis and Angiogenesis and Improves Neurological Function in Rats. *Stroke*, 1732–1737. https://doi.org/10.1161/01.STR.0000132196.49028.a4

Wang, Z., Liu, J., Zhong, N., Qin, Y., Zhou, H., & Li, K. (2012). Changes in the brain intrinsic organization in both on-task state and post-task resting state. *NeuroImage*, *62*(1), 394–407. https://doi.org/10.1016/j.neuroimage.2012.04.051

Warburg, O. (1956). On the Origin of Cancer Cells. *Science*, *123*(3191), 309–314.

Ward, N. L., & LaManna, J. C. (2004). The neurovascular unit and its growth factors: Coordinated response in the vascular and nervous systems. *Neurological Research*, *26*(8), 870–883. https://doi.org/10.1179/016164104X3798

Ward, N. S., Brown, M. M., Thompson, A. J., & Frackowiak, R. S. J. (2003). Neural correlates of motor recovery after stroke: a longitudinal fMRI study. *Brain*, *126*(11), 2476–2496. https://doi.org/10.1093/brain/awg245

Warnert, E. A. H., Murphy, K., Hall, J. E., & Wise, R. G. (2015). Noninvasive assessment of arterial compliance of human cerebral arteries with short inversion time arterial spin labeling, (August 2014), 461–468. https://doi.org/10.1038/jcbfm.2014.219

Watts, M. E., Pocock, R., & Claudianos, C. (2018). Brain Energy and Oxygen Metabolism: Emerging Role in Normal Function and Disease, *11*(June), 1–13. https://doi.org/10.3389/fnmol.2018.00216

Wegner, C., Filippi, M., Korteweg, T., Beckmann, C., Ciccarelli, O., De Stefano, N., …

Matthews, P. M. (2008). Relating functional changes during hand movement to clinical parameters in patients with multiple sclerosis in a multi-centre fMRI study. *European Journal of Neurology*, *15*(2), 113–122. https://doi.org/10.1111/j.1468-1331.2007.02027.x

Whelton, S., Chin, A., Xin, X., & He, J. (2002). Effect of Aerobic Exercise on Blood Pressure: A Meta-Analysis of Randomized, Controlled Trials. *Annals of Internal Medicine*, (136), 493–503.

Winkler, A. M., Ridgway, G. R., Webster, M. A., Smith, S. M., & Nichols, T. E. (2014). Permutation inference for the general linear model. *NeuroImage*, *92*, 381–397. https://doi.org/10.1016/j.neuroimage.2014.01.060

Wise, R. G., Harris, A. D., Stone, A. J., & Murphy, K. (2013). Measurement of OEF and absolute CMRO2: MRI-based methods using interleaved and combined hypercapnia and hyperoxia. *NeuroImage*, *83*(0), 135–147. https://doi.org/10.1016/j.neuroimage.2013.06.008

Witte, M. E., Geurts, J. J. G., de Vries, H. E., van der Valk, P., & van Horssen, J. (2010, August 1). Mitochondrial dysfunction: A potential link between neuroinflammation and neurodegeneration? *Mitochondrion*. Elsevier. https://doi.org/10.1016/j.mito.2010.05.014

Witte, M. E., Mahad, D. J., Lassmann, H., & van Horssen, J. (2014). Mitochondrial dysfunction contributes to neurodegeneration in multiple sclerosis. *Trends in Molecular Medicine*, *20*(3), 179–187. https://doi.org/10.1016/j.molmed.2013.11.007

Woolrich, M. W., Behrens, T. E. J., Beckmann, C. F., Jenkinson, M., & Smith, S. M. (2004). Multilevel linear modelling for FMRI group analysis using Bayesian inference, *21*, 1732–1747. https://doi.org/10.1016/j.neuroimage.2003.12.023

Woolrich, M. W., Ripley, B. D., Brady, M., & Smith, S. M. (2001). Temporal Autocorrelation in Univariate Linear Modeling of FMRI Data, *1386*, 1370–1386. https://doi.org/10.1006/nimg.2001.0931

Wu, T., Wang, J., Wang, C., Hallett, M., Zang, Y., Wu, X., & Chan, P. (2012). Basal ganglia circuits changes in Parkinson's disease patients. *Neuroscience Letters*, *524*(1), 55–59. https://doi.org/10.1016/j.neulet.2012.07.012.Basal

Wuerfel, J., Bellmann-strobl, J., Brunecker, P., Aktas, O., Mcfarland, H., Villringer, A., & Zipp, F. (2004). Changes in cerebral perfusion precede plaque formation in multiple sclerosis : a longitudinal perfusion MRI study. *Brain*, *127*(1), 111–119. https://doi.org/10.1093/brain/awh007

Wylezinska, M., Cifelli, A., Jezzard, P., Palace, J., & Alecci, M. (2003). Thalamic

neurodegeneration in relapsing-. *Neurology*, (60), 1949–1954.

Xiao, L., Ohayon, D., Mckenzie, I. A., Sinclair-wilson, A., Wright, J. L., Fudge, A. D., … Richardson, W. D. (2016). Rapid production of new oligodendrocytes is required in the earliest stages of motor-skill learning, *19*(9). https://doi.org/10.1038/nn.4351

Xiong, J., Ma, L., Wang, B., Narayana, S., Duff, E. P., Gary, F., & Fox, P. T. (2009). Long-term Motor Training Induced Changes in Regional Cerebral Blood Flow in Both Task and Resting States. *NeuroImage*, *45*(1), 75–82. https://doi.org/10.1016/j.neuroimage.2008.11.016.Long-term

Xu, T., Yu, X., Perlik, A. J., Tobin, W. F., Zweig, J. A., Tennant, K., & Jones, T. (2009). Rapid formation and selective stabilization of synapses for enduring motor memories. *Nature*, *462*(December), 915–920. https://doi.org/10.1038/nature08389

Zahiri, N., Abollahi, I., Nabavi, S. M., Ehsani, F., Arab, A. M., Shaw, I., … Sangelaji, B. (2017). Interference Effect of Prior Explicit Information on Motor Sequence Learning in Relapsing-Remitting Multiple Sclerosis Patients. *Malaysian Journal of Medical Sciences*, *24*(1), 69–80. https://doi.org/10.21315/mjms2017.24.1.8

Zeller, D., & Classen, J. (2014). Plasticity of the motor system in multiple sclerosis. *Neuroscience*, *283*, 222–230. https://doi.org/10.1016/j.neuroscience.2014.05.043

Zhang, H., Long, Z., Ge, R., Xu, L., Jin, Z., Yao, L., & Liu, Y. (2014). Motor Imagery Learning Modulates Functional Connectivity of Multiple Brain Systems in Resting State. *PLoS ONE*, *9*(1), e85489. https://doi.org/10.1371/journal.pone.0085489

Zhang, Y., Brady, M., & Smith, S. (2001). Segmentation of brain MR images through a hidden Markov random field model and the expectation-maximization algorithm. *IEEE Transactions on Medical Imaging*, *20*(1), 45–57. https://doi.org/10.1109/42.906424

Zhou, F., Zhuang, Y., Gong, H., Wang, B., Wang, X., Chen, Q., … Wan, H. (2014). Altered Inter-Subregion Connectivity of the Default Mode Network in Relapsing Remitting Multiple Sclerosis : A Functional and Structural Connectivity Study. *PLoS ONE*, *9*(7), e101198. https://doi.org/10.1371/journal.pone.0101198

Zhu, S., Fang, Z., Hu, S., Wang, Z., & Rao, H. (2013). Resting State Brain Function Analysis Using Concurrent BOLD in ASL Perfusion fMRI, *8*(6), 4–12. https://doi.org/10.1371/journal.pone.0065884

Zivadinov, R, Bergsland, N., Dolezal, O., Hussein, S., Seidl, Z., Dwyer, M. G., … Hora, D. (2013). Evolution of Cortical and Thalamus Atrophy and Disability Progression in Early Relapsing-Remitting MS during 5 Years. *Brain*, (34), 1931–1939.

Zivadinov, Robert, Havrdova, E., Bergsland, N., Tyblova, M., Hagameier, J., Seidl, Z., … Horakova, D. (2013). Thalamic Atrophy Is Associated with Development of Clinically. *Radiology*, *268*(3), 831–841. https://doi.org/10.1148/radiol.13122424/-/DC1

Zlokovic, B. V. (2011). Neurovascular pathways to neurodegeneration in Alzheimer ' s disease and other disorders. *Nature Reviews Neuroscience*, *12*(December), 723–738. https://doi.org/10.1038/nrn3114

Zou, Q., Wu, C. W., Stein, E. A., Zang, Y., & Yang, Y. (2009). Static and Dynamic Characteristics of Cerebral Blood Flow during the Resting State. *NeuroImage*, *48*(19), 515–524. https://doi.org/10.1016/j.neuroimage.2009.07.006.Static